

การศึกษาเชิงทฤษฎีของการถ่ายโอนอิเล็กตรอนที่เหนี่ยวนำด้วยแสงในฟลาโวนอยด์จากข้อมูล  
การจำลองพลวัตเชิงโมเลกุล

นายเกียรติศักดิ์ ลักษณะงาม

วิทยานิพนธ์นี้เป็นส่วนหนึ่งของการศึกษาตามหลักสูตรปริญญาวิทยาศาสตรดุษฎีบัณฑิต  
สาขาวิชาเคมี ภาควิชาเคมี  
คณะวิทยาศาสตร์ จุฬาลงกรณ์มหาวิทยาลัย  
ปีการศึกษา 2555  
ลิขสิทธิ์ของจุฬาลงกรณ์มหาวิทยาลัย

บทคัดย่อและแฟ้มข้อมูลฉบับเต็มของวิทยานิพนธ์ตั้งแต่ปีการศึกษา 2554 ที่ให้บริการในคลังปัญญาจุฬาฯ (CUIR)  
เป็นแฟ้มข้อมูลของนิสิตเจ้าของวิทยานิพนธ์ที่ส่งผ่านทางบัณฑิตวิทยาลัย

The abstract and full text of theses from the academic year 2011 in Chulalongkorn University Intellectual Repository(CUIR)  
are the thesis authors' files submitted through the Graduate School.

THEORETICAL INVESTIGATION OF PHOTOINDUCED ELECTRON TRANSFER IN  
FLAVODOXIN FROM MOLECULAR DYNAMICS SIMULATION DATA

Mr. Kiattisak Lugsanangarm

A Dissertation Submitted in Partial Fulfillment of the Requirements  
for the Degree of Doctor of Philosophy Program in Chemistry

Department of Chemistry

Faculty of Science

Chulalongkorn University

Academic Year 2012

Copyright of Chulalongkorn University

Thesis Title THEORETICAL INVESTIGATION OF PHOTOINDUCED  
ELECTRON TRANSFER IN FLAVODOXIN FROM MOLECULAR  
DYNAMICS SIMULATION DATA

By Mr. Kiattisak Lugsanangarm

Field of Study Chemistry

Thesis Advisor Associate Professor Sirirat Kokpol, Ph.D.

Thesis Co-advisor Assistant Professor Somsak Pianwanit, Ph.D.  
Professor Karl Peter Wolschann, Ph.D.

---

Accepted by the Faculty of Science, Chulalongkorn University in Partial Fulfillment of the  
Requirements for the Doctoral Degree

.....Dean of the Faculty of Science  
(Professor Supot Hannongbua, Dr. rer. nat.)

#### THESIS COMMITTEE

.....Chairman  
(Assistant Professor Warinthorn Chavasiri, Ph.D.)

.....Thesis Advisor  
(Associate Professor Sirirat Kokpol, Ph.D.)

.....Thesis Co-advisor  
(Assistant Professor Somsak Pianwanit, Ph.D.)

.....Thesis Co-advisor  
(Professor Karl Peter Wolschann, Ph.D.)

.....Examiner  
(Professor Thawatchai Tuntulani, Ph.D.)

.....Examiner  
(Associate Professor Vudhichai Parasuk, Ph.D.)

.....Examiner  
(Associate Professor Pornthep Sompornpisut, Ph.D.)

.....External Examiner  
(Nadtanet Nunthaboot, Ph.D.)

เกียรติศักดิ์ ลักษณะงาม: การศึกษาเชิงทฤษฎีของการถ่ายโอนอิเล็กตรอนที่เหนี่ยวนำด้วยแสงในฟลาโวกอกซินจากข้อมูลการจำลองพลวัตเชิงโมเลกุล. (THEORETICAL INVESTIGATION OF PHOTOINDUCED ELECTRON TRANSFER IN FLAVODOXIN FROM MOLECULAR DYNAMICS SIMULATION DATA)  
 อ. ที่ปรึกษาวิทยานิพนธ์หลัก: รศ.ดร. ศิริรัตน์ ก๊กผล, อ. ที่ปรึกษาวิทยานิพนธ์ร่วม: ผศ.ดร. สมศักดิ์ เพ็ชรวิช, ศ.ดร. คาร์ล ปีเตอร์ โวลชาน, 186 หน้า.

การถ่ายโอนอิเล็กตรอนที่เหนี่ยวนำด้วยแสง (PET) ในเอนไซม์มีบทบาทสำคัญในกระบวนการทางชีววิทยาจำนวนมาก ในงานวิจัยนี้ได้ทำการศึกษา PET ในฟลาโวกอกซินจากแบบที่เรียดีซัลโฟวิบริโอ วัลการิส สายพันธุ์ มิยาซากิ เอฟ (FD-DvMF) และจากเฮลิโคแบคเตอร์ ไพโลไร (FD-HP) ด้วยเทคนิคการจำลองโมเลกุลหลายเทคนิค ซึ่งเอนไซม์ทั้งคู่จับกับโมเลกุลเอฟเอ็มเอ็นที่ทำหน้าที่เป็นโคแฟกเตอร์ โครงสร้างของ FD-DvMF จำนวน 4 โครงสร้าง (ชนิดดั้งเดิมและชนิดกลายพันธุ์ W59F, Y97F และ W59F-Y97F) ถูกสร้างขึ้นด้วยเทคนิคการจำลองฮอมอโลยี ในขณะที่โครงสร้างของ FD-HP ชนิดดั้งเดิมได้นำมาจากธนาคารข้อมูลโปรตีน ใช้เทคนิคการจำลองพลวัตเชิงโมเลกุล (MD) สำหรับระบบทั้งห้าเพื่อศึกษาอันตรกิริยาการเข้าจับระหว่างเอฟเอ็มเอ็นกับฟลาโวกอกซินและสมบัติทางพลวัต การคำนวณพลังงานเสรีแบบแยกบ่งชี้ว่าบริเวณ 10-ลูปมีผลต่อการเข้าจับมากที่สุด ทั้งนี้เนื่องมาจากพันธะไฮโดรเจนระหว่างหมู่ฟอสเฟตกับกรดอะมิโนทำการวิเคราะห์หลัก PET โดยใช้โครงรูปจำนวนมากจากผลของ MD ร่วมกับทฤษฎีของคาทิกานีและมาทาคะด้วยการปรับค่าเข้ากับข้อมูลการรบกวนฟลูออเรสเซนซ์ที่ได้จากการทดลอง ผลพบว่าอัตราการถ่ายโอนอิเล็กตรอนเฉลี่ยจาก Trp59 ใน FD-DvMF ชนิดดั้งเดิม และจาก Tyr92 ใน FD-HP ไปยัง Iso ที่สถานะเร้า (Iso\*) มีค่าเร็วที่สุด นอกจากนี้ยังพบว่าพลังงานไฟฟ้าสถิตและการเปลี่ยนแปลงพลังงานเสรีมาตรฐานของปฏิกิริยาเป็นปัจจัยหลักที่ส่งผลต่ออัตราการถ่ายโอนอิเล็กตรอนชนิดเร็ววดยิ่ง ได้ทำการศึกษาการถ่ายโอนประจุด้วยวิธีทางเคมีควอนตัม ผลการคำนวณพบว่าสถานะกระตุ้นที่หนึ่งมีลักษณะเป็นสถานะเร้าแบบเฉพาะที่ ในขณะที่สถานะกระตุ้นที่สองมีลักษณะเป็นสถานะถ่ายโอนประจุ

ภาควิชา.....เคมี.....	ลายมือชื่อนิสิต.....
สาขาวิชา.....เคมี.....	ลายมือชื่อ อ.ที่ปรึกษาวิทยานิพนธ์หลัก.....
ปีการศึกษา.....2555.....	ลายมือชื่อ อ.ที่ปรึกษาวิทยานิพนธ์ร่วม.....
	ลายมือชื่อ อ.ที่ปรึกษาวิทยานิพนธ์ร่วม.....

# # 5172229823: MAJOR CHEMISTRY

KEYWORDS: PHOTOINDUCED ELECTRON TRANSFER / FLAVODOXIN / MOLECULAR DYNAMICS SIMULATION / ELECTRON TRANSFER RATE

KIATTISAK LUGSANANGARM: THEORETICAL INVESTIGATION OF PHOTOINDUCED ELECTRON TRANSFER IN FLAVODOXIN FROM MOLECULAR DYNAMICS SIMULATION DATA. ADVISOR: ASSOC. PROF. SIRIRAT KOKPOL, Ph.D., CO-ADVISOR: ASST. PROF. SOMSAK PIANWANIT, Ph.D., PROF. KARL PETER WOLSCHANN Ph.D., 186 pp.

Photoinduced electron transfer (PET) in enzyme plays significant roles in many biological processes. In this work, PET in flavodoxin from *Desulfobivrio vulgaris*, strain Miyazaki F (FD-*Dv*MF) and from *Helicobacter pylori* (FD-HP), in which both bind one molecule of FMN as a cofactor, were studied using several molecular modeling techniques. Four FD-*Dv*MF structures (wild type, W59F, Y97F and W59F-Y97F) were generated by homology modeling while the wild type structure of FD-HP was taken from the protein data bank. Molecular dynamics (MD) simulations of all five systems were carried out to investigate FMN-enzyme binding interaction as well as their dynamic properties. The decomposition free energy calculations indicate that the 10-loop region has the highest contribution to the binding, which is due to the H-bonding between phosphate subsite and amino acids. Ensemble of conformations obtained from the MD simulations of the five systems was supplied into the Kakitani and Mataga theory to analyze the PET mechanisms by fitting with experimental fluorescence quenching data. It was found that the mean electron transfer rate from Trp59 to excited Iso (Iso\*) in the wild type was the fastest among the four FD-*Dv*MF and it is from Tyr92 to Iso\* for the FD-HP. In addition, the net electrostatic energy and the standard free energy change of the reaction are the most influential factors for the ultrafast electron transfer rate. The charge transfer (CT) was further studied by using quantum chemistry method. The calculations reveal that the  $S_1$  state is the locally excited state while the  $S_2$  state shows CT state characteristic.

Department: ..... Chemistry ..... Student's Signature .....

Field of Study: ..... Chemistry ..... Advisor's Signature .....

Academic Year: ..... 2012 ..... Co-advisor's Signature .....

Co-advisor's Signature .....

## ACKNOWLEDGEMENTS

I would like to express my gratitude to many people who have supported, encouraged and fulfilled during the time of my Ph.D. student duration. The most sincerely gratitude to my supervisor: Assoc. Prof. Dr. Sirirat Kokpol for giving me the great opportunity to study in Ph.D. course under The Royal Golden Jubilee Ph.D. scholarship in 2008. I deeply acknowledge all of the advices not only for the studying, the scientific thinking but also how to be a good researcher. The second is my co-advisor: Assist. Prof. Dr. Somsak Pianwanit who give me the guidance and suggestions. He always gives me the simple explanation of the uneasy topic. I would like to acknowledge Prof. Dr. Fumio Tanaka, who introduced me into the electron transfer story. He also always encourages, guide and support me with the very interesting work. Especially thank to Prof. Dr. Karl Peter Wolschann and Prof. Dr. Leticia González and Dr. Stephan Kupfer for taking care, guidance and useful suggestions during the time of my staying at Vienna, Austria in 2012. I am grateful to Prof. M. Kitamura for kindly providing the numerical data of absorption spectrum of flavodoxin from *helicobacter pylori*. All comrades are also thanked for the fulfillment the happiness. I would like to thank The Royal Golden Jubilee Ph.D. Program (3.C.CU/50/S.1), from Chulalongkorn University and The Thailand Research Fund (TRF) for providing financial support. The Computational Chemistry Unit Cell, Chulalongkorn University and National Electronics and Computer Technology Center (NECTEC) are acknowledged for providing computing facilities.

Finally I would like to sincerely thank my beloved family for the understanding, encouraging, fulfilling the happiness and their standing beside me all the time.

## CONTENTS

	Page
ABSTRACT IN THAI .....	iv
ABSTRACT IN ENGLISH .....	v
ACKNOWLEDGEMENTS .....	vi
CONTENTS .....	vii
LIST OF TABLES .....	xii
LIST OF FIGURES .....	xiii
LIST OF ABBREVIATIONS .....	xx
<b>CHAPTER I INTRODUCTION .....</b>	<b>1</b>
1.1 RESEARCH RATIONALES AND THEORIES .....	1
1.1.1 FLAVOPROTEIN .....	1
1.1.2 ELECTRON TRANSFER .....	4
1.1.3 ELECTRON TRANSFER THOERIES .....	4
1.1.3.1 MARCUS THEORY .....	6
1.1.3.2 KAKITANI AND MATAGA (KM) THOERY .....	7
1.2 RESEARCH METHODOLOGY .....	8
1.3 OBJECTIVES .....	9
1.4 SCOPE OF THIS DISSERTATION .....	10
1.5 EXPECTED BENEFICIAL OUTCOMES .....	10
<b>CHAPTER II PROTEIN STRUCTURES, DYNAMIC AND THERMODYNAMIC PROPERTIES OF WILD TYPE AND MUTATED FLAVODOXIN FROM <i>DESULFOVIBRIO VULGARIS</i> STRAIN MIYAZAKI F. ....</b>	<b>12</b>
2.1 ABSTRACT .....	13
2.2 INTRODUCTION .....	13
2.3 METHODS .....	16
2.3.1 Structural Modeling .....	16
2.3.2 Calculation of the Atomic Charge of FMN .....	17

	Page
2.3.3 Molecular Dynamics Simulation .....	17
2.3.4 MM-PBSA Free Energy Calculation .....	18
2.3.5 Calculations of Decomposition Free Energy per Residue.....	18
2.4. RESULTS .....	19
2.4.1 Evaluation of the quality of the predicted models .....	19
2.4.2 Comparison of Protein Structures Among the Four FD-DvMF Variants .....	21
2.4.3 Accessibility of Water Molecules to FMN .....	21
2.4.5 Dynamic Properties of the four FD-DvMF variants .....	24
2.4.6 Hydrogen Bonding Dynamics .....	28
2.4.7 Decomposition free energy per residue at FMN Binding Site .....	32
2.4.8 Free Energy of FMN Binding .....	33
2.4.9 The contribution of the total binding energies .....	35
2.5 DISCUSSION .....	36
<b>CHAPTER III ANALYSIS OF PHOTOINDUCED ELECTRON TRANSFER IN</b>	
<b>WILD TYPE FLAVODOXIN FROM <i>DESULFOVIBRIO VULGARIS</i> STRAIN</b>	
<b>MIYAZAKI F.</b> .....	39
3.1 ABSTRACT .....	40
3.2 INTRODUCTION .....	40
3.3 METHOD .....	42
3.3.1 Homology modeling and MD calculation .....	42
3.3.2 ET theory .....	42
3.3.3 Electrostatic Energy in the Protein .....	43
3.3.4 Fluorescence Decays .....	44
3.3.5 Quantum chemical calculation .....	45
3.4 RESULTS .....	46
3.4.1 Geometrical factors of FD .....	46
3.4.2 Fluorescence decays .....	50
3.4.3. ET rates .....	53



	Page
3.4.4 ES energy .....	53
3.4.5 Dipole moment of the Trp59-Iso*-Tyr97 system .....	54
3.4.6 Charge transfer interaction .....	55
3.4.7 Correlation .....	56
3.5 DISCUSSION .....	58
<b>CHAPTER IV GLOBAL ANALYSES OF PHOTOINDUCED ELECTRON TRANSFER IN WILD TYPE AND MUTATED FLAVODOXIN FROM <i>DESULFOVIBRIO VULGARIS</i> STRAIN MIYAZAKI F. ....</b>	62
4.1 ABSTRACT .....	63
4.2 INTRODUCTION .....	63
4.3 METHOD .....	65
4.3.1 Protein Structures and Dynamic of the WT, Y97F, W59F and DM variant FDs .....	65
4.3.2 ET Theory .....	65
4.3.3 ES Energy in the Proteins .....	67
4.3.4 Calculation of Fluorescence Decays .....	68
4.3.5 Determination of ET Parameters .....	69
4.4 RESULTS .....	70
4.4.1 Comparison of Protein Structures around Iso among the Four FD Systems ...	70
4.4.2 Analyses of the Fluorescence Dynamics .....	74
4.4.3 ET Parameters .....	79
4.4.4 ES Energies in the Proteins .....	79
4.4.5 ET Rates .....	81
4.5 DISCUSSION .....	84
<b>CHAPTER V CONFORMATIONAL FLEXIBILITY AND THERMODYNAMIC PROPERTIES OF FLAVODOXIN FROM <i>HELICOBACTER PYLORI</i> .....</b>	88
5.1 ABSTRACT .....	89
5.2 INTRODUCTION .....	89

	Page
5.3 METHODS .....	91
5.3.1 Protein and ligand preparation .....	91
5.3.2 Molecular dynamics simulations .....	91
5.3.3 The root of mean square fluctuation .....	92
5.3.4 Decomposition free energy per residue .....	92
5.4 RESULT AND DISCUSSION .....	93
5.4.1 Comparison of the protein structure between Holo- and Apo-flavodoxin .....	93
5.4.2 Hydrogen binding analyses .....	96
5.4.3 Decomposition free energy per amino acid residues at the binding site .....	99
5.4.4 The dynamical flexibility of the amino acids at the active site .....	102
5.5 CONCLUSION .....	107
<b>CHAPTER VI THEORETICAL ANALYSIS OF PHOTOINDUCED ELECTRON TRANSFER IN FLAVODOXIN FROM <i>HELICOBACTER PYLORI</i></b> .....	108
6.1 ABSTRACT .....	109
6.2 INTRODUCTION .....	109
6.3 THEORETICAL METHODS .....	110
6.3.1 Method of MD simulation .....	110
6.3.2 Method of theoretical analyses .....	111
6.3.2.1 ET theory .....	111
6.3.2.2 Electrostatic energy in the FD-HP .....	113
6.3.3 Fluorescence Decays .....	114
6.4 RESULTS .....	115
6.4.1 Dynamics of geometry around Iso .....	115
6.4.2 Ultrafast fluorescence dynamics .....	117
6.4.3 ET parameters .....	118
6.4.4 ET rate and related physical quantities .....	119
6.4.5 Energy gap law and Dutton law .....	122
6.5 DISCUSSION .....	125

	Page
<b>CHAPTER VII TDDFT AND MS-RASPT2 STUDY OF PHOTOINDUCED</b>	
<b>INTERMOLECULAR CHARGE TRANSFER IN <i>H. PYLORI</i> FLAVODOXIN .....</b>	127
7.1 ABSTRACT .....	128
7.2 INTRODUCTION .....	128
7.3 COMPUTATIONAL DETAILS .....	130
7.4 RESULTS AND DISCUSSION .....	134
7.4.1 Comparison the TD-DFT between global hybrid functional and long-range corrected hybrid functional .....	134
7.4.2 RASSCF and MS-RASPT2 calculation .....	141
7.5 CONCLUSION .....	142
<b>CHAPTER VIII CONCLUSIONS.....</b>	144
8.1 CONCLUSIONS .....	144
8.2 RESEARCH LIMITATIONS .....	146
8.3 SUGGESTION AND FUTURE WORK .....	146
SUPPLEMENTAL INFORMATION OF CHAPTER II .....	147
SUPPLEMENTAL INFORMATION OF CHAPTER III .....	152
SUPPLEMENTAL INFORMATION OF CHAPTER IV .....	155
SUPPLEMENTAL INFORMATION OF CHAPTER V .....	160
SUPPLEMENTAL INFORMATION OF CHAPTER VI .....	162
REFERENCES.....	163
APPENDIX .....	183
BIOGRAPHY.....	186

## LIST OF TABLES

		Page
Table 2.1	Number of water molecules in contact with FMN .....	23
Table 2.2	The mean RMSD of the four FD- <i>Dv</i> MF variants .....	26
Table 2.3	Comparison of the amino acid residues with a low and a high RMSF value among the four FD- <i>Dv</i> MF variants .....	27
Table 2.4	The percent occupation of the H-bond between FMN and surrounding amino acids .....	30
Table 2.5	Decomposition free energy per residue in the four FD- <i>Dv</i> MF variants .....	34
Table 2.6	Binding free energy of FMN .....	34
Table 2.7	Experimental binding free energy of flavin in FD- <i>Dv</i> MF .....	36
Table 3.1	Physical constants of Iso and aromatic amino acids .....	48
Table 3.2	Physical constants contained in KM theory .....	52
Table 4.1	Geometrical factors relative to Iso in the mutated FD systems obtained by MD.	72
Table 4.2	The best-fit ET parameters .....	77
Table 4.3	Energy gap law of ET in FD .....	82
Table 5.1	Percentage occupation of H-bonds between FMN cofactor and surrounding amino acids .....	99
Table 6.1	Donor-acceptor distance .....	119
Table 6.2	Best-fit ET parameter in FD-HP .....	124
Table 6.3	Physical quantity related to ET rate .....	124
Table 7.1	Comparison the excitation energies, oscillator strength and orbital transition obtained by means of TDDFT by using the X- Ray geometry .....	137

## LIST OF FIGURES

	Page
Figure 1.1	The three-dimensional structure of FMN bound flavodoxin obtained by homology modeling approach. The FMN is indicated in ball and stick model ... 2
Figure 1.2	Time-resolved fluorescence of wild type and the three mutated variants FD which were excited at 410 nm and observed at 530 nm. The solid lines are the simulations with two exponential or single-exponential functions. .... 2
Figure 1.3	Schematic representation of the FMN binding site of FD from <i>H. Pylori</i> . .... 3
Figure 1.4	Representation of the potential energy surface which describe the ET process. The energy barrier ( $\Delta G^*$ ), the Gibbs free energy change ( $\Delta G^0$ ) and the total reorganization energy ( $\lambda$ ) are indicated. .... 5
Figure 1.5	Molecular orbital description of the photoinduced electron transfer process. .... 6
Figure 1.6	The overall procedure for ET analysis . .... 9
Figure 2.1	Three-dimensional structures of the four FD- <i>DvMF</i> variants at the FMN binding site, as predicted by homology modeling. .... 20
Figure 2.2	Comparison verified-3D analysis between the template and four predicted FD- <i>DvMF</i> variants. The compatibility of amino acids in their environments are indicated by the positive scores. .... 21
Figure 2.3	Shape of the protein surface at the FMN binding site in the four FD- <i>DvMF</i> variants. It is apparent that the FMN binding site is rather small in the WT and Y97F, compared to that in the W59F and DM variants. .... 22
Figure 2.4	The RDF of the number of water molecules near FMN. The integrated number of water molecules is indicated in green for WT, red for W59F, deep blue for Y97F and light blue for DM. The number of water molecules seems complementary with the number of H-bonds between FMN and the nearby amino acids of FD- <i>DvMF</i> . .... 24
Figure 2.5	Time-dependent changes in the RMSD of the four FD- <i>DvMF</i> variants. Black lines indicated that for the entire FD- <i>DvMF</i> , green lines the peptide backbone and blue lines the FMN molecule .... 25

	Page
Figure 2.6	The RMSF for the four FD-DvMF variants. .... 25
Figure 2.7	Comparison of the rigid (blue) and flexible (red) parts among the four FD-DvMF variants. The rigid and flexible parts were determined by taking an average over 7 ns. .... 27
Figure 2.8	H-bond distance between the Tyr99OH and Trp59 peptide O in the four FD-DvMF variants. The distances between the H atom of the Tyr99OH and the Trp59 peptide O are shown. .... 29
Figure 2.9	Comparison of the distance distribution with hundred percent occupation among the four FD-DvMF variants. The distances between the H atoms and the proton acceptors are shown here. The proton donor-acceptor pair satisfies the two criteria for H-bond formation of (i) the bond angle $> 120^\circ$ and (ii) the donor-acceptor heavy atoms $< 3.5 \text{ \AA}$ . .... 32
Figure 2.10	Decomposition free energy of amino acids at the FMN binding site. The energies are shown with green bars for WT, red bars for W59F, deep blue bars for Y97F and light blue bars for DM. .... 33
Figure 3.1	Structure of FD obtained by a method of homology modeling. .... 47
Figure 3.2	Center to center distances between Iso and nearby aromatic amino acids in WT. Rc denotes center to center distance. Trp59, Tyr97, Trp16 and Tyr99 indicate the distances between Iso and Trp59, between Iso and Tyr97, between Iso and Trp16, and between Iso and Tyr99. .... 49
Figure 3.3	Edge to edge distances between Iso and nearby aromatic amino acids in WT. Re denotes edge to edge distance. Trp59, Tyr97, Trp16 and Tyr99 indicate the distances between Iso and Trp59, between Iso and Tyr97, between Iso and Trp16, and between Iso and Tyr99. .... 49
Figure 3.4	Inter-planer angles between Iso and nearby aromatic amino acids in WT. Trp59, Tyr97, Trp16 and Tyr99 indicate the distances between Iso and Trp59, between Iso and Tyr97, between Iso and Trp16, and between Iso and Tyr99. ... 50

Figure 3.5	Fluorescence decays of WT with two lifetime components. The observed decay $F_{obs}$ is given by Eq. 3.6. $F_{calc}$ is the calculated decay and obtained with the best-fit ET quantities listed in Table 3.2. Upper panel is deviation given by Eq. 3.10 in text. The value of $\chi^2$ was $3.42 \times 10^{-3}$ . .....	51
Figure 3.6	Fluorescence decays of FD  $F_{obs}$ and $F_{calc}$ denotes the observed and calculated fluorescence intensities. Upper panel shows deviation between the observed and calculated intensities. ..	51
Figure 3.7	ET rate from aromatic amino acids to Iso* in FD. Trp59, Tyr97, Trp16 and Tyr99 indicate ET rates from these amino acids to Iso*. ET rate is expressed in unit of $ps^{-1}$ . .....	53
Figure 3.8	$ES$ energy between ionic species produced by ET and ionic amino acids in WT. $E_{iso}$ denotes $ES$ energy between Iso anion and all ionic amino acids. $E_{59}$ , $E_{97}$ , $E_{16}$ and $E_{99}$ indicate electrostatic energy between aromatic cations (Trp59, Tyr97, Trp16 and Tyr99, respectively) and all ionic amino acid residues. $\epsilon_0 = 5.85$ was used as described in text. ....	54
Figure 3.9	Dipole moment in the system of Iso*-Tyr97-Trp59 in WT FD.  Iso (center) is sandwiched by Trp59 (upper) and Tyr97 (lower). This conformation was obtained by a snapshot of MD structure, where only Iso, Trp59 and Tyr97 were extracted. The direction of the dipole moment was from Iso* to Trp59, which shows part of charge in Trp59 transferred to Iso*, since the direction should be in the Iso plane without charge transfer interaction between Trp59 and Iso*. ....	55
Figure 3.10	Charge transfer and interaction energy in the system of Trp59-Iso*-Tyr97 in WT. Dipole moment of Iso* alone was 10.0 D, of which direction was in the plane of Iso. Interaction energy was obtained by Eq. 3.11. ....	56

Figure 3.11	Correlation between interaction energy and charge densities A: Correlations between the interaction energy and charge density of Iso. B: correlation of Trp59, and C: correlation of Tyr97. Interaction energies were obtained by Eq. 3.11. ....	58
Figure 3.12	Electronic delocalization of molecular orbitals in the configuration without appreciable charge transfer. Optimized configuration at 360 ps had low dipole moment and apparently no charge transfer took place. Panels A and B shows electronic delocalization of molecular orbitals No. 91 and 86, respectively. Orbital No. of HOMO was 94. The electronic delocalization among the three chromophores may yields the non-zero interaction energy. ....	60
Figure 4.1	Comparison of the protein structures among the WT and the Y97F, W59F and DM FD variants. A: WT, B: Y97F, C: W59F and D: DM. These structures were determined by homology modeling using the X-ray structure of flavodoxin <i>Desulfovibrio vulgaris</i> , strain Hildengorouh (PDB code: 1J8Q) as the template. ....	71
Figure 4.2	Time-dependent changes in $R_c$ between Iso and the aromatic amino acids. A: Y97F, B: W59F and C: DM. Tyr97, Trp59, etc. in the inserts denote the distances between Iso and Tyr97, and between Iso and Trp59, etc., respectively. ....	73
Figure 4.3	Fluorescence decays of the Y97F, W59F and DM FD variants. A: Y97F, B: W59F and C: DM. Upper panels in A, B and C represent deviations between the observed (Fobs) and calculated (Fcalc) fluorescence decays. Obtained ET parameters are listed in Table 4.2. ....	76
Figure 4.4	Net $ES$ energy in the WT and variant FDs. A: WT, B: Y97F, C: W59F and D: DM. Net $ES$ energy means sum of $ES$ energies of Iso and the aromatic amino acids. ET rate depends on net $ES$ energy [see Eq. 4.1 and Eq. 4.5 in text]. Trp59, Tyr97, Trp16 and Tyr99 in inserts denote net energies of Trp59, Tyr97, Trp16 and Tyr99, respectively. ....	80



	Page
Figure 4.5	ET rates in the mutated FD systems. .... 84
Figure 4.6	Energy gap law of ET in FD. The ET rate is expressed in unit of $\text{ps}^{-1}$ . Total free energy gap ( $-\Delta G_{ij}^0$ ) is given by Eq. 4.16. Numerical data are listed in Table 4.3. $(\ln k_j^i) / \lambda_j^i$ vs. $-\Delta G_{ij}^0 / \lambda_j^i$ were plotted according to Eq. 4.17. Insert indicates an approximate parabolic function of the plot. .... 87
Figure 5.1	The three dimensional structure of <i>H. pylori</i> flavodoxin. (A) Protein structure of <i>H. pylori</i> flavodoxin, which consisted of five- $\beta$ sheets and four- $\alpha$ helix shape of amino acids. (B) The close-view at the FMN binding site. The FMN and three important loops for binding are indicated in yellow. .... 90
Figure 5.2	Comparison of the RMSF between the Apo- and Holo-FDs. Amino acid residues indicated in the Figure displayed great difference between Apo- and Holo-FDs. .... 94
Figure 5.3	Comparison of the main segments between Apo- (green) and Holo- (blue) FDs. The FMN cofactor is shown by ball and stick model. The red color indicates the highly flexible region. The entire protein was divided into 5 parts as indicated residue Nos. in black. .... 95
Figure 5.4	Comparison of the total energy of Holo-FD and Apo-FD. Holo form is indicated in blue color and Apo form in green color. .... 95
Figure 5.5	H-bond formation between FMN and surrounding amino acids. Upper panel shows schematic representation of the H-bond. Lower panel shows the histogram of H-bond distance distribution. .... 98
Figure 5.6	The decomposition free energy per amino acid residue for FMN binding. The Figure shows the contribution of individual amino acid at loop-10, loop-50 and loop-90 to FMN binding energy. .... 101
Figure 5.7	Contribution of the side-chain and the backbone of individual amino acid residue at loop-10, loop-50 and loop-90 to the FMN binding free energy. .... 101
Figure 5.8	The electrostatic and van der Waals energies per residue at loop-10, loop-50 and loop-90 for the FMN binding. .... 102

	Page
Figure 5.9	Distribution of the dihedral angles of $\chi_1$ and $\chi_2$ of amino acids at the FMN binding site. The distribution of the Apo-FD is indicated in blue, and one of Holo-FD in red. .... 106
Figure 6.1	Absorption and fluorescence spectra of FD-HP. The absorption peaks were at 378 nm and 452 nm in visible wavelength region. Fluorescence peak was at 521 nm. FD-HP was dissolved in 10 mM Tris-HCl buffer at pH 8.0. Optical density at the excitation wavelength (450 nm) was ca. 0.1 upon the fluorescence measurements. .... 116
Figure 6.2	The protein structures near Iso binding site in FD-HP and DVFD obtained by MD simulation. Iso is stacked with Tyr92 in FD-HP (A), while it is sandwiched by Trp59 and Tyr97 in DVFD (B). Mean center-to-center distance ( $R_c$ ) between Iso and Tyr92 was 0.56 nm, which are similar to those of $R_c$ between Iso and Tyr97 in WT DVFD and W59F DVFD. .... 116
Figure 6.3	Time-evolution of $R_c$ between Iso and nearby aromatic amino acids Tyr92, Trp64 and Tyr121 were three closest aromatic amino acids to Iso among five in FD-HP. Number of snapshots was 50000 with 0.1 ps time intervals. Mean values of $R_c$ over 50000 snapshots are listed in Table 6.1. .... 117
Figure 6.4	Observed and calculated fluorescence intensities. Upper panel shows deviation between the observed and calculated intensities obtained by Eq. 6.11, and lower panel the observed (blue dots), calculated intensities (red line) with KM theory by Method A, and pulsed laser (black line). The emission was monitored at 530 nm. Half-width of the laser was ca. 0.2 ps at 410 nm. The protein was dissolved into 10 mM Tris-HCl (pH 8.0) buffer. Absorbance of the sample at 410 nm (excitation) was ca. 3 in a cell-cuvettes with 1 cm optical pass. .... 118
Figure 6.5	Time-evolution of ET rate. Panel A represents ET rates from Trp64, Tyr92 and Tyr121 to Iso*, and Panel B, ET rate from Tyr92. Panel C represents distribution of logarithmic ET rate from Tyr92 to Iso*. .... 120

	Page
Figure 6.6	ES energy between photoinduced ionic species and ionic groups in the protein. Panel A indicates ES energies between Iso anion or donor cations and ionic groups in the protein. Panel B indicates net ES energy between the photoproducts and ionic groups in the protein, given by Eq. 6.5. .... 121
Figure 6.7	Correlation between the logarithmic ET rate and net ES energy or Rc in FD-HP. Panel A indicates relationship between the logarithmic ET rate from Tyr92 to Iso* (Energy gap law), Panel B relationship between the logarithmic ET rate and the net ES energy and Panel C relationship between the logarithmic ET rate and Rc (Dutton law). .... 123
Figure 6.8	Relationship between Rc and various energies of Tyr92 in FD-HP. Panel A shows Rc - net ES energy relation, Panel B, Rc - total free energy gap, and Panel C, Rc - sum of total free energy gap and solvent reorganization energy. Solid red lines in the Panels show approximate linear functions between these quantities. .... 126
Figure 7.1	The three dimensional structure involved in the calculation. .... 131
Figure 7.2	Molecular orbital for RASSCF (26,2,2;11,4,8) calculation. .... 133
Figure 7.3	UV/Vis spectra of <i>H. pylori</i> FD. .... 134
Figure 7.4	Comparison of the experimental and calculated spectra of the TDDFT/TZVP of the X-ray configuration using water solvation model. .... 139
Figure 7.5	Comparison of the experimental and calculated spectra of the TDDFT/TZVP of the X-ray configuration using dielectric constant equal 4. .... 140
Figure 7.6	Frontier molecular orbital of TD-CAM-B3LYP\\X-ray level of theory. .... 141

**LIST OF ABBREVIATION**

3D	=	Three Dimension
CT	=	Charge Transfer
FD-DvMF	=	Flavodoxin from <i>Desulfovibrio vulgaris</i> , Miyazaki F
FD-HP	=	Flavodoxin from <i>Helicobacter Pylori</i>
ET	=	Electron Transfer
FD	=	Flavodoxin
FMN	=	Flavin mononucleotide
FMN-BP		FMN binding protein
GS	=	Ground State
HOMO	=	Highest Occupied Molecular Orbital
HP	=	<i>Helicobacter pylori</i>
KM	=	Kakitani and Mataga
LE	=	Locally Excited State
LUMO	=	Lowest Occupied Molecular Orbital
MD	=	Molecular Dynamic
MO	=	Molecular Orbital
MS-RASPT2	=	Multi-State Second-Order Perturbation Theory Restricted Active Space
PES	=	Potential Energy Surface
PET	=	Photoinduced Electron Transfer
Phe	=	Phenylalanine
RASSCF	=	Restricted Active Space Self-Consistent Field
TD-DFT	=	Time-Dependent Density Functional Theory
Trp	=	Tryptophan
Tyr	=	Tyrosine
UV	=	Ultraviolet

# CHAPTER I

## INTRODUCTION

### 1.1 RESEARCH RATIONALES AND THEORIES

#### 1.1.1 FLAVOPROTEIN

Flavoproteins are involved in many oxidation-reduction reactions in all living organisms as mammals, plants microorganisms, including pathogenic bacteria. The photochemistry and photophysics of flavoprotein have been of considerable interest because of their biochemical versatility in light-harvesting. The flavoproteins contain one of the prosthetic group termed “flavin molecules” as the reaction center that are flavin mononucleotide (FMN), flavin adenine dinucleotide (FAD) or riboflavin (RF, commonly known as vitamin B<sub>2</sub>).[1] Most of flavoproteins contain the aromatic amino acids, tryptophan (Trp) and tyrosine (Tyr), near the flavin molecule.

Flavodoxin (FD), a small group of flavoproteins, has a molecular weight of 15-23 kDa.[2] They contain a non covalent-bound FMN as the reaction center. The non-pathogenic FD from *Desulfovibrio vulgaris* strain Miyazaki F. has been chosen as a studied model because of the small molecular size, non-toxicity of the host bacterium and easy expression, for the investigation of the protein folding, protein-ligand recognition and stability, including evaluation of ET components.[3] In 1980 Kitamura and co-workers successfully characterized and studied its biochemical properties. The FD strain Miyazaki F. contain 148 amino acid residues (Figure 1.1).[4] However, the three dimensional structure of FD strain Miyazaki F. has not been experimentally determined yet. Furthermore, its fluorescence intensity measured by means of the conventional fluorescence spectroscopy is too low.[5] In 2002, Mataga and co-worker extensively studied the ultra-fast fluorescence dynamics of wild type (WT) and three mutant types, Y98F (Tyr98 is replaced by Phe), W60F (Trp60 is replaced by Phe), and the double mutants W60F-Y98F in the femtosecond time domain by using an up-conversion technique.[6] They found that the fluorescence were remarkable quenched and considered to be induced by photoinduced electron transfer (PET) from tryptophan (Trp) and/or tyrosine (Tyr) to the excited flavin molecule (Iso\*). The ultra-short fluorescence lifetimes were 0.158 ps in the WT, 0.322 ps in W60F, 0.245 ps in Y98F and 18 ps in the W60F-Y98F. The corresponding time-dependent fluorescence decays

of those variants are shown in Figure 1.2. (Due to the methionine was absence from the protein structure used for modeling the protein structures of FD, the amino acid sequence are shifted below. Therefore, in WT FD, hereafter the crucial Trp60 and Tyr98 are pronounced to be Trp59 and Tyr97, respectively.)

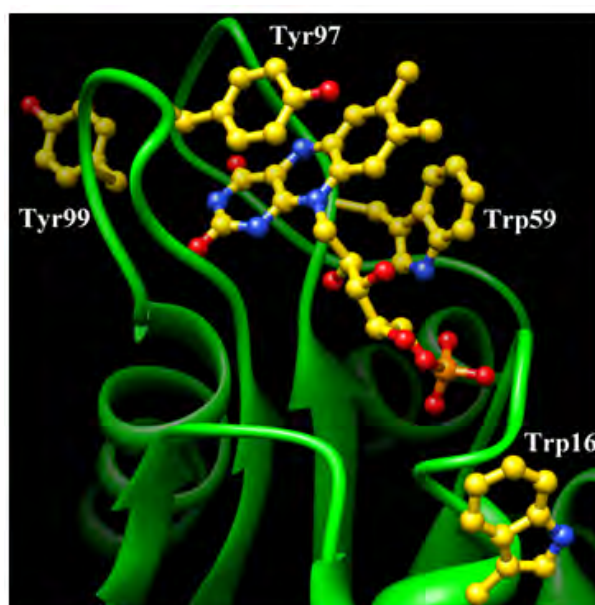


**Figure 1.1** The three-dimensional structure of FMN bound flavodoxin obtained by homology modeling approach. The FMN is indicated in ball and stick model. [7]

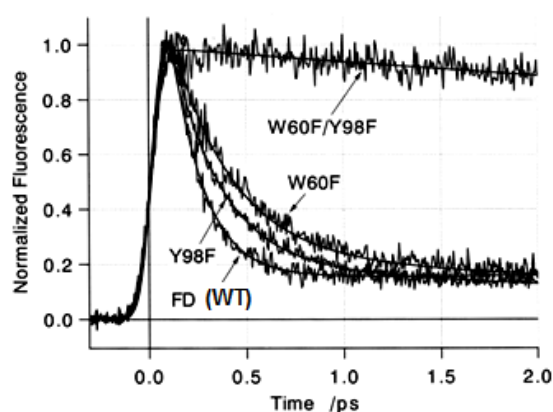


**Figure 1.2** Time-resolved fluorescence of wild type and the three mutated variants FD which were excited at 410 nm and observed at 530 nm. The solid lines are the simulations with two exponential or single-exponential functions.[6]

The pathogenic bacterium, *Helicobacter pylori* (*H. pylori*) can course type-B gastritis and peptic-ulcer diseases, gastric carcinoma and mucosa-associated lymphoid-tissue lymphoma. FD of this bacterium can be categorized into the long-chain type FD. It composed of 164 amino acid residue. Its protein structure at the FMN binding site shared a similar pattern with FD from *Desulfovibrio vulgaris*, strain Miyazaki F. except for the stacking chromophore. In this protein only Tyr92 is located nearby FMN while the Trp is absence, see Figure 1.3.

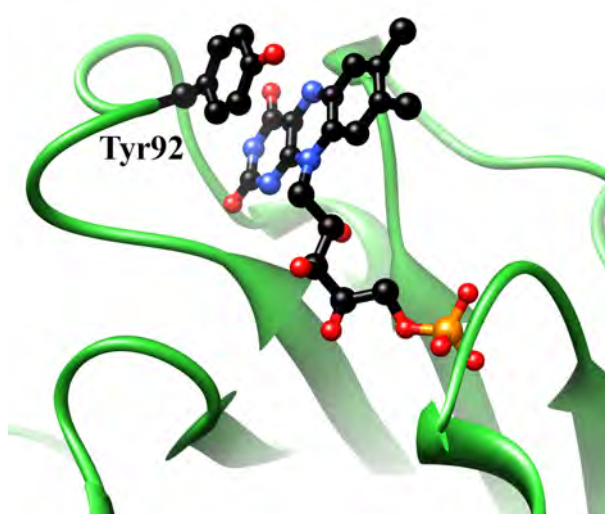


Figure 1.3 Schematic representation of the FMN binding site of FD from *H. Pylori*.

The three-dimensional structure of FD from *Desulfovibrio vulgaris*, strain Miyazaki F. has not been experimental determined. However, in the case of FD from *H. pylori* its X-ray crystallographic structure has been determined.[8] The fluorescence decay of FD from *Desulfovibrio vulgaris*, strain Miyazaki F. for WT and the three mutated type (W60F, Y98F, and double mutation) have been reported by Mataga *et. al.* (2002) [6] and *H. pylori* was measured by collaborate team in Japan (unpublished data). It shows the fluorescence decayed with lifetimes of 173 fs (amplitude, 0.963) and 2.08 ps (0.037), ~ 1.9 fold faster than lifetimes of W60F in Miyazaki F.

Therefore, it is of interest to investigate the interactions involving for the FMN association to protein FD and analyze the ET mechanism in FD-DvMF and FD-HP. In this research the three-dimensional structure of FDs from *Desulfovibrio vulgari* strain Miyazaki F. will be predicted by means of homology modeling. The predicted models and FD from *H. pylori*

(known structure) are then further be used to study their dynamic properties by MD simulations in order to compare among the five FD variants. The structural dynamic and thermodynamic properties will be investigated using MD simulation. Subsequently, the complex coordinate will be extracted from MD trajectory to study the ET analyses and charge transfer by quantum calculation technique.

### **1.1.2 ELECTRON TRANSFER**

The electron transfer (ET) is of fundamental interest in the field of chemistry, biology and physics. Numerous essential processes in biology and chemistry are involving ET reactions such as photosynthesis, respiration and other important biological processes, including bioelectronics and biosensor.[5, 9-13] Beside, the study of ET in simple model has become a very useful to gain fundamental knowledge of ET mechanism.

### **1.1.3 ELECTRON TRANSFER THOERIES**

Considering the electron transfer process between a donor D and an receptor A, either D or A may be in an excited state ( $D^*$  or  $A^*$ ), this process is known as photoinduced electron transfer (PET). The reactant state will have a potential energy which is a function of many coordinates including solvent coordinates, leading to a multidimensional potential energy surface (PES). At transition state, PES can be reduced to a one-dimensional profile (Figure 1.4). For ET to occur, the reactant state normally distort along the reaction coordinate from its equilibrium position ① to position ② or the transition state where ET is occurred. The resulting product state then relaxes to its equilibrium at position ③ .[14]



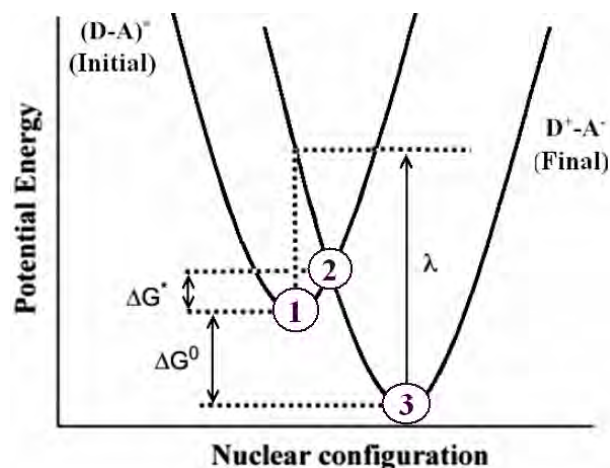


**Figure 1.4** Representation of the potential energy surface which describe the ET process. The energy barrier ( $\Delta G^*$ ), the Gibbs free energy change ( $\Delta G^0$ ) and the total reorganization energy ( $\lambda$ ) are indicated.

The ET reaction can be classified according to the magnitude of the splitting of ②. There are two kinds of the change in PES which corresponding to the ET process. They can be classified into :

- i) In the case of the sufficient electronic interaction (splitting  $> k_B T$ ), the large splitting could be observed. This reaction is called adiabatic.
- ii) If the electronic interaction is small (splitting  $< k_B T$ ), the reaction is called non-adiabatic. In this case, the system tends to be retained their original electronic configuration when passing across the intersection (ET process).

When considering the ET process (Figure 1.5) the process first starts by light excitation. The electron which localized at the Highest Occupied Molecular Orbital (HOMO) state of acceptor is excited up to the Lowest Occupied Molecular Orbital (LUMO) state of the corresponding species. Subsequently, the electron on the HOMO state of the donor species (higher energy than the HOMO state of acceptor site) rapidly transfer into the unoccupied hole on the HOMO state of acceptor, at this point, leading to the orbital interaction between D and A. The charge separation (CS) state will be existed followed by the transfer of the excited electron into the unoccupied hole on the HOMO state of donor. This is so-called charge recombination (CR) state.[14]

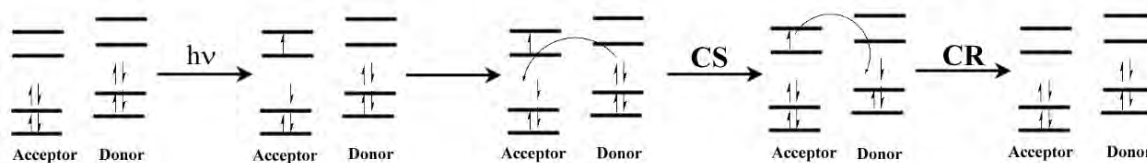


**Figure 1.5** Molecular orbital description of the photoinduced electron transfer process.

### 1.1.3.1 MARCUS THEORY

In 1956 Rudolph A. Marcus proposed the ET theory to explain the rates of electron transfer reactions.[13] He received the Nobel Prize in Chemistry in 1992 regarding to his equation. The equation was formulated in order to explain the outer sphere electron transfer reactions, which is the electron donor (D) and acceptor (A) species aren't directly linked to each other). The original electron transfer formulated by Marcus was developed by Noel S. Hush in order to describe the inner sphere electron transfer reactions, which is the D and A are linked with covalent bond). The later known as Marcus-Hush theory.

Considering the Marcus's equation, it has been proposed based on the traditional Arrhenius equation as:

1. The pre-exponential term in the Arrhenius equation has been provided, based on the electronic coupling interaction ( $H_{ab}$ ) between the reactant and product state of the ET reaction.
2. The activation energy can be determined based on a parameter called the reorganization energy ( $\lambda_s$ ), which is the energy required to distort the initial coordinates and its surroundings environment in order to reach the equilibrium configuration of the final coordinates and the Gibbs free energy ( $\Delta G^0$ ).[15]

Marcus-Hush theory is used to describe the ET rates over the last several decades. The most important of the prediction by Marcus-Hush theory is that the electron transfer rate which will increase as the ET reaction becomes more exergonic and reach the point which has maximum ET rate ( $-\Delta G^0 = \lambda_s$ ). Past that point, the electron transfer rate will decrease as the reaction becomes more exergonic which is called "Marcus inverted region."

Marcus theory (Marcus-Hush) for ET in proteins is:

$$k_{ET} = \frac{2\pi}{\hbar} \frac{H_{ab}^2}{\sqrt{4\pi\lambda_s k_B T}} \exp \left\{ -\frac{(\Delta G^0 - e^2 / \varepsilon_0 R + \lambda_s + ES)^2}{4\lambda_s k_B T} \right\} \quad (1.1)$$

$H_{ab}$  is electronic coupling interaction between donor and acceptor at donor-acceptor.  $\Delta G^0$  is standard free energy gap between products and reactants.  $ES$  represents electrostatic energy.  $\hbar$ ,  $k_B$  and  $T$  are Planck constant, Boltzmann constant and temperature, respectively.  $\lambda_s$  is known as solvent reorganization energy and expressed as:

$$\lambda_s = e^2 \left( \frac{1}{2a_1} + \frac{1}{2a_2} - \frac{1}{R} \right) \left( \frac{1}{\varepsilon_\infty} - \frac{1}{\varepsilon_0} \right) \quad (1.2)$$

where  $a_1$  and  $a_2$  are radii of acceptor and donor when these reactants are assumed to be spherical, and  $\varepsilon_\infty$  and  $\varepsilon_0$  are optical and static dielectric constants.

### 1.1.3.2 KAKITANI AND MATAGA (KM) THOERY

Kakitani and Mataga have formulated a theory applicable both to adiabatic (strong coupling) and non-adiabatic (weak coupling) ET processes [16] developing from the Marcus-Hush theory.

$$k_{ET} = \frac{\nu_0}{1 + \exp\{\beta(R - R_0)\}} \sqrt{\frac{k_B T}{4\pi\lambda_s}} \exp \left[ -\frac{\{\Delta G^0 - e^2 / \varepsilon_0 R + \lambda_s + ES\}^2}{4\lambda_s k_B T} \right] \quad (1.3)$$

In KM theory, only the pre-exponential term is different from the Marcus theory. The term in Eq. 1.3  $\nu_0$  is frequency and  $\beta$  is a coefficient related to ET process. The ET process has been classified to be adiabatic, when  $R < R_0$ , and non-adiabatic when  $R > R_0$  where  $R$  were defined as the center-to-center distance and  $R_0$  the critical distance. The other constants are common among Eqs. 1.1 – 1.3. The standard free energy change ( $\Delta G^0$ ) by expressed with ionization potential of electron donor,  $E_{IP(donor)}$  and  $G_{ISO(acceptor)}^0$  is standard Gibbs energy related to electron affinity of the excited acceptor, as shown in Eq. 1.4.

$$\Delta G^0 = E_{IP(donor)} - G_{ISO(acceptor)}^0 \quad (1.4)$$

Since the structure in protein is always dynamic, therefore, the adiabatic and non-adiabatic properties can be incorporated all the time. The verifications of the theory for analysis of the ET are very important. The suitable ET theory should be applicable for both kinds of such processes. The verified results of the FMN-binding proteins [17-18] indicate that the KM theory can provide more satisfactory results than Marcus-Hush theory. The fact that the ET parameters which contained in both Marcus-Hush theory and KM theory quite similar except for the  $1 + \exp\{\beta(R - R_0)\}$  term in the KM theory. This term is important for the non-adiabatic ET process where the  $R > R_0$ . This may be the reason why the KM theory can explain the ET process better than Marcus-Hush theory.

## 1.2 RESEARCH METHODOLOGY

The method of fluorescence decay analysis, related to the ET rate and physical quantities in the ET theory is demonstrated in Figure 1.6. It is consecutive procedure as:

- 1.2.1 The ensemble of protein conformations was calculated by using MD simulation.
- 1.2.2 The ET rate and related physical quantities in the KM ET theory, given by Eq. 1.3 as  $\nu_0^q$ ,  $\beta^q$ , and  $R_0^q$  for Trp and Tyr,  $G_{Iso}^0$  and  $\epsilon_0$  are to be determined.
- 1.2.3 The guess initial values for the ET analysis were obtained from the previously related work. For FD from *Desulfovibrio vulgaris*, strain Miyazaki F., the ET initial parameters were taken from ET analysis of FMN-BP, and the result of this strain were further used for ET analysis of FD from *H. pylori*.
- 1.2.4 The fluorescence decay is calculated over the MD time.
- 1.2.5 The minimum Chi-square is calculated in order to justify the best fit between the observed and calculated fluorescence decay.
- 1.2.6 The new ET parameters are generated by the non-linear least squares method. The calculation is being processed which the less Chi-square value than the previous calculation is to be obtained. Step 1.2.4 to 1.2.6 is repeated until the minimum value of the Chi-square is obtained.

- 1.2.7 The calculated fluorescence decay, ET rates and related physical quantities in the ET theory are obtained, when the minimum value of the Chi-square is obtained.

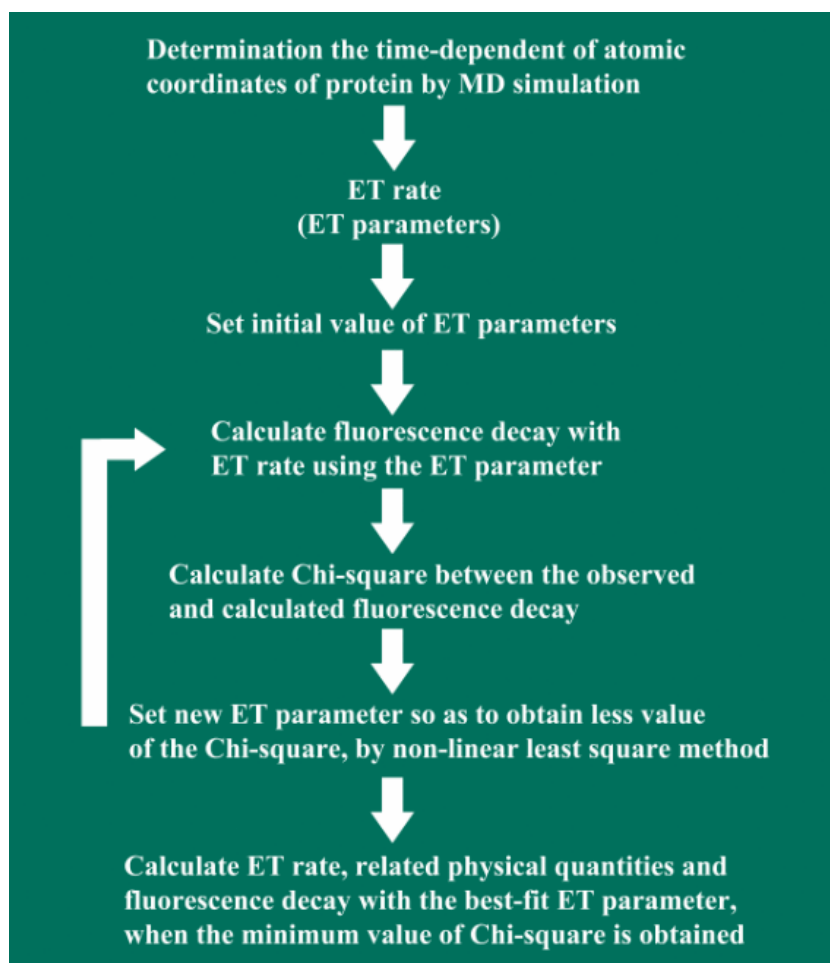


**Figure 1.6** The overall procedure for ET analysis.

### 1.3 OBJECTIVES

- 1.3.1** To investigate dynamical properties and important interaction involved in the binding of flavin mononucleotide (FMN) for both *Desulfovibrio vulgaris* strain Miyazaki F. and *Helicobacter pylori* (*H. pylori*).
- 1.3.2** To study the factor and relationship of the ET components contained in the theory which affect the electron transfer rate in both flavodoxins.

## 1.4 SCOPE OF THIS DISSERTATION

The purposes of this thesis are to investigate the interaction involved in the binding of FMN cofactor and the dynamic properties of the whole protein for both non-pathogenic (*Desulfovibrio vulgaris* strain Miyazaki F. and pathogenic (*H. pylori*) bacteria by molecular dynamic (MD) simulations. The FD-*Dv*MF for both wild-type and three variants were chosen as the first model due to there are experimental fluorescence decay data including the FMN binding information available. Then the FD-HP was analyzed. The MD results of FD-*Dv*MF showing that during the MD production time, the shape of FMN binding site are changed even though either one or two amino acids were changed. This led to the difference in rearrangement of FMN and surrounded amino acids. Such rearrangement and their thermodynamic stabilization have been discussed in Chapter II. Subsequently, the PET mechanisms were focused. The fluorescence decay data of FD-*Dv*MF were combined with ensemble of protein coordinates obtained from MD simulations. The influencing parameters on the ET rate in the KM ET theory have been determined and then discussed on Chapter III and Chapter IV.

The structural dynamic and thermodynamics property of FMN binding in wild-type FD-HP has also been calculated and described in Chapter V. The PET mechanism and the influential parameters which affected on the ET rate have been analyzed and discussed in Chapter VI. In addition to clarify the ET mechanism, the charge transfers (CT) mechanism has been studied by simulating the UV-visible spectra of FD-HP and comparing with the experimental information. These comparisons can point out that the TDDFT with either high amount of exact exchange or long-range correction can provide an appropriate CT mechanism, as discussed in Chapter VII.

## 1.5 EXPECTED BENEFICIAL OUTCOMES

- 1.5.1 Information of the dynamic properties and important interactions involved in the binding of FMN to flavodoxin from *Desulfovibrio vulgaris* strain Miyazaki F. and *H. pylori*.
- 1.5.2 Relationship of parameters which are influential upon the ET rate for both flavodoxins could be applied in the field of biosensors and bioelectronics and fulfill specific requirements.

We hope that combining these results should provide the better understanding in PET and the relationship of parameters which influential upon the ET rate for both flavodoxins. The long term goal of these fundamental knowledge are to aid PET analyses, engineering of flavoprotein redox potentials, including biosensors and bioelectronics.

**CHAPTER II**  
**PROTEIN STRUCTURES, DYNAMIC AND THERMODYNAMIC**  
**PROPERTIES OF WILD TYPE AND MUTATED FLAVODOXIN**  
**FROM *DESULFOVIBRIO VULGARIS* STRAIN *MIYAZAKI F.***

---

**Homology Modeling and Molecular Dynamics Simulations of Wild Type and**  
**Mutated Flavodoxins from *Desulfovibrio vulgaris* (Miyazaki F):**  
**Insight into FMN-Apoprotein Interactions**

**Kiattisak Lugsanangarm, Somsak Pianwanit, Sirirat Kokpol and Fumio Tanaka**

---

*Department of Chemistry, Faculty of Science, Chulalongkorn University,*  
*Bangkok 10330, Thailand*

---

**This article has been published in Journal: Molecular Simulation. Page 1164-1178.**

**Volume: 37. Issue 14, Year: 2011.**

---



## 2.1 ABSTRACT

The flavodoxin from *Desulfovibrio vulgaris*, strain Miyazaki F (FD-*Dv*MF) binds one molecule of FMN as a cofactor, and is considered to associate with electron transport reactions. However, although the three dimensional structure of the related flavodoxin from *D. vulgaris* strain Hildenborough (FD-*Dv*H) has been determined, that for FD-*Dv*MF has not. In this work, the protein structures of the wild type (WT) and the W59F, Y97F and W59F-Y97F substitutional mutants of FD-*Dv*MF have been predicted by a homology modeling approach. Subsequently, the dynamic properties of these four FD-*Dv*MF variants were investigated by molecular dynamics (MD) simulations. The results revealed that peptide O of Trp59 formed H-bond with Tyr99OH only in Y97F, leading to FMN being buried deeper inside the protein than in the other three variants and reducing the accessibility of water to FMN. The phosphate oxygen atoms formed extensive H-bonds with amino acid residues in the 10-loop region in all variants resulting in the highest degree of stabilization. The OH groups of the ribityl-chain and the isoalloxazine ring formed H-bonds with amino acid residues of the 60-loop and 90-loop regions, respectively. The decomposition free energy calculations suggest the greatest contribution come from the 10-loop region, which is compatible with the published data. That the calculated binding and decomposition free energies were both greatest in Y97F is proposed to be due to the H-bond between peptide O of Trp59 and Tyr99OH.

## 2.2 INTRODUCTION

Flavoproteins are ubiquitously distributed in various microorganisms [1, 9, 19] and pathogenic bacteria [2, 20] and in specific tissues of multicellular plants and animals, such as in milk, brain, kidney, liver and heart of mammals and in leafy vegetables.[1] Flavoproteins play an essential role in many oxido-reduction reactions,[21-23] whilst in some systems flavins function as photoreceptors.[24] Their photochemistry and photophysics have been of considerable interest due to their important role in light-harvesting biological mechanisms.[1, 10] The one important characteristic that classifies flavoproteins is that they bind with one of the flavin molecules, flavin mononucleotide (FMN), flavin adenine dinucleotide (FAD) or riboflavin (RF, more commonly known as vitamin B2), as a cofactor.[1, 22-23] In the case of FAD and FMN, they consisted of an isoalloxazine chromophore (Iso) connected to a ribityl adenine diphosphate or ribityl phosphate

chain, respectively. Naturally, flavin has the three different redox states; that is the (i) oxidized form, (ii) a one electron reduced radical semiquinone, and (iii) a two-electron fully reduced hydroquinone.[1, 22-23] Recently, because of this biochemical versatility, flavoproteins have become a popular model for both experimental studies, such as on the electron transfer process,[6, 25-31] and including rational drug design,[20] and also in theoretical works [32-34] on their conformational dynamics.

Flavodoxins (FDs) are small flavoproteins with a molecular weight of 15 - 23 kDa and have been isolated from a variety of microorganisms. FDs are considered to function as electron-transfer proteins in various metabolic pathways.[2] They contain one molecule of non covalently-bound FMN as a cofactor, and exhibit a high negative reduction potential for the semiquinone / hydroquinone couple of the bound FMN cofactor, and accordingly the semiquinone state is stable. The redox properties of the bound FMN in FDs are very different from those of the free FMN.

Since the late 1960's the FD from *Desulfovibrio vulgaris* strain Miyazaki F (FD-*Dv*MF) has been chosen as an alternative FD model, due to the non-toxic nature of the host bacterium, for the evaluation of electron transfer components.[3] As such, FD-*Dv*MF was first characterized and studied for its biochemical properties by Kitamura *et al.*[4] *In vitro* analysis revealed that the dissociation constant of FD-*Dv*MF was 0.38 nM, compared to 0.24 nM for the related FD from *Desulfovibrio vulgaris* Hildenborough (FD-*Dv*H). The redox potential of these two closely related FDs was also slightly different, being  $E_1 = -434$  and  $-440$  mV for the oxidized-semiquinone reaction of FD-*Dv*MF and FD-*Dv*H, respectively, and  $E_2 = -151$  and  $-143$  mV for the semiquinone-2-electron reduced reaction, respectively.[4] However, these two strains shared a similar physiology.[10] Although a fair amount of theoretical work has been published for FD-*Dv*H to iterate the empirical data, in contrast very little is known about the conformational dynamics and structural stability, including the energetic aspects, of FD-*Dv*MF.

Recently, the three-dimensional structures of numerous FDs have been determined, including FD-*Dv*H [35] and the FDs from *Anacystis nidulans*,[36] *Clostridium beijerinckii*,[37] *Escherichia coli*,[38] *Anabaena 7120*,[39] a red algae,[40] *Chondrus crispus* [41] and *H. pylori*,[8] by X-ray crystallography. In contrast, the structure of FD-*Dv*MF, has not been determined yet, although Kitamura *et al.*[4] have determined the primary structure and redox potentials of FD-*Dv*MF.

Ultrafast photophysics of FD-*Dv*MF has been extensively investigated in the wild type (WT), and the Y97F (Tyr97 is replaced by Phe), W59F (Trp59 is replaced by Phe) and W59F-Y97F double mutant (DM) (both Trp59 and Tyr97 are replaced by Phe) substitution based mutant variants.[6] The fluorescence lifetimes of FD-*Dv*MF were 0.158 ps in the WT, 0.245 ps in Y97F and 0.322 ps in W59F but 18 ps in the DM. These ultra-short lifetimes are ascribed to the photoinduced electron transfer (ET) from Trp59 and Tyr97 to the excited isoalloxazine (Iso\*).[25, 27-28, 42-43] Differences in the fluorescence lifetimes between Y97F and W59F were elucidated by means of ET donor-acceptor distances, using the crystal structure of FD-*Dv*H.[6] However, it is not clear whether the donor – acceptor distances evaluated for the FD-*Dv*H are valid for the elucidation of ET rates (inverse of the lifetimes).

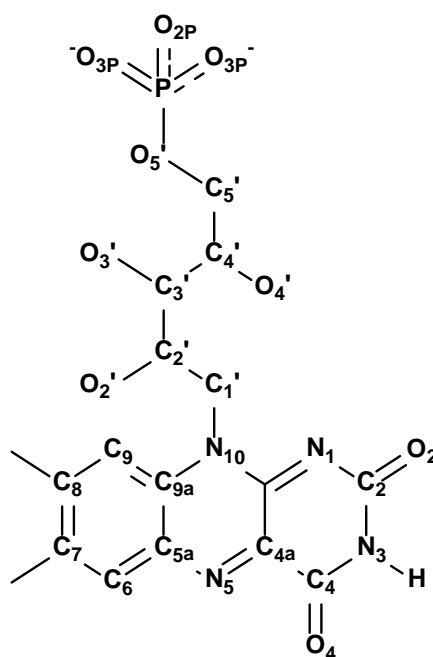


**Chart 1** Chemical structure and numbering of the FMN atoms.

Homology modeling has been a useful tool to predict the protein structure when the primary structure is known but the three dimensional structure is not known. However, it depends on the knowledge of at least the 3D structure of a closely related homologous protein with a considerable sequence identity to the target.[44] Homology modeling has also been used to

predict the protein structure of the FD from *Escherichia coli*,[45] and subsequently the constructed model was used to calculate the binding affinity of FMN.[46-48] However, a thorough analysis of the binding energy of the cofactors, including FMN, in flavoproteins has not been reported yet. In the present work we first predicted the structures and detailed the important interaction of the WT, and the substitution-based mutants W59F, Y97F and DM, of FD-*Dv*MF by means of homology modeling. The predicted models were then further used to investigate their dynamic properties by molecular dynamics (MD) simulations, and compared among these four FD-*Dv*MF variants. Finally, the interactions between FMN and the apoproteins were analyzed qualitatively by the MM-PBSA method between FMN and the apoproteins of the four FD-*Dv*MF variants. The observations in this study should help to further the understanding and complement the knowledge of the structural stability of FD-*Dv*MF, especially with respect to the ET and engineering of flavoprotein redox potentials, including for biosensors and bioelectronics.[11]

## 2.3 METHODS

### 2.3.1 Structural Modeling

The amino acid sequence of the WT FD-*Dv*MF was obtained from the previously reported work.[4] Table S1 shows a comparison of the sequence identity and similarity, the amino acid residues at positions 59 and 97, and the X-ray crystallographic resolution of the four FDs, which are somewhat similar except in the three-dimensional structural resolution. Considering the crystal structures of the two mutants, Y98W (PDB: 1F4P) and S35C (PDB: 1J8Q), the Y98W mutant has Trp59 / Trp97 residues that do not match to the target. In addition, the two WT structures (PDB: 1FX1 and 1BUS) display either {an amino acid sequence identity (66%) and similarity (76%) that is not different from} or {100% identity to} S35C, but the resolution of the WT is much higher than that for S35C (2.0 vs. 1.35 Angstroms). Therefore, the structure S35C (PDB: 1J8Q) was selected as the template for our study due to the higher resolution of its structure. The three dimensional structure of FD-*Dv*MF was then constructed using the Modeler Module of the Discovery Studio 2.0 (<http://www.discoverystudios.com>). Ten satisfactory models were generated from the Modeler Module and then the density optimization potential energy (DOPE) was used to justify the best quality model (defined as the structure with lowest DOPE score), which was then selected for further study. Subsequently, the target structure was

energetically minimized with 1000 steps using steepest decent minimization, followed by another 1000 steps of conjugate gradient minimization. This initial structure was further replaced by phenylalanine at position 59 (W59F), at position 97 (Y97F) or at both 59 and 97 (DM). All constructed 3D models of FD-*Dv*MF were submitted to the Protein Model Data Base (PMDB; 3D protein models obtained by structure prediction methods [49]) and can be accessed by PM0076923, PM0076926, PM0076924 and PM0076925 for the WT, W59F, Y97F and DM variants, respectively.

### 2.3.2 Calculation of the Atomic Charge of FMN

In this study, the FMN molecule was optimized using the HF/6-31G\* level of the theory by using the Gaussian 03 program.[50] The restrained electrostatic potential (RESP) method was used to compute the atomic partial charge. The FMN topology was constructed using the antechamber program in the Amber10 software package.[51]

### 2.3.3 Molecular Dynamics Simulation

The Amber10 program and amber03 force field were used for MD.[51] All missing hydrogen atoms of the protein were added using the LEaP module. First, all four FD-*Dv*MF variant structures were minimized with 1000 steps of steepest decent minimization, followed by 2000 steps of conjugate gradient minimization to remove the geometrical strain. Subsequently, the complexes were then solvated by 5760 TIP3P water molecules employing the periodic boundary extending to 10 Å from the complex. To neutralize the negative charges, 19 sodium counter ions were added to regions with the largest positive Coulombic potentials. Subsequently, 3000 steps of conjugated gradient minimization were performed on the whole system. This minimized solvated system was then used as the starting structure for the subsequent MD simulations. The MD systems were set under the isobaric-isothermal ensemble (*NPT*) with a constant pressure and temperature of 1 atm and 300 K, respectively. The Berendsen algorithm was used in order to control the temperature. Electrostatic interaction was corrected by the particle mesh Ewald method. In order to relax the position of the water molecules, we performed MD simulations for 135 ps by fixing the solute structure. After that, we performed an equilibrium MD simulation for about 3 ns. In all the simulations, bonds involving hydrogen were constrained

by applying the SHAKE algorithm [52] and were carried out with a 2 fs time step. We observed that the systems were well equilibrated by temperature, total energy and root of mean square deviation (RMSD). We used MD data from 3 ns to 10 ns (net 7 ns) of the production run to investigate the time dependent characteristics of the WT and the three mutated FD-DvMF variants.

### 2.3.4 MM-PBSA Free Energy Calculation

The binding free energy ( $\Delta G^0$ ) between FMN and the protein moiety was computed using the MM-PBSA method.[52-54] Five hundred MD snapshots (14 ps time intervals for 7 ns) were used to calculate the MM-PBSA free energy, after sodium counter ions and water molecules were stripped off. The average binding free energy ( $\Delta G_{bind}^0$ ) was calculated from the average molecular mechanical gas-phase energies ( $\Delta E_{MM}$ ), solvation free energies ( $\Delta G_{sol}^0$ ) and entropy contributions ( $-T\Delta S$ ), which were estimated from the normal-mode analysis of the binding reaction as detailed below in Eqs. 2.1 – 2.3:

$$\Delta G_{bind}^0 = \Delta G_{sol}^0 + \Delta E_{MM} - T\Delta S \quad (2.1)$$

$$\Delta E_{MM} = \Delta E_{elec} + \Delta E_{vdw} - \Delta E_{int} \quad (2.2)$$

$$\Delta G_{sol}^0 = \Delta G_{pol}^0 + \Delta G_{nonpol}^0 \quad (2.3)$$

Here  $\Delta E_{MM}$  is the molecular mechanics energy, which can be divided into the three parts of the electrostatic ( $\Delta E_{es}$ ), van der Waals ( $\Delta E_{vdw}$ ) and internal ( $\Delta E_{int}$ ) energies. The internal energy was neglected here as usual.  $\Delta G_{sol}^0$  is the solvation free energy and  $T\Delta S$  is the product of temperature and entropy change.  $\Delta G_{sol}^0$  was obtained by the generalized Born approach. We used  $\epsilon = 1$  for the solute and  $\epsilon = 80$  for the solvent in the calculation of  $\Delta G_{sol}^0$ . The *molsurf* program was used to calculate the non-polar solvation free energy.

### 2.3.5 Calculations of Decomposition Free Energy per Residue

The individual contribution of the decomposition energies of amino acid residues in the 10-loop (residues 10 - 16), 60-loop (residues 57 – 62) and 90-loop (residues 93 – 101) regions

were also studied using MM-PBSA calculations,[52-54] with the Amber10 software.[51] The coordinates of the atoms of 500 snapshots with 14 ps time intervals for 7.0 ns of the MD production run were used for the calculation of decomposition free energies per residue. The solvation free energy was estimated using polar and non-polar contributions according to Eq. 2.3. The molecular mechanic energy was calculated without cutoff for the evaluation of non-bonded interactions. The conformational entropies ( $T\Delta S$ ) were also calculated.

## 2.4. Results

### 2.4.1 Evaluation of the quality of the predicted models

The chemical structure and numbering of the FMN atoms is shown in Chart 1. Figure 2.1 shows the three-dimensional structures of the WT, W59F, Y97F and DM variants of FD-*Dv*MF as obtained by homology modeling. To assess the structural reliability of the WT and the three mutated FD-*Dv*MF variants, Ramachadran plots were employed.[55-56] The results demonstrated that the backbone angles in all four FD-*Dv*MF variants were in the allowed region (Figure S2.1, **Supplemental Information of Chapter II**). Using the web-based ProSA program, which is based on the energy of the structure using a distance based pair potential,[55-56] we found that the overall predicted structures have Z-scores (displayed in the context of all known protein structures by X-ray and NMR spectroscopy) of -7.99, -8.08 -8.02 and -8.00 for the WT, W59F, Y97F and DM, respectively, whilst that for the template (1J8Q) was only -7.94, as shown in Figures S2.2 and S3. Furthermore, we analyzed the compatibility of all amino acid residues with their environment using the Verify-3D approach from the same web server, where a score over 0.2 is considered reliable.[56-57] It is of note that in Figure 2.2, all starting FD-*Dv*MF variants are clearly properly folded with respect to the template and there are no residues with a negative score.

Through these assessments of the quality of the modeled structure, we conclude that the predicted models are reliable enough to characterize and so we used them to further investigate the dynamic behavior and interaction between the FMN cofactor and FD-*Dv*MF.

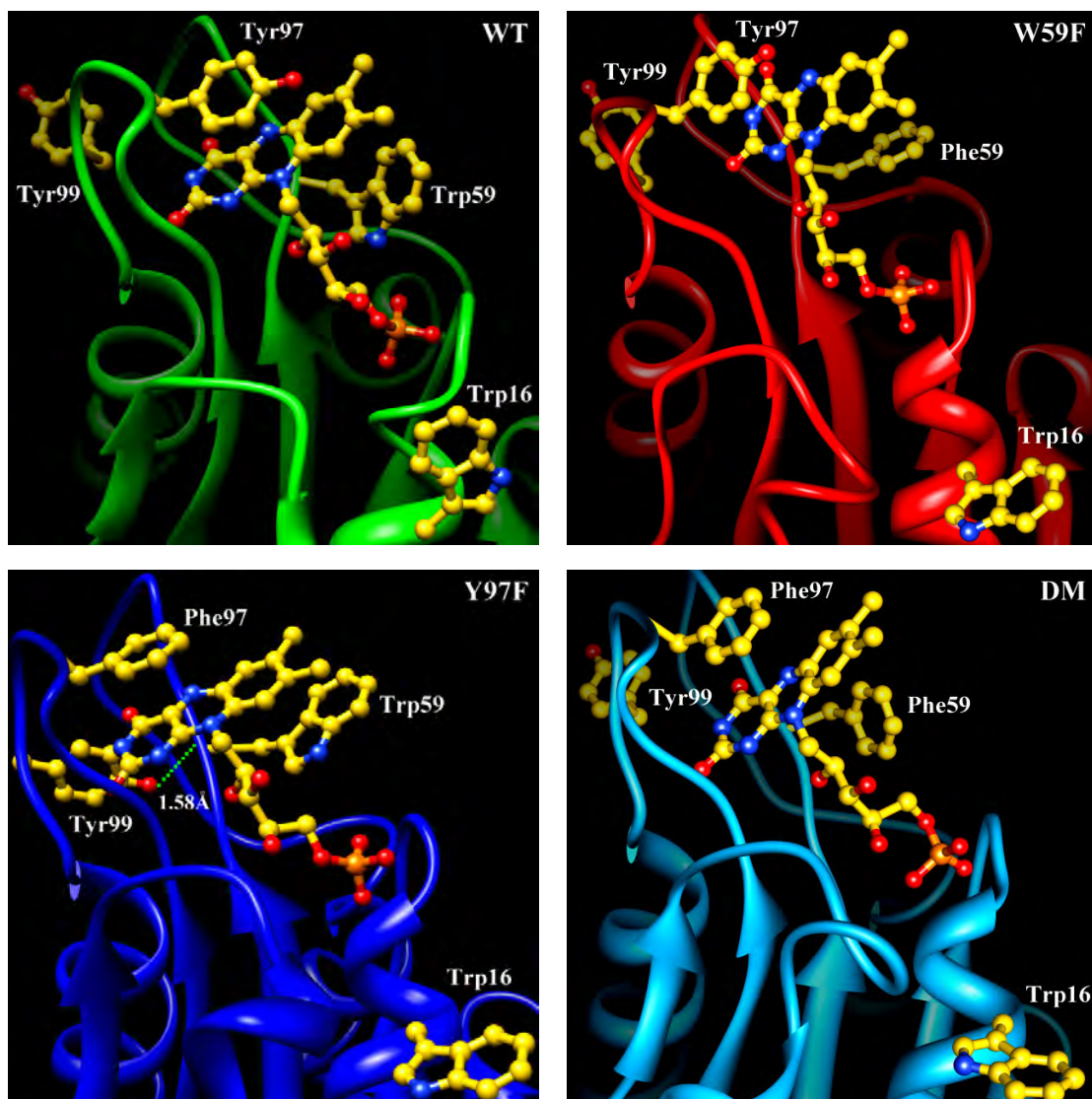


**Figure 2.1** Three-dimensional structures of the four FD-*Dv*MF variants at the FMN binding site, as predicted by homology modeling.



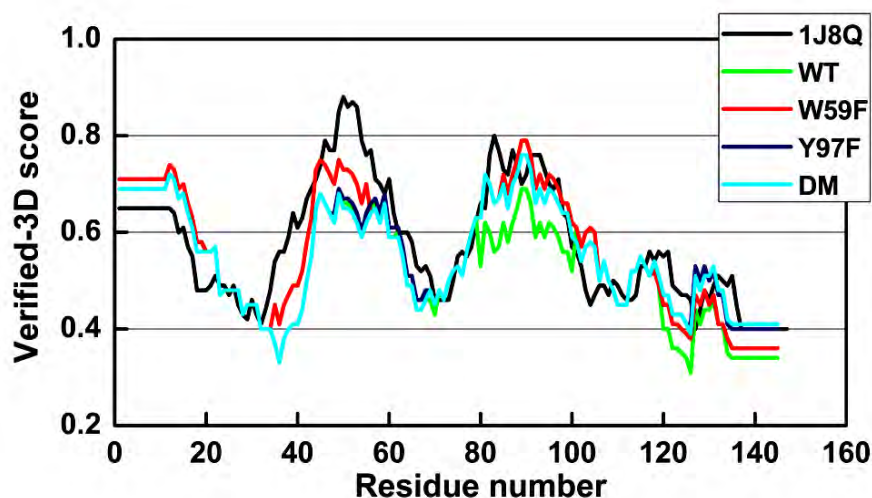


**Figure 2.2** Comparison verified-3D analysis between the template and four predicted FD-*DvMF* variants. The compatibility of amino acids in their environments are indicated by the positive scores

## 2.4.2 Comparison of Protein Structures Among the Four FD-*DvMF*

### Variants

The mean center to center distances between Iso and Tyr97 were 5.4 Å in the WT [58] and 5.5 Å in W59F, whilst between Iso and Trp59 they were 6.4 Å in the WT and 7.8 Å in Y97F.[59] The mean inter-planar angles between Iso and Tyr97 were 14 deg in WT and 18.6 deg in W59F, whilst between Iso and Trp59 they were -43 deg in the WT and 31.2 deg in Y97F.[59] These results suggest that the local structure of the WT FD-*DvMF* near the Iso binding site is quite different from that of the Y97F or W59F mutants.

### 2.4.3 Accessibility of Water Molecules to FMN

Figure 2.3 illustrates the protein surface at the FMN binding sites for all four FD-*DvMF* variants, with the focus being on the Iso moieties where the phosphate group was completely buried inside the proteins, but part of the ribityl and Iso groups were exposed to the water layer. The space of the ribityl-binding site in Y97F was quite narrow compared to the other three FD-*DvMF* variants, and a part of ribityl group was buried inside the protein. The degree of exposure of FMN to the water layer was also illustrated in the space-filling model in Figure S2.4

(Supplemental Information of Chapter II), where it is apparent that FMN is buried the most in Y97F, followed by the WT, whilst in W59F and DM the FMN is exposed to the water layer. The agreement is that the number of water molecules in the first solvent layer in contact with FMN was highest in W59F, followed by DM, WT and lastly Y97F (Table 2.1). From examination of the second solvation layer (5 Å), it is apparent that whilst FMN is buried the most in Y97F, it is exposed to water the most in W59F. The buried structure of FMN in Y97F may be ascribed to H-bond formation between Trp59 and Tyr99, as shown in Figure 2.1 and discussed below.

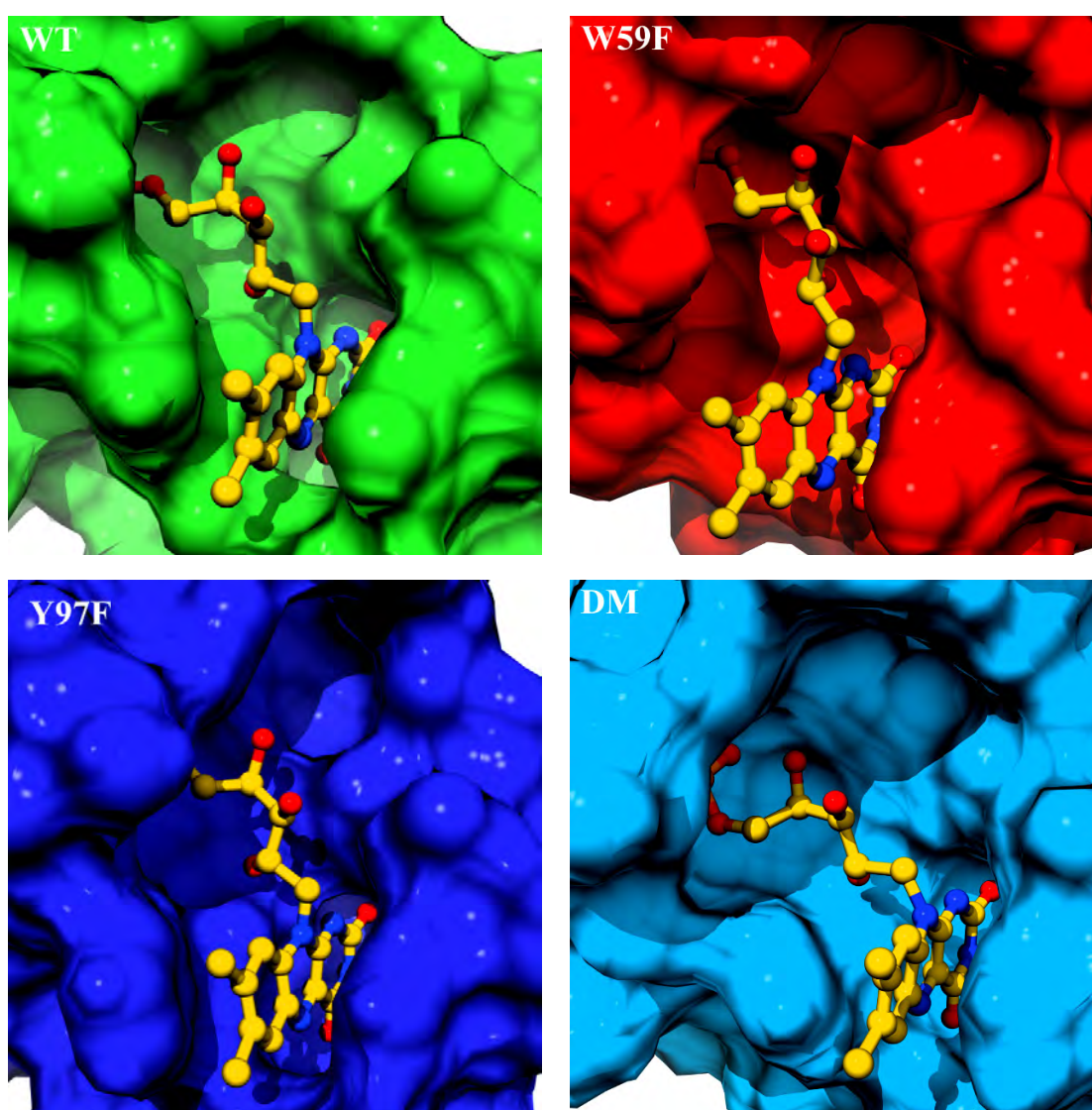


**Figure 2.3** Shape of the protein surface at the FMN binding site in the four FD-*Dv*MF variants. It is apparent that the FMN binding site is rather small in the WT and Y97F, compared to that in the W59F and DM variants.

**Table 2.1** Number of water molecules in contact with FMN

Solvation layer	Amount of water molecules			
	WT	W59F	Y97F	W59F-Y97F (DM)
First <sup>a</sup>	18.5	23.6	17.4	20.5
Second <sup>b</sup>	40.8	47.3	37.6	41.6

Number of water molecules in the <sup>a</sup> first layer (within 3.5 Å) and the <sup>b</sup> second layer (within 5 Å) from the FMN atoms.

Figure 2.4 shows the radial distribution function (RDF) of the water molecules at the FMN binding site. No water molecule was found near N1, which may be ascribed to the presence of the bulky ribityl side chain at N10. The average number of water molecules located near N3 was about 1.7 in WT, 1.1 in W59F, 1.5 in Y97F and 1.6 in DM. In W59F an average of about four water molecules were present at N5, and 0.7 at O2, but the presence of water molecules at N5 and O2 was negligible in the other FD-*Dv*MF variants. At O4, 1.6 water molecules were present in W59F, 0.8 in Y97F and 1.2 in DM, but none were found in the WT. At the O2' and O5' phosphate oxygen atoms, very few water molecules existed, because these phosphate oxygen atoms formed H-bonds with the surrounding amino acid residues, as described later. However, about two water molecules were located at the O3' and O4' atoms in all four FD-*Dv*MF variants. These results suggest that in W59F an appreciable amount of water molecules are located near to Iso, which is in accordance with the result of the number of water molecules accessible to FMN (Table 2.1), and also with the quite large space at the FMN binding site in W59F.

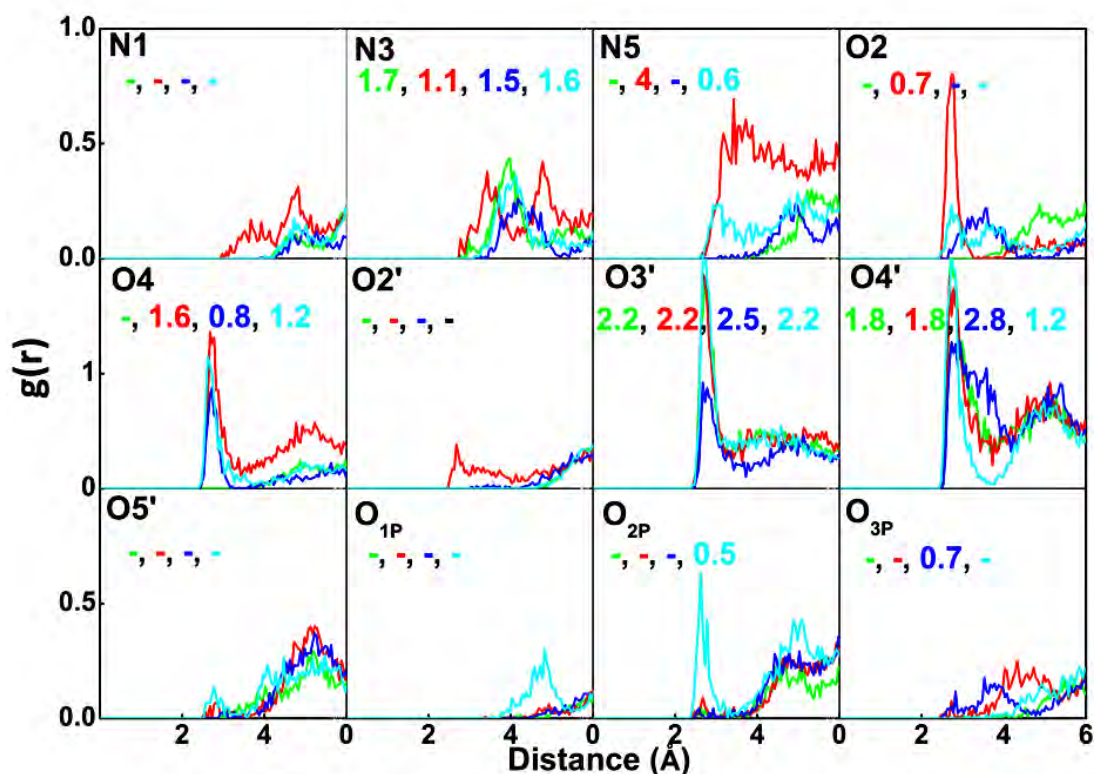
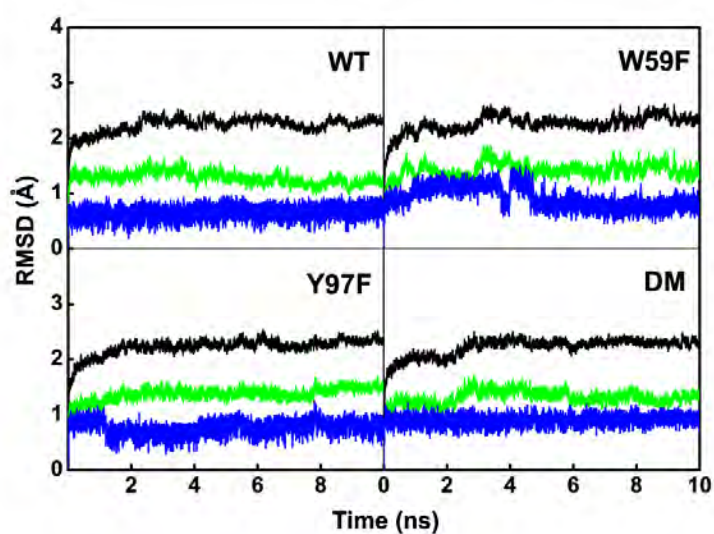


**Figure 2.4** The RDF of the number of water molecules near FMN. The integrated number of water molecules is indicated in green for WT, red for W59F, deep blue for Y97F and light blue for DM. The number of water molecules seems complementary with the number of H-bonds between FMN and the nearby amino acids of FD-*Dv*MF.

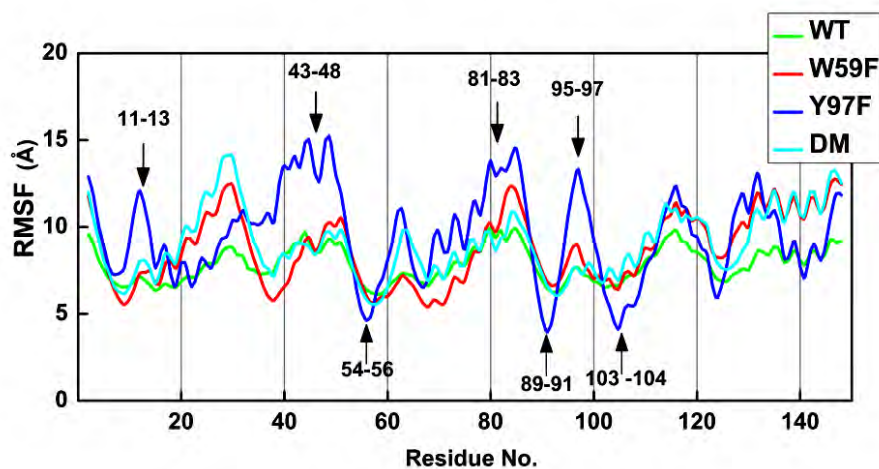
### 2.4.5 Dynamic Properties of the four FD-*Dv*MF variants

Figure 2.5 shows the time-dependent changes in the RMSD [51] from the starting structures that were obtained by homology modeling. The RMSDs for all four FD-*Dv*MF variants were well equilibrated after 3 ns of simulation time, and the mean RMSDs of the entire protein were all similar (Table 2.1). However, the RMSD of the backbone region was highest in W59F and lowest in WT, whilst the RMSD of FMN was also lowest in WT but highest in the DM (see Table 2.2), perhaps due to the increased motional freedom of FMN following replacement of both the bulky Trp and Tyr with the smaller Phe. Figure 2.6 shows the RMSF for the four FD-*Dv*MF variants, whilst the peptide chains with low and high RMSF values are summarized in Table 2.3. The RMSF values were low in the amino acid residues around Trp16, Gly60, Cys92, Cys101 and Lys124 in the WT, around Ser9, Ala37, Gly60, Cys92 and Cys101 in W59F, around Gly55,

Ala88, Pro103 and Lys124 in Y97F, and around Gly8, Gly55 and Cys92 in the DM. The protein structures should be rigid at these amino acid residues. The values of RMSD were high in the amino acid residues around Val3, Ala42, Ala82 and Gly115 in the WT, around Asn2, Glu27, Arg49, Gly83, Gly116 and Asp134 in W59F, and around Asn2, Thr11, Gly44, Arg49, Gly115, Gly127 and Asp128 in Y97F, and around Gly22, Glu27, Gly85, Leu114 and Arg130 in DM. The protein structures should be flexible at these amino acid residues.



**Figure 2.5** Time-dependent changes in the RMSD of the four FD-DvMF variants. Black lines indicated that for the entire FD-DvMF, green lines the peptide backbone and blue lines the FMN molecule.



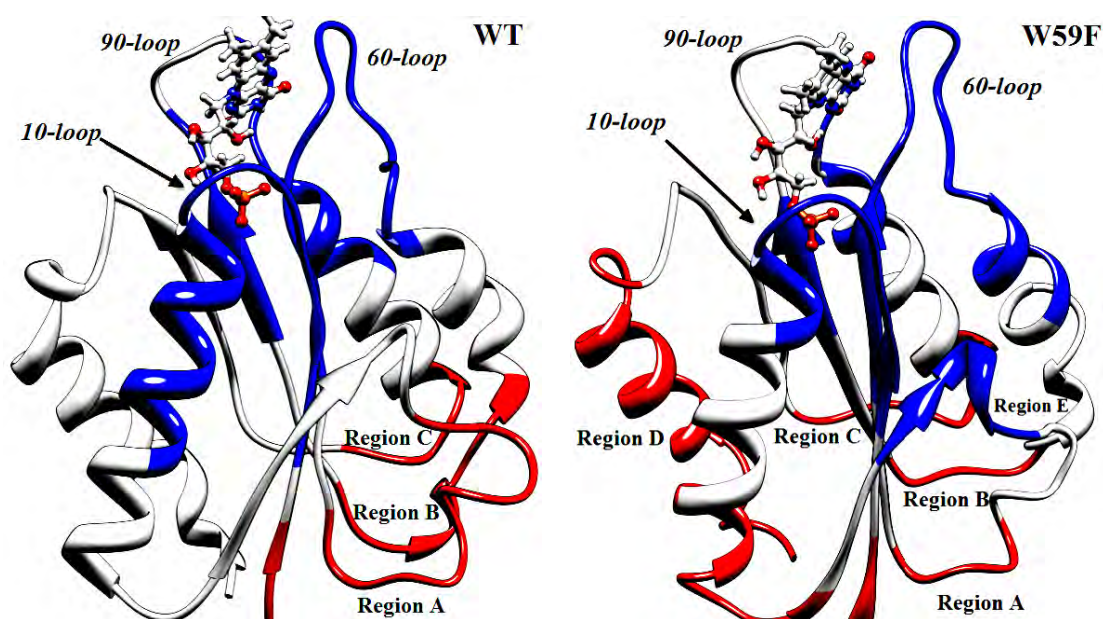
**Figure 2.6** The RMSF for the four FD-DvMF variants.

**Table 2.2** The mean RMSD of the four FD-*Dv*MF variants<sup>a</sup>

Protein part	WT	W59F	Y97F	W59F-Y97F
Entire protein	2.28 ± 0.08	2.32 ± 0.10	2.28 ± 0.07	2.30 ± 0.06
Backbone	1.26 ± 0.10	1.45 ± 0.11	1.41 ± 0.08	1.34 ± 0.09
FMN	0.68 ± 0.12	0.87 ± 0.19	0.78 ± 0.13	0.91 ± 0.09

<sup>a</sup>The mean was taken over 7 ns of production time with 14 time intervals. Means within a row or a column followed by a different letter are significantly different ( $P < 0.05$ ).

Figure 2.7 illustrates the location of the rigid (in blue) and flexible (in red) parts of the structures of the four FD-*Dv*MF variants. In the WT, the 10-loop, 60-loop and part of 90-loop regions were rigid, whilst regions A, B and C were flexible. In W59F, the rigid part of the 10-loop domain is reduced and instead region E became rigid and region D became flexible, in addition to regions A, B and C being flexible. In Y97F, the entire 10-loop region is flexible, whilst the flexible region in region C is reduced. In the DM variant, the 10-loop region was neither rigid nor flexible. Instead, most parts of regions C and D were flexible. Thus, even though only one or two amino acid residues (Trp59 and / or Tyr97) were replaced with Phe, the dynamic properties of the whole FD-*Dv*MF protein were remarkably modified in the mutant variants and especially the DM.



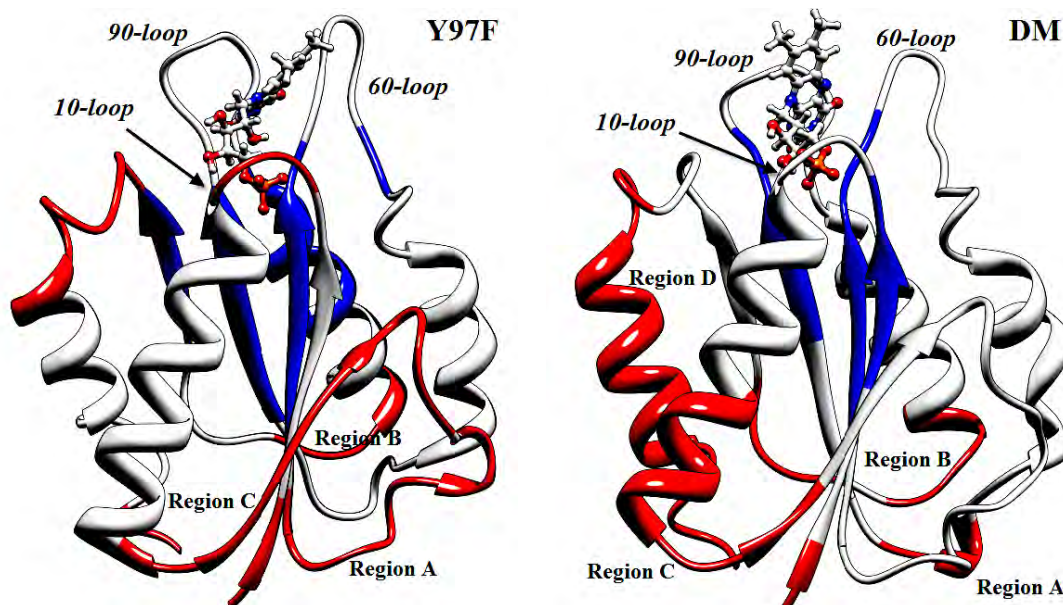


**Figure 2.7** Comparison of the rigid (blue) and flexible (red) parts among the four FD-DvMF variants. The rigid and flexible parts were determined by taking an average over 7 ns.

**Table 2.3** Comparison of the amino acid residues with a low and a high RMSF value among the four FD-DvMF variants<sup>a</sup>

FD-DvMF variant	Rigid part	Flexible part
WT	Thr14-Ala15-Trp16-Val17	Ala1-Asn2-Val3-Leu4-Ile5
	Thr58-Trp59-Gly60-Asp61	Val40-Glu41-Ala42-Glu43-Gly44
	Phe90-Gly91-Cys92-Gly93	Thr80-Gly81-Ala82-Gly83-Lys84
	Tyr99-Phe100-Cys101-Gly102	Ser112-Gly113-Leu114-Gly115- Ala116-Asp117
	Ser122-Leu123-Lys124-Ile125	
W59F	Val6-Tyr7-Gly8-Ser9-Thr10-Thr11	Ala1-Asn2-Val3
	Arg35-Asp36-Ala37-Gly38-Gln39	Ile25-Ala26-Glu27-Ala28-Gly29
	Thr58-Phe59-Gly60-Asp69-Phe70	Glu47-Gly48-Arg49-Asp50-Leu51
	Phe90-Gly91-Cys92-Gly93	Gly81-Ala82-Gly83-Lys84-Gly85
	Tyr99-Phe100-Cys101-Gly192	Ser112-Gly116 Asp134-Asp135
Y97F	Leu53-Phe54-Gly55-Cys56-Ser57	Ala1-Asn2-Val3

	Glu65-Leu66-Ala88-Cys89-Phe90	Thr10-Thr11-Gly12
	Cys101-Gly102-Pro103-Val104- Asp105-Ala106	Ala42-Glu43-Gly44-Leu45-Cys46
	Ser122-Leu123-Lys124-Ile125	Glu47-Gly48-Arg49-Asp50
		Gly113-Leu114-Gly115- Ala116
		Asp126-Gly127-Asp128-Pro129
	Val6-Tyr7-Gly8-Ser9	Ala1-Asn2-Gly22-Arg23-Asp24
	Leu53-Phe54-Gly55-Cys56-Ser57-Thr58-Phe59	Ile25-Ala26-Glu27-Ala28-Gly29
<b>DM</b>	Phe90- Gly91-Cys92-Gly93-Asp94	Gly83-Lys84-Gly85-Arg86
		Ser112-Gly113-Leu114-Gly115
		Asp128-Pro129-Arg130-Thr131

<sup>a</sup>Rigid and flexible parts were selected by RMSF values of less than 7 Å and more than 10 Å, respectively. Those that fall in between are defined as neither rigid nor flexible.

## 2.4.6 Hydrogen Bonding Dynamics

The criteria for real H-bond formation may require (i) a bond angle of X-H...Y greater than 120°, (ii) the distance between the heavy atoms of the donor and acceptor to be less than 3.5 Å and (iii) H-bond energies that vary from a few kcal mol<sup>-1</sup> to tens of kcal mol<sup>-1</sup>, depending on the donor and acceptor.[60] In this work, the energetic aspect, however, will be neglected because the calculation time required to obtain it is logistically too consuming and the other two criteria have previously been shown to be sufficient to successfully evaluate the important H-bond interactions.[55-56, 61-62] Figure 2.8 shows the H-bond dynamics between Tyr99OH and Trp59 (Op), which clearly satisfied both criteria for likely H-bond formation. A H-bond between the Tyr99OH and the Trp59 peptide O was found in Y97F, but not in the other three FD-DvMF variants, as described later. Because of this H-bond the position of Tyr99 shifted towards Trp59 in Y97F. Trp59 is located in loop-60 and Tyr99 in loop-90, with FMN sandwiched between these loops. Accordingly, the space between both loops became narrower in Y97F than those in the other three FD-DvMF variants, as stated earlier.



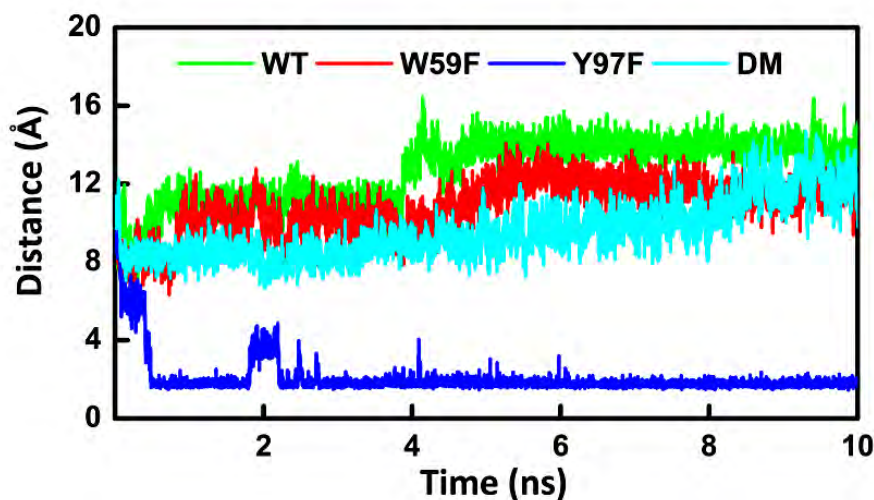


**Figure 2.8** H-bond distance between the Tyr99OH and Trp59 peptide O in the four FD-*DvMF* variants. The distances between the H atom of the Tyr99OH and the Trp59 peptide O are shown.

The percent occupancies of the potential H-bonds between FMN and the surrounding amino acid residues are listed in Table 2.4. The two criteria for likely H-bond formation (see above) were also satisfied here. Within the 10-loop region of all four FD-*DvMF* variants, H-bonds were formed between Ser9OH with O<sub>3p</sub>, Thr10NH(p) with O<sub>1p</sub>, Thr11OH with O<sub>2p</sub>, Thr11NH(p) with O<sub>2p</sub> and O<sub>1p</sub>, Gly12NH(p) with O<sub>2p</sub>, Asn13NH(p) with O<sub>2p</sub>, Thr14OH with O<sub>3p</sub> and Thr14NH(p) with O<sub>3p</sub>. For the other H-bond pairs, only Ser57OH with O5' and O<sub>3p</sub> at the 60-loop region was found in all four FD-*DvMF* variants. For W59F, no H-bond was formed in the 90-loop region, whilst Ser9, Thr10, Thr11, Gly12 and Asn13 (10-loop) located near the phosphate, Asn13, Thr14, Ser57 and Thr58 (10-loop and 60-loop) located near the ribityl chain, and Gly60, Asp61, Asp94 and Tyr99 (60-loop and 90-loop) located near the Iso ring. Thus, the replacement of Trp (W59F), Tyr (Y97F) or both of them (DM) by Phe remarkably modified the H-bond pairs between FMN and the nearby amino acid residues.

**Table 2.4** The percent occupation of the H-bond between FMN and surrounding amino acids<sup>a</sup>

Loop	Residue	Atom in amino acid <sup>b</sup>	Atom in FMN <sup>c</sup>	Occupancy (%)			
				WT	W59F	Y97F	DM
10-loop	Ser9	OG-HG	O <sub>2P</sub>	97.6	72.0	85.8	--
	Ser9	OG-HG	O <sub>3P</sub>	100.0	99.5	100.0	88.1
	Ser9	OG-HG	O <sub>1P</sub>	--	--	63.1	93.4
	Thr10	OG1-HG1	O <sub>1P</sub>	97.3	99.9	87.9	--
	Thr10	N-H (p)	O <sub>2P</sub>	98.8	69.5	71.7	--
	Thr10	N-H (p)	O <sub>1P</sub>	99.9	100.0	100.0	99.9
	Thr10	N-H (p)	O <sub>3P</sub>	89.1	--	75.7	--
	Thr10	OG1-HG1	O <sub>2P</sub>	--	51.8	--	--
	Thr11	OG1-HG1	O5'	58.3	--	--	78.4
	Thr11	OG1- HG1	O <sub>2P</sub>	100.0	95.3	96.7	98.0
	Thr11	OG1-HG1	O <sub>1P</sub>	--	--	69.2	55.3
	Thr11	N-H (p)	O <sub>2P</sub>	100.0	99.9	99.9	99.1
	Thr11	N- H (p)	O <sub>1P</sub>	75.8	92.8	99.6	94.4
	Gly12	N-H (p)	O <sub>2P</sub>	99.8	95.3	95.9	91.7
	Gly12	N-H (p)	O <sub>1P</sub>	--	--	--	84.4
	Asn13	N-H (p)	O <sub>2P</sub>	99.4	95.3	100.0	100.0
	Asn13	N-H (p)	O <sub>3P</sub>	--	79.3	77.8	86.7
	Asn13	N-H (p)	O <sub>1P</sub>	--	--	--	77.1
	Asn13	ND2-HD22	O5'	--	86.9	97.0	--
	Asn13	ND2-HD22	O <sub>2P</sub>	--	84.5	99.7	60.5
Thr14	OG1-HG1	O <sub>3P</sub>	100.0	94.7	100.0	100.0	
Thr14	N-H (p)	O <sub>3P</sub>	100.0	99.3	100.0	100.0	
Thr14	OG1-HG1	O5'	--	--	52.9	--	
60-loop	Ser57	OG-HG	O5'	54.2	54.6	71.3	53.5
	Ser57	OG-HG	O <sub>1P</sub>	100.0	100.0	99.8	--
	Ser57	OG-HG	O <sub>3P</sub>	87.0	71.4	76.3	51.4
	Thr58	N-H (p)	O2'	83.7	--	63.7	99.0

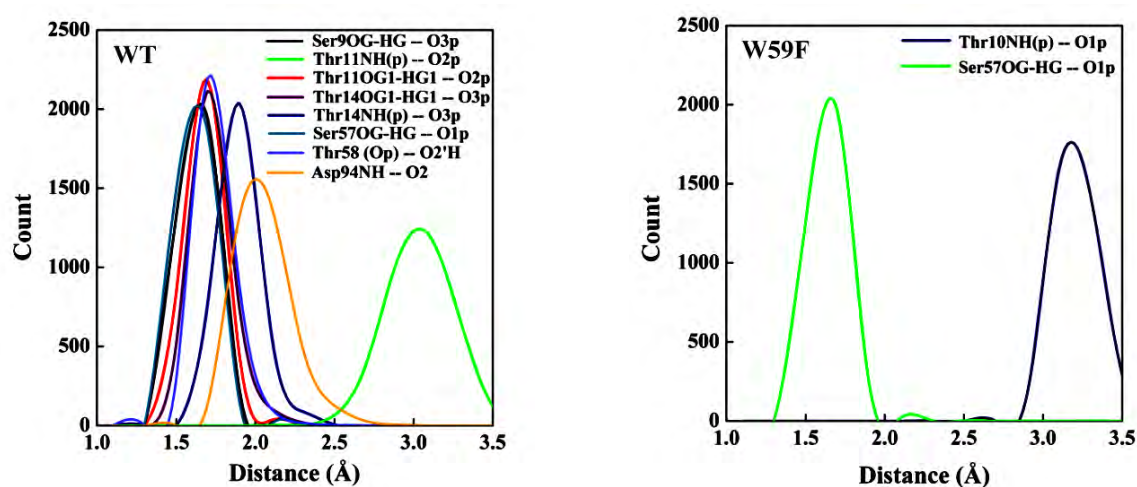
	Thr58	O (p)	O2'H	100.0	--	98.4	99.9
	Trp59	NE1-HE1	O <sub>1P</sub>	74.8	--	--	--
	Gly60	O (p)	N3H	--	77.57	--	--
	Gly60	N-H (p)	O4	--	--	--	62.6
	Asp61	N-H (p)	O4	92.4	--	83.1	--
	Asp61	N-H (p)	N5	83.3	--	87.1	--
90-loop	Asp94	N-H (p)	N1	95.2	--	98.0	96.8
	Asp94	N-H (p)	O2	100.0	--	100.0	100.0
	Tyr99	O (p)	N3H	77.9	--	100.0	100.0

<sup>a</sup>Data were obtained by Amber10.[51]

<sup>b</sup>Atomic notations are given in a PDB file. p in parentheses denotes peptide.

<sup>c</sup>Atomic notations are as given in Chart 1.

Figure 2.9 shows the distribution of the donor proton and acceptor distance. In all four FD-*Dv*MF variants, the H-bonds mostly occurred between amino acid residues in the 10-loop region and the phosphate group, with those involving Ser9, Thr11, Thr14 and Ser57 being the strongest in the WT, and then followed by Y97F, DM and W59F (in decreasing order), as judged from the number of H-bonds.



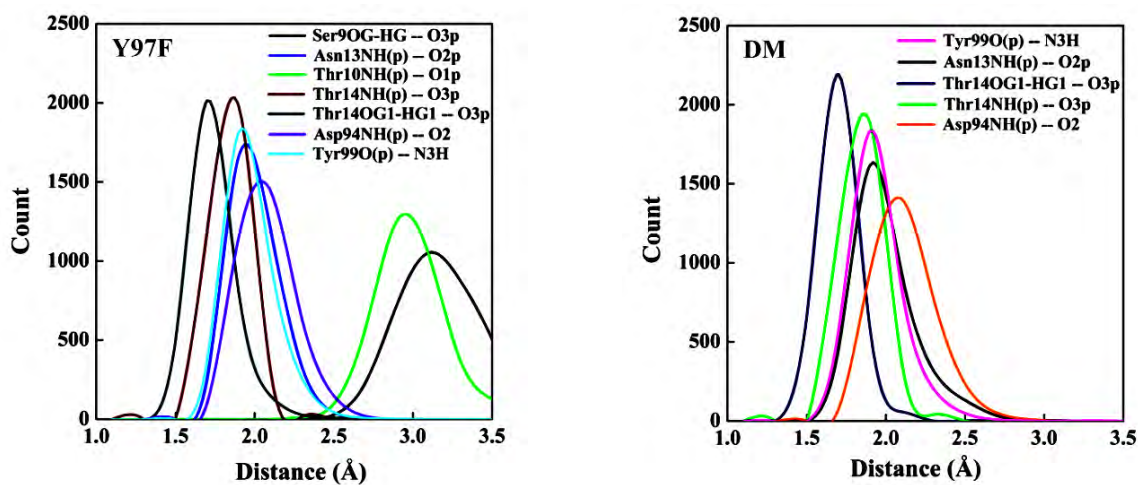


**Figure 2.9** Comparison of the distance distribution with hundred percent occupations among the four FD-*DvMF* variants. The distances between the H atoms and the proton acceptors are shown here. The proton donor-acceptor pair satisfies the two criteria for H-bond formation of (i) the bond angle  $> 120^\circ$  and (ii) the donor-acceptor heavy atoms  $< 3.5 \text{ \AA}$ .

#### 2.4.7 Decomposition free energy per residue at FMN Binding Site

The decomposition free energy per amino acid residue is defined as the stabilized energy upon the binding of the amino acid to a protein. If these amino acid residues are located near the FMN binding site, then their decomposition free energy per residue should be influenced by the interaction between FMN and the amino acid residues. FMN was surrounded by the 10-loop, 60-loop and 90-loop regions (see Figure 2.7), and the decomposition free energies per residue at these three regions are shown in Figure 2.10, whilst the mean decomposition free energies per residue of the four FD-*DvMF* variants are summarized in Table 2.5. At the 10-loop region, the highest decomposition free energy was found in Y97F followed by W59F, DM and lastly the WT. At the 60-loop region, the decomposition free energies were considerably lower than those at the 10-loop region, and the order was also somewhat changed, being (highest to lowest) WT  $>$  Y97F  $>$  DM  $>$  W59F. Finally, the 90-loop region had the lowest decomposition free energies of all three loops and was ordered differently again as Y97F  $>$  DM  $>$  WT  $>$  W59F. It is evident that the 10-loop region has the greatest decomposition free energy per residue among the three loops, although the order of the magnitude of the energy was different between the three loop regions.

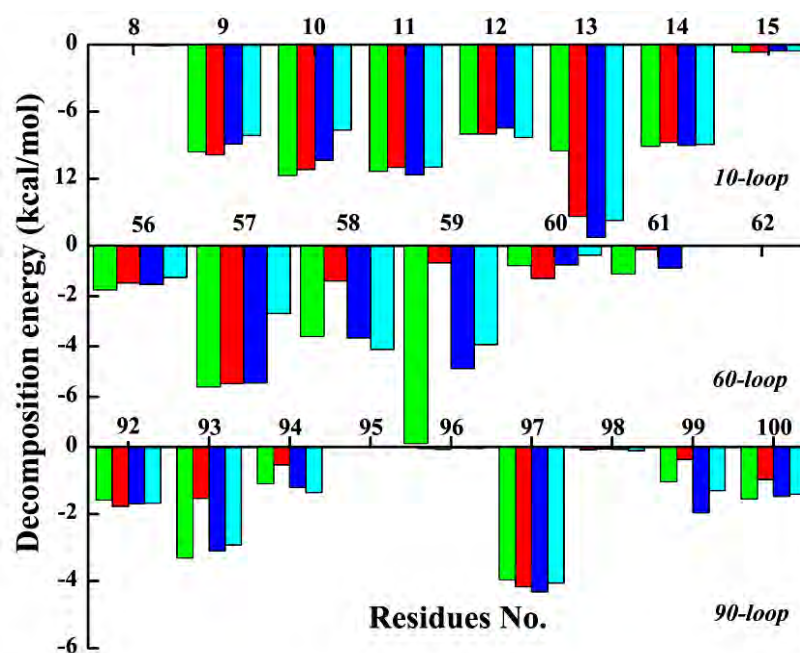


**Figure 2.10** Decomposition free energy of amino acids at the FMN binding site. The energies are shown with green bars for WT, red bars for W59F, deep blue bars for Y97F and light blue bars for DM.

#### 2.4.8 Free Energy of FMN Binding

The free energy changes upon the binding of FMN to the proteins are shown in Table 2.6. They consist of the molecular mechanical gas-phase energies ( $\Delta E_{MM}$ ) and the solvation free energy ( $\Delta G_{sol}^0$ ), in addition to the entropy term ( $T\Delta S$ ), as shown by Eq. 2.1. The average of these quantities is listed in Table 2.6, taken over 7 ns with a time interval of 14 ps. The total enthalpy energy ( $\langle \Delta E_{Tot} \rangle_{AV}$ ), derived as follows  $\langle \Delta E_{Tot} \rangle_{AV} = \langle \Delta E_{elec} \rangle_{AV} + \langle \Delta E_{vdw} \rangle_{AV} + \langle \Delta E_{solv} \rangle_{AV}$ , was -22.07 kcal / mol in WT, -18.92 kcal / mol in W59F, -22.97 kcal / mol in Y97F and -18.0 kcal / mol in DM. The mean was -20.49 kcal / mol. The electrostatic energies were all positive, but all the other enthalpy changes and entropy terms were negative. The negative value solvation energies contributed the most to the negative binding free energies of FMN in all four FD-DvMF variants. The order of the magnitude of the binding free energy was Y97F > WT > W59F > DM, which was the same as that observed with the decomposition free energy per residue.

**Table 2.5** Decomposition free energy per residue in the four FD-DvMF variants<sup>a</sup>

Energy	WT	W59F	Y97F	DM
10-loop <sup>b</sup>	-8.54 ± 3.70	-9.25 ± 4.47	-9.30 ± 5.00	-8.60 ± 4.51
60-loop <sup>c</sup>	-3.45 ± 2.28	-1.74 ± 1.90	-2.86 ± 2.08	-2.00 ± 1.87
90-loop <sup>d</sup>	-1.39 ± 1.41	-1.05 ± 1.34	-1.53 ± 1.48	-1.42 ± 1.38
Total	-13.38 ± 2.92	-12.04 ± 2.71	-13.69 ± 5.61	-12.02 ± 5.07

<sup>a</sup>Energy is expressed in units of kcal / mol.

The <sup>b</sup>10-loop, <sup>c</sup>60-loop and <sup>d</sup>90-loop regions consist of amino acid residues 9 - 15, 56 - 61 and 92 - 100, respectively.

Data are shown as the mean ± 1 SD. Means within a row or a column followed by a different letter are significantly different (P<0.05).

**Table 2.6** Binding free energy of FMN<sup>a</sup>

	WT	W59F	Y97F	DM
$\langle \Delta E_{elec} \rangle_{AV}$ <sup>b</sup>	229.5 ± 16.2	231.9 ± 22.8	235.3 ± 15.8	230.6 ± 25.0
$\langle \Delta E_{vdw} \rangle_{AV}$ <sup>c</sup>	-43.0 ± 5.0	-28.7 ± 5.7	-41.6 ± 4.7	-36.6 ± 5.4
$\langle \Delta E_{MM} \rangle_{AV}$ <sup>d</sup>	186.6 ± 15.6	203.3 ± 21.2	193.5 ± 14.9	194.1 ± 23.8
$\langle \Delta G_{nonpol}^0 \rangle_{AV}$	-5.25 ± 0.11	-4.70 ± 0.22	-5.26 ± 0.09	-4.97 ± 0.11
$\langle \Delta G_{pol}^0 \rangle_{AV}$	-273.7 ± 11.7	-277.7 ± 16.43	-284.3 ± 12.5	-264.5 ± 16.9
$\langle \Delta G_{sol}^0 \rangle_{AV}$ <sup>e</sup>	-279.0 ± 11.7	-282.4 ± 16.43	-289.6 ± 12.5	-269.5 ± 16.9
$\langle T\Delta S \rangle_{AV}$ <sup>f</sup>	-28.0 ± 15.4	-25.4 ± 15.5	-28.7 ± 16.0	-26.8 ± 15.3
$\Delta G_{bind}^0$ <sup>g</sup>	-64.4 ± 17.9	-53.8 ± 18.1	-67.5 ± 18.0	-48.5 ± 18.4
$Kd_{cal}^h$	1.2 x 10 <sup>-38</sup>	8.1 x 10 <sup>-31</sup>	8.4 x 10 <sup>-41</sup>	6.63 x 10 <sup>-27</sup>

<sup>a</sup>The method of the calculation is as described in the MM-PBSA free energy calculation section of methods of analyses in text. The energies were obtained by taking average over 7 ns with 14 ps time intervals, and are shown as the mean ± 1 SD. Energy is expressed in units of kcal / mol.

<sup>b</sup>Electrostatic energy between all atoms in FMN and all other atoms in the FD protein.

<sup>c</sup>Van der Waals interaction energy.

<sup>d</sup>Molecular mechanics energy calculated by Eq. 2.2.

<sup>e</sup> Solvation free energy calculated by Eq. 2.3.

<sup>f</sup>  $T = 298$  K. See calculation of decomposition energy of amino acids section of methods of analyses for the calculation of entropy change in text.

<sup>g</sup> The binding free energy was calculated by Eq. 2.1 in the text.

<sup>h</sup>  $\Delta G_{bind}^0 = RT \ln(Kd_{cal})$ , where the units of  $Kd_{cal}$  are in nM.

#### 2.4.9 The contribution of the total binding energies

Finally, since the binding free energy of FMN relates to the dissociation constant of FMN, then the experimentally derived dissociation constants ( $K_d$ ) and binding free energies ( $\Delta G_{Exp}^0$ ) of FMN, RF and lumiflavin in the FD from *Anabaena* (Table 2.7) were compared with the herein theoretically derived values for FD-DvMF. For *Anabaena*, the mean values of  $\Delta G_{Exp}^0$  are -10.8 kcal / mol for FMN, -5.82 kcal / mol for RF and -5.05 kcal / mol for lumiflavin. The contribution of the phosphate group to  $\Delta G_{Exp}^0$  may be obtained by  $\Delta G_{Exp}^0$  (FMN) -  $\Delta G_{Exp}^0$  (RF), which yields a value of - 4.98 kcal / mol (46%), and that for the ribityl group by  $\Delta G_{Exp}^0$  (RF) -  $\Delta G_{Exp}^0$  (lumiflavin), yielding - 0.77 kcal / mol (7%). Thus, the contribution of the isoalloxazine ring to  $\Delta G_{Exp}^0$  may be 47%. These values for the FD from *Anabaena* agree well with the theoretical values for the FD-DvMF variants, where from the decomposition of free energy per residue (Table 2.5), in a similar manner, the contribution was evaluated as being 64% from the 10-loop region (mostly interacts with the phosphate group), 10% from the 90-loop region (mostly interacts with the ribityl group), and 26% from the isoalloxazine ring. Therefore, the calculated contributions of all three parts of FMN to the total binding free energies were in qualitatively good accordance with the experimental contributions.

**Table 2.7** Experimental binding free energy of flavin in FD-*Dv*MF

FD source		Ligand	$K_d$	$\Delta G_{Exp}^0$ <sup>c</sup> (kcal / mol)
<i>Anabaena</i>	WT	FMN	0.26±0.06	-13.1±0.1
<i>PCC7119</i> <sup>a</sup>	Y94F		1.04±0.15	-12.3±0.1
	W57F		8.33±0.49	-11.02±0.03
<i>Anabaena</i>	WT	Riboflavin	3.15±0.8	-6.14±0.01
<i>PCC7119</i> <sup>b</sup>	Y94F		180.7±1.0	-5.11±0.01
	W57F		22.9±1.2	-6.33±0.03
	WT	Lumiflavin	189.7 ±1.8	-5.05±0.01

Data are obtained from Ref.[63].

<sup>a</sup> Dissociation equilibrium constant of the ligands in unit of nM.

<sup>b</sup> Dissociation equilibrium constant of the ligands in unit of  $\mu$  M.

<sup>c</sup> Experimentally determined by binding free energy of the ligands, according to the equation,

$$\Delta G_{Exp}^0 = RT \ln(K_d).$$

## 2.5 DISCUSSION

Protein structures of the WT, W59F, Y97F and DM FD-*Dv*MF variants were first predicted by homology modeling, the optimal models selected using DOPE analysis and then checked by ProSA and Verify-SD software. Then the dynamic properties of these systems were studied by MD simulation. Bound FMN in all four FD-*Dv*MF variants was surrounded by the 10-loop, 60-loop and 90-loop regions, and sandwiched by the 60-loop and 90-loop regions. Only in the Y97F variant were Trp59 in 60-loop region and Tyr99 in the 90-loop region found to form H-bonds. The superimposition of the whole protein of all variants showed slight differences at the FMN binding site, and these can be classified into two groups. The first group is comprised of that found with the WT and the W59F and Y97F variants, and the second group is that found with the DM. In the DM variant, the conformations of the negatively charged amino acids at the binding site, Asp61 and Asp62, are shifted closer to Tyr99 than in the other variants (Figure S2.5, **Supplemental Information of Chapter II**), leading to a blocking of the ability of Tyr99 to rotate to form a H-bond with the amino acid at position 59. This different conformation, with respect to that seen in the WT (group 1) might be due to the high hydrophobicity of Phe resulting in the



cooperative stacking form of the three components (Phe59 – Iso – Phe97). Note here that Phe has a hydrophobicity value of 100, while Tyr is 63 and glycine is 0. The backbone of these negatively charged amino acid residues of all variants except for the DM are located slightly distal to the Tyr99 residue. Therefore, more space is allowed for the Tyr99 residue of the Y97F variant to rotate and form such a H-bond, as indicated by the dark blue arrow in Figure S2.5 (**Supplemental Information of Chapter II**). However, we could not observe this behavior in the case of the WT and W59F variants, perhaps due to the larger van der Waal's radius of Tyr97. We propose that the larger van der Waal's radius of Tyr97 in the WT and W59F mutant sterically affects the movement of Tyr99, whilst the smaller van der Waal's radius of Phe97 in the Y97F mutant FD is less sterically hindering.

The binding affinity of FMN was qualitatively studied in azoreductase from *Enterococcus faecalis* with an index of drugscore.[46] Zhou *et al.*[47] calculated the decomposition free energy per residue of FMN (4.35 kcal / mol) as one of the amino acid residues in chorismate synthase from *Shigella flexneri*. In the four FD-*DvMF* variants studied here the decomposition free energy per residue of FMN were significantly higher at 18.0, 17.7, 16.6 and 13.6 kcal / mol in the DM, WT, W59F and Y97F variants, respectively.

In the present work, we first systematically investigated the molecular interactions of FMN with the protein parts in the four FD-*DvMF* variants, by means of MM-PBSA. The order of both the decomposition free energy per residue and the binding free energy of FMN were Y97F > WT > W59F > DM. The decomposition free energy per residue equates to the stabilization energy upon the binding of an amino acid into a loop, and was by far the highest in the 10-loop region. Thus, the amino acid residues of the 10-loop region of FD-*DvMF* interact with FMN the strongest of the three loops. H-bond formation between the phosphate oxygen atoms and the amino acid residues in the 10-loop region could contribute to the higher interaction level with the 10-loop region. Accordingly, it is reasonable that the decomposition free energy per residue was parallel to the binding free energy of FMN among the four systems (compare the data in Tables 2.5 and 2.6). That the greatest binding free energy of FMN was seen with Y97F may be ascribed to the H-bond formation between the Trp59 of the 60-loop region and the Tyr99 of the 90-loop region, which then causes FMN to be buried the most into the protein among the four systems. H-bond energies may also contribute to the binding free energy of FMN.

The order of the numbers of water molecules accessible to FMN was W59F > DM > WT > Y97F, which does not correlate well with that for  $\langle \Delta E_{solv} \rangle_{AV}$  at Y97F > W59F > WT > DM, suggesting that water molecules near FMN and outside the protein do not contribute very much to the solvation energy.

Indeed, from the published experimental dissociation constants ( $K_d$ ) and binding free energies ( $\Delta G_{Exp}^0$ ) of FMN, RF and lumiflavin in the FDs from the related *Anabaena* PCC7119 (Table 2.7), the contribution of the phosphate group (46%) and isoalloxazine ring (47%) were the most significant factors, while the ribityl group contributed some 7%, which is in broad accord with that theoretically evaluated for FD-*Dv*MF and presented here (Table 2.5). Our results reveal a contribution of 64% from the 10-loop region (mostly interacts with the phosphate group), 10% from the 90-loop region (mostly interacts with the ribityl group), and 26% from the isoalloxazine ring. The experimental binding free energy, between FMN and apo-FD, of the corresponding mutated variants has not been determined yet. However, our results are consistent with the published data of the FD from *Anabaena* PCC7119 (Table 2.7), where the mutated FDs show a higher binding free energy or likelihood to dissociate than the WT one.[63]

Ultrafast fluorescence dynamics of the four FD-*Dv*MF variants have been investigated by means of an up-conversion method.[6] The fluorescence lifetimes of WT were shortest, because the photoinduced electron transfer takes place both from Trp59 and Tyr97 to the excited Iso. Quantitative analysis of the photoinduced electron transfer has not been performed, because the protein structures were not known. The results of the present work could enable us to quantitatively analyze the photoinduced electron transfer in FD-*Dv*MF [58] as FMN binding proteins[18, 64-65] and AppAs,[66-67] with the observed ultrafast fluorescence dynamics of four FD-*Dv*MF systems.[6]

## CHAPTER III

### ANALYSIS OF PHOTOINDUCED ELECTRON TRANSFER IN WILD TYPE FLAVODOXIN FROM *DESULFOVIBRIO VULGARIS* STRAIN MIYAZAKI F.

---

#### Analysis of Photoinduced Electron Transfer in Flavodoxin

Kiattisak Lugsanangarm<sup>a</sup>, Somsak Pianwanit<sup>a</sup>, Sirirat Kokpol<sup>a,b\*</sup>, Fumio Tanaka<sup>c\*</sup>,  
Haik Chosrowjan<sup>d</sup>, Seiji Taniguchi<sup>d</sup> and Noboru Mataga<sup>d</sup>

---

<sup>a</sup> *Department of Chemistry, Faculty of Science, Chulalongkorn University,  
Bangkok, 10330, Thailand*

<sup>b</sup> *Center of Excellence for Petroleum, Petrochemicals, and Advanced Materials, Chulalongkorn  
University, Bangkok, 10330, Thailand*

<sup>c</sup> *Department of Biochemistry, Center for Excellence in Protein Structure and Function,  
Faculty of Science, Mahidol University, Bangkok, 10400, Thailand*

<sup>d</sup> *Division of Laser BioScience, Institute for Laser Technology, Utsubo-Honmachi, 1-8-4,  
Nishiku, Osaka 550-0004, Japan*

### 3.1 ABSTRACT

Flavodoxin (FD) from *Desulfovibrio vulgaris*, strain Miyazaki F., is a small flavoprotein that is considered to function in the transport of electrons between proteins. The observed fluorescence dynamics of FD revealed two lifetime components, a major (0.92) component at 0.158 ps and a minor (0.08) one at longer than 500 ps. Photoinduced electron transfer (ET) from Trp59 and/or Tyr97 to the excited isoalloxazine (Iso\*) in FD were analyzed with atomic coordinates determined by molecular dynamic simulations (MD), the Kakitani and Mataga ET theory and the observed fluorescence dynamics with and without the minor longer decay component. The observed fluorescence decay with its long tail was not satisfactorily reproduced by the present method. We interpreted the longer lifetime component to be free flavin mononucleotide (FMN) liberated from the protein. The ET rate was faster from Trp59 to Iso\* than that from Tyr97 to Iso\*, despite the fact that the donor-acceptor distance was shorter in Tyr97 – Iso\* (mean 0.54 nm) than in Trp59 – Iso\* (mean 0.64 nm), as elucidated by means of electrostatic (*ES*) energy. Interactions in the Trp59 - Iso\* - Tyr97 system were quantum chemically studied using the conformations extracted from 46 MD snapshots at 40 ps time intervals with a PM6 semi-empirical molecular orbital (MO) method of the conformations. Dipole moments of the systems were mostly much greater than that of Iso\* alone, and its directions were from Iso\* to Trp59. MO analyses revealed that charge transfer takes place mostly from Trp59 to Iso\*, which is in accordance with the ET analysis. Correlations between interaction energies and charge density were also examined. Absolute value of the energy increased with amount of the charge transferred.

### 3.2 INTRODUCTION

Flavoproteins play an important role in oxidation-reduction reactions in all living organisms as mammals, plants and microorganisms.[68] Some flavoproteins function as photoreceptors.[69-72] Photoinduced electron transfer (ET) in these flavin photoreceptors is the first step of their functions. Various electron transfer theories have been modeled for bulk solutions.[16, 73-75] However, it is not clear whether these theories are applicable to ET in proteins. It has been difficult to quantitatively analyze ET in proteins, because the microenvironment around the ET donor and acceptor are heterogeneous, and ET theories in

proteins contain several unknown parameters. We have quantitatively analyzed ET in flavoproteins, from their time-resolved fluorescence and molecular dynamic simulations (MD) with an ET theory.[18, 64, 66-67]

Flavodoxins (FD) are a group of small flavoproteins with a molecular weight of 15-23 kDa, that have been isolated from a variety of microorganisms. Flavodoxins are considered to function as electron transport proteins in various metabolic pathways.[22-23, 76] They contain a single molecule of non covalent-bound flavin mononucleotide (FMN) as the reaction center. The FD from *Desulfobivrio vulgaris*, strain Miyazaki F., was first characterized by Kitamura *et al.*[4] Revealing that the dissociation constant of FMN from FD was 0.38 nM, and its redox potentials were  $E_1 = -434$  mV for the oxidized-semiquinone reaction and  $E_2 = -151$  mV for the semiquinone-2-electron reduced reaction.

The three dimensional structure of FD has not been experimentally determined yet, so we obtained the potential structure of the FD by means of homology modeling method (unpublished work). According to this structure, the FD isoalloxazine ring (Iso) is sandwiched by the Tyr97 and Trp59 residue, which is reassuringly similar to that reported for the FD from *Desulfobivrio vulgaris*, Hildenborough.[35]

The fluorescence dynamics of wild type (WT), Y97F (Tyr97 is replaced by Phe), W59F (Trp59 is replaced by Phe), and the double mutants W59F-Y97F (DM) were measured in the sub-picoseconds time domain by means of the fluorescence up-conversion method by Mataga *et al.*[6] These ultra-short lifetimes are considered to have been induced by ET from the aromatic amino acids to the excited isoalloxazine (Iso\*).[25, 27-28, 77] The observed fluorescence dynamics of the WT FD contains two lifetime components, 0.158 ps (0.92) and longer than 500 ps (0.08). The longer lifetime component was interpreted as being due to FMN liberated from the FD,[32-33] even though the dissociation constant is very low (0.38 nM).[4]

It is required to establish a method to analyze ET mechanism in proteins. To contribute to it, we have investigated ET mechanism in FD from the fluorescence dynamics and also charge transfer interaction in Trp59 - Iso\* - Tyr97 systems with a semi-empirical molecular orbital method (MO).

### 3.3 METHOD

#### 3.3.1 Homology modeling and MD calculation

The three dimensional structure of FD has not yet been determined by X-ray diffraction method or NMR spectroscopy. Therefore, we deduced its likely structure by means of homology modeling [44] using the Modeller module of the Discovery Studio 2.0 (Website, <http://www.discoverystudios.com>). MD calculations were performed using the Amber 10 software package,[51] as described elsewhere.[18, 64, 66-67] In addition, a total of 5760 water molecules were added to complete the system.

#### 3.3.2 ET theory

The original Marcus ET theory [73] has been modified in the various ways.[16, 74-75] In the present analysis the Kakitani and Mataga (KM) theory [16] was used, because it has given satisfactory results for static ET analyses in several flavoproteins,[32-33] and dynamic ET analyses in FMN-bp [18, 66] and AppA.[66-67] The ET rate as described by KM theory [16] is expressed by Eq. 3.1.

$$k_{ET}^j = \frac{\nu_0^q}{1 + \exp\{\beta^q(R_j - R_0^q)\}} \sqrt{\frac{k_B T}{4\pi\lambda_s^{qj}}} \exp\left[-\frac{\{\Delta G_q^0 - e^2 / \varepsilon_0 R_j + \lambda_s^{qj} + ES_j\}^2}{4\lambda_s^{qj} k_B T}\right] \quad (3.1)$$

where  $k_{ET}^j$  is the ET rate from a donor  $j$  to Iso\*, and the index  $q$  denotes Trp or Tyr.  $\nu_0^q$  is an adiabatic frequency,  $\beta^q$  ET process coefficient.  $R_j$  and  $R_0^q$  are the donor  $j$ -Iso distance and its critical distance for the ET process, respectively.  $R_j$  was expressed as a center-to-center (Rc) distance rather than an edge-to-edge distance.[18, 32-33, 64, 66-67] The ET process is adiabatic when  $R_j < R_0^q$ , and non-adiabatic when  $R_j > R_0^q$ . The terms  $k_B$ ,  $T$  and  $e$  are the Boltzmann constant, temperature and electron charge, respectively.  $ES_j$  is the electrostatic ( $ES$ ) energy, which is described in Eq. 3.5 below.

The solvent reorganization energy ( $\lambda_s^{qj}$ ) is [73] of the ET donor  $q$  and  $j$ , is expressed as Eq. 3.2.

$$\lambda_S^{qi} = e^2 \left( \frac{1}{2a_{Iso}} + \frac{1}{2a_q} - \frac{1}{R_j} \right) \left( \frac{1}{\varepsilon_\infty} - \frac{1}{\varepsilon_0} \right) \quad (3.2)$$

where  $a_{Iso}$  and  $a_q$  are the radii of Iso and Trp or Tyr when these reactants are assumed to be spherical, and  $\varepsilon_\infty$  and  $\varepsilon_0$  are the optical and static dielectric constants, respectively. The optical dielectric constant used in this study was 2.0. The radii of Iso, Trp and Tyr were determined as before,[18, 32-33, 64, 66-67] with the value of  $a_{Iso}$ ,  $a_{Trp}$  and  $a_{Tyr}$  being 0.224, 0.196 and 0.173 nm, respectively.

The standard free energy change was expressed with the ionization potential of the ET donor,  $E_{IP}^q$ , as shown in Eq. 3.3.

$$\Delta G_q^0 = E_{IP}^q - G_{Iso}^0 \quad (3.3)$$

$G_{Iso}^0$  is the standard Gibbs energy related to electron affinity of Iso\*. The values of  $E_{IP}^q$  for Trp and Tyr were 7.2 eV and 8.0 eV, respectively.[78]

### 3.3.3 Electrostatic Energy in the Protein

Protein systems contain many ionic groups, which may have an influence upon the ET rate. FD contains Iso as the ET acceptor and the potential ET donors as Trp16, Trp59, Tyr97 and Tyr99. In term of charged residues, FD has 12 Glus, 15 Asps, 2 Lyss, 8 Args amino acid residues plus two negative charges at the FMN phosphate. The *ES* energy between the Iso anion or donor cation and these ionic groups in the protein is expressed by Eq. 3.4.

$$E(j) = \sum_{i=1}^{12} \frac{C_j \cdot C_{Glu}}{\varepsilon_0 R_j (Glu - i)} + \sum_{i=1}^{15} \frac{C_j \cdot C_{Asp}}{\varepsilon_0 R_j (Asp - i)} + \sum_{i=1}^2 \frac{C_j \cdot C_{Lys}}{\varepsilon_0 R_j (Lys - i)} + \sum_{i=1}^8 \frac{C_j \cdot C_{Arg}}{\varepsilon_0 R_j (Arg - i)} + \sum_{i=1}^2 \frac{C_j \cdot C_P}{\varepsilon_0 R_j (P - i)} \quad (3.4)$$

The values of  $j = 0$  for the Iso anion, and  $j = 1$  for Trp16<sup>+</sup>,  $j = 2$  for Trp59<sup>+</sup>,  $j = 3$  for Tyr97<sup>+</sup> and  $j = 4$  for Tyr99<sup>+</sup>.  $C_j$  is charge of the aromatic ionic species  $j$ , and is equal to  $-e$  for  $j = 0$  and  $+e$  for  $j = 1$  to 4. Thus,  $C_{Glu} (= -e)$ ,  $C_{Asp} (= -e)$ ,  $C_{Lys} (= +e)$ ,  $C_{Arg} (= +e)$  and  $C_P (= -e)$

are the charges of Glu, Asp, Lys, Arg and phosphate anions, respectively. We assumed that these groups are all in an ionic state in solution. The distances between the aromatic ionic species  $j$  and the  $i$ -th Glu ( $i = 1 - 12$ ) are denoted as  $R_j(\text{Glu} - i)$ , while that between the aromatic ionic species  $j$  and the  $i$ -th Asp ( $i = 1 - 15$ ) are denoted as  $R_j(\text{Asp} - i)$ , and so on.

$ES_j$  in Eq. 3.5 was expressed as follows:

$$ES_j = E(0) + E(j) \quad (3.5)$$

Here  $j$  has values from 1 to 4, and represents the  $j$ th ET donor as described above.

### 3.3.4 Fluorescence Decays

The observed fluorescence decay of FD has been reported by Mataga *et al.*, [6] and we used two kind decays as the observed fluorescence decay. The first one is derived from the experimentally observed decay and is evaluated as shown in Eq. 3.6.

$$F_{obs}(t) = 0.92 \exp(-t/0.158) + 0.08 \exp(-t/500) \quad (3.6)$$

where the lifetimes are indicated in unit of ps.

However, the decay was also alternatively evaluated as shown in Eq. 3.7, where the minor component with a lifetime of greater than 500 ps was neglected, since this was interpreted as being due to free FMN dissociated from the protein. [32-33]

$$F_{obs}(t) = \exp(-t/0.158) \quad (3.7)$$

The calculated fluorescence decay is expressed as Eq. 3.8.

$$F_{calc}(t) = \left\langle \exp - \left\{ \sum_{j=1}^4 k_{ET}^j(t') \right\} t \right\rangle_{AV} \quad (3.8)$$



Fluorescence decays were calculated up to 2 ps with time intervals of 0.002 ps, since the decay was measured in this time range.[6] Note that  $\langle \dots \rangle_{AV}$  means the averaging procedure of the exponential function in Eq. 3.8 over  $t'$  up to 2 ns with 0.1 ps time intervals. In addition, Eq. 3.8 assumes that the decay function at every instant of time,  $t'$ , during the MD time range can be always expressed by the exponential function. The present method is mathematically equivalent to the one by Henry and Hochstrasser,[34] when the time range (2 ns) of MD data is much longer than one (2 ps) of fluorescence data, as described in the **Supplemental Information of Chapter III**.

The unknown ET parameters ( $\nu_0^q$ ,  $\beta^q$ , and  $R_0^q$  for Trp and Tyr,  $G_{iso}^0$  and  $\varepsilon_0$ ) contained in the KM theory were determined so as to obtain the minimum value of  $\chi^2$ , defined by Eq. 3.9, by means of a non-linear least squares method, according to the Marquardt algorithm, as previously reported.[18, 64, 66] These were then used to obtain the minimum value of  $\chi^2$ , as defined by Eq. 3.9.

$$\chi^2 = \frac{1}{N} \sum_{i=1}^N \frac{\{F_{calc}(t_i) - F_{obs}(t_i)\}^2}{F_{calc}(t_i)} \quad (3.9)$$

Here,  $N$  denotes number of time intervals of the fluorescence decay, and was 1000. Deviation between the observed and calculated intensities was expressed by Eq. 3.10.

$$Deviation(t_i) = \frac{\{F_{calc}(t_i) - F_{obs}(t_i)\}}{\sqrt{F_{calc}(t_i)}} \quad (3.10)$$

### 3.3.5 Quantum chemical calculation

Dipole moments of the Trp59-Iso\*-Tyr97 systems, of which configurations were extracted from the MD simulations. MO calculations were performed by a semi-empirical (PM6 method) with the MOPAC2009 software. The key words, EF (geometrical optimization), PRECISE (accurate calculation), PM6 (semi-empirical Hamiltonians), XYZ (geometry expressed by (x,y,z) coordinates), GEO-OK (neglect check on abnormal access of atoms), EPS (dielectric constant for COSMO solvation energy) and EXCITED (first excited singlet state to be optimized)

were used for the calculation (for details of these Keywords visit the website: <http://openmopac.net/>).

The charge densities of Trp59, Iso\* and Tyr97 were obtained as the sums of Mulliken charge of the constituent atoms in Trp59, Iso\* and Tyr97, respectively. This interaction energy (kcal / mol) of the Trp59-Iso\*-Tyr97 system was calculated by Eq. 3.11.

$$\Delta E = \Delta H_f(\text{Trp59} - \text{Iso}^* - \text{Tyr97}) - \Delta H_f(\text{Trp59}) - \Delta H_f(\text{Iso}^*) - \Delta H_f(\text{Tyr97}) \quad (3.11)$$

In Eq. 3.11  $\Delta H_f(\text{Trp59} - \text{Iso}^* - \text{Tyr97})$ ,  $\Delta H_f(\text{Trp59})$ ,  $\Delta H_f(\text{Iso}^*)$  and  $\Delta H_f(\text{Tyr97})$  were heat of formation of Trp59-Iso\*-Tyr97 system, Trp59 system, Iso\* system and Tyr97 system, respectively. The heat of formation contains the total electronic energy, the core-core repulsion energy between atoms and the heat of formation of all constituent atoms.

## 3.4 RESULTS

### 3.4.1 Geometrical factors of FD

The protein structure of FD at the FMN binding site was determined by the method of homology modeling, and is shown in Figure 3.1. Time-dependent changes in the center-to-center ( $R_c$ ) distances in the Iso\* and Tyr97, Trp59, Trp16, Tyr99 pairs are shown in Figure 3.2, while the changes in the edge-to-edge distances ( $R_e$ ) are shown in Figure 3.3. Of these aromatic amino acids Trp16 is clearly by far the furthest away from Iso, and oscillates the most over time, followed by Tyr99 as determined by both  $R_c$  and  $R_e$  values. However although both Trp59 and Tyr97 are closer, remain relatively more static over time and are somewhat close in distance from Iso to each other, interestingly they show an inversion between  $R_c$  and  $R_e$  values. Thus by  $R_c$  Tyr97 is the closet residue to Iso, while conversely by  $R_e$  it is Trp 59. Figure 3.4 shows the time-dependent changes in inter-planar angles between Iso and the aromatic amino acids, with the mean distances listed in Table 3.1. The mean  $R_c$  value between Iso and Tyr97 was 0.54 nm, which was the closest of the aromatic amino acid residues. The other  $R_c$  values between Iso and Trp59, Trp16 and Tyr97 were 0.64, 1.72 and 1.3 nm, respectively, while the corresponding values of  $R_e$  were 0.301, 0.247, 1.18 and 0.533 nm for Iso to Tyr97, Trp59, Trp16 and Tyr99, respectively. Thus,  $R_e$  was shortest in the Iso-Trp59 pair, although the shortest  $R_c$  value was

between Iso-Tyr97. This discrepancy is because Iso and Tyr97 are almost parallel as seen by the inter-planar angle. Indeed, the inter-planar angles between Iso and the aromatic amino acids were 14, -43, -18 and 24 deg in Tyr97, Trp59, Trp16 and Tyr99, respectively. The  $R_c$  between Iso and Tyr97, for instance, was the shortest and they are almost parallel in orientation.

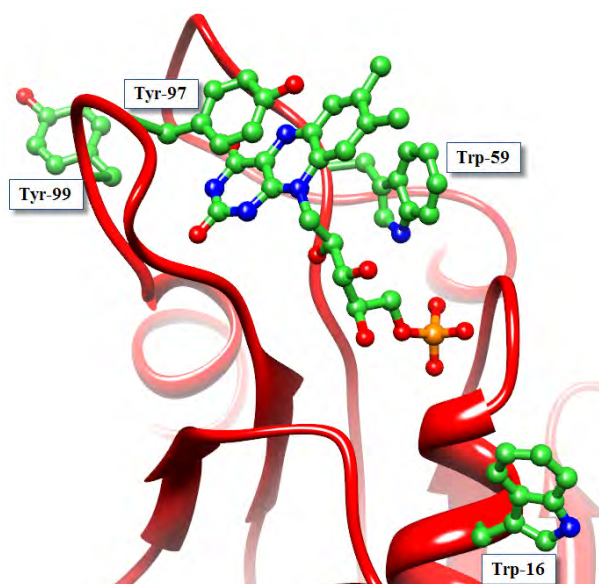


**Figure 3.1** Structure of FD obtained by a method of homology modeling.

**Table 3.1** Physical constants of Iso and aromatic amino acids <sup>a</sup>

Physical quantity	Iso	Tyr97	Trp59	Trp16	Tyr99
$Rc^b$ (nm)		0.536 $\pm 0.0009$	0.642 $\pm 0.0010$	1.72 $\pm 0.0053$	1.28 $\pm 0.0024$
$Re^c$ (nm)		0.301 $\pm 0.0015$	0.247 $\pm 0.0015$	1.18 $\pm 0.0045$	0.533 $\pm 0.0026$
Inter-planar angle (deg)		14.0 $\pm 0.05$	-42.8 $\pm 0.05$	-18.0 $\pm 0.06$	23.5 $\pm 0.07$
$ES$ energy <sup>d</sup> (eV)	2.83 $\pm 0.0006$	-2.93 $\pm 0.0009$	-2.85 $\pm 0.0006$	-0.0993 $\pm 0.0001$	-0.118 $\pm 0.0002$
$ES^e$ (eV)		-0.0942	-0.0172	2.73	2.71
ET rate <sup>f</sup> (ps <sup>-1</sup> )		(1.26 $\pm$ 0.007) $\times 10^{-3}$	7.11 $\pm$ 0.015	(5.33 $\pm$ 0.048 ) $\times 10^{-55}$	(1.15 $\pm$ 0.033) $\times 10^{-50}$

<sup>a</sup> The physical quantities were obtained taking average over MD time (2 ns) at time intervals of 0.1 ps. Mean  $\pm$  SE was shown.

<sup>b</sup> Center to center distance

<sup>c</sup> Edge to edge distance

<sup>d</sup>  $ES$  energy between Iso anion produced by ET and all ionic amino acids, between Tyr97 cation and all ionic amino acids, between Trp cation and all ionic amino acids, and so on. <sup>e</sup>  $ES$  energy given by Eq. 3.5 <sup>f</sup> ET rate given by Eq. 3.1.

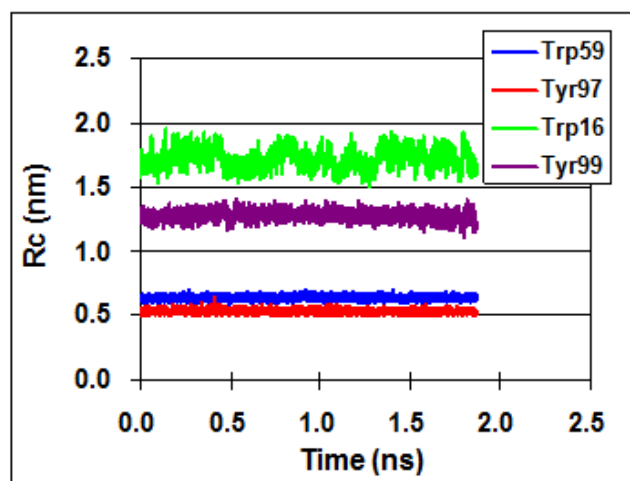


**Figure 3.2** Center to center distances between Iso and nearby aromatic amino acids in WT. Rc denotes center to center distance. Trp59, Tyr97, Trp16 and Tyr99 indicate the distances between Iso and Trp59, between Iso and Tyr97, between Iso and Trp16, and between Iso and Tyr99.

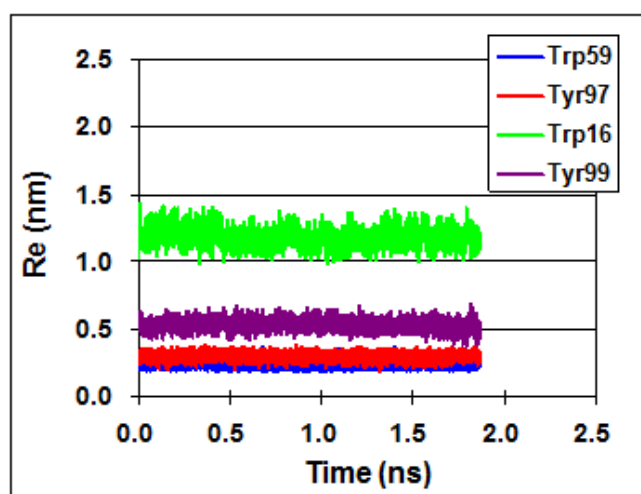


**Figure 3.3** Edge to edge distances between Iso and nearby aromatic amino acids in WT. Re denotes edge to edge distance. Trp59, Tyr97, Trp16 and Tyr99 indicate the distances between Iso and Trp59, between Iso and Tyr97, between Iso and Trp16, and between Iso and Tyr99.

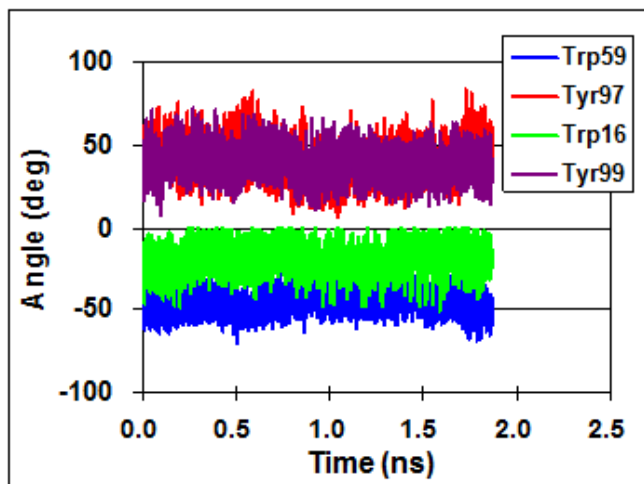
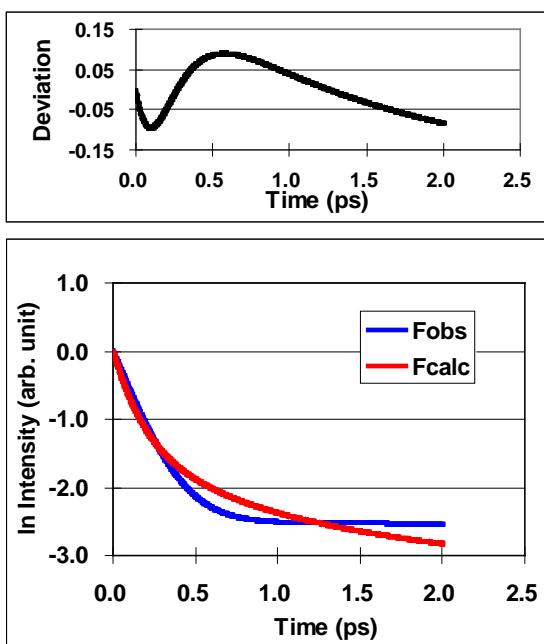


**Figure 3.4** Inter-planer angles between Iso and nearby aromatic amino acids in WT.

Trp59, Tyr97, Trp16 and Tyr99 indicate the distances between Iso and Trp59, between Iso and Tyr97, between Iso and Trp16, and between Iso and Tyr99.

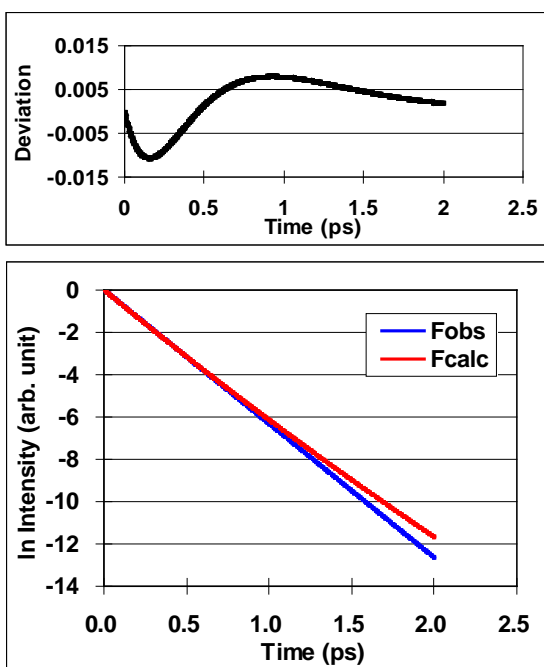
### 3.4.2 Fluorescence decays

Figure 3.5 shows the observed ( $F_{\text{obs}}$ ) and calculated ( $F_{\text{calc}}$ ) fluorescence decays of the FD. The calculated decay was obtained with the best-fit ET quantities and listed in Table 3.2. The physical quantities for Trp and Tyr, respectively, were  $\nu_0 = 2.06 \times 10^3$  and  $5.00 \times 10^2 \text{ ps}^{-1}$ ,  $\beta = 21.9$  and  $9.99 \text{ nm}^{-1}$  and  $R_0 = 0.518$  and  $0.694 \text{ nm}$ . In addition,  $G_{\text{Iso}}^0 = 7.54 \text{ eV}$  and  $\epsilon_0 = 2.16$ . The value of  $\chi^2$  was  $3.42 \times 10^{-3}$ . The agreement between the observed and calculated decays was not good, and the long tail with a fluorescent decay of more than 500 ps lifetime [6] could not be reproduced. Figure 3.6 shows fluorescence decays with Eq. 3.7 as the observed fluorescence dynamics. When the longer lifetime fluorescence decay (500 ps) was assumed to be due to free FMN dissociated from the protein and so ignored, the fluorescence decay could be evaluated with Eq. 3.7 as the observed fluorescence dynamics (Figure 3.6). The physical quantities determined with Eq. 3.7 for Trp and Tyr, respectively, were  $\nu_0 = 3.08 \times 10^3$  and  $2.46 \times 10^3 \text{ ps}^{-1}$ ,  $\beta = 55.6$  and  $9.64 \text{ nm}^{-1}$ ,  $R_0 = 0.772$  and  $0.676 \text{ nm}$ ,  $G_{\text{Iso}}^0 = 7.67 \text{ eV}$  and  $\epsilon_0 = 5.85$ . These parameters were determined by analyzing the fluorescence decays of the WT, W59F, Y97F and W59F-Y97F double mutation FD's together at once .



**Figure 3.5** Fluorescence decays of WT with two lifetime components.

The observed decay  $F_{obs}$  is given by Eq. 3.6.  $F_{calc}$  is the calculated decay and obtained with the best-fit ET quantities listed in Table 3.2. Upper panel is deviation given by Eq. 3.10 in text. The value of  $\chi^2$  was  $3.42 \times 10^{-3}$ .



**Figure 3.6** Fluorescence decays of FD

$F_{obs}$  and  $F_{calc}$  denotes the observed and calculated fluorescence intensities.

Upper panel shows deviation between the observed and calculated intensities.

**Table 3.2** Physical constants contained in KM theory <sup>a</sup>

The observed decay	Trp			Tyr			$G_{Iso}^0$ (eV)	$\epsilon_0$	$\chi^2$
	$\nu_0$ (ps <sup>-1</sup> )	$\beta$ (nm <sup>-1</sup> )	$R_0$ (nm)	$\nu_0$ (ps <sup>-1</sup> )	$\beta$ (nm <sup>-1</sup> )	$R_0$ (nm)			
Two lifetimes	2056	21.9	0.518	500	9.99	0.694	7.54	2.16	3.42 x 10 <sup>-3</sup>
Single lifetime <sup>b</sup>	3087	55.6	0.772	2455	9.64	0.676	7.67	5.85	9.55 x 10 <sup>-5</sup>

<sup>a</sup> Meanings of the physical constants are described in Eq. 3.1, and below.

<sup>b</sup> Data were taken from unpublished work.



### 3.4.3. ET rates

Figure 3.7 shows representative time-dependent changes in ET rates from Trp59, from Tyr97, from Trp16 and from Tyr99 to Iso\*. The mean ET rates are also listed in Table 3.1. The mean ET rates were  $1.26 \times 10^{-3} \text{ ps}^{-1}$  from Tyr97,  $7.11 \text{ ps}^{-1}$  from Trp59,  $5.33 \times 10^{-55} \text{ ps}^{-1}$  from Trp16, and  $1.15 \times 10^{-50} \text{ ps}^{-1}$  from Tyr99. It is noted that ET rate was fastest from Trp59, despite that the donor-acceptor distance was shortest between Iso and Tyr97 (see Table 3.1).

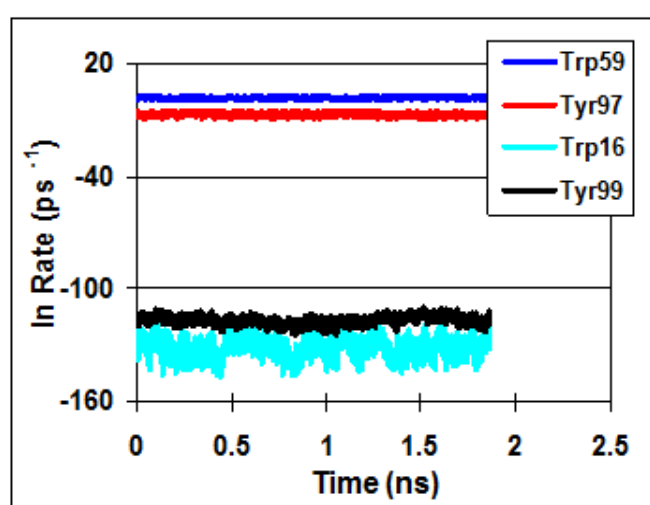


**Figure 3.7** ET rate from aromatic amino acids to Iso\* in FD

Trp59, Tyr97, Trp16 and Tyr99 indicate ET rates from these amino acids to Iso\*. ET rate is expressed in unit of  $\text{ps}^{-1}$ .

### 3.4.4 ES energy

The time-dependent changes in the ES energies are shown in Figure 3.8. The mean energies were 2.83 eV at Iso anion, -2.93 eV at Tyr97 cation, -2.85 eV at Trp59 cation, -0.099 eV at Trp16 cation, and -0.118 eV at Tyr99 cation (see Table 3.1). Net ES energy given by Eq. 3.5 are important for the ET rate (see Eq. 3.1). The values of net ES energies were -0.0942 eV for Tyr97, -0.0172 eV for Trp59, 2.73 eV for Trp16, and 2.71 eV for Tyr99.

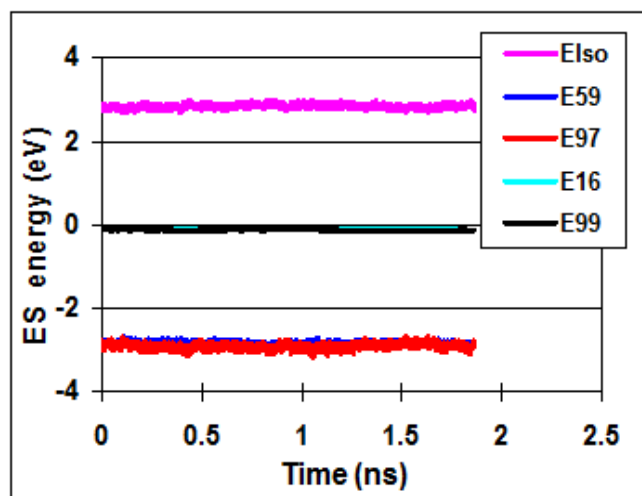


**Figure 3.8** *ES* energy between ionic species produced by ET and ionic amino acids in WT.

Eiso denotes *ES* energy between Iso anion and all ionic amino acids. E59, E97, E16 and E99 indicate electrostatic energy between aromatic cations (Trp59, Tyr97, Trp16 and Tyr99, respectively) and all ionic amino acid residues.  $\epsilon_0 = 5.85$  was used as described in text.

### 3.4.5 Dipole moment of the Trp59-Iso\*-Tyr97 system

Figure 3.9 shows a typical dipole moment of the Trp59-Iso\*-Tyr97 system, which conformation was obtained from a snapshot of the MD trajectory. The dipole moment was 22.9 D, and its direction was from Iso\* to Trp59. The COSMO solvation effect of the electronic states was introduced, using the dielectric constant value of  $\epsilon_0 = 5.85$  (see Table 3.2). The dipole moment of Iso\* alone was 12.4 D, and its direction was in the plane of Iso\*. Figure 3.10(A) shows time-dependent change in the dipole moment of Trp59-Iso\*-Tyr97 systems. Every snapshot of MD structures at 40 ps time intervals was geometrically optimized. The dipole moment changed with time from 10.4 to 32.3 D. Mean dipole moment was 22.0 D.

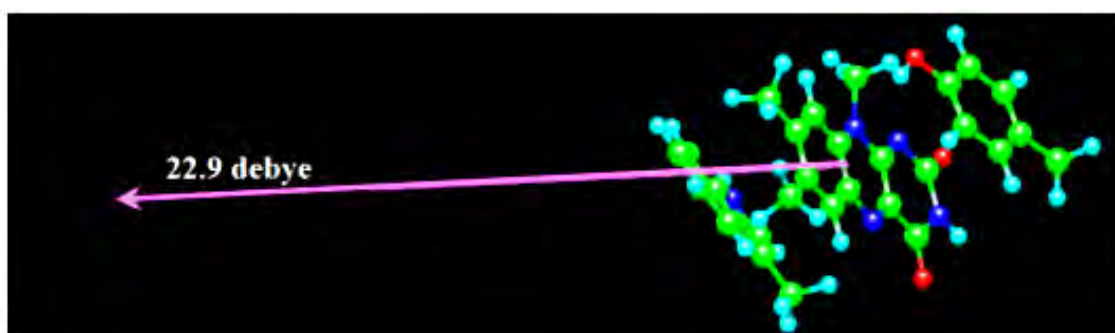
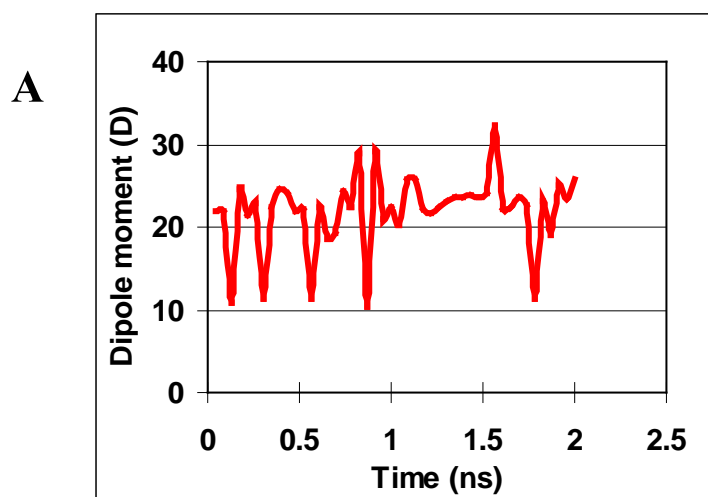


**Figure 3.9** Dipole moment in the system of Iso\*-Tyr97-Trp59 in WT FD.

Iso (center) is sandwiched by Trp59 (upper) and Tyr97 (lower). This conformation was obtained by a snapshot of MD structure, where only Iso, Trp59 and Tyr97 were extracted. The direction of the dipole moment was from Iso\* to Trp59, which shows part of charge in Trp59 transferred to Iso\*, since the direction should be in the Iso plane without charge transfer interaction between Trp59 and Iso\*.

### 3.4.6 Charge transfer interaction

In the present work the terminology “charge transfer” is used when a non-zero partial charge in any of Trp, Tyr and Iso\* is obtained by MO. Iso\* must be negatively charged after ET and Trp59/Tyr97 should be positively charged (cationic) because they will be loose an electron. Time-dependent changes in the charge densities of Trp59, Tyr97 and Iso\* are shown in Figure 3.10(B). Charge densities of Iso were always negative or zero. Mean charge density of Iso was -0.568. Charge densities of Trp59 were always positive or zero. Mean charge density of Trp59 was 0.465. Charge densities at Tyr97 were mostly zero, but sometimes displayed positive charge densities, which shows that Tyr97 can be a charge donor to Iso\* in the Trp59-Iso\*-Tyr97 system. Mean charge density of Tyr97 was 0.103. Figure 3.10(C) shows time-evolution of the interaction energy in Trp59-Iso\*-Tyr97 system, which was obtained by Eq. 3.11. The interaction energy varied from -22 kcal / mol to 15 kcal / mol. Mean interaction energy was -14.9 kcal / mol. In the six snapshots the interaction energies were positive, which implies that the interaction among Trp59, Iso\* and Tyr97 was repulsive.



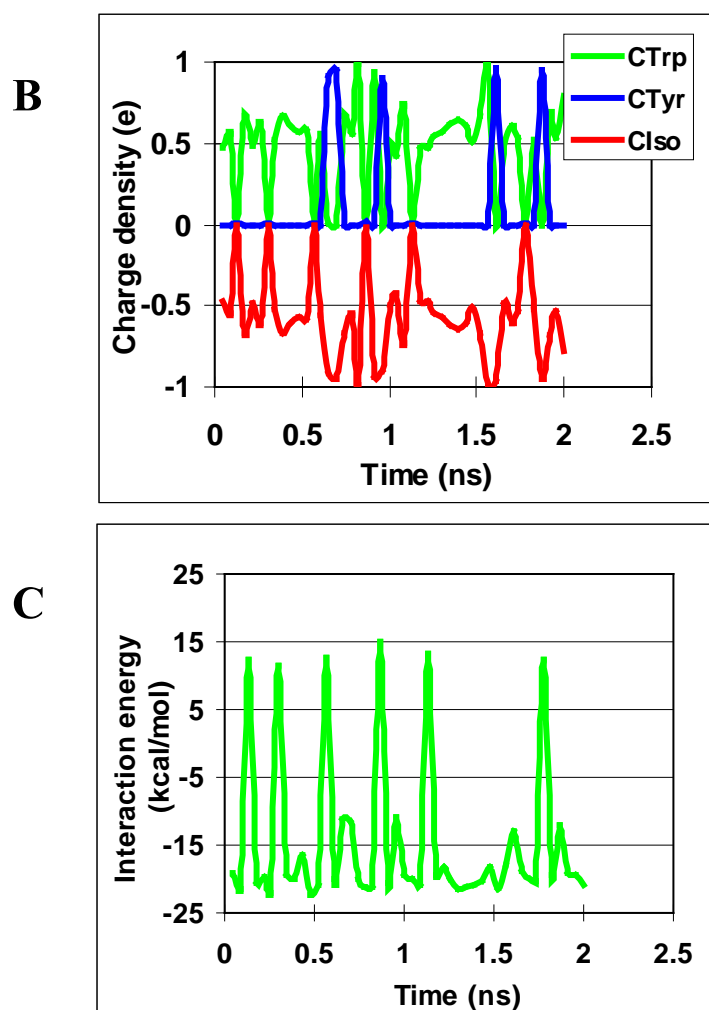
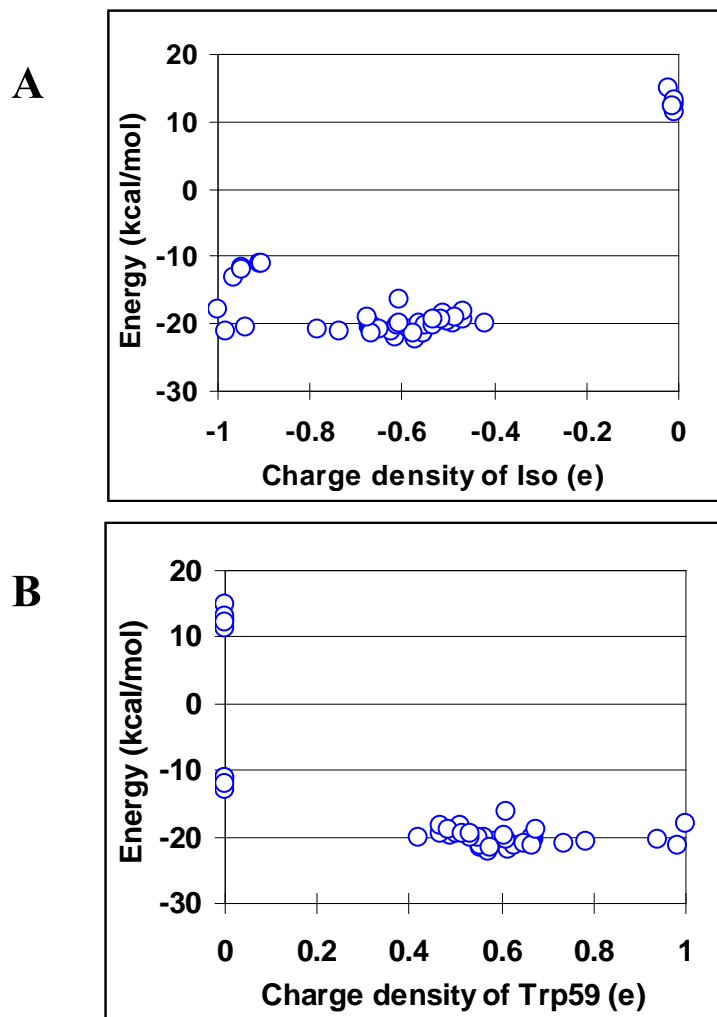


**Figure 3.10** Charge transfer and interaction energy in the system of Trp59-Iso\*-Tyr97 in WT. Dipole moment of Iso\* alone was 10.0 D, of which direction was in the plane of Iso. Interaction energy was obtained by Eq. 3.11.

### 3.4.7 Correlation

Figure 3.11(A) shows the correlation between the interaction energy and charge density at Iso\*. The interaction energy (absolute value) displayed a tendency to increase with the charge density. It is noted that the interaction energies were positive when the charge densities of Iso\* were closed to zero. Correlation between interaction energy and charge density of Trp59 is shown in Figure 3.11(B). Interaction energy was around -20 kcal / mol, when the amount of charge densities transferred from Trp59 to Iso\* were from 0.4 to 1.0. When no charge transfer occurred, the interaction energies were around -12 kcal / mol and around 13 kcal / mol. Even in the negative

energies no charge transfer occurred. Figure 3.11(C) shows correlation between the interaction energy and charge density of Tyr97. In Tyr97 mostly no charge transfer occurred, but about 0.95 of charge transferred from Tyr97 to Iso\* at the energy around -12 kcal / mol. When the interaction energies were positive, the charge transferred little from Tyr97 to Iso\*.



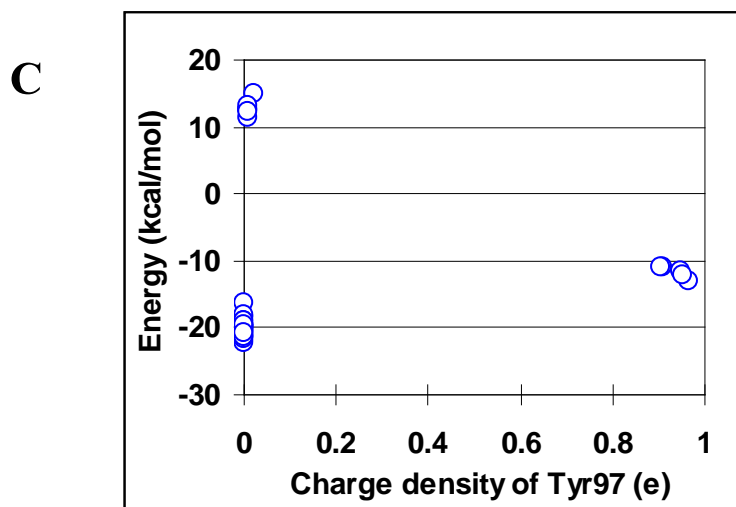


**Figure 3.11** Correlation between interaction energy and charge densities

A: Correlations between the interaction energy and charge density of Iso. B: correlation of Trp59, and C: correlation of Tyr97. Interaction energies were obtained by Eq. 3.11.

### 3.5 DISCUSSION

In the present work we have studied the dynamic properties of ET donors and acceptor in FD by MD, and analyzed the ET mechanism using the KM theory and the MD data from the observed fluorescence dynamics. Agreements between the observed and calculated fluorescence dynamics were very good, when the longer lifetime component of the observed fluorescence dynamics ( $> 500$  ps) [6] was neglected. We could not reproduce the observed fluorescence decay with the longer lifetime component by the present method of analysis. Two reasons for this are conceivable. Firstly, the sample was somehow not stable at the fluorescence measurements by an up-conversion instrument system, even though the dissociation constant of FMN is very low (0.38 nM), [4] and thereby the  $[FMN] / [FD-FMN]$  is estimated to be  $1.23 \times 10^{-3}$  at  $[FD-FMN] = 2.5 \times 10^{-4}$  M for the fluorescence measurements. If we assume that  $[FMN]$  and  $[FD-FMN]$  are proportional to amplitudes of the shorter lifetime and the longer lifetime, respectively, then  $[FMN] / [FD-FMN] = 0.087$  (9 %), [6] which is much larger than one stated above. However, these ratios cannot be compared because of the difference in experimental condition (with and without laser pulsed, [6] and [4] respectively). Therefore, if the sample of WT used for the measurements was not fresh enough, then the intense laser energy could bring the irreversible dissociation of FMN. [26] Secondly, the mathematic model (see Eq. 3.8) which assumes that the

fluorescence decays exponentially at every instant of MD time, is not valid and so the WT FD consists of two completely different conformers. We support the former interpretation (without the longer lifetime component), because we did not see the predicted conformational change of the second option in the MD snapshots in the time range of 10 ns in WT (see Figure S3.1 in **Supplemental Information of Chapter III**), and we could reasonably analyze four fluorescence decays of WT, W59F, Y97F and W59F-Y97F double mutated FDs (unpublished work).

In the present analysis the ET rate was  $7.1 \text{ ps}^{-1}$  (lifetime 0.141 ps) from Trp59 to Iso\*, and  $0.0013 \text{ ps}^{-1}$  from Tyr97 in WT. ET rate from Trp59 was ca. 6000 time faster than one from Tyr97, despite that  $R_c$  between Iso and Trp59 was longer by 0.1 nm than one between Iso and Tyr97. Experimental average lifetimes were 0.158 ps in WT, 0.808 ps in Y97F and 1.20 ps in W59F.[6] Apparently our result disagrees with the experimental data if we assume that the ET rates of Trp59 and Tyr97 in the WT FD are similar to those of Trp59 in Y97F and Tyr97 in W59F, respectively. However, this assumption is not correct, according to the results of total analyses with the four FD systems together at once (unpublished work). According to this work ET rates were  $5.40 \text{ ps}^{-1}$  (lifetime 0.185 ps) in Trp59 of Y97F and  $3.18 \text{ ps}^{-1}$  (lifetime 0.314 ps) in Tyr97 of W59F. ET rate from Trp59 was 1.3 times faster in WT compared to one in Y97F which may be due to  $ES$  energy changes, and ET rate from Tyr97 was 2400 times slower in WT compared to one in W59F. The reason why ET rates from Trp59 and Tyr97 in WT are different from those in the mutated FDs may be due to the changes in  $ES$  energy among the proteins.

MO analyses revealed that charge transfer takes place mostly from Trp59 to Iso\*, which is in accordance with the ET data. However, charge transfer occasionally occurred from Tyr97 to Iso\* (5 times among 46 snapshots), though ET rate from Tyr97 was much slower than one from Trp59. The mean interaction energy obtained by Eq. 3.11 as evaluated over 46 snapshots at 40 ps time intervals was -15 kcal / mol. The interaction energy (absolute value) was greater as the amount of transferred charge at Iso\* increased. The interaction energy, however, was not zero, even though no charge transfer takes place. The phenomena were also observed in FMN-bp system.[65] The occupied molecular orbitals calculated are delocalized between Iso\* and Trp59 or Tyr97, even though no charge transfer occurred as in FMN-bp.[79] Figure 3.12 shows the electronic delocalization between Iso\* and Tyr97 in A and between Iso\* and Trp59 in B. This suggests that electrons distribute uniformly between Iso\* and Trp59, and so apparently no charge

transfer occurred. The electronic delocalization may yield non-zero interaction energy among the chromophores.

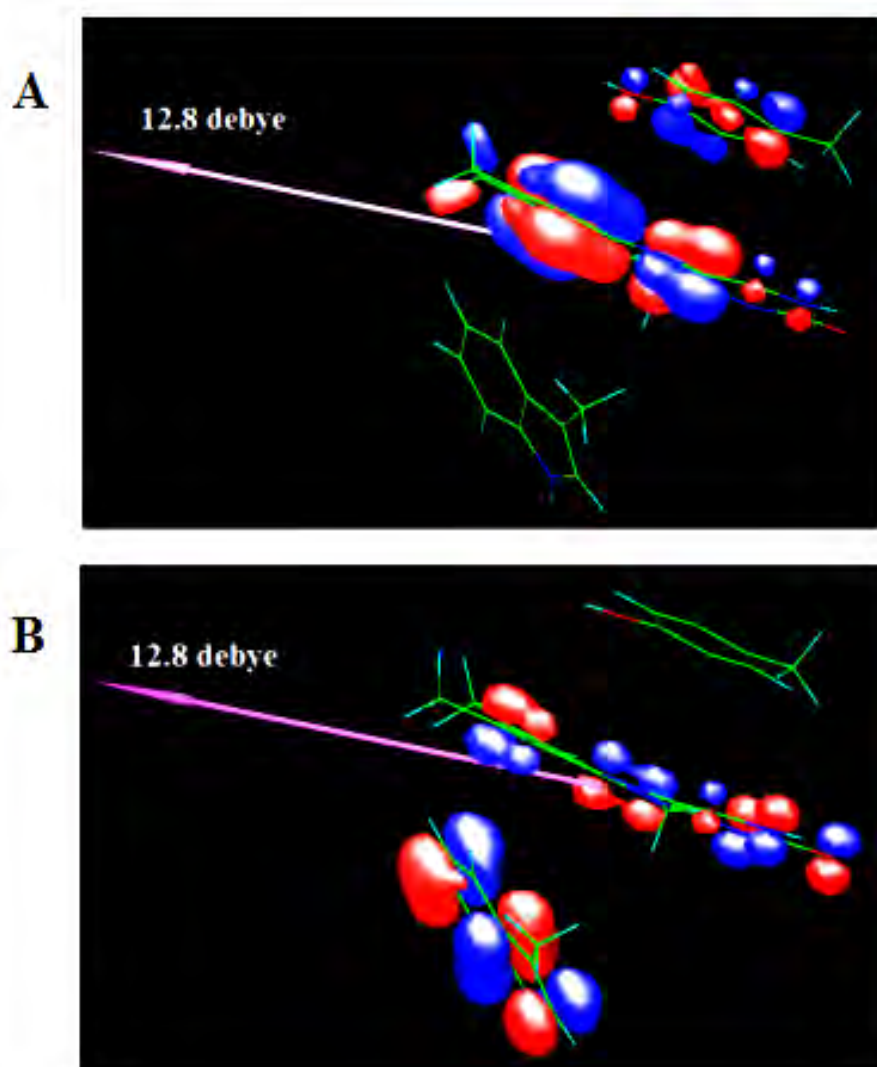


**Figure 3.12** Electronic delocalization of molecular orbitals in the configuration without appreciable charge transfer. Optimized configuration at 360 ps had low dipole moment and apparently no charge transfer took place. Panels A and B shows electronic delocalization of molecular orbitals No. 91 and 86, respectively. Orbital No. of HOMO was 94. The electronic delocalization among the three chromophores may yields the non-zero interaction energy.

It is important to consider which factors are influential upon ET rate. Effect of variation in  $\nu_0$  on ET rate is considered to be not much compared to the other factors.  $\beta$  and  $R_0$  may be influential factors on ET rate when  $R_j$  is longer than  $R_0$  (non-adiabatic process). It is not



unreasonable that factors contained in  $-\frac{\{\Delta G_q^0 - e^2 / \epsilon_0 R_j + \lambda_s^{qj} + ES_j\}^2}{4\lambda_s^{qj} k_B T}$  in exponential function (see Eq. 3.1) are important.  $R_j$  is influential through  $\lambda_s^{qj}$  and  $-e^2 / \epsilon_0 R_j$ . Effect of  $\lambda_s^{qj}$  variation on ET rate may be compensated by  $\lambda_s^{qj}$  in the denominator. Accordingly,  $\Delta G_q^0 + ES_j$  may be most important factors.  $ES_j$  varies quite a lot with time because it directly depends on the structural dynamics of the protein, while  $\Delta G_q^0$  keeps constant. Recently the effect of change in one charge was reported on ultrafast fluorescence dynamics and ET rates from Trp and/or Tyr to Iso\* in FMN-bp.[80]

Relationship between ET process and electron transfer process in dark is worthy to discuss. The donor-acceptor distance dependence of  $\lambda_s^{qj}$  and  $-e^2 / \epsilon_0 R_j$  are common in the both processes except for the distance.  $ES$  energy of Iso anion and other ionic amino acids is also common between the both electron transfer processes. Many of flavoproteins involve in electron transfer processes in dark. ET analyses of the flavoproteins could also help to understand the electron transfer in the ground state of Iso.

**CHAPTER IV**  
**GLOBAL ANALYSES OF PHOTOINDUCED ELECTRON TRANSFER IN**  
**WILD TYPE AND MUTATED FLAVODOXIN FROM *DESULFOVIBRIO***  
***VULGARIS* STRAIN MIYAZAKI F.**

---

**Photoinduced Electron Transfer in Wild Type and Mutated Flavodoxin from *Desulfovibrio***  
***vulgaris*, strain Miyazaki F.: Energy Gap Law**

**Kiattisak Lugsanangarm<sup>a</sup>, Somsak Pianwanit<sup>a</sup>, Sirirat Kokpol<sup>a,b</sup>, Fumio Tanaka<sup>c</sup>,**  
**Haik Chosrowjan<sup>d</sup>, Seiji Taniguchi<sup>d</sup> and Noboru Mataga<sup>d</sup>**

---

<sup>a</sup> *Department of Chemistry, Faculty of Science, Chulalongkorn University,*  
*Bangkok, 10330, Thailand*

<sup>b</sup> *Center of Excellence for Petroleum, Petrochemicals, and Advanced Materials, Chulalongkorn*  
*University, Bangkok, 10330, Thailand*

<sup>c</sup> *Department of Biochemistry, Center for Excellence in Protein Structure and Function,*  
*Faculty of Science, Mahidol University, Bangkok, 10400, Thailand*

<sup>d</sup> *Division of Laser BioScience, Institute for Laser Technology, Utsubo-Honmachi, 1-8-4,*  
*Nishiku, Osaka 550-0004, Japan*

---

**This article has been published in Journal: Journal of Photochemistry Photobiology A:**  
**Chemistry. Page 32-41. Volume: 219, Issue 1, Year: 2011**

---

#### 4.1 ABSTRACT

Time-dependent changes in the geometrical factors near the isoalloxazine (Iso) residue of FMN in three mutant isoforms [Y97F, W59F and W59F-Y97F (DM, double mutation)] of the flavodoxin (FD) from *Desulfovibrio vulgaris*, strain Miyazaki F, were obtained by molecular dynamics simulation (MD). The center to center distances from Iso to Trp59 in Y97F and to Tyr97 in W59F were 0.78 nm and 0.55 nm, respectively. The remarkable fluorescence quenching in these proteins has been explained in terms of photoinduced electron transfer (ET) from the Trp59 and/or Tyr97 residues to the excited isoalloxazine (Iso\*). The ultrafast fluorescence dynamics of the wild type (WT) and the Y97F, W59F and DM variant FDs reported by Mataga *et al.* (*J. Phys. Chem. B*, **2002**, *106*, 8917–8920), were simultaneously analyzed by the electron transfer theory of Kakitani and Mataga (KM theory) and the atomic coordinates determined by MD, according to a non-linear least squares method. Agreements between the observed and calculated decays were all very good. The obtained physical constants contained in the KM theory were, for Trp and Tyr, respectively, a frequency factor ( $\nu_0$ ) of  $3.09 \times 10^3 \text{ ps}^{-1}$  and  $2.46 \times 10^3 \text{ ps}^{-1}$ , an ET process coefficient ( $\beta$ ) of  $55.6 \text{ nm}^{-1}$  and  $9.64 \text{ nm}^{-1}$ , a critical transfer distance ( $R_0$ ) of 0.772 nm and 0.676 nm, plus a free energy related to the electron affinity of Iso\* ( $G_{Iso}^0$ ) of 7.67 eV. These constants were common to all three mutant FD systems. In contrast, the static dielectric constant depended on the FD systems, being 4.78, 4.04 and 2.28 in the Y97F, W59F and DM variant FDs, respectively. The mean ET rate to Iso\* was fastest from Trp59 in Y97F among the three systems. The total free energy gap in the FD systems was obtained as a sum of the net electrostatic (ES) energy between ion pairs and the standard free energy gap. A plot of  $\ln k_{ET} / \lambda_S$  vs.  $-\Delta G_T^0 / \lambda_S$  in all ET donors, where  $k_{ET}$  is ET rate,  $\lambda_S$  is the reorganization energy and  $\Delta G_T^0$  is the total free energy gap, revealed that  $\ln k_{ET} / \lambda_S$  can be expressed by a parabolic function of  $-\Delta G_T^0 / \lambda_S$  and the ET process in FD took place mostly in the normal region.

#### 4.2 INTRODUCTION

The electron transfer phenomena in proteins are of importance in the fields of physics, chemistry and biology.[13-14, 19] Photoinduced electron transfer (ET) plays an essential role in photosynthetic systems and photoreceptors in plants and microorganisms. In the last decade a

number of new flavin photoreceptors have been found.[30, 69, 81-98] In these BLUF (blue-light using flavin) units of the flavin photoreceptors, Trp and/or Tyr residues exist near isoalloxazine (Iso), and ET from Tyr to the excited isoalloxazine (Iso\*) is considered to be the first step of the bacterial photo-regulation of photosynthesis. DNA photolyase and cryptochrome also contain flavins.[99] Femtosecond dynamics of DNA photolyase has been investigated by a transient absorption spectroscopy.[100-101]

Most flavoproteins other than flavin photoreceptors contain the aromatic amino acids Trp and Tyr near the Iso residue. These flavoproteins are practically non-fluorescent, but they emit fluorescence with a very short lifetime upon excitation with a sub-picosecond light pulse.[6, 29, 31-33, 42, 102] This remarkable fluorescence quenching is ascribed to ultrafast ET from the Trp and / or Tyr residues to the Iso\*.[25, 27-28, 77] Since the seminal work on electron transfer theory by Marcus,[13, 73-74] many researchers have further developed the theory of ET.[16, 75, 103-106] However, these theories have been modeled for ET in bulk solution. It is not clear whether they are applicable to ET in proteins, where a reliable method to quantitatively analyze ET in proteins is still required.

In the previously work, the differences in the fluorescence lifetimes between Y97F and W59F were elucidated by means of ET donor-acceptor distances of a static FD structure via X-ray crystallography [35] from *Desulfovibrio vulgaris*, Hildenborough.[6] However, we can not obtain a non-exponential decay of the flavoproteins by this method. Accordingly, we believe that the dynamic analysis with dynamic structures is more reliable for ET rate and the understanding of fluorescence dynamics. Therefore, we have developed the method to analyze ET in proteins by using the atomic coordinates determined by MD simulations, Kakitani and Mataga (KM) theory, and experimental fluorescence dynamics.[18, 64, 66-67] By using this approach for FMN binding protein (FBP) and AppA, the following conclusions on ET in flavoproteins have been derived; 1) a non-exponential decay can be reproduced when the time over (MD time) which the simulation is run exceeds the experimental decay time, 2) The electrostatic ( $ES$ ) energy between the ionic ET products and other ionic amino acids are influential upon the ET rates, 3) Trp and Tyr as ET donors have different ET parameters in KM theory as standard free energy gap ( $\Delta G^0$ ), frequency factor ( $\nu_0$ ), ET process coefficient ( $\beta$ ) and critical distance ( $R_0$ ), which will be described later, and 4) the static dielectric constant depends on the protein systems, which should be the local

dielectric constant near the ion pair. However, these characteristics of ET in proteins were obtained from only a few flavoprotein systems and so it is very important to apply the present method for many more flavoproteins, in order to test its general applicability and usefulness.

Here, the ultrafast fluorescence dynamics of WT (wild type), Y97F (Tyr97 is replaced by Phe), W59F (Trp59 is replaced by Phe) and DM (double mutation, both of Trp59 and Tyr97 are replaced by Phe) flavodoxin (FD) systems are analyzed simultaneously to obtain a precise feature of the ET mechanism in FD, and to further verify the validity of the method. The mechanism of ET in FD was compared to those in FBP [18, 64] and the flavin photoreceptor of AppA.[66-67]

## 4.3 METHOD

### 4.3.1 Protein Structures and Dynamic of the WT, Y97F, W59F and DM variant FDs

X-ray crystallography and or NMR based determination of the structure of FD is not available yet and so the structure of these systems were approximated by a homology modeling technique (unpublished work). In the present work, all systems are calculated for 5 ns. We found that all systems reached equilibrium, by RMSD analysis, after 3ns as shown in Figure S4.1 (Supplemental Information of Chapter IV). Therefore, we collected MD coordinate for analysis from 3-5 ns (net 2 ns).

### 4.3.2 ET Theory

KM theory was used for the analyses, because it explains the distance-dependent average ET rates of flavoproteins [33] and the fluorescence decays of FBP very well.[18] The ET rate by KM theory[16, 105-106] is expressed by Eq. 4.1;

$$k_j^i(t) = \frac{\nu_0^q}{1 + \exp\{\beta^q(R_j^i - R_0^q)\}} \sqrt{\frac{k_B T}{4\pi\lambda_j^i(t)}} \exp\left[-\frac{\{\Delta G_q^0 - e^2 / \epsilon_0^j R_j^i(t) + \lambda_j^i(t) + ES_j^i(t)\}^2}{4\lambda_j^i(t)k_B T}\right] \quad (4.1)$$

where  $i$  is the donating aromatic amino acid in the ET, such as Trp59, Tyr97, Tyr99 and Trp16,  $j$  denotes the FD system as WT, Y97F, W59F or DM variants and  $q$  denotes Trp or Tyr. In

Eq. 4.1, time-dependent variables,  $R_j^i(t')$ ,  $\lambda_j^i(t')$  and  $ES_j^i(t')$ , where  $t'$  is MD time, are explicitly indicated, but  $(t')$  parts of these variables were omitted in text.  $\nu_0^q$  is an adiabatic frequency of Trp or Tyr,  $\beta^q$  is a coefficient of the ET process for Trp or Tyr.  $R_0^q$  is a critical donor-acceptor distance between adiabatic and non-adiabatic ET.  $R_j^i$  is the distance between the Iso and the donor amino acid  $i$  in the FD system  $j$ , expressed as a center to center ( $R_c$ ) distance. The ET process is adiabatic when  $R_j^i < R_0^q$ , and non-adiabatic when  $R_j^i > R_0^q$ .  $ES_j^i$  is the net  $ES$  energy between the Iso anion or a donor cation and all other ionic groups in the FD system  $j$ , which will be described later.  $\epsilon_0^j$  is a static dielectric constant of the FD system  $j$ .  $k_B$ ,  $T$  and  $e$  are the Boltzmann constant, temperature and electron charge, respectively.  $\lambda_j^i$  is the solvent reorganization energy [33] of a donor  $i$  in the FD system  $j$  and is expressed in Eq. 4.2;

$$\lambda_j^i = e^2 \left( \frac{1}{2a_1} + \frac{1}{2a_2} - \frac{1}{R_j^i} \right) \left( \frac{1}{\epsilon_\infty} - \frac{1}{\epsilon_0^j} \right) \quad (4.2)$$

where  $a_1$  and  $a_2$  are the radii of the acceptor and donor, assuming these reactants are spherical. The optical dielectric constant ( $\epsilon_\infty$ ) used was 2.0. The radii of Iso, Trp and Tyr were determined in the following way: (1) The three dimensional sizes of lumiflavin for Iso, 3-methylindole for Trp, and *p*-methylphenol for Tyr were obtained by the semi-empirical molecular orbital method (PM3). (2) The volumes of these molecules were determined as asymmetric rotors. (3) Radii of the spheres having the same volumes of the asymmetric rotors were obtained. The value of  $a_1$  of Iso was 0.224 nm, and those of  $a_2$  for Trp and Tyr were 0.196 nm and 0.173 nm, respectively.

The standard free energy change was expressed with the ionization potential of the ET donor,  $E_q^{IP}$ , as in Eq. 4.3;

$$\Delta G_q^0 = E_q^{IP} - G_{Iso}^0 \quad (4.3)$$

where  $G_{Iso}^0$  is the standard Gibbs energy related to electron affinity of Iso\*. The  $E_q^{IP}$  values for Trp and Tyr were 7.2 and 8.0 eV, respectively, used in this analysis.

### 4.3.3 ES Energy in the Proteins

Protein systems contain many ionic groups, which may influence the ET rate. The *ES* energy between all ionic groups in the FD system  $j$ , including the phosphate anions of FMN, and Iso anion [ $ES_j(Iso)$ ], Trp59<sup>+</sup> [ $ES_j(Trp59)$ ], Tyr97<sup>+</sup> [ $ES_j(Tyr97)$ ], Tyr99<sup>+</sup> [ $ES_j(Tyr99)$ ] and Trp16<sup>+</sup> [ $ES_j(Trp16)$ ], are expressed by Eq. 4.4, respectively. FD contains 12 Glus, 15 Asps, 2 Lyss and 8 Args residues plus two negative charges at the FMN phosphate.

$$ES_j(w) = \sum_{i=1}^{12} \frac{C_w \cdot C_{Glu}}{\epsilon_0^j R_j^w(Glu-i)} + \sum_{i=1}^{15} \frac{C_w \cdot C_{Asp}}{\epsilon_0^j R_j^w(Asp-i)} + \sum_{i=1}^2 \frac{C_w \cdot C_{Lys}}{\epsilon_0^j R_j^w(Lys-i)} + \sum_{i=1}^8 \frac{C_w \cdot C_{Arg}}{\epsilon_0^j R_j^w(Arg-i)} + \sum_{i=1}^2 \frac{C_w \cdot C_P}{\epsilon_0^j R_j^w(P-i)} \quad (4.4)$$

In Eq. 4.4, any of Iso, Trp59, Tyr97, Trp16 and Tyr99 were represented by  $w$ .  $C_{Iso}$  is the charge of the Iso anion and is equal to  $-e$ .  $C_{Trp59}$ ,  $C_{Tyr97}$ ,  $C_{Trp16}$  and  $C_{Tyr99}$  are the charges of the Trp59, Tyr97, Trp16 and Tyr99 cations, respectively, and are all equal to  $+e$ .  $C_{Glu}$  and  $C_{Asp}$  are the charges of the Glu and Asp anions, respectively, and are equal to  $-e$ .  $C_{Lys}$  and  $C_{Arg}$  are the charges of the Lys and Arg cations, respectively, and are equal to  $+e$ .  $C_P$  is the charge of the FMN phosphate and is equal to  $-e$ . We assumed that these groups are all in an ionic state in solution since the fluorescence dynamics of the FD systems were measured in buffer solutions at pH 8. The distances between the chromophore  $w$  and  $i^{\text{th}}$  Glu ( $i = 1 - 12$ ) in the FD system  $j$  are denoted as  $R_j^w(Glu-i)$ . Here, *ES* energies were evaluated using only the ionic groups in the proteins. When *ES* energies were obtained with partial charge densities of all the atoms in the proteins, they did not differ much from those obtained with the present method.[58]

Net *ES* energies of the donor  $w$  in FD  $j$  are expressed as follows:

$$\text{For } k_j^i(t), ES_j^i = ES_j(Iso) + ES_j(i) \quad (4.5)$$

Here  $i$  represents Trp59, Tyr97, Trp16 and Tyr99 in the FD system  $j$ , respectively.

The values of *ES* energy, as given by Eq. 4.4, and, consequently, those for  $ES_j^i$ , as given by Eq. 4.5, were separately evaluated among the WT, Y97F, W59F and DM FD variants, because

the distances between the Iso anion and the ionic groups, and between the cations and ionic groups, were different among these four systems.

#### 4.3.4 Calculation of Fluorescence Decays

The observed fluorescence decays [6] of the WT, Y97F, W59F and DM systems are expressed by Eqs. 4.6 – 4.9, respectively.

$$F_{obs}^{WT}(t) = \exp(-t / \tau_1^{WT}) \quad (4.6)$$

$$F_{obs}^{Y97F}(t) = \alpha_1^{Y97F} \exp(-t / \tau_1^{Y97F}) + \alpha_2^{Y97F} \exp(-t / \tau_2^{Y97F}) \quad (4.7)$$

$$F_{obs}^{W59F}(t) = \alpha_1^{W59F} \exp(-t / \tau_1^{W59F}) + \alpha_2^{W59F} \exp(-t / \tau_2^{W59F}) \quad (4.8)$$

$$F_{obs}^{DM}(t) = \exp(-t / \tau_1^{DM}) \quad (4.9)$$

Here  $\tau_1^{WT} = 0.157$  ps,  $\tau_1^{Y97F} = 0.245$  ps ( $\alpha_1^{Y97F} = 0.85$ ),  $\tau_2^{Y97F} = 4.0$  ps ( $\alpha_2^{Y97F} = 0.15$ ),  $\tau_1^{W59F} = 0.322$  ps ( $\alpha_1^{W59F} = 0.83$ ),  $\tau_2^{W59F} = 5.5$  ps ( $\alpha_2^{W59F} = 0.17$ ),  $\tau_1^{DM} = 18$  ps. The calculated fluorescence decays of the WT and the Y97F, W59F and DM FD variants are expressed by Eqs. 4.10 – 4.13, respectively;

$$F_{calc}^{WT}(t) = \left\langle \exp \left[ - \left\{ k_{WT}^{Trp59}(t') + k_{WT}^{Tyr97}(t') + k_{WT}^{Tyr99}(t') + k_{WT}^{Trp16}(t') \right\} t \right] \right\rangle_{AV} \quad (4.10)$$

$$F_{calc}^{Y97F}(t) = \left\langle \exp \left[ - \left\{ k_{Y97F}^{Trp59}(t') + k_{Y97F}^{Tyr99}(t') + k_{Y97F}^{Trp16}(t') \right\} t \right] \right\rangle_{AV} \quad (4.11)$$

$$F_{calc}^{W59F}(t) = \left\langle \exp \left[ - \left\{ k_{W59F}^{Tyr97}(t') + k_{W59F}^{Tyr99}(t') + k_{W59F}^{Trp16}(t') \right\} t \right] \right\rangle_{AV} \quad (4.12)$$

$$F_{calc}^{DM}(t) = \left\langle \exp \left[ - \left\{ k_{DM}^{Tyr99}(t') + k_{DM}^{Trp16}(t') \right\} t \right] \right\rangle_{AV} \quad (4.13)$$

where  $k_{WT}^{Trp59}(t')$ ,  $k_{Y97F}^{Trp59}(t')$ ,  $k_{W59F}^{Tyr97}(t')$  and so on, in the calculated decays, represent the ET rates of Trp59 in WT, Trp59 in Y97F, Tyr97 in W59F, and so on, respectively. These ET rates are dependent on MD simulation time  $t'$  as shown in Eq. 4.1. In Eqs. 4.10 – 4.13,  $t'$  denotes MD time (0 – 2 ns), while  $t$  is fluorescence decay time (0 – 2 ps).

Fluorescence decays were calculated up to 2 ps with time intervals of 0.002 ps, since the decays were measured in this time range.[6]  $\langle \dots \rangle_{AV}$  represents the averaging procedure of the exponential function in Eqs. 4.10 – 4.13 over  $t'$  up to 2 ns with 0.1 ps time intervals. In Eqs. 4.10



– 4.13 we have assumed that the decay functions during the MD time ranges can always be expressed by exponential functions at every instant of time,  $t'$ . The present method is mathematically equivalent to the one by Henry and Hochstrasser,[34]when the time range (2 ns) of MD data is much longer than one (2 ps) of fluorescence data, as described in the **Supplemental Information of Chapter III.**

### 4.3.5 Determination of ET Parameters

The unknown ET parameters ( $\nu_0^{Trp}$ ,  $\nu_0^{Tyr}$ ,  $\beta^{Trp}$ ,  $\beta^{Tyr}$ ,  $R_0^{Trp}$ ,  $R_0^{Tyr}$ ,  $\varepsilon_0^{WT}$ ,  $\varepsilon_0^{Y97F}$ ,  $\varepsilon_0^{W59F}$ ,  $\varepsilon_0^{DM}$  and  $G_{Iso}^0$ ) contained in the KM theory (see Eq. 4.1) were determined so as to obtain the minimum value of  $\chi^2$ , defined by Eq. 4.14, by means of a non-linear least squares method, according to the Marquardt algorithm, as previously reported.[18, 64, 66-67]

$$\chi^2 = \frac{1}{N_{WT}} \sum_{i=1}^{N_{WT}} \frac{\{F_{calc}^{WT}(t_i) - F_{obs}^{WT}(t_i)\}^2}{F_{calc}^{WT}(t_i)} + \frac{1}{N_{Y97F}} \sum_{i=1}^{N_{Y97F}} \frac{\{F_{calc}^{Y97F}(t_i) - F_{obs}^{Y97F}(t_i)\}^2}{F_{calc}^{Y97F}(t_i)} + \frac{1}{N_{W59F}} \sum_{i=1}^{N_{W59F}} \frac{\{F_{calc}^{W59F}(t_i) - F_{obs}^{W59F}(t_i)\}^2}{F_{calc}^{W59F}(t_i)} + \frac{1}{N_{DM}} \sum_{i=1}^{N_{DM}} \frac{\{F_{calc}^{DM}(t_i) - F_{obs}^{DM}(t_i)\}^2}{F_{calc}^{DM}(t_i)} \quad (4.14)$$

where  $N_{WT}$ ,  $N_{Y97F}$ ,  $N_{W59F}$  and  $N_{DM}$  denote the number of time intervals of the fluorescence decays of the WT and the Y97F, W59F and DM FD variants, respectively, and were all 1000. Deviations of the four FD systems between the observed and calculated intensities are defined by Eq. 4.15;

$$Deviation(j;t_i) = \frac{\{F_{calc}^j(t_i) - F_{obs}^j(t_i)\}}{\sqrt{F_{calc}^j(t_i)}} \quad (4.15)$$

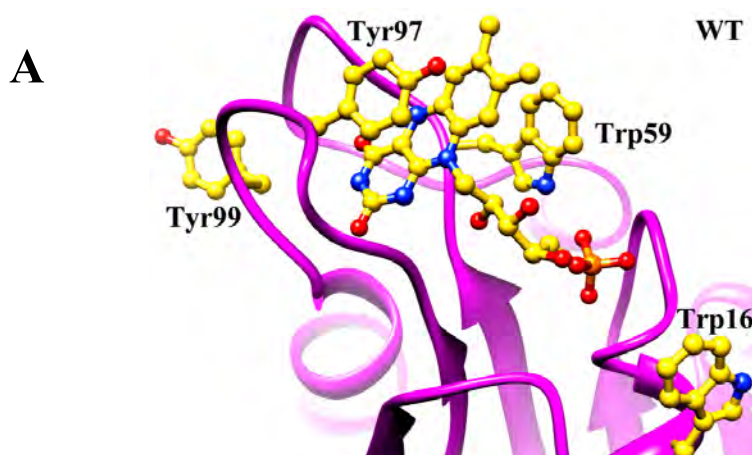
Here  $j = WT, W59F, Y97F$  and  $DM$ .

## 4.4 RESULTS

### 4.4.1 Comparison of Protein Structures around Iso among the Four FD Systems

Typical protein structures of the WT and the Y97F, W59F and DM variant FDs, as determined by homology modeling and MD, are shown in Figure 4.1. Time-dependent changes in the  $R_c$  between Iso and Tyr97, Trp59, Trp16 and Tyr99 are also shown in Figure 4.2. The changes in the mean edge to edge distances ( $R_e$ ) are shown in Figure S4.2 (**Supplemental Material of Chapter IV**).

The mean  $R_c$  and  $R_e$  values are listed in Table 4.1. The mean value of  $R_c$  between Iso and Trp59 in Y97F (0.78 nm) was significantly longer than that (0.64 nm) in the WT FD. The values of  $R_c$  for Trp16 and Tyr99 were quite different among the mutated FD variants. Thus, the  $R_c$  of Trp16 was longest (2.12 nm) in the Y97F FD and shortest (1.72 nm) in the WT, whilst for Tyr99 it was longest (1.36 nm) in W59F and shortest (1.04 nm) in Y97F. However, the values of  $R_e$  for Trp59 in Y97F and for Tyr97 in W59F were almost identical with those for Trp59 and Tyr97 in the WT. The time-dependent changes in the inter-planar angles between Iso and Trp59, Trp16 and Tyr99 in Y97F is shown in Figure S4.3 (**Supplemental Information of Chapter IV**). The time-dependent changes were remarkable in Tyr99 and Trp16. For Trp16, the angle carried from around 70 deg initially, increasing to 160 deg at 0.7 ns and then decreasing to 20 deg at 1.3 ns, while for Tyr99 it was initially around 50 deg, increased to 160 deg at 0.7 ns, decreased to 30 deg at 0.9 ns, and increased again to around 100 deg. The mean values of the angle are listed in Table 4.1. The angle between Iso and Trp59 varied considerably between Y97F (31 deg) and the WT (-43 deg), whilst



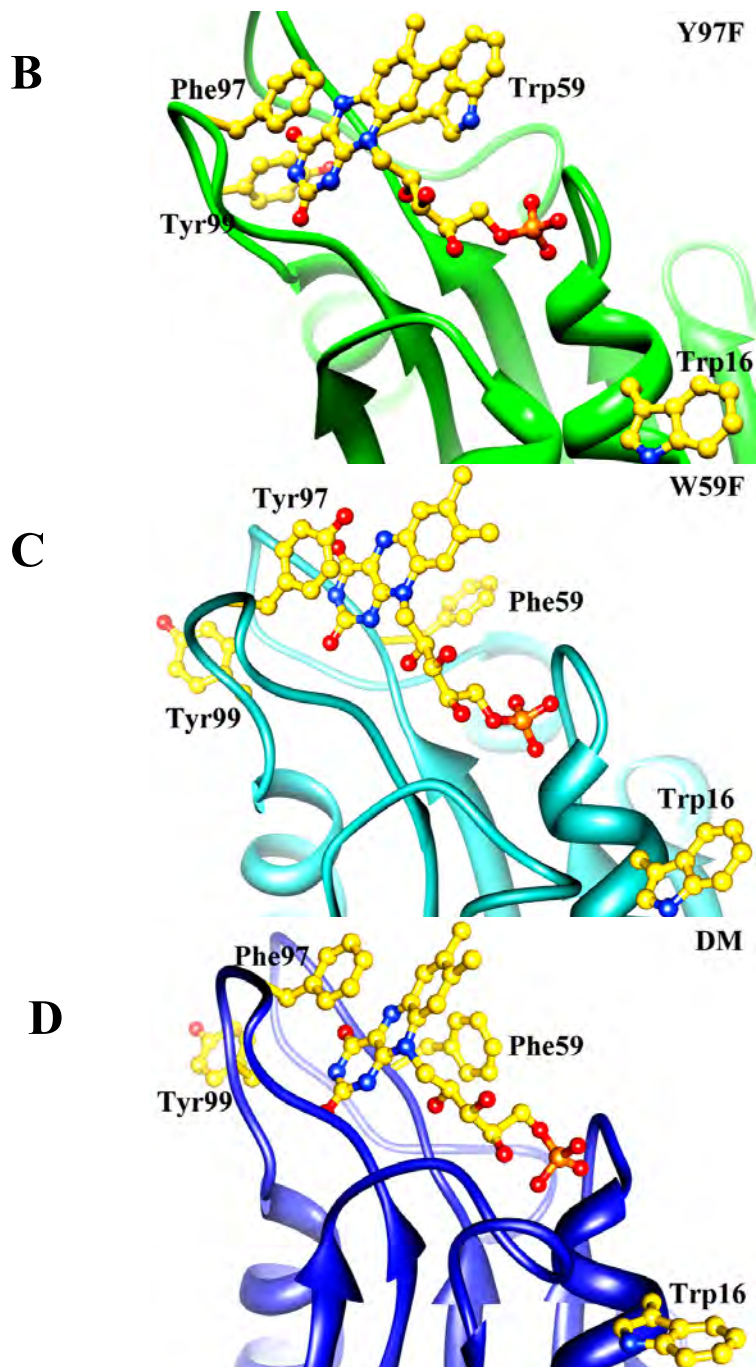


**Figure 4.1** Comparison of the protein structures among the WT and the Y97F, W59F and DM FD variants.

A: WT, B: Y97F, C: W59F and D: DM. These structures were determined by homology modeling using the X-ray structure of flavodoxin *Desulfovibrio vulgaris*, strain Hildengorough (PDB code: 1J8Q) as the template.

**Table 4.1** Geometrical factors relative to Iso in the mutated FD systems obtained by MD.<sup>a</sup>

Geometrical factor	Y97F		W59F		DM			WT <sup>b</sup>				
	Trp59	Tyr99	Trp16	Tyr97	Tyr99	Trp16	Tyr99	Trp16	Trp59	Tyr97	Tyr99	Trp16
$R_c^c$	0.78 ±	1.04 ±	2.12 ±	0.55 ±	1.36 ±	1.82 ±	1.35 ±	2.02 ±	0.64 ±	0.54 ±	1.28 ±	1.72 ±
(nm)	0.0001	0.0002	0.0003	0.0001	0.0005	0.0004	0.0005	0.0005	0.0010	0.0009	0.0024	0.0053
$R_e^d$	0.26 ±	0.34 ±	1.54 ±	0.30 ±	0.54 ±	1.39 ±	0.496 ±	1.44 ±	0.25 ±	0.30 ±	0.53 ±	1.18 ±
(nm)	0.0002	0.0005	0.0004	0.0001	0.0004	0.0004	0.0005	0.0005	0.0015	0.0015	0.0026	0.0045
Inter-planar angle(deg)	31.2 ±	61.3 ±	53.7 ±	18.6 ±	36.4 ±	-20.8 ±	-28.6 ±	30.9 ±	-42.8 ±	14.0 ±	23.5 ±	-18.1 ±
	0.13	0.25	0.22	0.07	0.08	0.08	0.09	0.14	0.05	0.05	0.07	0.06

<sup>a</sup> Mean ± SE. The means values were obtained taking an average over MD time (2 ns) with 0.1 ps time intervals. The distances and inter-planar angles are shown between Iso and the aromatic amino acids.

<sup>b</sup> Data were taken from Ref. [58].

<sup>c</sup> Center to center distance between Iso and the aromatic amino acids.

<sup>d</sup> Edge to edge distance.

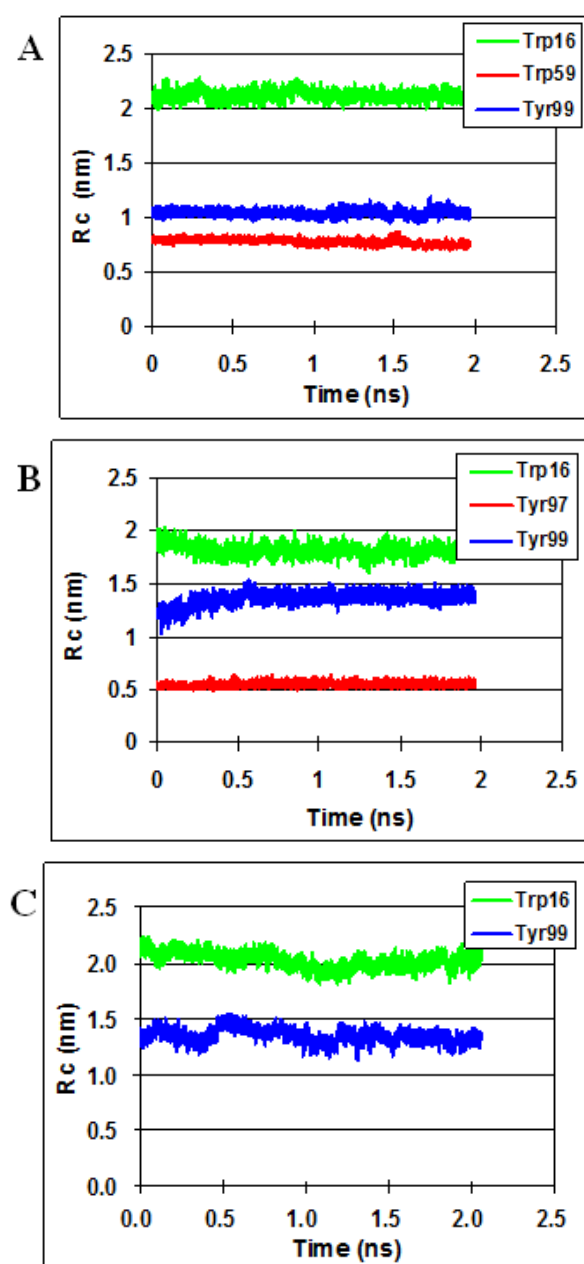


**Figure 4.2** Time-dependent changes in  $R_c$  between Iso and the aromatic amino acids.

A: Y97F, B: W59F and C: DM. Tyr97, Trp59, etc. in the inserts denote the distances between Iso and Tyr97, and between Iso and Trp59, etc., respectively.

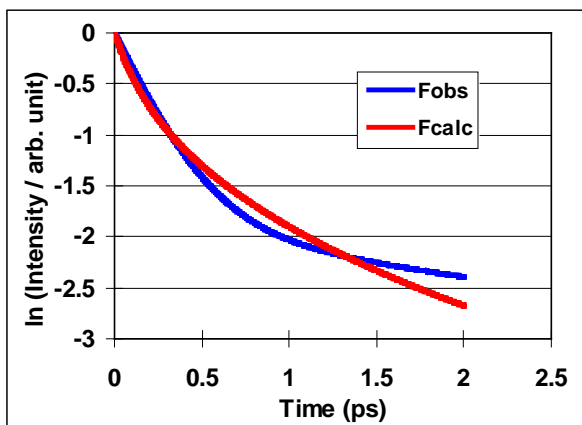
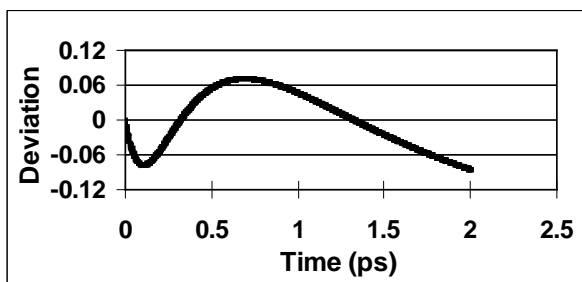
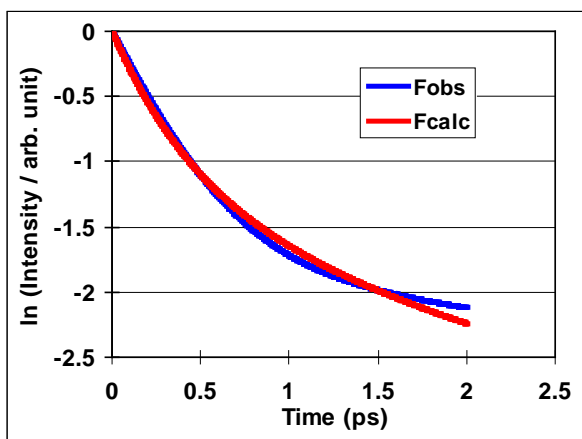
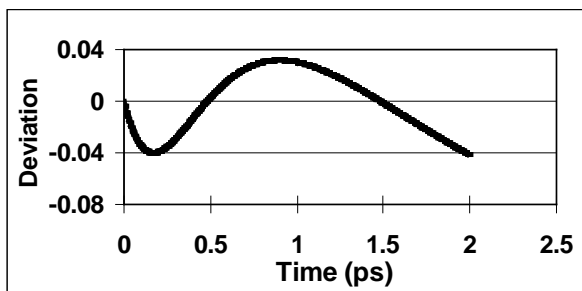
the angles between Iso and Tyr97 were similar in these systems (19 deg and 14 deg, respectively). The time-dependent changes in the inter-planar angles in the W59F and DM variants are shown in Figure S4.4 (**Supplemental Information IV**). Contrary to that seen in Y97F, the angles rapidly

fluctuate around constant values, except for Trp16 in the DM variant, which increased with time from 20 deg to 60 deg. The mean angle of Tyr97 in the W59F mutation did not differ much from that of the WT. The mean angles of Tyr99 were 61 deg in Y97F compared to -29 deg in the DM. The angles of Trp16 were 54 deg in Y97F, -21 deg in W59F and -18 deg in the WT FDs.

#### 4.4.2 Analyses of the Fluorescence Dynamics

Ultrafast fluorescence decays of the four FD systems were simultaneously analyzed with common ET parameters. Figure 4.3 shows the observed and calculated fluorescence decays of the Y97F, W59F and DM variant FDs. The upper panels of the decay plots show the deviations between the observed and calculated decays. The decays of the WT [58] and the double mutated FD were single exponential, whereas those of the Y97F and W59F variant FDs were non-exponential. It is striking that two nearly single exponential and two double-exponential decay functions were reproduced with the same ET parameters (Table 4.2) of  $\nu_0^q$ ,  $\beta^q$ ,  $R_0^q$  and  $\Delta G_q^0$  ( $q = \text{Trp or Tyr}$ ), despite that all of fluorescence decay exponentially before taking average over MD time range. It is reasonable to assume that the dielectric constant near the ET donor and acceptor ions depends on the FD systems, because the polarity near the Iso\* anion is different among the four FD systems.

If we consider that four decays were simultaneously analyzed with common parameters as  $\nu_0^q$ ,  $\beta^q$  and  $R_0^q$  ( $q = \text{Trp or Tyr}$ ) and also the intensities are expressed in logarithm, agreements between the observed and calculated decays were satisfactory [the total value of  $\chi^2$  ( $5.55 \times 10^{-4}$ )] and acceptable as compared with our previous work, FMN binding protein systems.[18]

**A****B**

C

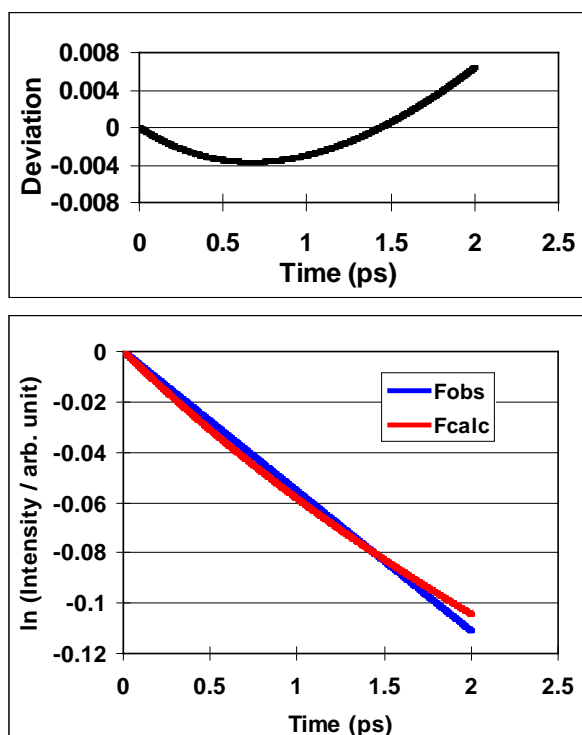


**Figure 4.3** Fluorescence decays of the Y97F, W59F and DM FD variants.

A: Y97F, B: W59F and C: DM. Upper panels in A, B and C represent deviations between the observed (Fobs) and calculated (Fcalc) fluorescence decays. Obtained ET parameters are listed in Table 4.2.



**Table 4.2** The best-fit ET parameters <sup>a</sup>

System		$\nu_0^{q^b}$ (ps <sup>-1</sup> )		$\beta^{q^b}$ (nm <sup>-1</sup> )		$R_0^{q^b}$ (nm)		$G_{Iso}^{0^b}$ (eV)	$\varepsilon_0^{j^b}$	$\chi^2^c$
		Trp	Tyr	Trp	Tyr	Trp	Tyr			
FD	Y97F								4.78	$2.61 \times 10^{-3}$
	W59F								4.04	$5.97 \times 10^{-4}$
	DM	3090	2460	55.6	9.64	0.772	0.676	7.67	2.28	$3.04 \times 10^{-5}$
	WT <sup>d</sup>								5.85	$5.90 \times 10^{-4}$
AppA <sup>c</sup>	WT								29.0	$4.60 \times 10^{-4}$
	Y21F	2304	2661	18.1	6.25	0.539	2.74	8.53	13.7	$3.08 \times 10^{-4}$
	W104F								2.45	$1.60 \times 10^{-4}$
FBP <sup>f</sup>	WT, W32Y, W32A	1016	197	21.0	6.64	0.570	0.0	8.97	9.86	$5.24 \times 10^{-4}$

<sup>a</sup>  $\nu_0^q$ ,  $\beta^q$ ,  $R_0^q$  ( $q = \text{Trp}$  or  $\text{Tyr}$ ) were common for the three mutated FD systems and the WT.  $\varepsilon_0^j$  depended on FD species  $j$ . These values were determined from the fluorescence dynamics of the WT and variant FDs by means of the best-fit procedure, as described in the text.

<sup>b</sup>  $\Delta G_q^0$  in Eq. 4.1 is obtained by Eq. 4.3 with  $G_{iso}^0$ . The values of  $\Delta G_q^0$  were -0.467 eV for Trp and 0.333 eV for Tyr.

<sup>c</sup> Chi-square was evaluated independently for each system. Total value of  $\chi^2$  was  $5.55 \times 10^{-4}$ .

<sup>d</sup> Data from Ref.[58]

<sup>e</sup> Data from Ref.[66-67]

<sup>f</sup> Data from Ref.[64] Three fluorescence decays of WT, W32Y and W32A FMN binding proteins were analyzed with common dielectric constant.

### 4.4.3 ET Parameters

The obtained ET parameters for the WT and the three mutant FD variants are listed in Table 4.2, along with those for the AppA and FBP taken from the literature for comparison. From these values,  $\Delta G_q^0$  was calculated by Eq. 4.3 to be -0.467 eV for Trp and 0.333 eV for Tyr. The adiabatic frequency ( $\nu_0^q$ ) of Trp in FD was ~1.3- and three-fold greater than that for AppA and FBP, respectively, whilst the  $\nu_0^q$  of Tyr in FD was 0.92- and 12.5-fold higher than that in AppA and FBP, respectively. The ET process coefficient ( $\beta^q$ ) of Trp in FD was three-fold and 2.6-fold greater than that in AppA and FBP, respectively, whilst the  $\beta^q$  of Tyr was 1.5-fold larger than that of both AppA and FBP. Finally, the  $R_0^q$  in FD was ca. 0.2 nm longer for Trp than that in AppA, but much shorter than that for the Tyr in AppA.

### 4.4.4 ES Energies in the Proteins

Figure S4.5 (**Supplemental Information IV**) shows the time-dependent changes in the *ES* energies of the Y97F, W59F and the DM FD variants, with the mean energies listed in Table 4.3. The mean energy [ $ES_j(Iso)$ ] between the Iso anion and all other ionic groups was lowest in the WT and some 1.20-, 1.28- and 2.42-fold higher in the Y97F, W59F and DM FD variants, respectively. The mean energies of the Trp59 cation in Y97F, and the Tyr97 cation in W59F, were 1.20- and 1.30-fold lower, respectively, than those in the WT FD. For the Tyr99 and Trp16 cations, the mean energy was lower in all three FD variants than the WT, starting from slightly lower in Y97F up to the dramatically so in the double mutation.

For ET rates, the sum of the energies of Iso and ET donors (net energy) are important (see Eq. 4.5). The time-dependent changes in the net *ES* energies ( $ES_j^i$ ) are shown in Figure 4.4. The mean net energy was -0.00159 eV for Trp59 in Y97F and -0.219 eV for Tyr97 in W59F, which were comparable to those in the WT at -0.0172 eV and -0.0942 eV, respectively. Fluctuations of these energies over time, i.e. time-dependent changes, may influence the non-exponential behavior of the fluorescence decay. *ES* energies from 5700 water molecules outside the protein and from partial charges of non-ionic amino acids in the protein were not evaluated here because they were relatively negligible with a contribution of less than 6% (to be submitted).

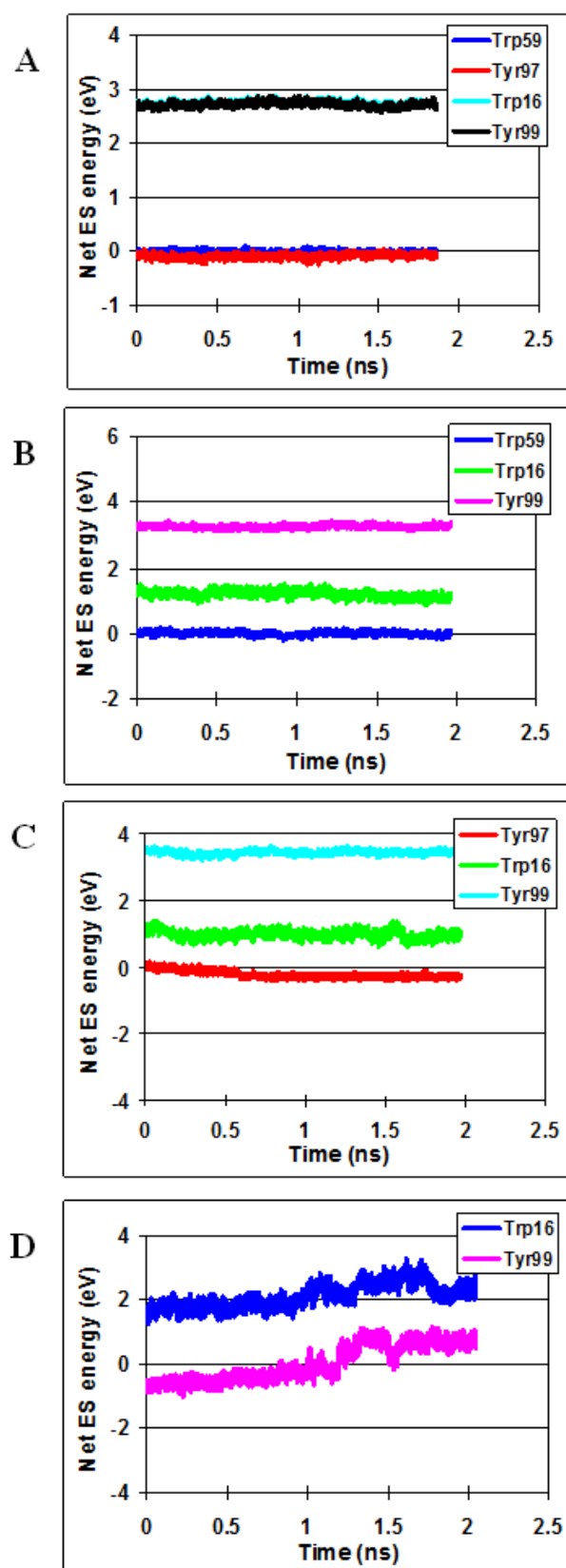


**Figure 4.4** Net *ES* energy in the WT and variant FDs

A: WT, B: Y97F, C: W59F and D: DM. Net *ES* energy means sum of *ES* energies of Iso and the aromatic amino acids. ET rate depends on net *ES* energy [see Eq. 4.1 and Eq. 4.5 in text]. Trp59, Tyr97, Trp16 and Tyr99 in inserts denote net energies of Trp59, Tyr97, Trp16 and Tyr99, respectively.

#### 4.4.5 ET Rates

ET rates were calculated with the best-fit ET parameters (see Table 4.2). Figure 4.5 shows the ET rates in the three variant FDs (Y97F, W59F and DM). The ET rate was fastest from Trp59 to Iso\* in Y97F, from Tyr97 in W59F and from Tyr99 in the DM. If Figure 4.4 and 4.5 are compared, it is evident that the ET rate becomes slower with increasing levels of the net *ES* energy, which implies that the *ES* energy plays an important role in determining the ET rate. The mean values of the ET rates are listed in Table 4.3, where that from Trp59 to Iso\* in Y97F ( $5.40 \text{ ps}^{-1}$ ) was slightly slower than that in the WT ( $7.11 \text{ ps}^{-1}$ ), whilst that from Tyr97 in W59F ( $3.18 \text{ ps}^{-1}$ ) was much faster than the corresponding value in the WT ( $1.26 \times 10^{-3} \text{ ps}^{-1}$ ). It is noted that the ET rates from Tyr99 to Iso\* were negligibly slow in the WT, Y97F and W59F FD variants, but became dramatically faster in DM.

**Table 4.3** Energy gap law of ET in FD <sup>a</sup>

Physical quantity	WT				W59F			Y97F			DM	
	Trp59	Tyr97	Trp16	Tyr99	Tyr97	Trp16	Tyr99	Trp59	Trp16	Tyr99	Trp16	Tyr99
$\ln k_j^i$ <sup>b</sup>	1.96	-6.68	-124.97	-114.99	1.14	-69.10	-155.82	1.60	-96.53	-139.87	-94.97	-2.60
$\lambda_j^i$ <sup>c</sup> (eV)	1.53	1.54	1.99	2.06	1.20	1.54	1.59	1.47	1.81	1.74	0.377	0.385
ES energy <sup>d</sup> (eV)	-2.85	-2.93	-0.0993	-0.118	-3.82	-2.62	-0.176	-3.41	-2.21	-0.150	-4.67	-6.80
Net ES energy <sup>e</sup> (eV)	-0.0172	-0.0942	2.73	2.71	-0.219	0.984	3.42	-0.00159	1.20	3.26	2.13	0.0131
$\Delta G_q^{0f}$ (eV)	-0.467	0.333	-0.467	0.333	0.333	-0.467	0.333	-0.467	-0.467	0.333	-0.467	0.333
ES energy between donor and acceptor <sup>g</sup>	-0.384	-0.460	-0.144	-0.193	-0.652	-0.196	-0.263	-0.386	-0.142	-0.289	-0.313	-0.470
$-\Delta G_{ij}^{0h}$ (eV)	0.868	0.221	-2.12	-2.86	0.583	-0.321	-3.49	0.855	-0.594	-3.31	-1.35	0.124
$-\Delta G_{ij}^0 / \lambda_j^i$	0.569	0.143	-1.07	-1.39	0.450	-0.209	-2.19	0.583	-0.329	-1.90	-3.58	0.322
$(\ln k_j^i) / \lambda_j^i$	1.28	-4.33	-62.84	-55.95	0.951	-44.95	-97.84	1.09	-53.46	-80.22	-251.93	-6.76

<sup>a</sup> ET rate is given by Eq. 4.1. Data of WT were taken from Ref. [58]

<sup>b</sup>  $k_j^i$  is expressed in unit of ps<sup>-1</sup>.

<sup>c</sup> Reorganization energy is given by Eq. 4.2.

d *ES* energies are given by Eq. 4.4. *ES* energies of Iso were 2.83 eV in WT, 3.60 eV in W59F, 3.41 eV in Y97F and 6.82 eV in DM.

e Net *ES* energies are given by Eq. 4.5.

f  $\Delta G_q^0$  is given by Eq. 4.3.

g *ES* energy between donor and acceptor is given by  $-e^2 / \epsilon_0^j R_j^i$  in Eq. 4.1.

h Total free energy gap is given by Eq. 4.16.

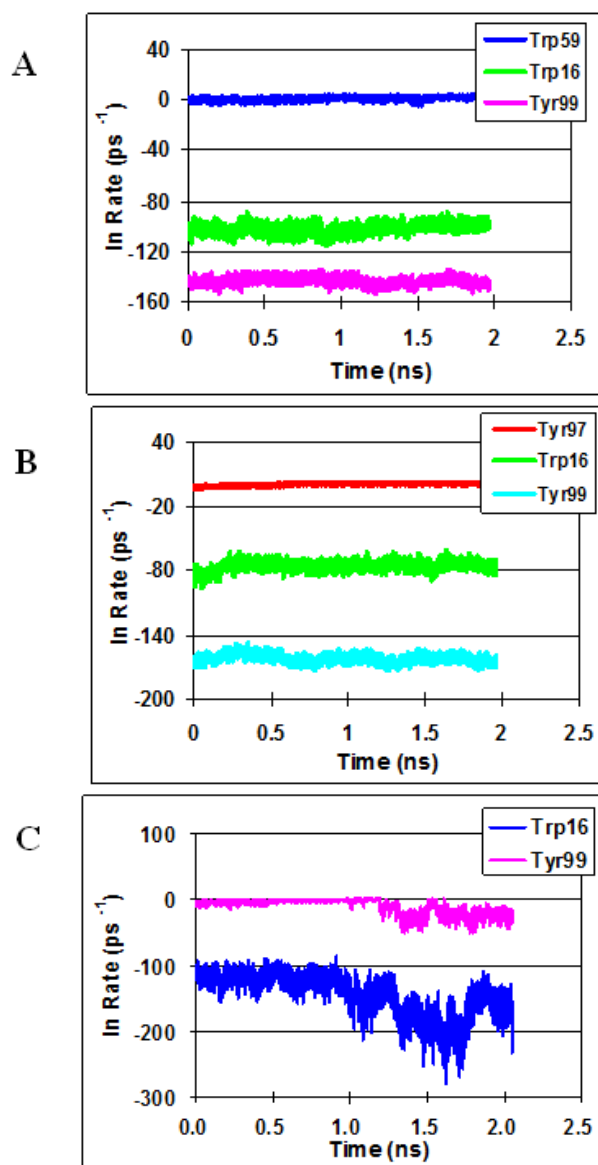


**Figure 4.5** ET rates in the mutated FD systems.

A: Y97F, B: W59F and C: DM. ET rates were calculated with the best-fit parameters listed in Table 4.2. Insert denotes ET donors.

#### 4.5 DISCUSSION

The observed fluorescence dynamics of the WT and the three mutated FD systems were simultaneously analyzed with common ET parameters. All fluorescence decays were satisfactorily reproduced with the best-fit ET parameters. The obtained ET parameters were



compared with those of the flavin photoreceptor AppA,[66-67] and also with those of FBP [18, 64] (see Table 4.2). The values of  $\nu_0^{Trp}$  and  $\nu_0^{Tyr}$  in FD were 3090 and 2460 ps<sup>-1</sup>, respectively, while they were 2304 and 2661 ps<sup>-1</sup> for Trp and Tyr, respectively, in AppA. In both protein systems  $\nu_0^{Tyr}$  was greater than  $\nu_0^{Trp}$ , which is remarkably different from that of FBP.

$\nu_0^q$  is related to the electronic interaction energy between the donor and the acceptor. In AppA, the greater  $\nu_0^q$  in Tyr was elucidated in terms of the hydrogen bond chain, Tyr21-Gln63-Iso\*.[66-67] In FD, the  $R_c$  value between Iso and Tyr97 was very short (0.55 nm) compared to the  $R_c$  of Trp59, which may be the reason why  $\nu_0^{Tyr}$  was greater than  $\nu_0^{Trp}$ , whilst  $\beta^{Trp}$  and  $\beta^{Tyr}$  did not differ much compared to those of AppA. The value of  $R_0^{Trp}$  in FD was 0.772 nm, which is considerably longer than that in AppA (0.539 nm). However, the  $R_0^{Tyr}$  in AppA was remarkably longer than that in FD, and this may be due to the long chain of hydrogen bonds from Tyr21 to Iso\* through Gln63.[67]

In FBP, the  $\epsilon_0$  used was common among the three systems of FBP, while different values of  $\epsilon_0$  were used in FD (this work) and in AppA.[66-67] Agreements between the observed and calculated fluorescence decays were greatly improved when the  $\epsilon_0$  values were changed with the protein system. Iso, in all FD systems, are partly exposed to the water layer (unpublished work).  $\epsilon_0^j$  ( $j = \text{WT, Y97F, W59F}$  and  $\text{DM}$ ) were somewhat lower than those found for AppA and FBP.

The ET rate from Trp59 to Iso\* in Y97F was faster than that from Tyr97 to Iso\* in W59F, despite the fact that the distance between Iso and Tyr97 in W59F was shorter than that between Iso and Trp59 in Y97F. A similar result was also found in the WT, and these results suggest that the donor-acceptor distance and  $\nu_0^q$  are not always critically important to the ET rate in the proteins. As shown in Figure 4.4 and 4.5, and also in Table 4.3, the ET rate became faster as the net  $ES$  energy ( $ES_j^i$ ) was reduced, which reveals that the net  $ES$  energy is the most important factor in determining the ET rate in the proteins. Figure 4.6 shows the relationship between the ln ET rate and the total free energy gap ( $\Delta G_{ij}^0$ ).  $\Delta G_{ij}^0$  was obtained from Eq. 4.16 (see Eq. 4.1).

$$-\Delta G_{ij}^0 = -(\Delta G_q^0 - e^2 / \epsilon_0^j R_j^i + ES_j^i) \quad (4.16)$$

The numerical data of these physical quantities are listed in Table 4.3. In the present FD systems the solvent reorganization energy ( $\lambda_j^i$ ) was found to vary from 0.385 (Tyr99 in DM) to 2.06 (Tyr99 in WT) with the ET donor (amount of variation 1.68 eV). On the other hand, the values of total free energy gap,  $\Delta G_{ij}^0$ , varied from -3.49 eV (Tyr99 in W59F) to 0.868 eV (Trp59 in WT), in which the net *ES* energy varied from 3.42 eV to -0.219 eV for Tyr99 and Tyr97, respectively, in W59F (amount of variation 3.64 eV.) Since the change in  $\Delta G_q^0$  was at most 0.8 eV and further amount of variation in *ES* energy between ion pair of the donor and acceptor  $-e^2 / \epsilon_0 R_j^i$  in Eq. 4.16 was at most 0.51 eV (varied from -0.652 eV (Tyr97 in W59F) to -0.142 eV (Trp16 in Y97F) ). It is considered that the net *ES* energy  $ES_j^i$  is most influential factor among the ET parameters.  $(\ln k_j^i) / \lambda_j^i$  may be plotted against  $-\Delta G_{ij}^0 / \lambda_j^i$  when  $\lambda_s^{jk}$  appreciably varies, as Eq. 4.17.

$$(\ln k_j^i) / \lambda_j^i \propto (-\Delta G_{ij}^0 / \lambda_j^i + 1)^2 \quad (4.17)$$

Pre-exponential factors in Eq. 4.1 may be almost constant upon the variation of  $-\Delta G_{ij}^0 / \lambda_j^i$ . The value of  $(\ln k_j^i) / \lambda_j^i$  was -252 at  $-\Delta G_{ij}^0 / \lambda_j^i$  (Trp16 in DM; see Figure 4.6) equals -3.58, and increased with  $-\Delta G_{ij}^0 / \lambda_j^i$ . The value of  $(\ln k_j^i) / \lambda_j^i$  became maximum at around 6 of  $-\Delta G_{ij}^0 / \lambda_j^i$ , and then decreased with  $-\Delta G_{ij}^0 / \lambda_j^i$ . The solid curve in Figure 4.6 was an approximate parabolic function,  $Y = -11.602X^2 + 21.105X - 14.834$ , where Y is  $(\ln k_j^i) / \lambda_j^i$ , and X is  $-\Delta G_{ij}^0 / \lambda_j^i$ . The results reveal that ET in FD mostly takes place in the normal region.

A number of works have reported on the free energy gap law in bulk solutions,[107-111] but rarely reported in proteins. The energy gap law was experimentally demonstrated in the ET processes in photosystem I and in the reaction center of the purple bacterium, *Rhodobacter sphaeroides*, by Iwaki *et al.*, where the ET takes place in the normal regions.[112] Turro *et al.* [113]found that ET in a homologous series of RuII diimines with cytochrome (cyt) *c* in its oxidized and reduced forms takes place in both the inverted region and normal region. ET in FD in the present work took place in the normal region.

Relationship between ET process and electron transfer process in dark is worth of discussion. The donor-acceptor distance dependence on  $\lambda_s^{qj}$  and  $-e^2 / \epsilon_0 R_j$  are common in both processes. *ES* energy of Iso anion and other ionic amino acids is also common between both

electron transfer processes. Many flavoproteins are involved in electron transfer processes in dark. ET analyses of the flavoproteins could also help to understand the electron transfer in the ground state of Iso in the proteins.

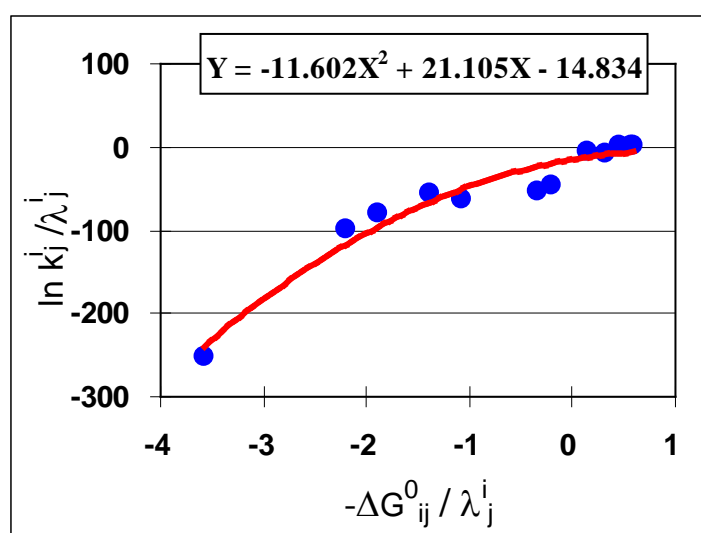


**Figure 4.6** Energy gap law of ET in FD

The ET rate is expressed in unit of  $\text{ps}^{-1}$ . Total free energy gap ( $-\Delta G_{ij}^0$ ) is given by Eq. 4.16.

Numerical data are listed in Table 4.3.  $(\ln k_j^i) / \lambda_j^i$  vs.  $-\Delta G_{ij}^0 / \lambda_j^i$  were plotted according to Eq.

4.17. Insert indicates an approximate parabolic function of the plot.

**CHAPTER V**  
**CONFORMATIONAL FLEXIBILITY AND THERMODYNAMIC**  
**PROPERTIES OF FLAVODOXIN FROM *HELICOBACTER PYLORI***

---

**Conformational Flexibility and Thermodynamic properties of Holo and Apo *Helicobacter pylori* flavodoxin: Molecular Dynamic Simulation approaches**

**Kiattisak Lugsanangarm<sup>1</sup>, Somsak Pianwanit<sup>1</sup>, Sirirat Kokpol<sup>1</sup>,  
Arthit Nueangaudom<sup>1</sup>, Fumio Tanaka<sup>1,2</sup>**

---

<sup>1</sup> *Department of Chemistry, Faculty of Science, Chulalongkorn University, Bangkok 10330, Thailand*

<sup>2</sup> *Division of Laser BioScience, Institute for Laser Technology, Utsubo-Honmachi, 1-8-4, Nishiku, Osaka 550-0004, Japan*

---

**This article is in preparation for publication (2013).**

---

## 5.1 ABSTRACT

The physically and thermodynamically conformational rearrangements of flavodoxins from bacterium *Helicobacter pylori*, for both Apo and Holo form, have been studied by molecular dynamic simulation. The results show that the whole protein of both types shared a similar pattern of the amino acid fluctuation except for the FMN binding site. The H-bond analyses reveal that amino acid which located at 10-loop can extremely form H-bond with phosphate subsite followed by loop-50 with ribityl subsite and loop-90 with Iso subsite. This is in accordance with the decomposition free energy analysis which shows that loop-10 shows the highest stabilization energy by  $-0.77$  kcal / mol, followed by loop-50 of  $-0.75$  kcal / mol, and lowest contribution has been found by loop-90 of  $-1.24$  kcal / mol. In addition to the binding free energy, Asn14, Thr54 and Tyr92 show the mostly contributed come from van der Waals interaction of their sidechain with the cofactor molecule. The dramatically change in dihedral angle upon FMN cofactor binding can be found for Asn14, Ala55, Tyr92 and Thr95 which can support the existing of an ensembles conformations of protein flavodoxin prior association with FMN.

## 5.2 INTRODUCTION

To date, approximately 50 percentage of the world population are infected by *Helicobacter pylori* (*H. pylori*).[114] This bacterium is gram-negative and colonized in the stomach. R.A. Alm and co-workers have demonstrated that *H. pylori* is related with gastroduodenal pathologies, including type B gastritis, stomach and duodenal ulcers,[115-116] adenocarcinoma [117] and stomach lymphomas.[118] Human with long-life infection by *H. pylori* for 20-30 years can be contracted with stomach cancer.

FD plays an important role for *H. pylori* survival, and functions as an electron acceptor of the pyruvate:flavodoxin oxidoreductase complex (PFOR) that catalyzes pyruvate oxidative decarboxylation.[119] Therefore, FD from *H. pylori* has been extensively studied in order to clearly understand on the folded-unfolded stability,[120-124] binding mechanism,[125-126] including finding lead inhibitor.[20] The crystal structure of FD from pathogen *H. Pylori* was first determined by J. Freigang and co-workers.[8] Figure 5.1(A) shows the protein structure of FD. It composed of 164 amino acid residues with five- $\beta$  sheets and four- $\alpha$  helix shape.[8, 127] FD from this bacterium can be classified as the long-chain FD.[2] The fifth  $\beta$ -strand (amino acid

No. Gly110 – Gln115) in FD from *H. pylori* is absent in the short-chain FD as *Desulfovibrio vulgaris*, Hildenborough and Miyazaki F. The fifth  $\beta$ -strand is believed to act as the protein signaling for the protein partner.[127] The FMN binding site is surrounded by groups of amino acids, which is categorized as loop-10 (from Phe8 – Ala17), loop-50 (Ala52- Gln61), and loop-90 (Leu86 – Ala97) (see Figure 5.1(B)). FD from this bacterium is somewhat different from the other flavodoxins not only in the number of amino acids but also in the characteristic at the FMN binding site. In most flavodoxins isoalloxazine (Iso) ring of FMN is in close proximity with an aromatic amino acid as tryptophan (Trp) and sometime is sandwiched by Trp and tyrosine (Tyr). FD from *H. pylori* contains only Tyr92 as the aromatic amino acid and Ala55 instead of Trp.[20]

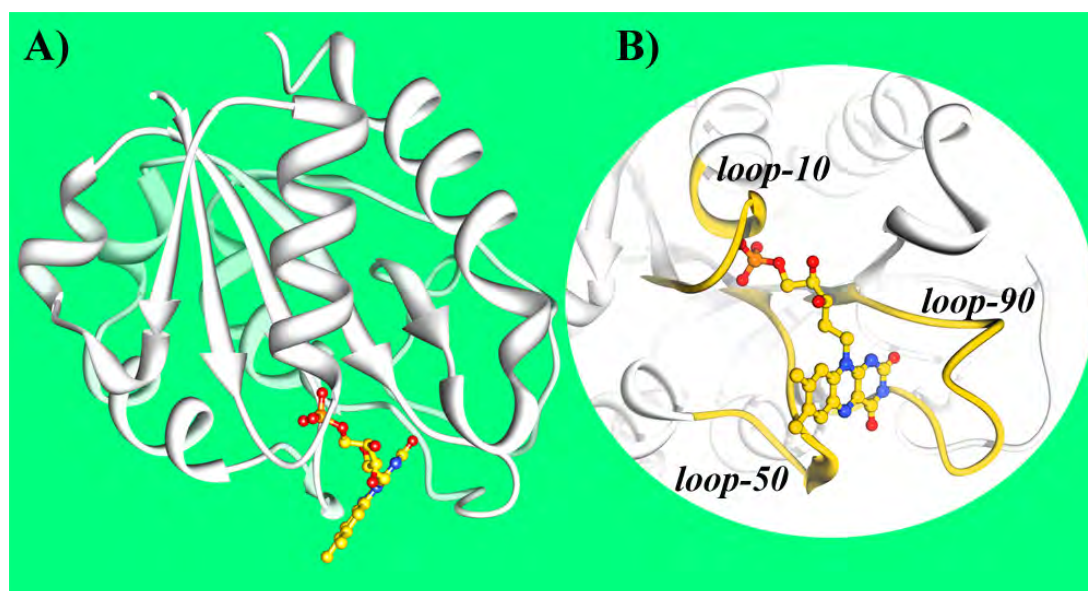


**Figure 5.1** The three dimensional structure of *H. pylori* flavodoxin. (A) Protein structure of *H. pylori* flavodoxin, which consisted of five-  $\beta$  sheets and four-  $\alpha$  helix shape of amino acids. (B) The close-view at the FMN binding site. The FMN and three important loops for binding are indicated in yellow.

Currently, the mechanism of FMN association with Apo-FD is not clearly understood. S. Ayuso-Tejedor and co-workers reported that alanine mutations of amino acid at the binding site which revealed that they did not change the association constant of FMN. Furthermore, the alanine-mutagenesis revealed that the aromatic ring of Tyr92 is important not only to stabilize the protein structure of native FD, but also recognize FMN to bind.

In this work, we have studied the structural and thermodynamic properties of Holo- and Apo-FDs. Moreover, the dihedral angle analyses of amino acids located at the FMN binding site revealed the difference pattern upon FMN binding to Apo-FD. This study can provide the molecular basis for FMN binding in the native FD and insight into the structural requirement on the structure-based drug design.

## 5.3 METHODS

### 5.3.1 Protein and ligand preparation

The starting crystallographic structure of *H. pylori* [8] was obtained from Protein Data Bank (PDB code: 1FUE), [Research Collaboratory for Structural Bioinformatics (RCSB) (<http://www.rcsb.org/pdb>)]. The missing hydrogen atoms were added by using Discovery studio 2.0 software packages. (Accelrys) The parameters of FMN cofactor were obtained from the previously work.[7] Subsequently, the protein was subjected for all hydrogen minimization by using AMBER version 10 software package.[51]

### 5.3.2 Molecular dynamics simulations

MD simulation was carried out by using Amber version 10. The amber03 force field was employed for protein topology.[51] The starting structure was first minimized with 2000 steps of steepest decent (SD) minimization, followed by 3000 steps of conjugate gradient (CG) minimization in order to remove the bad geometrical crashes. The protein complexed was then solvated with the explicit TIP3P c.a. 6660 water molecules. An appropriate sodium counter ions were added in order to neutralize the negative charges. Subsequently, 3000 steps of CG minimization were performed on the whole system with the periodic boundary extending to 10 Å from the complex. These minimized solvated systems were used as the starting structure for the following MD simulation. For apo-FD, the FMN molecule in crystallographic structure was removed and then a similar fashion of preparing approach with Holo-FD has been applied.

The MD simulations were carried out under the isobaric-isothermal ensemble (normal temperature and pressure, *NPT*) with a constant temperature of 298 K and constant pressure of 1 atm. The Particle Mesh Ewald (PME) method was used to correct the electrostatic

interaction,[128] and the bonds involving hydrogen were constrained by applying the SHAKE algorithm.[52] Subsequently, the complex was subjected to first MD simulation in order to relax the position of the water molecules (for 150 ps by fixing the solute structure). Then we performed additional MD simulations to reach 50 ns with the time interval of 0.002 ps. In order to study the protein conformational change and the thermodynamic quality upon the FMN binding, the single trajectory (FD complexed with FMN) and separated trajectory (Apo-FD and FMN, isolated system) have been calculated with the same MD protocol.

### 5.3.3 The root of mean square fluctuation

The root of mean square fluctuation (RMSF) of each amino acid, which represents the flexibility of each amino acid residue, was carried out by using *ptraj* module implemented in AMBER version 10.[51] The superposition of the trajectories to the reference conformation of amino acid over equilibrium time has been calculated. The RMSF defined as Eq. 5.1.

$$\text{RMSF}_{(i)} = \sqrt{\frac{1}{T} \sum_{t=1}^T (R_i(t) - R_i^{ref})^2} \quad (5.1)$$

Here  $R_i$  is the position vector of atom  $i$  (in this study, the  $C\alpha$ , N, and O atoms coordinates were evaluated).  $R_i^{ref}$  is the reference position of residue  $i$  and  $T$  is the total number of protein coordinate.

### 5.3.4 Decomposition free energy per residue

The decomposition energies of each amino acid were studied at the binding site of FMN molecule of loop-10 (residues Phe8 – Ala17), loop-50 (residues Ala52 – Gln61) and loop-90 (residues Leu86 – Ala97). We used one hundred snapshots of the last 30 ns (with time interval 0.3 ns) of the production phase to study decomposition free energy. The solvation free energy was estimated using polar and non-polar contributions according to Eq. 5.4. The cutoff for non-bonded interactions was neglected for molecular mechanic energy calculation.



## 5.4 RESULT AND DISCUSSION

### 5.4.1 Comparison of the protein structure between Holo- and Apo-flavodoxin

The longer MD time could provide the more reliable ensemble collection. In this work, the MD simulations of both Apo- and Holo-FD were carried out for 50 ns. The stability of the whole MD system can be investigated by the time evolution of the root of mean square deviation (RMSD), illustrated in Figure S5.1. It is clear that for both Apo- and Holo-FD reached the equilibration after 20 ns. Therefore, we have collected their configurations from 20 to 50 ns in order to investigate their dynamic behavior, structural difference at the binding site including their thermodynamic properties. The averaged RMSD of each part of both Apo- and Holo-FD have been summarized in Table S5.1, which shows that the RMSD of entire protein (backbone and sidechain) of Apo-FD is higher than one of Holo form. Being considered the RMSD of only backbone part (N, CA, C=O), we found that Holo-FD show higher value of RMSD compared to Apo-FD form. The mean value of the backbone RMSD in Holo form was 1.46 Å, while one of Apo form was 1.38 Å. This suggests that molecular volume of Holo-FD increases upon FMN binding. In addition to the dynamics of each amino acid, the RMSF analyses, with respect to the averaged structure, have been carried out. Figure 5.2 illustrates the comparison of RMSF between Apo- and Holo-FDs, which shows that RMSF shared a similar pattern along with the residue No. between Apo- and Holo-FDs, except for those at the FMN binding site. The amino acid residues which show significant difference in RMSF magnitude, were Asp11, Ser12, Gly13, Asn14 in loop10, Ala55, Gly56, Ala57, Gly58 in loop50, Asp90, Thr91, Tyr92 in loop90, and Gln144, Asp145, Asp146, Leu147, Thr148, and Asp149. This might be due to the lost of binding interaction between FMN molecule and Apo-FD.

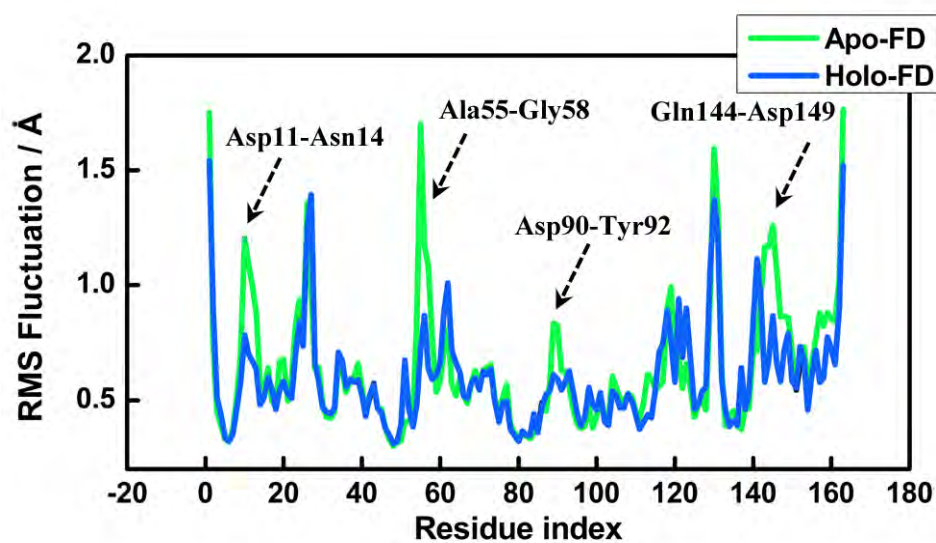


**Figure 5.2** Comparison of the RMSF between the Apo- and Holo-FDs. Amino acid residues indicated in the Figure displayed great difference between Apo- and Holo-FDs.

The superimposition of configuration which taken by averaging of the last 30 ns of the production time has been shown in Figure 5.3. Clearly, the structure of Apo-FD (green ribbon) and Holo-FD (blue ribbon) shared a similar pattern except the large different which can be found in 4 loops, namely, Asp11 – Asn14, Ala55 – Gly58, Asp90 – Tyr92, and Gln44 – Asp49. The protein backbones were quite similar between Apo- and Holo-FDs, except for the FMN binding site. Figure 5.4 shows time-evolutions of the total energy in the entire MD simulation time. It is evident that the energy of Holo-FD (blue line) was quite lower than one of Apo-FD (green line). This result reveals that the Apo-FD becomes much stable upon the binding of FMN.

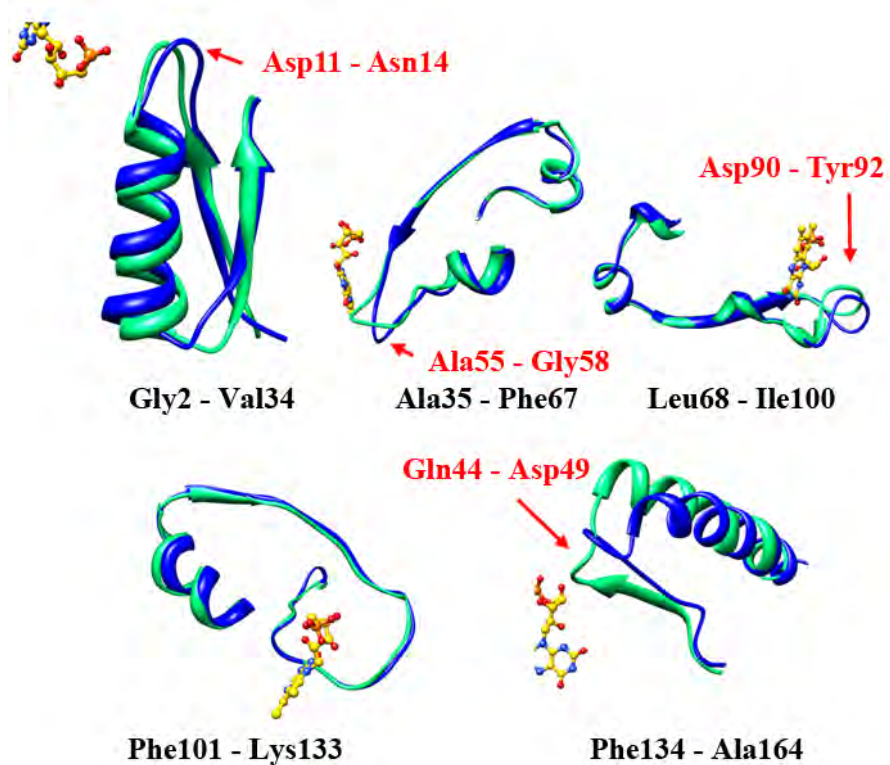


**Figure 5.3** Comparison of the main segments between Apo- (green) and Holo- (blue) FDs. The FMN cofactor is shown by ball and stick model. The red color indicates the highly flexible region. The entire protein was divided into 5 parts as indicated residue Nos. in black.

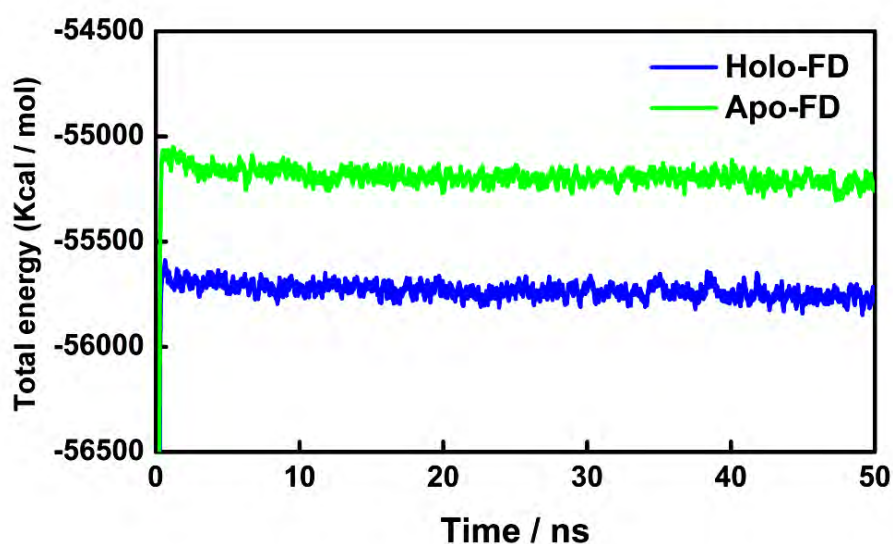


**Figure 5.4** Comparison of the total energy of Holo-FD and Apo-FD. Holo form is indicated in blue color and Apo form in green color.

### 5.4.2 Hydrogen binding analyses

H-bonds play a crucial role in bimolecular system.[129] In this study, the criteria for formation of H-bond were (i) the distance between the heavy atoms of the donor and acceptor to be less than 3.5 Å, (ii) a bond angle of X-H...Y to be greater than 120°. Figure 5.5(A) shows H-bond pairs between FMN and Apo-FD, and Figure 5.5(B) shows the H-bond distance of the corresponding atom pair. Ala97(NH: peptide), Thr95(O: peptide), Thr95 (OG1: side chain) and Asp88(NH: peptide) satisfied the both criteria, and form strong H-bonds with Iso O2, N3H, O4 and O2, respectively. Moderate H-bonds with the percentage of occupation around 40 % were observed in ribityl sidechain of FMN molecule [Asn14 (37.96%), Thr54 (35.34% and 34.14%)]. Slight H-bonds with % occupation lower than 40 % formation between amino acid in loop-10 [Thr10 (33.78%), Ser12 (18.60%, 16.02% and 15.26%), Asn14 (23.66%, 19.34 % and 13.50%)] with phosphate subsites. The H-bond formations between FMN and Apo-FD are summarized in Table 5.1. Ala97 (NH: peptide), Thr95 (O: peptide) and Thr95 (OG: side chain) strongly formed H-bond with O2, N3H and O4 of FMN, respectively, as judged from percent occupation. O2 of Iso also formed H-bond with Asn88 (NH: peptide). Ribityl O2' and O4' formed H-bonds with Thr54 (NH: peptide) and Asn14 (ND2: side chain), respectively. O3P formed H-bonds with Ser12 (OG: side chain), Thr10 (OG: side chain) and Asn14 (ND2: side chain). O1P formed H-bonds with Ser12 (OG: side chain) and Asn14 (ND2: side chain).

The experimentally side-directed alanine mutagenesis of amino acid at the phosphate subsite of *H. pylori* FD revealed a small effect on the dissociation constant.[125] This agrees well with our calculation results. Because in this region, Ser12 can only form moderately H-bone by 75 % occupation, while the rest play small contribution. The H-bond pattern in *H. pylori* FD were quite different from the observed one of strain *Miyazaki F.* [7] The H-bond formations in FD from *Miyazaki F.* are favorable between loop-10 and phosphate subsite.[7] The difference of this H-bond pattern may be due to the different in protein architecture.



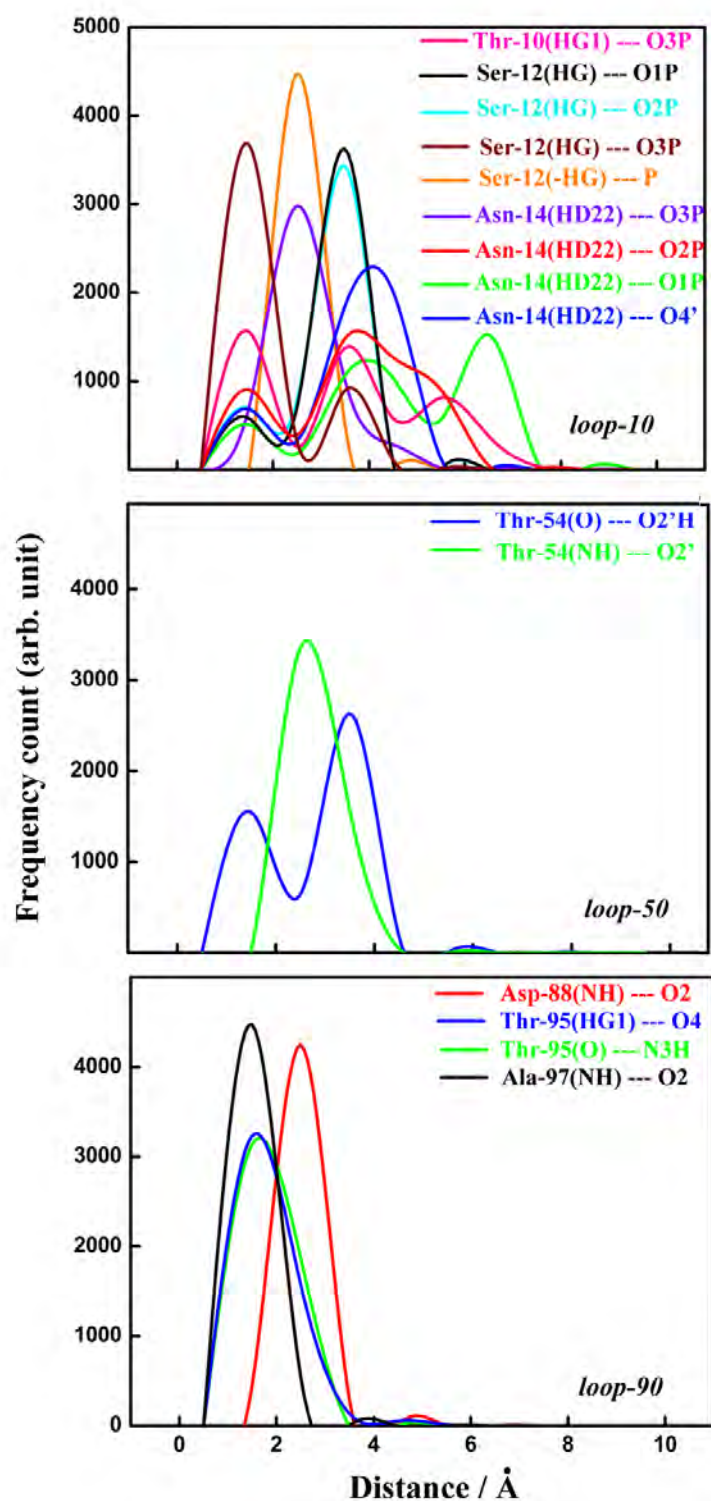


**Figure 5.5** H-bond formation between FMN and surrounding amino acids. Upper panel shows schematic representation of the H-bond. Lower panel shows the histogram of H-bond distance distribution.

**Table 5.1** Percentage occupation of H-bonds between FMN cofactor and surrounding amino acids<sup>a</sup>

Amino acid residue (Atom kind)	FMN	% Occupied	Distance (Å)	Angle (degree)
Ala97(NH)	O2	100.00	2.83 ( 0.11)	162.12( 9.24)
Thr95(O)	N3-H	99.58	2.94 ( 0.14)	160.62( 9.32)
Thr95(OG1-HG1)	O4	92.74	2.84 ( 0.19)	158.09(12.28)
Ser12(OG-HG)	O3P	75.70	2.60 ( 0.15)	167.07( 8.93)
Asp88(NH)	O2	74.96	3.16 ( 0.19)	150.07( 8.30)
Asn14(ND2-HD22)	O4'	37.96	3.03 ( 0.19)	150.1(16.00)
Thr54(O)	O2'-H	35.34	2.71 ( 0.13)	157.78(12.58)
Thr54(NH)	O2'	34.14	3.29 ( 0.15)	138.07( 9.80)
Thr10(OG1-HG1)	O3P	33.78	2.68 ( 0.18)	159.90( 9.19)
Asn14(ND2-HD22)	O1P	23.66	2.88 ( 0.16)	159.94(11.26)
Asn14(ND2-HD22)	O3P	19.34	2.89 ( 0.17)	159.00(10.86)
Ser12(OG-HG)	O1P	18.60	2.79 ( 0.33)	22.03 (18.32)
Ser12(OG-HG)	P	16.02	3.40 ( 0.08)	157.97( 8.78)
Ser12(OG-HG)	O2P	15.26	2.77 ( 0.34)	157.73(17.82)
Asn14(ND2-HD22)	O2P	13.50	2.86 ( 0.16)	157.38(11.30)

<sup>a</sup> See Chart 1 for definition of atomic labels. The last 30 ns of the production time which contain 5000 configurations with 6 ps time intervals were used for the analysis. The digits in parentheses denote the standard deviation

### 5.4.3 Decomposition free energy per amino acid residues at the binding site

The decomposition (DC) free energy of the amino acid residue represent the stability of protein complex upon those amino acid binding. We can assume that the amino acid which located near FMN molecule should be interacted and showing the influent on the stabilization energy. The FMN was surrounded by the loop-10, loop-50 and loop-90 regions (see Figure 5.1(B)). Figure 5.6 shows the DC plot of these three loops. At loop-10, Asn-14 shows the free

energy lower than  $-5$  kcal / mol. The amino acid Phe8, Gly9, Thr10, Ser12, Gly13, Ala15, and Ala17 show the energy contribution in the range of  $-0.02 \leq \Delta G_{bind} \leq -1.72$  kcal / mol. In this loop, there are residues Asp11 and Glu16 gave the small destabilization free energy. Focusing on loop-90, Tyr92 show is the most stabilization free energy upon the FMN binding by  $-4.83$  kcal / mol, while Gly87, Thr95, Phe96 and Ala97 provided a similar free energy contribution in the range of  $-0.05 \leq \Delta G_{bind} \leq -2.47$  kcal / mol. Compliant to the loop-10, there are Asp90 and Glu94 show the small destabilization free energy. Thr54 shows the most favor stabilization free energy by  $-2.27$  kcal / mol. Based upon the averaged binding free energy, loop-50 shows the lowest contribution upon FMN binding with respect to loop-10 and loop-90. The DC free energy separated into the residue sidechains (blue line) and backbones (green line) are depicted in Figure 5.7. In the loop-10, the lowest decomposition free energy was found by Asn14, Its sidechain show the source of the lowest DC energy. At the loop-90, sidechain of Tyr92 provided the interaction for stabilization, same as at loop-50 for Thr54. The classification of the contribution on that DC free energy into the van der Waals ( $E_{vdw} + G_{nonpol}$ ) and electrostatic ( $E_{ele} + G_{pol}$ ) energy term are shown in Figure 5.8. We found the van der Waals interaction play an important role in between the FMN and surrounded amino acids, in particular for Asn14, Thr54 and Tyr92. This is somewhat consistent with the mechanism as suggested by A. Lostao and co-workers. They reported that the electrostatic energies seem not to play a role in directing the binding mechanism.[126] In contrast, the hydrophobic encounter becomes the majority role involved in binding reaction. Based on the averaged contribution, loop-10 shows the highest stabilization energy by  $-0.77$  kcal / mol, followed by loop-50 of  $-0.75$  kcal / mol, and lowest contribution has been found by loop-90 of  $-1.24$  kcal / mol.



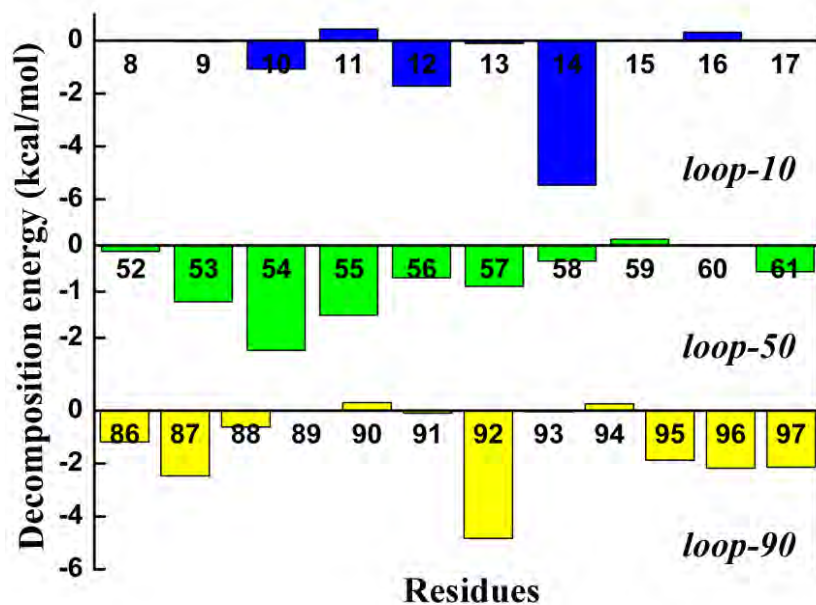


**Figure 5.6** The decomposition free energy per amino acid residue for FMN binding.

The Figure shows the contribution of individual amino acid at loop-10, loop-50 and loop-90 to FMN binding energy.

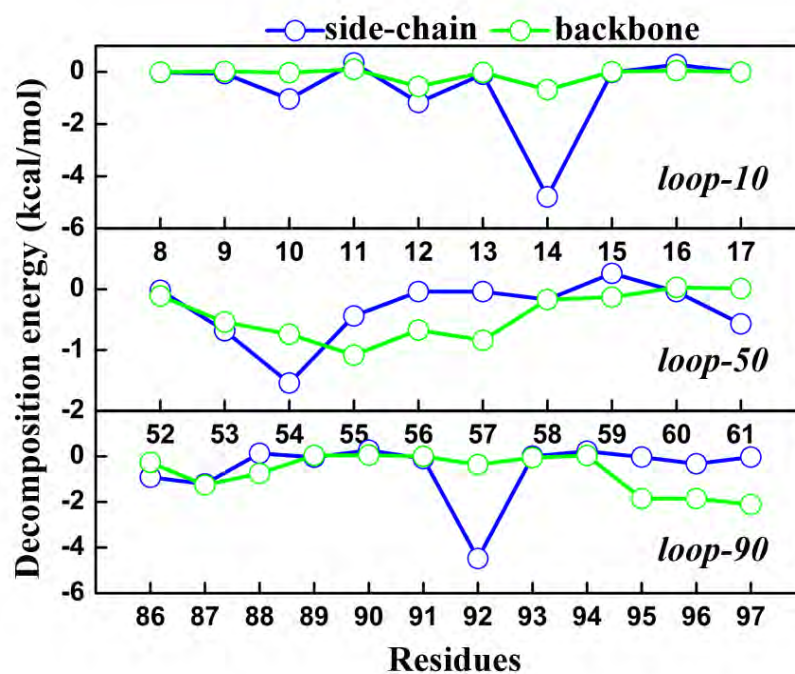


**Figure 5.7** Contribution of the side-chain and the backbone of individual amino acid residue at loop-10, loop-50 and loop-90 to the FMN binding free energy.

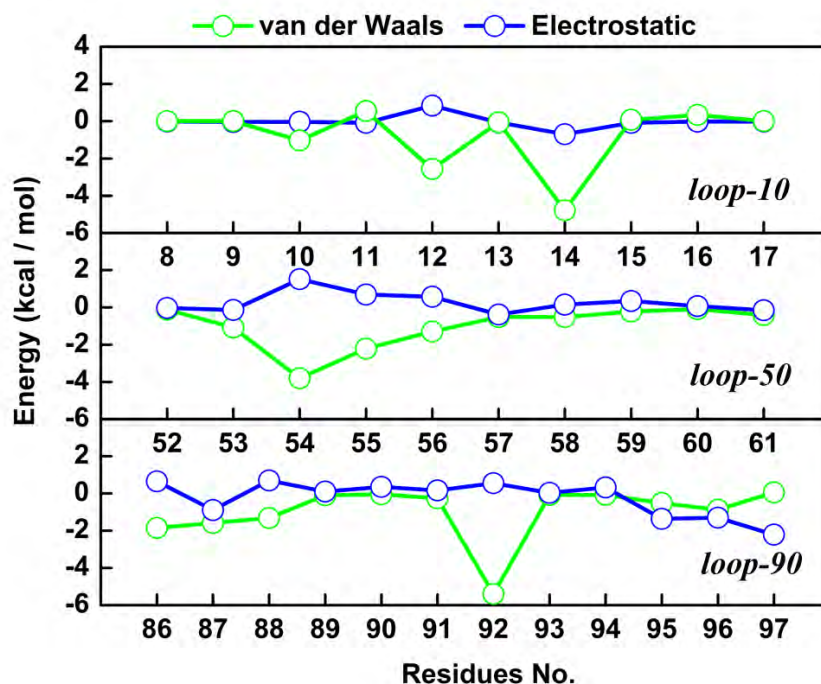


**Figure 5. 8** The electrostatic and van der Waals energies per residue at loop-10, loop-50 and loop-90 for the FMN binding.

#### 5.4.4 The dynamical flexibility of the amino acids at the active site

The conformational changes play a key role in the ligand binding to protein and help for stabilization its complex.[130] The aromatic amino acid at the binding site can control the FMN association as described as the "aromatic gate model" proposed by C. G. Genzor and co-workers.[131] In addition, T.A. Murray and co-workers reported the evidence of conformational changes associated to flavin binding to Apo-FD from *Desulfovibrio vulgaris*. [132] The dynamic of sidechain of Trp60 which located proximal to FMN associated conformational changes.[132] This suggests the role of dynamic, hydrophobic interaction, like  $\pi$ - $\pi$  interaction, between sidechain and Iso subsite. Therefore, the dynamic of sidechain at the FMN binding site between Apo- and Holo- form should be more clarified. To that end, MD simulation can provide insight at atomistic details. Figure 5.9 shows the dihedral angle of 16 amino acid residues at the FMN binding site (within 5 Å away from FMN molecule). Five thousand coordinates of the bound FD (single trajectory) and unbound (separated trajectory) have been extracted from the last 30 ns production time. These two situations of FD being studied are a good model to investigate the

dynamic of those residues upon FMN binding. The declaration variable  $\chi_1$  and  $\chi_2$  have been described in Figure 5.9. The plots of  $\chi_1$  versus  $\chi_2$  angle can describe how flexibility of sidechain of each individual residue is? We can classify the plot of dihedral angles into three groups. Group-I comprised of Thr10, Pro53, Ala57, Gly58, Gly87, Asp88, Phe96 and Ala97. In this group, the plot of  $\chi_1$  and  $\chi_2$  and also the frequency of population between Holo- (red meshed) and Apo-FD (blue meshed) are quite similar. This result implied that the binding of FMN molecule did not affect to the mobility of sidechain of these amino acid. Group-II comprised of Ser12, Asn14, and Gly98. These amino acids show a small difference pattern, angle or frequency of population. Group-III shows the highest difference among Apo- and Holo-FD, comprising of Ala55, Gln61, Tyr92 and Thr95. Clearly, Ala55 (this amino acid lying near Iso ring) of Holo-FD (red meshed) show the shift of  $\chi_1$  angle from c.a. 240 – 360 degree to a narrow dynamic range (red meshed) of c.a. 180 – 240 degree which was observed in Apo-FD. Interesting in the case of Tyr92, the shift of angle is observed in  $\chi_2$ . There are shifts of angle from c.a. 30 – 180 (based region of Apo-FD, blue meshed) to range c.a. 240 – 300 (based region of Holo-FD, red meshed). The conformational change of phenyl ring of Tyr92 in Holo-FD enabled to form  $\pi$ - $\pi$  interaction with Iso subsite. Interestingly, Thr95 is one of the most interesting amino acid in this work. Beside it can form H-bond with N3H and O4 of Iso subsite with  $\sim 100$  and 93 %, respectively, the dihedral angle of its sidechain show dramatically change between Apo- and Holo-FD. Therefore, the role of Thr95 for the involving of FMN molecule need to be further investigated.

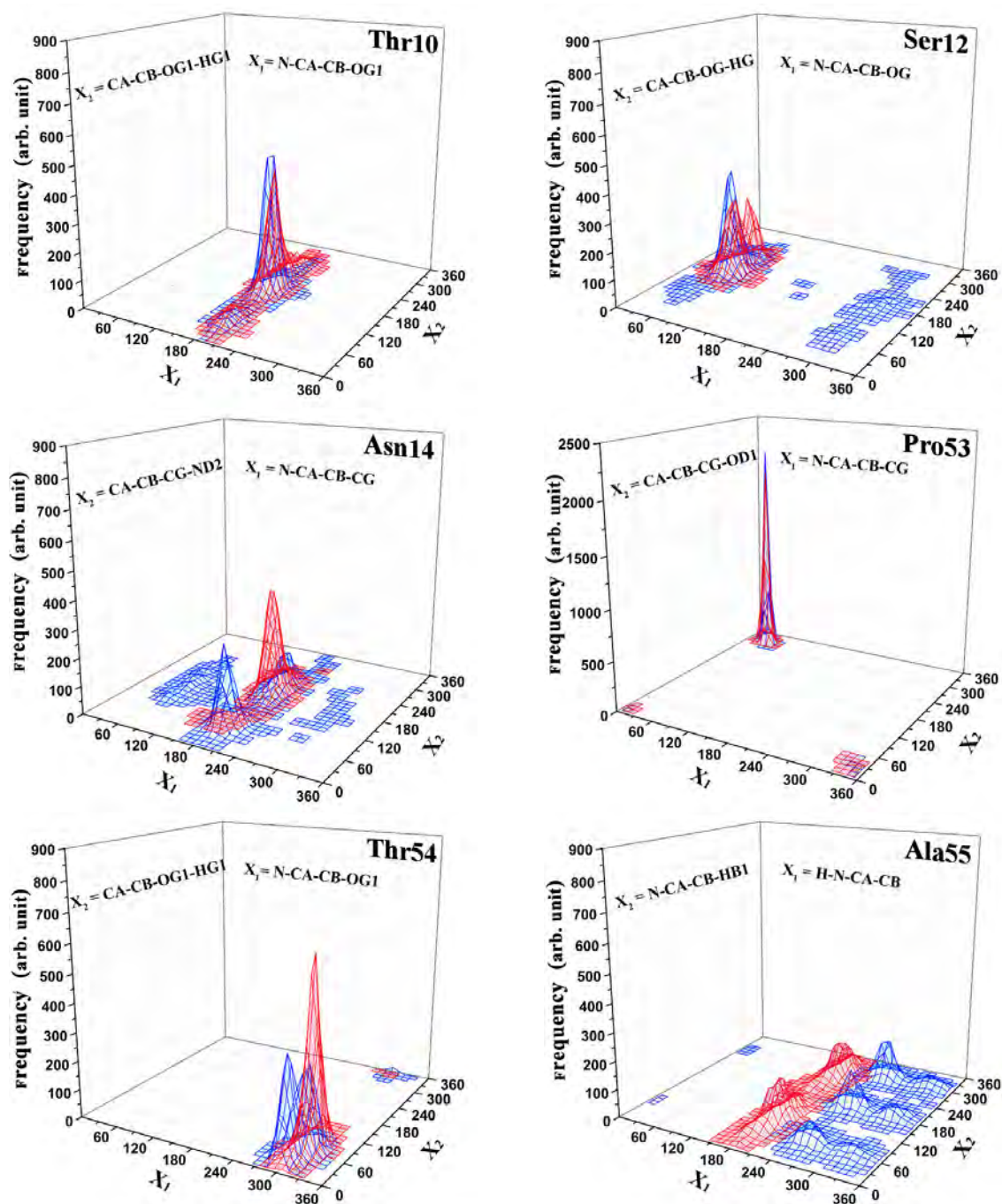


**Figure 5.9** Distribution of the dihedral angles of  $\chi_1$  and  $\chi_2$  of amino acids at the FMN binding site. The distribution of the Apo-FD is in blue, Holo-FD in red

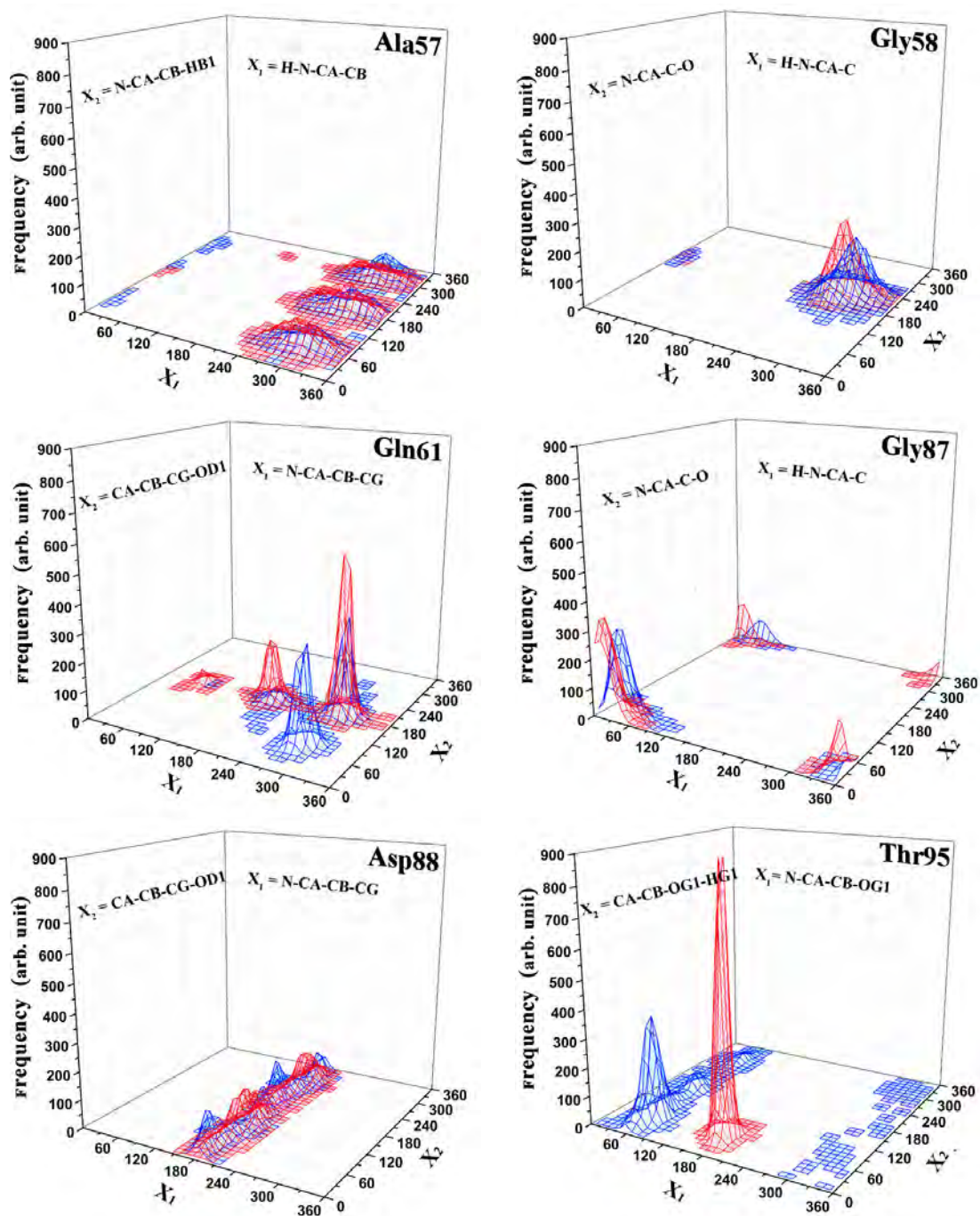


**Figure 5.9** Distribution of the dihedral angles of  $\chi_1$  and  $\chi_2$  of amino acids at the FMN binding site. The distribution of the Apo-FD is in blue, Holo-FD in red

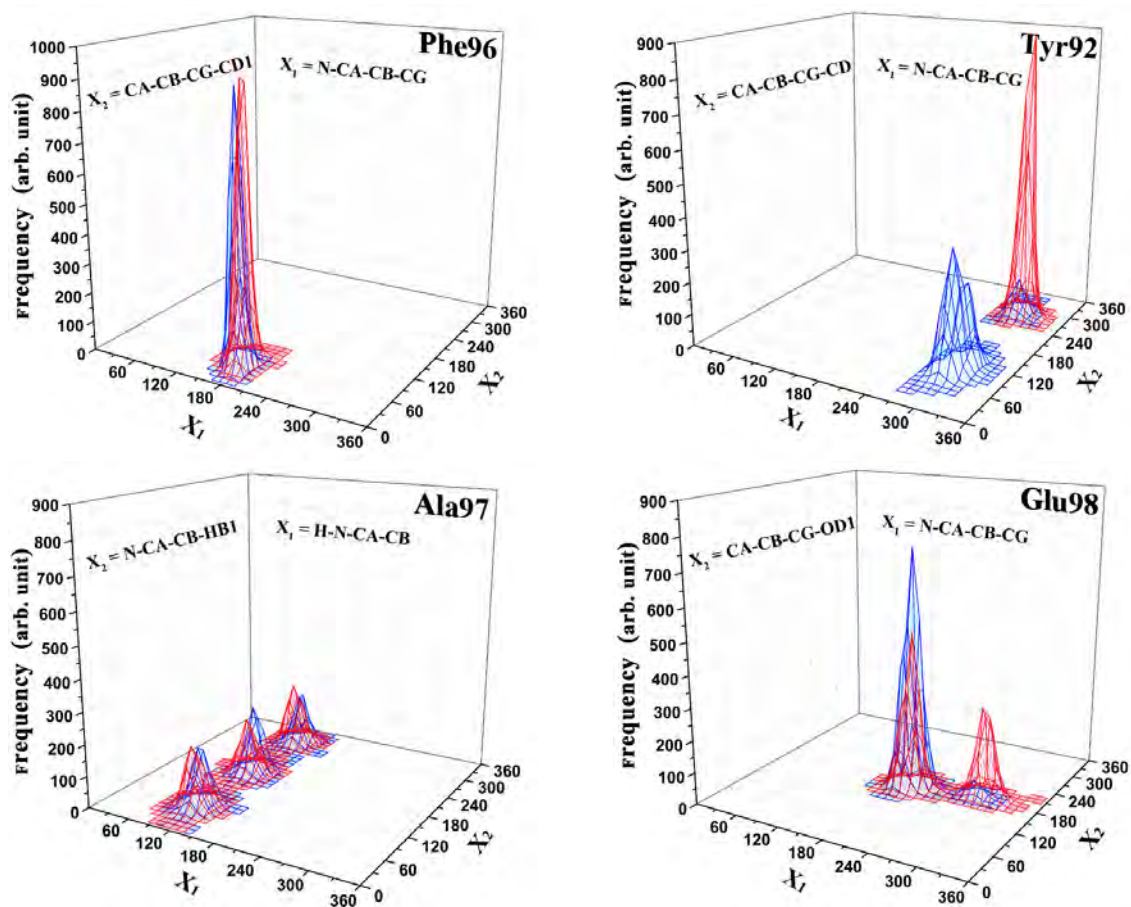


**Figure 5.9** Distribution of the dihedral angles of  $\chi_1$  and  $\chi_2$  of amino acids at the FMN binding site. The distribution of the Apo-FD is in blue, Holo-FD in red

## 5.5 CONCLUSION

In this work, we calculated MD simulations of explicit model of Apo- and Holo-flavodoxin to demonstrate the conformational adaptation attend the FMN complex formation energy and thermodynamic properties. In order to clarify such properties, fifty ns time length of a single and separate trajectories MD simulations have been carries out. The result shows that amino acid located at loop-90 as Asp88, Thr95 and Ala97 are favoring strongly formed H-bond with Iso moiety, while amino acid at loop-10 formed moderately H-bond with phosphate and ribityl part. The DC free energy analysis revealed that the favorable non-bonded van der Waals interactions contribute predominantly to the enthalpy upon FMN binding. In addition to the stabilization, amino acids at loop-10 provided the highest stabilization energy follow by loop-50 and lowest at loop-90, respectively.

The conformational flexibility analyses of amino acid at the binding site allowed us to figure out how the dynamic of each amino acid is? The simulation results clearly revealed that Asn14, Ala55, Gln61, Tyr92, Thr95 are influenced upon the cofactor association. The plots of dihedral angle of that sidechain are different in the positioned. This result is in accordance with the decomposition free energy analysis. An analysis of the separated free energy contributions also provides very informative information. The sidechain of these amino acid residues play an important role for FMN binding. We point these amino acids out, which might play dynamic role and support the conformational selection process for the FMN binding. For further understanding on the binding mechanism and the role of these amino acids, the folding-unfolding studies need to be further investigated.

**CHAPTER VI**  
**THEORETICAL ANALYSIS OF PHOTOINDUCED ELECTRON TRANSFER**  
**IN FLAVODOXIN FROM *HELICOBACTER PYLORI***

---

**Mechanism of Photoinduced Electron Transfer from Tyrosine to the Excited Flavin in  
Flavodoxin from *Helicobacter pylori***

**Kiattisak Lugsanangarm<sup>a</sup>, Somsak Pianwanit<sup>a</sup>, Arthit Nueangaudom<sup>a</sup>, Sirirat Kokpol<sup>a\*</sup>,  
Fumio Tanak<sup>a,d\*</sup>, Nadtanet Nunthaboot<sup>b</sup>, Takeshi Nakanishi<sup>c</sup>, Masaya Kitamura<sup>c</sup>, Seiji  
Taniguchi<sup>d</sup>, Haik Chosrowjan<sup>d\*</sup>**

---

<sup>a</sup> *Department of Chemistry, Faculty of Science, Chulalongkorn University, Bangkok 10330, Thailand,*

<sup>b</sup> *Department of Chemistry and Center of Excellence for Innovation in Chemistry, Faculty of Science, Mahasarakham University, Mahasarakham 44150, Thailand,*

<sup>c</sup> *Department of Applied Chemistry and Bioengineering, Graduate School of Engineering, Osaka City University, Osaka 558-8585, Japan*

<sup>d</sup> *Division of Laser BioScience, Institute for Laser Technology, Osaka 550-0004, Japan*

---

**This article is in preparation for publication (2013).**

---



## 6.1 ABSTRACT

Flavodoxin from *Helicobacter pylori* (FD-HP) contains flavin mononucleotide (FMN) as a cofactor. Tyr92, Trp64 and Tyr121 locate near isoalloxazine (Iso). The center-to-center distances ( $R_c$ ) from Tyr92, Trp64 and Tyr121 to Iso were obtained by molecular dynamics (MD) simulation. The mean values of  $R_c$  were 0.56, 1.55 and 1.92 nm, respectively. Photoinduced electron transfer (ET) from these aromatic amino acids to the excited Iso (Iso\*) was studied by ultrafast fluorescence dynamics obtained by means of a fluorescence up-conversion method. The fluorescence decayed with lifetimes of 173 fs (amplitude, 0.963) and 2.08 ps (0.037). The fluorescence intensities were analyzed with Kakitani and Mataga (KM) theory and atomic coordinates of the protein obtained by MD simulation, to obtain ET rate from the donors and related physical quantities. The ET rates from Tyr92 to excited Iso was  $23 \text{ ps}^{-1}$ . Those from Trp64 and Tyr121 were negligibly slow. The logarithmic ET rates displayed a parabolic behavior with a total free energy gap. A net electrostatic ( $ES$ ) energy between the photo-products and ionic groups inside the protein also displayed a parabolic behavior with the total free energy gap, which suggests that the parabolic energy gap law is ascribed to the net  $ES$  energy, and further the net  $ES$  energy is one of the most influential factors for the ultrafast ET rate. Dutton law predicts that the logarithmic ET rate decreases with  $R_c$ . The Dutton law was examined for the ET rate of Tyr92. However, no clear relationship between the logarithmic ET rates and  $R_c$ s were obtained. The reason for it was discussed comparing with Dutton law in flavin mononucleotide (FMN) binding protein.

## 6.2 INTRODUCTION

Photoinduced electron transfer (ET) phenomena have been central field of photochemistry and photobiology.[9, 19, 133-136] Since several flavin photoreceptors were found, ET in the flavoprotein photoreceptors has been investigated by many researchers.[30, 84, 137] Photochemistry of flavins was pioneered by Weber.[138] McCormick demonstrated strong quenching of flavin fluorescence by indole in isoalloxazine-( $\text{CH}_2$ )<sub>n</sub>-indole diads.[139] Berg and Visser reviewed on the time-resolved fluorescence spectroscopy of flavoproteins.[140] It was demonstrated that the remarkable quenching of flavin fluorescence by N,N'-dimethylaniline, indole and phenol in solution is ascribed to ET from the donors to the excited flavins, by means of

a picosecond-resolved transient absorption spectroscopy.[77] ET in flavodoxin (FD) from *Desulfovibrio vulgaris* in the picoseconds time domain [28] and in glucose oxidase in femtoseconds time domain has been also demonstrated by means of a transient absorption spectroscopy.[25]

Fluorescence is remarkably quenched in many of flavoproteins due to ET from Trp and/or Tyr to the excited isoalloxazine (Iso\*). The ultrafast fluorescence lifetimes of a number of flavoproteins were studied by means of a photon-counting method,[141] and a fluorescence up-conversion method.[6, 29, 31, 42-43, 80, 142] The fluorescence lifetimesv[80, 142-144] and decays [17-18, 58-59, 64, 145] have been analyzed with crystal structures and snapshots in water obtained by molecular dynamics (MD) simulation, using an electron transfer theory.

FDs are a group of small flavoproteins with a molecular weight of 15–23 kDa, that have been isolated from a variety of microorganisms, including *Helicobacter pylori* (*H. Pylori*) and *Desulfovibrio vulgaris*, Miyazaki F (DV). FDs are considered to function as electron transport proteins in various metabolic pathways.[146] *H.pylori* is a pathogen for type-B gastritis and peptic-ulcer diseases,[115] gastric carcinoma [147] and mucosa-associated lymphoid-tissue lymphoma.[118] It has been found that an inhibition of FD from *H. pylori* (FD-HP) by some compounds prevents the infections.[20] Crystal structure of FD-HP was determined by Freigang et al.[8] It contains Tyr92 near Iso, while FD from *Desulfovibrio vulgaris*, Miyazaki F. (FD-DvMF) has Trp59 and Tyr97 within 1 nm from isoalloxazine (Iso). Fluorescence from both FDs is strongly quenched as a consequence of ET from these aromatic amino acids to Iso\*. The ET mechanism in FD-DvMFs was studied with the structures determined by MD simulation.[58] In the present work the ultrafast fluorescence dynamics of FD-HP has been studied by means of the fluorescence up-conversion method. The ET mechanism in FD-HP has been comparatively examined with FD-DvMF and flavin mononucleotide (FMN) binding protein (FBP) from DV, by using MD simulation structures.

## 6.3 THEORETICAL METHODS

### 6.3.1 Method of MD simulation

The X-ray structure of FD-HP (PDB code 1FUE, Research Collaboratory for Structural Bioinformatics; <http://www.rcsb.org/pdb>) [8] was used as a starting structure of MD simulation

calculation. All missing hydrogen and heavy atoms were added by using Discovery studio 2.0 software packages. (Accelrys). The parameters of FMN cofactor were obtained from our previously work [7] whereas the AMBER03 force field [51] was used to describe the amino acid topologies. All MD simulations were carried out by using the AMBER 10 suite of programs.[51] First, the structure was minimized with 2000 steps of steepest decent (SD) minimization, followed by 3000 steps of conjugate gradient (CG) minimization to remove the bad geometrical crashes. Second, the protein was solvated with 6660 TIP3P water molecules in a cubic box. The energy of the protein-added water molecules was minimized, keeping the protein fixed. Subsequently, the SD with 2000 steps and then CG minimizations with 3000 steps were performed on the whole system with the periodic boundary extending to 1 nm from the complex. The MD simulations were carried out under the isobaric-isothermal ensemble (normal temperature and pressure, *NPT*) with a constant temperature at 298 K and with constant pressure at 1 atm. The electrostatic interaction was corrected by the Particle Mesh Ewald (PME) method.[128] The SHAKE algorithm was employed to constrain all bonds involving hydrogen atoms.[52] The non-bonded pair interactions were treated with a cut-off distance of 1 nm. The MD simulations were performed over 50 ns with the time step of 2 fs. The MD coordinates were collected every 0.1 ps during the last 5 ns of the production time and used for further analyses.

### 6.3.2 Method of theoretical analyses

#### 6.3.2.1 ET theory

The original Marcus ET theory [15, 73] has been modified in various ways [16, 74-75, 103-104, 148-150] In the present analysis, the Kakitani and Mataga (KM) theory [16, 148-150] was used, because it is applicable for both adiabatic and non-adiabatic ET processes, and has been found to give satisfactory results for static [80, 142-144] and dynamic [17-18, 58-59, 64, 145] ET analyses in several flavoproteins. The ET rate described by KM theory is expressed by Eq. 6.1;

$$k_{ET}^j = \frac{\nu_0^q}{1 + \exp\{\beta^q(R_j - R_0^q)\}} \sqrt{\frac{k_B T}{4\pi\lambda_s^{qi}}} \exp\left[-\frac{\{\Delta G_q^0 - e^2 / \epsilon_0^p R_j + \lambda_s^{qi} + ES_j\}^2}{4\lambda_s^{qi} k_B T}\right] \quad (6.1)$$

Here  $k_{ET}^j$  is the ET rate from a donor  $j$  to Iso\*, and index  $q$  denotes Trp or Tyr.  $\nu_0^q$  is an adiabatic frequency,  $\beta^q$  is the ET process coefficient.  $R_j$  and  $R_0^q$  are the donor  $j$ -Iso distance and its critical distance between adiabatic and non-adiabatic ET process, respectively.  $R_j$  is expressed as a center-to-center distance ( $R_c$ ) rather than edge-to-edge ( $R_e$ ) distance.[17-18, 58-59, 64, 80, 142-145] The ET process is adiabatic when  $R_j < R_0^q$ , and non-adiabatic when  $R_j > R_0^q$ .  $k_B$ ,  $T$  and  $e$  are Boltzmann constant, temperature and electron charge, respectively.  $ES_j$  is a net electrostatic ( $ES$ ) energy, which is described below. FD-HP contains 2 Trps (Trp64 and Trp155) and 3 Tyrs (Tyr92, Tyr104 and Tyr121) among 164 amino acid residues. In the present work the ET rates from Trp64, Tyr92 and Tyr121 of these aromatic amino acids to Iso\* were taken into account for the analysis, because the donor-acceptor distances were relatively short.

$\lambda_s^{qj}$  is a solvent reorganization energy [15, 73] of the ET donor  $q$  and  $j$ , and is expressed as Eq. 6.2.

$$\lambda_s^{qj} = e^2 \left( \frac{1}{2a_{Iso}} + \frac{1}{2a_q} - \frac{1}{R_j} \right) \left( \frac{1}{\epsilon_\infty} - \frac{1}{\epsilon_0^p} \right) \quad (6.2)$$

where  $a_{Iso}$  and  $a_q$  are the radii of Iso and Trp or Tyr, with these reactants being assumed to be spherical, and  $\epsilon_\infty$  and  $\epsilon_0^p$  are optical and static dielectric constants inside the protein. The static dielectric constant for the solvent reorganization energy and  $ES$  energy between Tyr92 cation and Iso anion was expressed by  $\epsilon_0^p = \epsilon_0^{DA}$ , while  $\epsilon_0^p = \epsilon_0$  in the other donor-acceptor pairs, because the  $R_c$  for Tyr92 was quite close shorter than 1 nm, and hence no amino acid exists between the donor and acceptor, The  $R_c$  between Trp64 or Tyr121 and Iso were longer than 1 nm where many amino acids exist. The situation in the Iso-Tyr92 pair may be quite different from the  $ES$  energy between the ionic species of photoproducts and the other ionic groups in the protein where there are many amino acids between them, as described below. The optical dielectric constant used was 2.0. The radii of Iso ( $a_{Iso}$ ), Trp ( $a_{Trp}$ ) and Tyr ( $a_{Tyr}$ ) used were 0.224, 0.196 and 0.173 nm, respectively.[17, 58-59, 64, 145]

The standard free energy gap was expressed with the ionization potential of the ET donor,  $E_{IP}^q$ , as Eq. 6.3;

$$\Delta G_q^0 = E_{IP}^q - G_{Iso}^0 \quad (6.3)$$

Here,  $G_{Iso}^0$  is standard Gibbs energy related to electron affinity of Iso\*. The values of  $E_{IP}^q$  for Trp and Tyr were 7.2 eV and 8.0 eV, respectively.[78]

### 6.3.2.2 Electrostatic energy in the FD-HP

Protein systems contain many ionic groups, which may influence the ET rate. The FMN cofactor in FD-HP has 2 negative charges at the pyrophosphate, while the protein itself contains 13 Glu, 14 Asp, 13 Lys and 2 Arg residues.

The *ES* energy between Iso anion or donor cation  $j$  and all other ionic groups in the protein is expressed by Eq. 6.4;

$$E(j) = \sum_{i=1}^{13} \frac{C_j \cdot C_{Glu}}{\epsilon_0 R_j(Glu - i)} + \sum_{i=1}^{14} \frac{C_j \cdot C_{Asp}}{\epsilon_0 R_j(Asp - i)} + \sum_{i=1}^{13} \frac{C_j \cdot C_{Lys}}{\epsilon_0 R_j(Lys - i)} + \sum_{i=1}^2 \frac{C_j \cdot C_{Arg}}{\epsilon_0 R_j(Arg - i)} + \sum_{i=1}^2 \frac{C_j \cdot C_P}{\epsilon_0 R_j(P - i)} \quad (6.4)$$

where  $j = 0$  for the Iso anion,  $j = 1$  for the Trp64 cation and  $j = 2$  for Tyr92 cation and  $j = 3$  for Tyr 121 cation.  $C_j$  is the charge of the aromatic ionic species  $j$ , that is  $-e$  for  $j = 0$  and  $+e$  for  $j = 1$  to 3.  $C_{Glu}$  ( $= -e$ ),  $C_{Asp}$  ( $= -e$ ),  $C_{Lys}$  ( $= +e$ ),  $C_{Arg}$  ( $= +e$ ) and  $C_P$  ( $= -e$ ) are the charges of the Glu, Asp, Lys and Arg residues plus the phosphate anions, respectively. We assumed that these groups are all in ionic state in solution. The values of  $pK_a$  of ionic amino acids in water were 4.3 in Glu, 3.9 in Asp, 10.5 in Lys, and 12.5 in Arg. In the protein these values of  $pK_a$  may be modified in the range of  $\pm 0.3$ . Histidine displays 6.0 of  $pK_a$  in water. All measurements were performed in 10 mM Tris-HCl (pH 8.0) buffer, where His should be neutral in the solution. The distances between the aromatic ionic species  $j$  and the  $i^{\text{th}}$  Glu ( $i = 1 - 13$ ) are denoted as  $R_j(Glu - i)$ , while the distances between the aromatic ionic species  $j$  and the  $i^{\text{th}}$  Asp ( $i = 1 - 14$ ) are denoted as  $R_j(Asp - i)$ , and so on. The dielectric constant in this *ES* energy was  $\epsilon_0$  as discussed above.

$ES_j$  in Eq. 6.1 was expressed as follows:

$$ES_j = E(0) + E(j) \quad (6.5)$$

Here  $j$  is from 1 to 3, and represents  $j$ th ET donor as described above.

### 6.3.3 Fluorescence Decays

The calculated decay curve expressed by Eq. 6.6, was obtained from a calculated decay function given below.

$$F_{calc}^c(t) = \int_0^t P(t-t') F_{calc}^f(t') dt' \quad (6.6)$$

Eq. 6.6 shows a convolution of the calculated decay function  $F_{calc}^f(t')$  given by Eq. 6.7 with an instrumental response,  $P(t-t')$ .

$$F_{calc}^f(t) = \left\langle \exp - \left\{ \sum_{j=1}^3 k_{ET}^j(t') \right\} t \right\rangle_{AV} \quad (6.7)$$

The fluorescence decay functions were calculated up to 3 ps, because the fluorescence dynamics was measured in this time range. In Eq. 6.7  $\langle \dots \rangle_{AV}$  means the averaging procedure of the exponential function in Eq. 6.7 over  $t'$  (MD simulation time) up to 5 ns with 0.1 ps time intervals. In Eq. 6.7 we assumed that the decay function at every instant of time,  $t'$ , during the MD time range can be always expressed by the exponential function. The decay expressed by Eq. 6.7 can be non-exponential after the averaging procedure, because the ET rate depends on MD simulation time  $t'$ . The present method is mathematically equivalent to the reported one [34] when the time range (5 ns) of MD simulation data is much longer than one (3 ps) of fluorescence data. The mathematical basis of this approach is described in **Supplemental Information of Chapter III**. Unknown ET parameters contained in KM theory were  $\nu_0^q$ ,  $\beta^q$ , and  $R_0^q$  for Trp and Tyr,  $G_{Iso}^0$ ,  $\varepsilon_0$  and  $\varepsilon_0^{DA}$ . These parameters were determined so as to obtain

the minimum value of  $\chi_A^2$  defined by Eq. 6.8, by means of a non-linear least square method according to Marquardt algorithm.

$$\chi^2 = \frac{1}{N} \sum_{i=1}^N \frac{\{F_{calc}^c(t_i) - F_{obs}(t_i)\}^2}{F_{calc}^c(t_i)} \quad (6.8)$$

Here  $F_{obs}(t_i)$  is the observed fluorescence intensity at  $t = t_i$ , and  $N = 153$ .

The observed fluorescence decay function of FD-HP,  $F_{obs}^f(t)$ , was extracted from the observed fluorescence intensities by means of a deconvolution procedure with a two-exponential function as expressed by Eq. 6.9;

$$F_{obs}^f(t) = \alpha_1 \exp(-t / \tau_1) + \alpha_2 \exp(-t / \tau_2) \quad (6.9)$$

Here the lifetimes were obtained as  $\tau_1 = 0.173$  ps ( $\alpha_1 = 0.963$ ) and  $\tau_2 = 2.08$  ps ( $\alpha_2 = 0.037$ ).

## 6.4 RESULTS

### 6.4.1 Dynamics of geometry around Iso

Absorption and fluorescence spectra of FD-HP are shown in Figure 6.1. The protein was dissolved into 10 mM Tris-HCl (pH 8.0) buffer. Absorption spectrum displayed two peaks at 378 nm and 452 nm in visible wavelength region. The wavelengths at absorption maxima were similar to those of free FMN. Fluorescence peak was at 521 nm, which was shorter by ca. 10 nm than one of free FMN in aqueous solution. A snapshot obtained by MD simulation of FD-HP around Iso is shown in Figure 6.2(A). Two Trps, Trp64 and Trp155, and three Tyrs, Tyr92, Tyr104 and Tyr121, exist in FD-HP as potential ET donors. Only one aromatic amino acid, Tyr92, locates near Iso within 1 nm, while Iso is sandwiched by Trp59 and Tyr97 in FD-DvMF (Figure 6.2(B)). Dynamics of Rc between Iso and Tyr92, between Iso and Trp64 and between Iso and Tyr121 are illustrated in Figure 6.3. Three closest aromatic amino acids to Iso are shown among the five in FD-HP. Fluctuation of Tyr92 in Rc was rather little compared to the other amino acids. Mean

values of  $R_c$  over MD time are listed in Table 6.1, together with those of FD-*Dv*MF and FBP for comparison. The values of  $R_c$  were 0.56 nm in Tyr92, 1.55 nm in Trp64 and 1.92 nm in Tyr121. The values of Tyr97 are 0.54 nm in WT FD-*Dv*MF, 0.55 nm in W59F (Trp59 replaced by Phe) FD-*Dv*MF.[59] The values of Trp are 0.64 nm in WT FD-*Dv*MF and 0.78 in Y97F (Tyr97 replaced by Phe) FD-*Dv*MF,[59] 0.70 nm in Trp32 of FBP.[145]

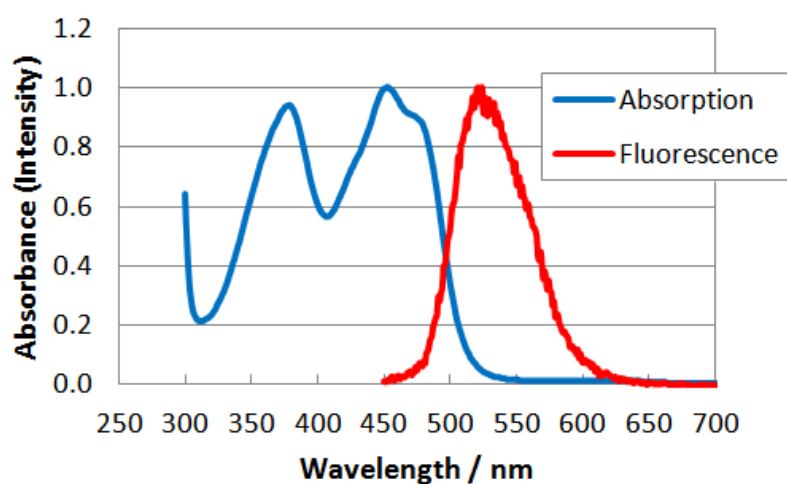


**Figure 6.1** Absorption and fluorescence spectra of FD-HP. The absorption peaks were at 378 nm and 452 nm in visible wavelength region. Fluorescence peak was at 521 nm. FD-HP was dissolved in 10 mM Tris-HCl buffer at pH 8.0. Optical density at the excitation wavelength (450 nm) was ca. 0.1 upon the fluorescence measurements.

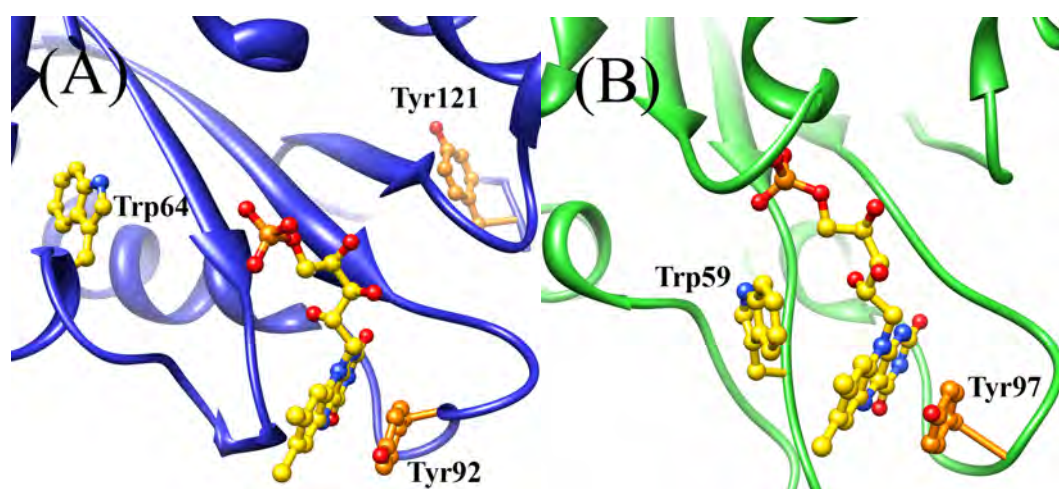


**Figure 6.2** The protein structures near Iso binding site in FD-HP and FD-*Dv*MF obtained by MD



simulation

Iso is stacked with Tyr92 in FD-HP (A), while it is sandwiched by Trp59 and Tyr97 in FD-*Dv*MF (B). Mean center-to-center distance ( $R_c$ ) between Iso and Tyr92 was 0.56 nm, which are similar to those of  $R_c$  between Iso and Tyr97 in WT FD-*Dv*MF and W59F FD-*Dv*MF.[59]

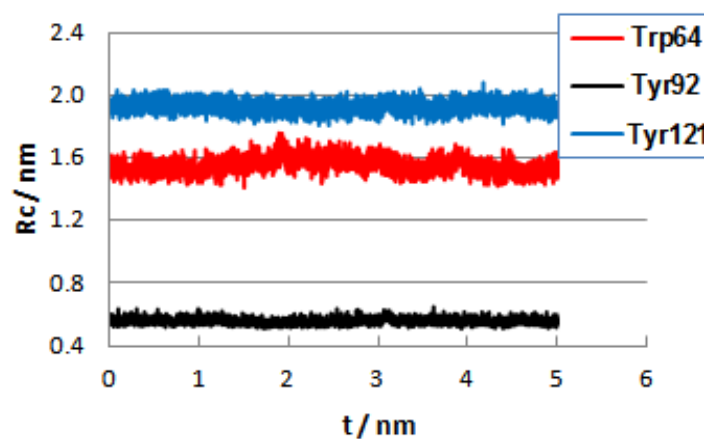


**Figure 6.3** Time-evolution of  $R_c$  between Iso and nearby aromatic amino acids

Tyr92, Trp64 and Tyr121 were three closest aromatic amino acids to Iso among five in FD-HP. Number of snapshots was 50000 with 0.1 ps time intervals. Mean values of  $R_c$  over 50000 snapshots are listed in Table 6.1.

### 6.4.2 Ultrafast fluorescence dynamics

Ultrafast fluorescence dynamics were measured by means of the fluorescence up-conversion method. Figure 6.4 shows the decays of FD-HP at 530 nm of the emission. The observed intensities are shown with dots. The decay did not display any emission-wavelength dependence. The experimental intensities were first approximated with a two-exponential function, by means of the deconvolution procedure as described at Section 6.3.6. The obtained decay function is given by Eq. 6.9. The lifetimes were 173 fs and 2.08 ps, with pre-exponential factors of 0.963 and 0.037, respectively.

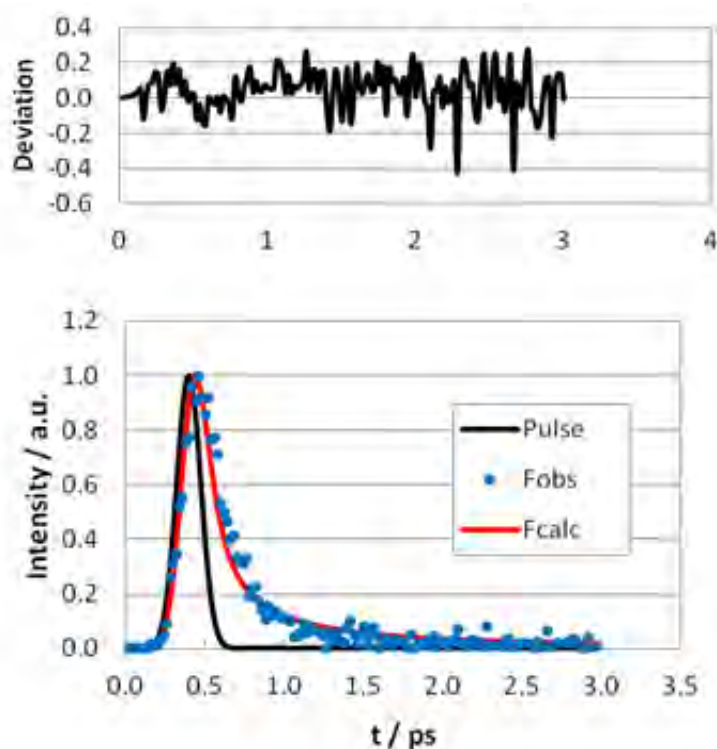


**Figure 6.4** Observed and calculated fluorescence intensities

Upper panel shows deviation between the observed and calculated intensities obtained by Eq. 6.11, and lower panel the observed (blue dots), calculated intensities (red line) with KM theory, and pulsed laser (black line). The emission was monitored at 530 nm. Half-width of the laser was ca. 0.2 ps at 410 nm. The protein was dissolved into 10 mM Tris-HCl (pH 8.0) buffer. Absorbance of the sample at 410 nm (excitation) was ca. 3 in a cell-cuvettes with 1 cm optical pass.

### 6.4.3 ET parameters

The observed fluorescence intensities were analyzed with three methods as described at Section 6.3.6. The calculated decay function shown in Figure 6.4 (red line). The ET parameters contained in KM theory are listed in Table 6.2. The values related to Trp as  $\nu_0$  (Trp),  $\beta$  (Trp) and  $R_0$  (Trp) may not be accurate, because ET rate from Trp64 was negligibly slow (see Table 6.3). The values of  $\chi^2$  were  $1.62 \times 10^{-2}$ . The unknown variable ET parameters were  $\nu_0^q$ ,  $\beta^q$ , and  $R_0^q$  (for Trp and Tyr),  $G_{iso}^0$ ,  $\varepsilon_0$  and  $\varepsilon_0^{DA}$ . The values of  $\nu_0^q$ ,  $\beta^q$ , and  $R_0^q$  for Tyr were  $610 \text{ ps}^{-1}$ ,  $6.0 \text{ nm}^{-1}$  and  $1.2 \text{ nm}$ , respectively. The values of  $G_{iso}^0$ ,  $\varepsilon_0$ , and  $\varepsilon_0^{DA}$  were 7.2 eV, 3.8 and

2.3, respectively. The static dielectric constant ( $\epsilon_0^{DA}$ ) between Tyr92 and acceptor were lower than one of the entire protein ( $\epsilon_0$ ). This is reasonable because no amino acid exists between them like a kind of vacuum.

The  $R_0$  (Tyr) was much longer in FD-HP (1.2 nm) than one in FD-*Dv*MF (0.68 nm), which suggests that ET process in FD-HP is adiabatic, while it is both adiabatic and non-adiabatic in FD-*Dv*MF depending on  $R_c$ . The value of  $G_{Iso}^0$  were lower in FD-HP than one in FD-*Dv*MF. The static dielectric constant of the entire protein ( $\epsilon_0$ ) was also lower in FD-HP than one in FD-*Dv*MF, which suggests that polarity inside the protein is lower in FD-HP than one in FD-*Dv*MF. The maximum wavelength of the fluorescence spectrum of FD-HP was shorter by 10 nm than FMN in aqueous solution, which supports the low polarity inside the protein.

#### 6.4.4 ET rate and related physical quantities

In Figure 6.5(A) time-evolutions of logarithmic ET rates are shown from the three donors. The ET rates from Trp64 and Tyr121 were negligibly slow compared to one from Tyr92, which reveals that ultrafast decay of FD-HP is ascribed to ET solely from Tyr92 to Iso\*. The ET rate from Tyr92 is shown more in detail in Figure 6.5(B). Figure 6.5(C) shows a distribution of the logarithmic ET rate from Tyr92. The logarithmic ET rate displayed a sharp peak at around 4. Mean values of the ET rates are listed in Table 6.3. The mean ET rates from Tyr92 were 22.5 ps<sup>-1</sup>. The ET rates from Trp64 and Tyr121 were negligibly slow.

**Table 6.1** Donor-acceptor distance<sup>a)</sup>

WT (FD-HP)		WT <sup>b)</sup> (FD- <i>Dv</i> MF)		Y97F <sup>b)</sup> (FD- <i>Dv</i> MF)	W59F <sup>b)</sup> (FD- <i>Dv</i> MF)	WT <sup>c)</sup> (FBP)	
Trp64	Tyr92	Tyr121	Trp59	Tyr97	Trp59	Tyr97	Trp32
1.55	0.56	1.92	0.64	0.54	0.78	0.55	0.70

<sup>a)</sup> Mean values of center to center distances between Iso and donors indicated are listed over 50,000 snapshots in WT from *H. pylori*, 20,000 snapshots in flavodoxins from *Desulfovibrio vulgaris*, Miyazaki F.

<sup>b)</sup> Data are taken from Ref.[58-59]

<sup>c)</sup> Data taken from Ref.[17]

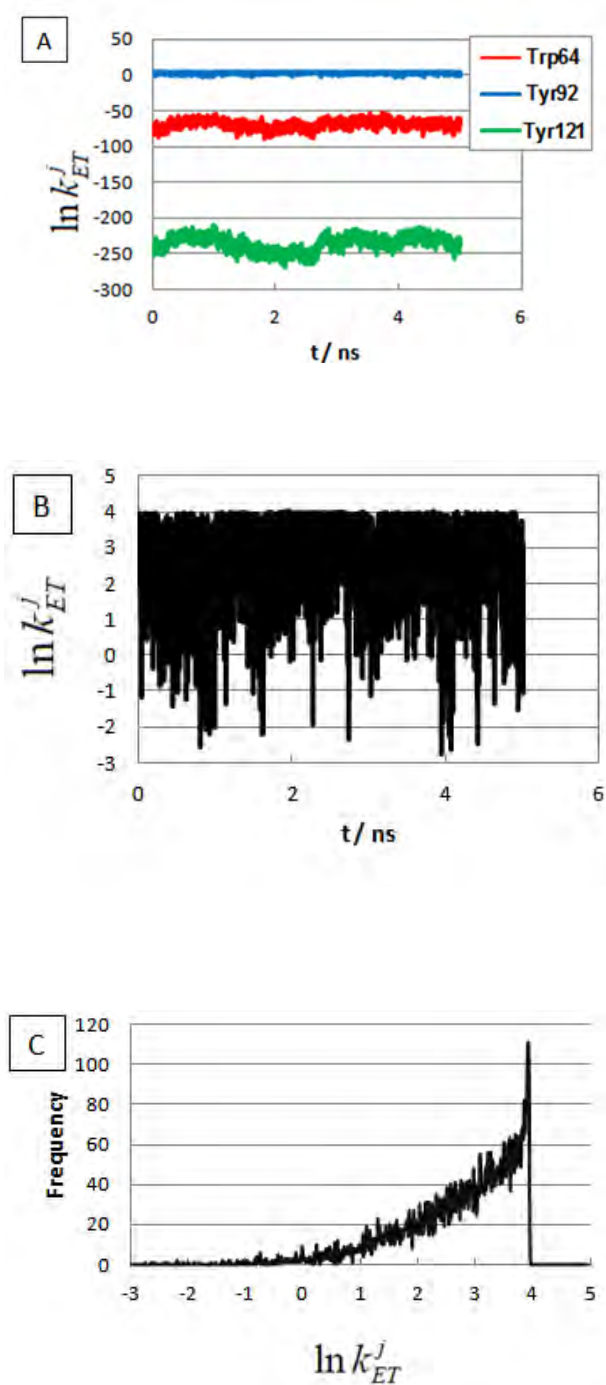


**Figure 6.5** Time-evolution of ET rate

Panel A represents ET rates from Trp64, Tyr92 and Tyr121 to Iso\*, and Panel B, ET rate from Tyr92. Panel C represents distribution of logarithmic ET rate from Tyr92 to Iso\*.

Time-evolutions of  $ES$  energies between Iso anion and ionic groups inside the protein [ $E(0)$  in Eq. 6.4], and between the donor cation and ionic groups inside the protein [ $E(j)$ ] are shown in Figure 6.6(A). The net  $ES$  energies between the photo-products and the ionic groups [ $ES_j$  in Eq. 6.5] are illustrated in Figure 6.6(B). The  $E(0)$  of Iso anion was highly positive and varied at around 4.5 eV. Repulsion energies by phosphate anions may greatly contribute to it, because the distances between the two negative charges and Iso anion were within 1 nm. The  $E(j)$  of Tyr92 varied at around -4.5 eV, and accordingly the net  $ES$  energies obtained as the sum of them were close to zero as in Figure 6.6(B). The net  $ES$  energies of Trp64 and Tyr121 were much greater than one of Tyr92. The mean values of the net  $ES$  energies are also listed in Table 6.3. The mean values were -0.12 to -0.17 eV in Tyr92 depending the Method used, while those of Trp64 and Tyr121 were 1.6 – 2.4 eV and 3.9 – 6.0 eV, respectively. The  $ES$  energy between Iso anion and a donor cation was greatest in Tyr92 among the donors, because Iso – Tyr92 distance was shortest. The solvent reorganization energy was least in Tyr92 among the donors. The energy increases with the donor-acceptor distance [see Eq. 6.2].

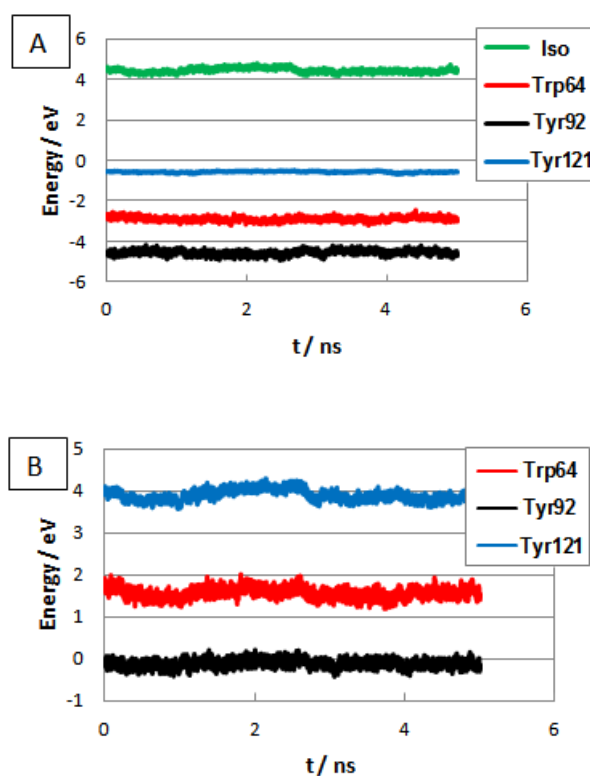


**Figure 6.6** ES energy between photoinduced ionic species and ionic groups in the protein

Panel A indicates ES energies between Iso anion or donor cations and ionic groups in the protein. Panel B indicates net ES energy between the photoproducts and ionic groups in the protein, given by Eq. 6.5.

These physical quantities including ET rates are compared to those of FD-*Dv*MF [59] as listed in Table S6.1 (**Supplemental Information of Chapter VI**). These values were obtained by simultaneous analysis among four FD-*Dv*MF mutated isoforms, WT, W59F, Y97F and W59F/Y97F. Despite that Rcs between Iso and Tyrs are similar among FD-HP, WT FD-*Dv*MF and W59F FD-*Dv*MF, the ET rate from Tyr92 was fastest in FD-HP, as 6.4 ps<sup>-1</sup> in FD-HP, 1.3 x 10<sup>-3</sup> ps<sup>-1</sup> in WT FD-*Dv*MF, and 5.0 ps<sup>-1</sup> in W59F FD-*Dv*MF.

#### 6.4.5 Energy gap law and Dutton law

Total free energy gap is expressed by Eq. 6.13;

$$-\Delta G_T^0 = -\Delta G_q^0 + e^2 / \epsilon_0^q R_j - ES_j \quad (6.13)$$

Meaning of every term in the right hand side is described below Eq. 6.1. Figure 6.7(A) shows a relationship of the  $\ln k_{ET}^j$  of Tyr92 with  $-\Delta G_T^0$ , which is called the energy gap law. Variations of these quantities are ascribed to the structural fluctuation of FD-HP revealed by MD simulation. The relationship was well described with a parabolic function expressed as a function,  $Y = -36.75X^2 + 19.7X + 1.29$ , where Y is  $\ln k_{ET}^j$  and X,  $-\Delta G_T^0$ . Figure 6.7(B) shows a relationship between  $\ln k_{ET}^j$  and  $-ES_j$ . The dependence of  $\ln k_{ET}^j$  on  $-ES_j$  was also well approximated with a parabolic function,  $Y = -21.6X^2 - 4.44X + 3.73$ , where Y is  $\ln k_{ET}^j$  and X,  $-ES_j$ . These results reveal that the parabolic energy gap law in FD-HP is ascribed greatly to the net ES energy. Figure 6.7(C) shows a relationship between  $\ln k_{ET}^j$  and Rc, which is called as Dutton law.[19, 74] According to Moser et al.,[74] the logarithmic ET rates linearly decrease with the edge-to-edge donor-acceptor distances. Figure 6.7(C) reveals no such linear relation, as predicted by Moser et al.[74]

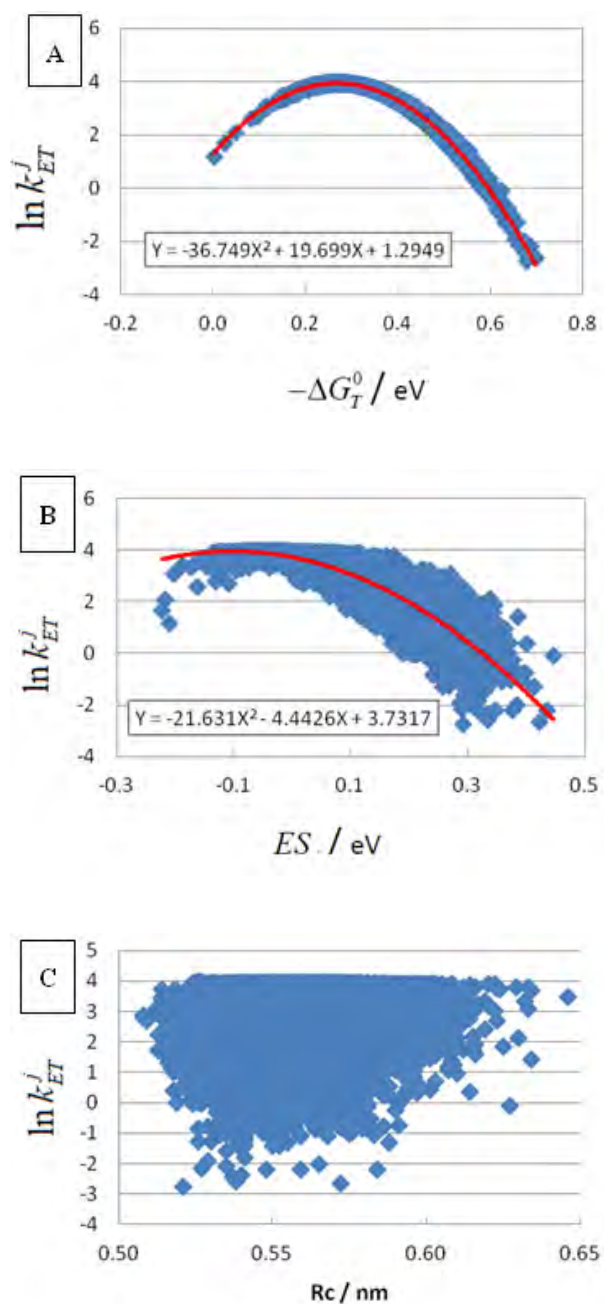


**Figure 6.7** Correlation between the logarithmic ET rate and net ES energy or Rc in FD-HP.

Panel A indicates relationship between the logarithmic ET rate from Tyr92 to Iso\* (Energy gap law), Panel B relationship between the logarithmic ET rate and the net ES energy and Panel C relationship between the logarithmic ET rate and Rc (Dutton law).

**Table 6.2** Best-fit ET parameter in FD-HP

System	$\nu_0$ (ps <sup>-1</sup> )		$\beta$ (nm <sup>-1</sup> )		$R_0$ (nm)		$G_{Iso}^0$ (eV)	$\epsilon_0$	$\epsilon_0^{DA}$	$\chi^2$
	Trp	Tyr	Trp	Tyr	Trp	Tyr				
FD-HP <sup>a</sup>	1019	611	21.0	6.01	0.666	1.15	7.16	3.76	2.25	$1.62 \times 10^{-2}$
FD-DvMF <sup>b</sup>	3090	2460	55.6	9.64	0.772	0.676	7.67	4.24	-	$5.55 \times 10^{-4}$

<sup>a</sup> The observed intensities were used for the analysis with a convolution procedure.

<sup>b</sup> The results of simultaneous analyses of WT, W59F, Y97F, W59F/Y97F flavodoxins, Miyazaki F. [59] are listed for the comparison.

**Table 6.3** Physical quantity related to ET rate<sup>a)</sup>

System	$k_{ET}^j$ <sup>b)</sup> (ps <sup>-1</sup> )			$ES_j$ <sup>c)</sup> (eV)			$-e^2 / \epsilon_0^d R_j$ <sup>d)</sup> (eV)			$\lambda_s^{aj}$ <sup>e)</sup> (eV)		
	Trp64	Tyr92	Tyr121	Trp64	Tyr92	Tyr121	Trp64	Tyr92	Tyr121	Trp64	Tyr92	Tyr121
FD-HP	$3.97 \times 10^{-27}$	22.5	$1.24 \times 10^{-95}$	1.58	-0.117	3.88	-0.247	-1.15	-0.198	1.39	0.268	1.55
	(3.11)											

<sup>a</sup> Mean values over 50,000 snapshots are listed.

<sup>b</sup> ET rate given by Eq. 6.1.

<sup>c</sup> Net  $ES$  energy between the photo-products and ionic groups inside the protein, given by Eq. 6.5.

<sup>d</sup>  $ES$  energy between Iso anion and a donor cation, appeared in Eq. 6.1.



## 6.5 DISCUSSION

It was found that the ultrafast fluorescence dynamics of FD-HP is ascribed to very fast ET from Tyr92 to Iso\*. ET rate of  $23 \text{ ps}^{-1}$  from Tyr92 to Iso\* in FD-HP was much faster than Tyr97 in WT of FD-*Dv*MF ( $0.001 \text{ ps}^{-1}$ ) [59] and faster than Tyr97 in W59F FD-*Dv*MF ( $5.0 \text{ ps}^{-1}$ ), despite that Rc (0.56 nm) between these Tyrs and Iso are similar. The dependence of the logarithmic ET rate on the total free energy gap displayed the parabolic behavior as in FD-*Dv*MF [59] and FBP.[17, 151] The parabolic behavior of the logarithmic ET rates is mainly ascribed to the net *ES* energy as shown in Figure 6.7(B). It has been also demonstrated that the net *ES* energy is a key factor for the ET rate in WT, E13K (Glu13 replaced by Lys), E13R (Glu13 replaced by Arg, E13T (Glu13 replaced by Thr) and E13Q (Glu13 replaced by Gln) FBP isoforms,[142, 151] in addition to Rc.

The linear relationship between the logarithmic ET rates and Rc obtained by Moser et al.[19, 74] suggests that ET rate mainly depends on Rc in the electronic coupling term as in Marcus-Hush ET rate,[74] and in KM theory [Eq. 6.1]. In FBP the logarithmic ET rates from Trp32 to Iso\* displayed a clear parabolic behavior against Rc, not linear,[151] in which Rc of Trp32 to Iso is 0.70 nm. The reason for it may be that the electronic coupling term is important, when the ET rates are rather slow as in ET processes of photosynthetic reaction centre and dark electron transfer in proteins,[19, 74] but the nuclear term may be important, when ET rates are ultrafast.[151] The parabolic behavior against Rc can be elucidated only by the nuclear term. In FD-HP the relationship between the logarithmic ET rates and Rc was neither linear nor parabolic. It is of interest why the logarithmic ET rates – Rc relationship is parabolic in Trp32 of FBP, but not in Tyr92 of FD-HP, despite that the ET rates in the both systems are similar. Figure 6.8 shows dependencies of various energies contained in the nuclear term of Eq. 6.1 on Rc in FD-HP. The  $ES_j$  of Tyr92 tends to decrease (increase in absolute value) with Rc (slope of -1.6), when it was approximated with a linear function. Total free energy gap ( $\Delta G_T^0$ ) also tends to decrease a little with Rc with the slope -0.4. The  $\Delta G_T^0$  contains both of  $ES_j$  and  $-e^2 / \epsilon_0^p R_j$  between Iso anion and Tyr92 cation. The *ES* energy of the ion pair should increase (decrease in absolute value) with Rc, and accordingly slope of the total free energy gap against Rc became more mild with little negative slope. The solvent reorganization energy,  $\lambda_s^{ij}$ , should increase

with  $R_c$  as shown in Eq. 6.2 with positive slope. Accordingly the dependency of  $\Delta G_T^0 + \lambda_S^{qj}$  [entire energies in the square term in the exponential function, see Eq. 6.1] on  $R_c$  became negligible.

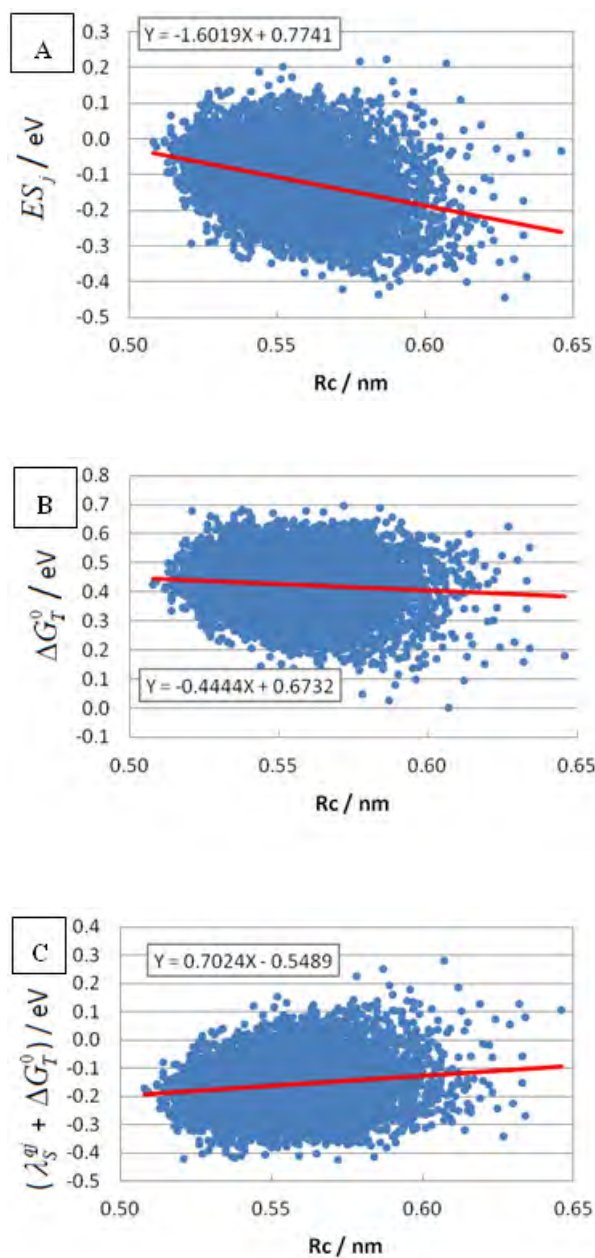


**Figure 6.8** Relationship between  $R_c$  and various energies of Tyr92 in FD-HP

Panel A shows  $R_c$  - net  $ES$  energy relation, Panel B,  $R_c$  - total free energy gap, and Panel C,  $R_c$  - sum of total free energy gap and solvent reorganization energy. Solid red lines in the Panels show approximate linear functions between these quantities.

**CHAPTER VII**  
**INTERMOLECULAR CHARGE TRANSFER CALCULATION OF**  
***HELICOBACTER PYLORI* FLAVODOXIN**

---

**TDDFT and MS-RASPT2 Study of Photoinduced  
Intermolecular Charge Transfer in *H. Pylori* Flavodoxin**

**Kiattisak Lugsanangarm<sup>1</sup>, Stephan Kupfer<sup>2</sup>, Peter Wolschann<sup>3</sup>,  
Somsak Pianwanit<sup>1</sup>, Sirirat Kokpol<sup>1</sup>, Fumio Tanaka<sup>1,4</sup>, Leticia González<sup>3\*</sup>**

---

<sup>1</sup> *Department of Chemistry, Faculty of Science, Chulalongkorn University, Bangkok 10330,  
Thailand*

<sup>2</sup> *Institute of Photonic Technology (IPHT) Jena, Albert-Einstein-Str. 9, 07745, Jena, Germany*

<sup>3</sup> *Institute of Theoretical Chemistry, University of Vienna, Vienna 1090, Austria*

<sup>4</sup> *Division of Laser BioScience, Institute for Laser Technology, Utsubo-Honmachi, 1-8-4, Nishiku,  
Osaka 550-0004, Japan*

---

**This article is in preparation for publication (2013).**

---

## 7.1 ABSTRACT

The UV-Visible absorption electronic spectra of *helicobacter pylori* (*H. pylori*) flavodoxin (FD) have been studied by means of Time-Dependent Density Functional Theory (TDDFT) and Multi-State Restricted Active Space Perturbation Theory of second order/Restricted Active Space Self-Consistent Field (MS-RASPT2/RASSCF). Upon experimental light excitation, FD shows the charge transfer (CT) absorption band. The TDDFT calculations with varies of the hybrid exact exchange and long-range correction functional show the inconsistent of the CT state. We found that performing TDDFT by global exact exchange (B3LYP-35, B97D and PBE0) provided that the  $S_1$  state can be assigned to the dark CT state in which the wave functions were transferred from Tyr to Iso, while the  $S_2$  state is assigned to be the locally excited (LE) state inside Iso moiety. On the other hand, the long range-corrected functional (CAM-B3LYP, M06-2X and  $\omega$ B97XD) provide the opposite result. Moreover, the effect of solvations has been studied by performing such TDDFTs by using water solvation and mimicked protein environment. The red-shift of the excitation energy can be found by going from the less polar environment to the polar media. This result implied that the CT states are preferably stabilized in polar media. This disagreement of the TDDFT results have been further studies by performing MS-RASPT2/RASSCF (26,2,2;11,4,8) level of theory. The result confirms that the  $S_1$  state is more pronounced to be the LE state, while the  $S_2$  state shows the CT characteristic.

## 7.2 INTRODUCTION

In recent year, the intermolecular charge transfer has been extensively studied by both experimental and theoretical approaches. On the experimental viewpoint, there is some information at the atomistic level which cannot be provided. Therefore, the theoretical study is needed. One of the challenging in the calculation is to study the charge transfer (CT) mechanism of the stacking configuration chromophores. The DNA base sequences were extensively used in theoretical studies.[152-156] However, the stacking conformations are still found in the other important protein. [1, 9, 157]

Flavodoxin (FD) is a flavoprotein which contains FMN as cofactor. FD can be found in both non-pathogenic namely *Hildenborough* and pathogenic bacteria as *Helicobacter Pylori* (*H. pylori*).[2, 119, 124, 158] The FMN molecule can be divided into three parts, namely Isoalloxazine (Iso), ribityl side chain and phosphate subsite, see Chart 7.1.[157] The last two subsites are necessary for the FMN binding to apo-protein, while the Iso part is recognized for the most important part in photoinduced charge transfer (PCT) mechanism.[22] Physiologically, FD consists of amino acid as tyrosine (Tyr) which lying stacking to Iso moiety. FD has attracted considerable attention as simple model for CT studies. The experimental UV-visible spectrum of this FD is reported. Furthermore, the fluorescence dynamic decay of FD (unpublished work) is studied by using transient up-conversion method. The result shows that the fluorescence dynamics can be characterized by a single exponential decay function with the life time of 210 femto-seconds. This quenching has been proposed due to PCT from Tyr (ground state) to the excited Iso (Iso\*). On the mechanism viewpoint, upon light excitation the oxidized FMN act as electron acceptor because of the relatively low energy, while the Tyr (ground state) act as electron donor due to the higher energy level of HOMO. Subsequently, the electron lying on HOMO of Tyr will transfer to the Iso\* causing fluorescence quenching.

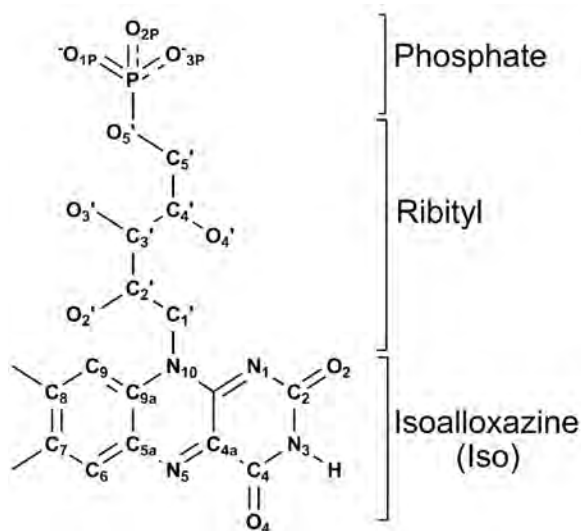


**Chart 7.1** Chemical structure and numbering of the FMN atoms.

Currently, the time-dependent density functional theory (TDDFT) method has been extensively used for the excited state calculation. The hybrid exact exchange and range-separated correction functional, namely B3LYP-35, PBE0, CAM-B3LYP,  $\omega$ B97XD, B97D and M06-2X have been employed in to predict the absorption spectra. These functionals show a good compromise between the accuracy and computation cost. Furthermore, the inclusion of the solvent effect in calculation yields the more reliable result for the CT character. The interpretation of the UV-visible spectra of FD from *H. pylori*, however, is never straightforward though the mechanism of PCT. Therefore, it is meaningful to investigate how the PCT mechanism of this system is? Additionally, a very recent study by D. Escudero and co-workers [159] showed the applicability of multi-configurational methodology as Restricted Active Space Self-Consistent Field (RASSCF) calculation. This means has been proved to be adequate for evaluating the CT in many  $\pi$ -electron systems.

In this work, we have analyzed the UV-Visible spectra by comparing the results obtained from conventional hybrid and correlation functional and more recent density functional specifically designed for the dispersion interaction and long-range CT transitions. The accuracy of such density functionals have been confirmed by RASSCF followed by MS-RASPT2 in which providing the more reliable result for the excitation properties.[160] This result can provide the information for better understanding on photophysical properties of this system.

### 7.3 COMPUTATIONAL DETAILS

The geometry of two chromophores (FMN and Tyr92) has been extracted from the experimental structure (PDB code: 1FUE).[8] The FMN has been modified to Lumiflavin (Lf) by removing the ribityl and phosphate moieties, remaining methyl group attached at N<sub>10</sub> position. Tyr92 was substituted with 4-methylphenol, see Figure 7.1.

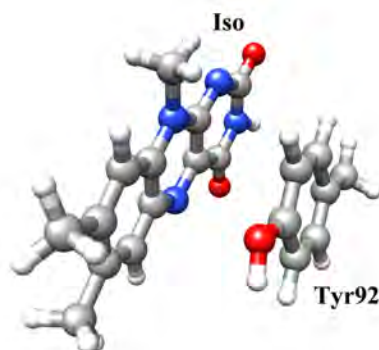


**Figure 7.1** The three dimensional structure involved in the calculation.

Focusing on the X-ray structure, the vertical excitation energies have been evaluated on those structures by using TDDFT [161-163] method with the TZVP basis set. Six density functionals as B3LYP-35, PBE0, B97D, CAM-B3LYP, M06-2X and  $\omega$ B97XD have been employed. The solvent effect as water has been included by the integral equation formalism for the polarizable continuum model (IEFPCM).[164] The mimicked protein environment has been study by using dielectric equal four [165] in order to study the effect of solvation on the electronic excited state. Their vertical excitation energies and the oscillator strength of ten excited states have been calculated. All TDDFT calculations have been calculated by using Gaussian09 program.[166]

In order to confirm the wave function transfer, the MS-RASPT2/RASSCF calculations have been performed by focusing on the molecular orbital which play an active role for CT between Iso and Tyr chromophores. Ten states of configuration interaction (CI) have been involved in this calculation in which the state-averaging (SA) approach has been employed to optimize molecular orbital basis set which describing the low-lying electronic state. In RASSCF, the standard active orbital are spitted into three subspaces, namely RAS1, RAS2, and RAS3. RAS1 described molecular orbital with large occupation number and only the maximum number of electron hole is allowed. RAS3 described the virtual molecular orbitals with the small occupations number in which only the maximum number of electron is allowed. RAS2 is equivalent to the active space of CASSCF calculation. Additionally, the majority different is that all possible configurations have to be included in RAS2 for CASSCF, whereas those configurations have been divided into subspace for RASSCF

approach. Therefore, the computational cost for RASSCF is drastically reduced. In the RASSCF fashion, the notation which has been involved by Sauri and co-worker [167] can be used to denote the active space. The index  $n$  denotes the number of active electron,  $l$  is the maximum number of the hole in RAS1,  $m$  is the maximum number of electron in RAS3 and  $i, j, k$  denote the number of active orbital in RAS1, RAS2, and RAS3 subspace, respectively. In this work, the number of all active electrons is 26, and the number of orbitals for RAS1, RAS2 and RAS3 are 11, 4 and 8, respectively. The basis set of 6-31G(d) has been used and the graphical inspection method was used for selection of the orbitals in which they played an active space role, see Figure 7.2. The active spaces have been constructed by concerning both Iso and Tyr moieties. The p-orbitals of the plane of two chromophores have been included. Furthermore, the lone pair electrons of N<sub>3</sub>, and N<sub>10</sub> were taken into account. Therefore, the active space contained 26 electrons and 23 molecular orbitals. Regarding the TDDFT calculations, the HOMO, LUMO, LUMO+1 and LUMO+2 have been assigned into RAS2 subspace, while the other occupied and unoccupied molecular orbitals were distributed into RAS1 and RAS3, respectively. The state-average calculations over ten roots with equal weight have been applied and the Cholesky decomposition has been applied to generate two-electron integral.[168] Subsequently, the excitation energies were calculated in which the correlation effect of all 26 electrons have been treated with the second-order perturbation theory. All MS-RASPT2/RASSCF have been calculated with MOLCAS version 7.8 software.[168-170]



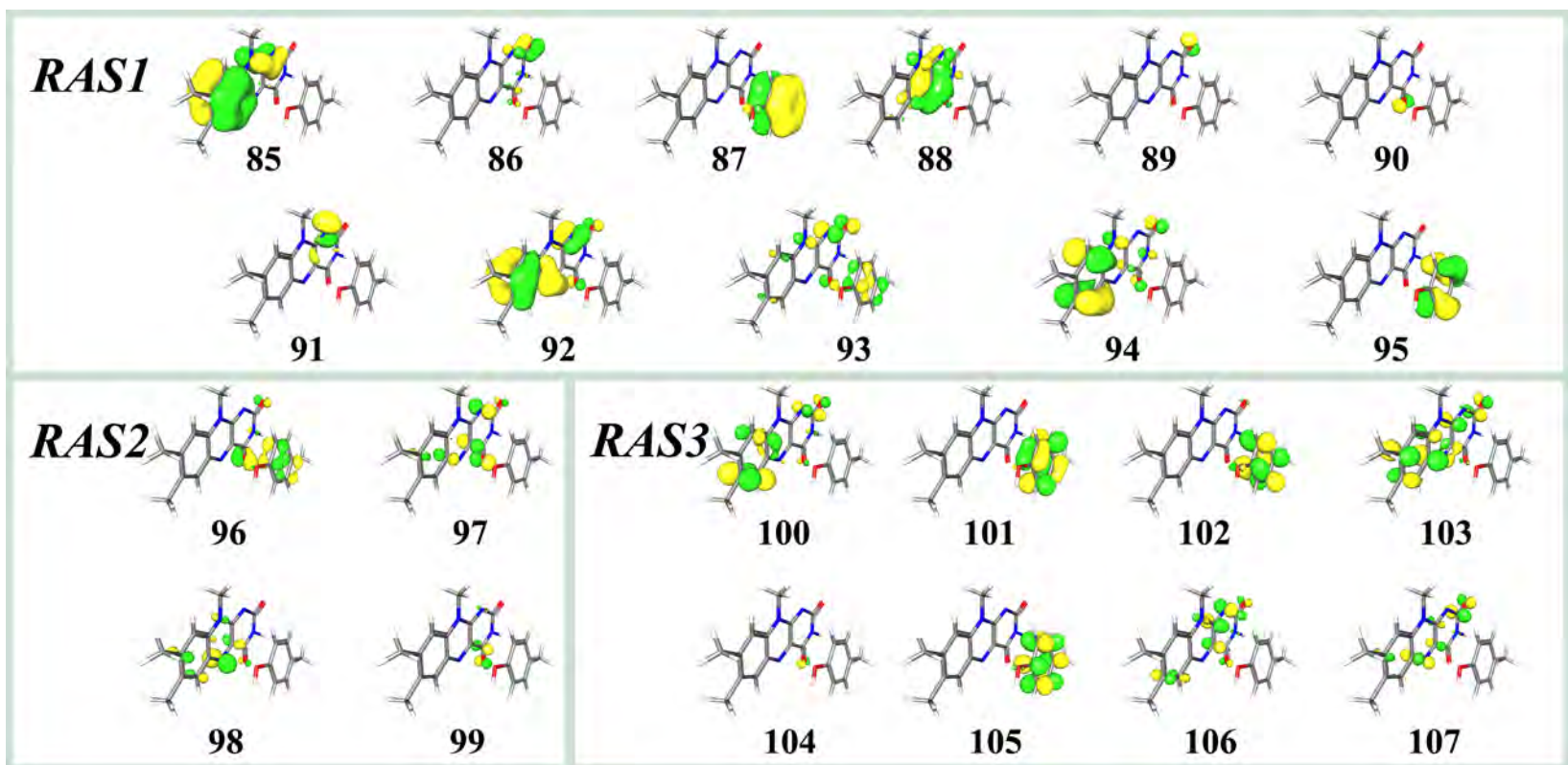
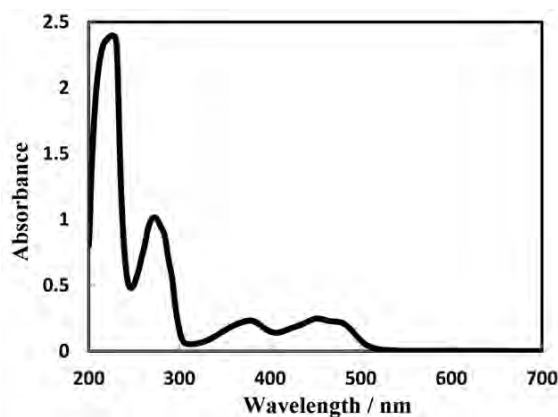


Figure 7. 2 Molecular orbital for RASSCF (26,2,2;11,4,8) calculation.

## 7.4 RESULTS AND DISCUSSION

### 7.4.1 Comparison the TDDFT between global hybrid functional and long-range corrected hybrid functional

The TDDFT calculation is widely used to study the excitation mechanism. Because it can provide fairly reasonably and comparable vertical excitation results compare to the experimental data. The accuracy of TDDFT is tested with a number of variety systems. A recent work by R. Improta and co-workers has shown the applicable of TDDFT on the CT in DNA based sequences model. To our knowledge, however, the CT mechanism in FD from *H. pylori* upon light excitation has never been studied. Furthermore, the CT mechanism needs to be clearly understood. Figure 7.3 shows the experimental UV-visible spectrum. One of two intense peaks at around 450 and 380 nm are reported correspond to the CT mechanism in FD, namely *H. pylori*, *Miyazaki F* and also *Hildenborough*. Those two latter proteins, however, have different protein structures, particularly the stacking counterpart compared with *H. pylori* FD. Therefore, this becomes a challenge in order to understanding its photophysics.



**Figure 7.3** UV/Vis spectra of *H. pylori* FD.

In the present work, the excitation energy, oscillator strength and the wave function transition have been calculated by using the X-ray geometry of FD from *H. pylori*. The difference six functional

such as global hybrid exact exchange and increased amount of exact exchange including the range-separated correction have been involved in order to see the effect of amount of exact exchange on the related quantities. The ten singlet excited states have been involved in the calculations. Furthermore, the effects of solvation and protein environment on such quantities of all calculation were mimicked by using water solvation model and the dielectric constant equal four. The fitting of the experimental UV-visible spectra and the calculated one using water solvation model are shown in Figure 7.4. We found that all TDDFT calculations provided fairly well spectrum. Considering the fitting profile, they can be divided into two groups, based on the similar pattern of excitation. First group comprised of TD-B3LYP-35, TD-PBE0 and B97D functional and the second group is comprised of TD-CAM-B3LYP, TD- $\omega$ B97XD and TD-M06-2X.

For the TD-B3LYP-35, TD-PBE0 and TD-B97D functionals, the  $S_1$  are pronounced to be the dark CT state with all magnitudes of the oscillator strength close to zero, see Table 7.1. The first intense peak of two boarder shoulders are assigned to the transition of  $S_0 \rightarrow S_2$  ( $f_{TD-B3LYP-35} = 0.20$ ,  $f_{TD-PBE0} = 0.15$  and  $f_{TD-B97D} = 0.05$ , respectively), and the second peak was assigned to  $S_0 \rightarrow S_3$  for TD-B3LYP-35 ( $f_{TD-B3LYP-35} = 0.26$ ),  $S_0 \rightarrow S_5$  for TD-PBE0 ( $f_{TD-PBE0} = 0.23$ ) and  $S_0 \rightarrow S_6$  for TD-B97D ( $f_{TD-B97D} = 0.17$ ), respectively. As mentioned above, to mimic the protein environment at the active site, we involved the dielectric equal four for all calculations, see Figure 7.5. The excitation energy of the  $S_1$  for TD-B3LYP-35 and TD-B97D were stabilized by ca. 0.03 eV, by going from the mimicked protein environment to the water solvation model, while TD-PBE0 the excitation energy was unchanged. On the other hand, the second group (TD-CAM-B3LYP, TD-M06-2X and TD- $\omega$ B97XD) shows that all of the first absorption band can be assigned to the transition of  $S_0 \rightarrow S_1$  and can be pronounced to the localized excited state (LE, excitation within conjugated  $\pi$  system of Iso). The TD-CAM-B3LYP shows the excitation energy of 2.82 eV with the  $f_{TD-CAM-B3LYP}$  of 0.24 for both water and mimicked protein environment. A similar result can be found for TD-M06-2X functional in which the mimicked protein environment shows the excitation of 2.86 eV. It was stabilized by 0.01 eV to the water solvation model. It should be note that in the case of TD- $\omega$ B97XD the excitation energy of mimicked protein environment was lower than the water solvation model. The  $S_0 \rightarrow S_2$  of these functional are more pronounced to be the dark CT state,

while all of the second absorption bands at ca. 350 nm can be assigned to the  $S_0 \rightarrow S_4$  transition. Concerning the mimicked protein environment fitting profile of the first group, the second shoulder at ca. 350 nm was assigned to the transition of  $S_0 \rightarrow S_4$  in the case of TD-B3LYP-35,  $S_0 \rightarrow S_5$  for TD-PBE0 and  $S_0 \rightarrow S_7$  for TD-B97D, respectively. It is interesting to note that all functional of the second group for both solvation model share a similar pattern for the wave function transition which is the first intense absorption peak correspond to  $S_0 \rightarrow S_1$  and the second intense peak is  $S_0 \rightarrow S_4$  while the third one can be assigned to the transition of  $S_0 \rightarrow S_9$ .

Table 7.1 summarizes the excitation energy, oscillator strength and the wave function transition of ten singlet excitation. We found that the water solvation and the mimicked protein environment provided the similar results. The dark CT state  $S_1$  of the first group is red-shift by ca. 0.03 eV by going from the mimicked protein environment to the water solvation model except for the TD-PBE0 (unchanged). The result shows that the dark CT state  $S_2$  of the second group is not affected from changing the environment except for the TD-M06-2X in which the CT state was red-shifted by ca. 0.03 eV by going from the mimicked protein environment to the water solvation model. This means that the CT states are more affected and preferable due to polar media. Next considering the LE state, we found that all TDDFT functions provided almost the same excitation energies (deviated less than 0.02 eV) between mimicked protein environment to the water solvation model except for TD- $\omega$ B97XD which show the blue-shifted (destabilized) by ca. 0.55 eV. Addition to the LE state, the wave function transition of these LE correspond to the moving inside Iso moiety, see Figure 7.6.

In summary, the disagreement between the hybrid exact exchange and the long-range correction TDDFT function might be due to amount of the exact exchange and clearly proved could cause an underestimate CT state. Therefore, the high level of calculation which yielded the high accuracy as MS-RASPT2/RASSCF need to be used to verify whether the CT state in this system is the  $S_1$  or  $S_2$  state.

**Table 7.1** Comparison the excitation energies, oscillator strength and orbital transition obtained by means of TDDFT by using the X-Ray geometry.

State	System	Excitation energy <sup>1</sup> (oscillator strength)							Character						
		B3LYP-35	B97D	PBE0	CAM-B3LYP	M06-2X	$\omega$ B97XD	MS-RASPT2	B3LYP-35	B97D	PBE0	CAM-B3LYP	M06-2X	$\omega$ B97XD	RASSCF
$S_1$	Water model	2.56 (0.01)	1.45 (0.00)	2.27 (0.00)	2.82 (0.24)	2.85 (0.24)	2.83 (0.24)	3.07 (0.49)	96 -> 97	96 -> 97	96 -> 97	95 -> 97	95 -> 97	95 -> 97	LE
	Dielectric 4	2.59 (0.01)	1.48 (0.00)	2.27 (0.00)	2.82 (0.24)	2.86 (0.26)	2.82 (0.24)		CT <sup>2</sup>	CT	CT	LE <sup>3</sup>	LE	LE	
$S_2$	Water model	2.74 (0.17)	2.19 (0.09)	2.59 (0.15)	3.10 (0.00)	3.13 (0.00)	3.20 (0.01)	4.41 (0.06)	95 -> 97	95 -> 97	95 -> 97	96 -> 97	96 -> 97	96 -> 97	CT
	Dielectric 4	2.76 (0.20)	2.18 (0.05)	2.59 (0.15)	3.10 (0.00)	3.16 (0.00)	3.20 (0.01)		LE	LE	LE	CT	CT	CT	
$S_3$	Water model	3.35 (0.26)	2.37 (0.00)	3.05 (0.00)	3.38 (0.00)	3.25 (0.00)	3.33 (0.00)	4.78 (0.32)	93 -> 97	94 -> 97	92 -> 97	92 -> 97	92 -> 97	92 -> 97	LE
	Dielectric 4	3.38 (0.00)	2.21 (0.05)	3.05 (0.00)	3.38 (0.00)	3.18 (0.00)	3.33 (0.00)		CT	LE	LE	LE	LE	LE	
$S_4$	Water model	3.43 (0.02)	2.39 (0.00)	3.25 (0.02)	3.56 (0.24)	3.62 (0.25)	3.59 (0.23)	4.91 (0.18)	93 -> 97	93 -> 97	94 -> 97	94 -> 97	94 -> 97	94 -> 97	CT/LE
	Dielectric 4	3.42 (0.09)	2.30 (0.00)	3.25 (0.02)	3.56 (0.24)	3.72 (0.23)	3.59 (0.23)		CT	LE	LE	LE	CT	LE	
$S_5$	Water model	3.46 (0.00)	2.41 (0.01)	3.34 (0.23)	3.99 (0.00)	4.10 (0.00)	3.95 (0.00)	5.05 (0.13)	92 -> 97	92 -> 97	93 -> 97	91 -> 97	91 -> 97	91 -> 97	LE
	Dielectric 4	3.46 (0.15)	2.42 (0.00)	3.34 (0.23)	3.99 (0.00)	3.95 (0.00)	3.95 (0.00)		LE	CT	CT	LE	LE	LE	

**Table 7.1** Comparison the excitation energies, oscillator strength and orbital transition obtained by means of TDDFT by using the X-Ray geometry. (Continue)

State	System	Excitation energy <sup>1</sup> (oscillator strength)							Character						
		B3LYP-35	B97D	PBE0	CAM-B3LYP	M06-2X	$\omega$ B97XD	MS-RASPT2	B3LYP-35	B97D	PBE0	CAM-B3LYP	M06-2X	$\omega$ B97XD	RASSCF
$S_6$	Water model	4.07 (0.00)	2.96 (0.17)	3.42 (0.0)	4.11 (0.00)	4.12 (0.00)	4.22 (0.00)	5.56  (0.27)	91 -> 97 LE	91 -> 97 LE	91 -> 97 CT	93 -> 97 CT	93 -> 97 CT	93 -> 97 CT	LE
	Dielectric 4	3.91 (0.00)	2.85 (0.00)	3.41 (0.00)	4.11 (0.00)	4.14 (0.00)	4.22 (0.00)		91 -> 97 LE	90 -> 97 LE	91 -> 97 LE	93 -> 97 CT	93 -> 97 CT	93 -> 97 CT	
$S_7$	Water model	4.57 (0.02)	3.01 (0.01)	4.18 (0.00)	4.74 (0.00)	4.81 (0.03)	4.73 (0.00)	5.57  (0.61)	90 -> 97 LE	90 -> 97 LE	88 -> 97 LE	89 -> 97 LE	90 -> 97 LE	87 -> 97 LE	LE
	Dielectric 4	4.60 (0.01)	3.02 (0.16)	4.17 (0.00)	4.75 (0.00)	4.74 (0.00)	4.73 (0.00)		89 -> 97 LE	91 -> 97 LE	88 -> 97 LE	89 -> 97 LE	87 -> 97 LE	87 -> 97 LE	
$S_8$	Water model	4.74 (0.02)	3.41 (0.01)	4.25 (0.01)	4.80 (0.00)	4.88 (0.02)	4.80 (0.00)	5.70  (0.81)	86 -> 97 CT	89 -> 97 LE	90 -> 97 LE	87 -> 97 LE	87 -> 97 LE	89 -> 97 LE	LE
	Dielectric 4	4.64 (0.01)	3.29 (0.01)	4.25 (0.01)	4.80 (0.00)	4.84 (0.06)	4.80 (0.00)		86 -> 97 CT	89 -> 97 LE	90 -> 97 LE	87 -> 97 LE	95 -> 98 CT	89 -> 97 LE	
$S_9$	Water model	4.83 (0.10)	3.46 (0.00)	4.39 (0.07)	4.95 (0.35)	5.00 (0.44)	5.10 (0.02)	6.21  (0.61)	89 -> 97 LE	96 -> 98 LE	89 -> 97 LE	95 -> 98 LE	95 -> 98 CT	89 -> 97 LE	CT/LE
	Dielectric 4	4.72 (0.06)	3.47 (0.00)	4.38 (0.06)	4.95 (0.35)	5.00 (0.41)	4.98 (0.36)		90 -> 97 LE	96 -> 98 CT	89 -> 97 LE	95 -> 98 LE	89 -> 97 LE	95 -> 98 LE	
$S_{10}$	Water model	4.96 (0.00)	3.70 (0.07)	4.44 (0.02)	5.09 (0.01)	5.16 (0.03)	5.10 (0.02)	-	96 -> 98 CT	88 -> 97 LE	87 -> 97 LE	88 -> 97 LE	96 -> 99 CT	96 -> 100 CT	-
	Dielectric 4	4.87 (0.01)	3.66 (0.00)	4.44 (0.02)	5.09 (0.01)	5.07 (0.01)	5.10 (0.02)		86 -> 97 CT	87 -> 97 LE	87 -> 97 LE	96 -> 100 CT	88 -> 97 LE	93 -> 101 LE	

(1) The excitation energy are given in eV. (2) CT denotes the Charge Transfer state in which the charges were transferred from Tyr to Iso moiety. (3) LE denotes Localized Excited state in Iso moiety, and HOMO and LUMO correspond to molecular orbital number 96 and 97, respectively. (4) The MS-RASPT2/RASSCF approach was calculated in gas phase.

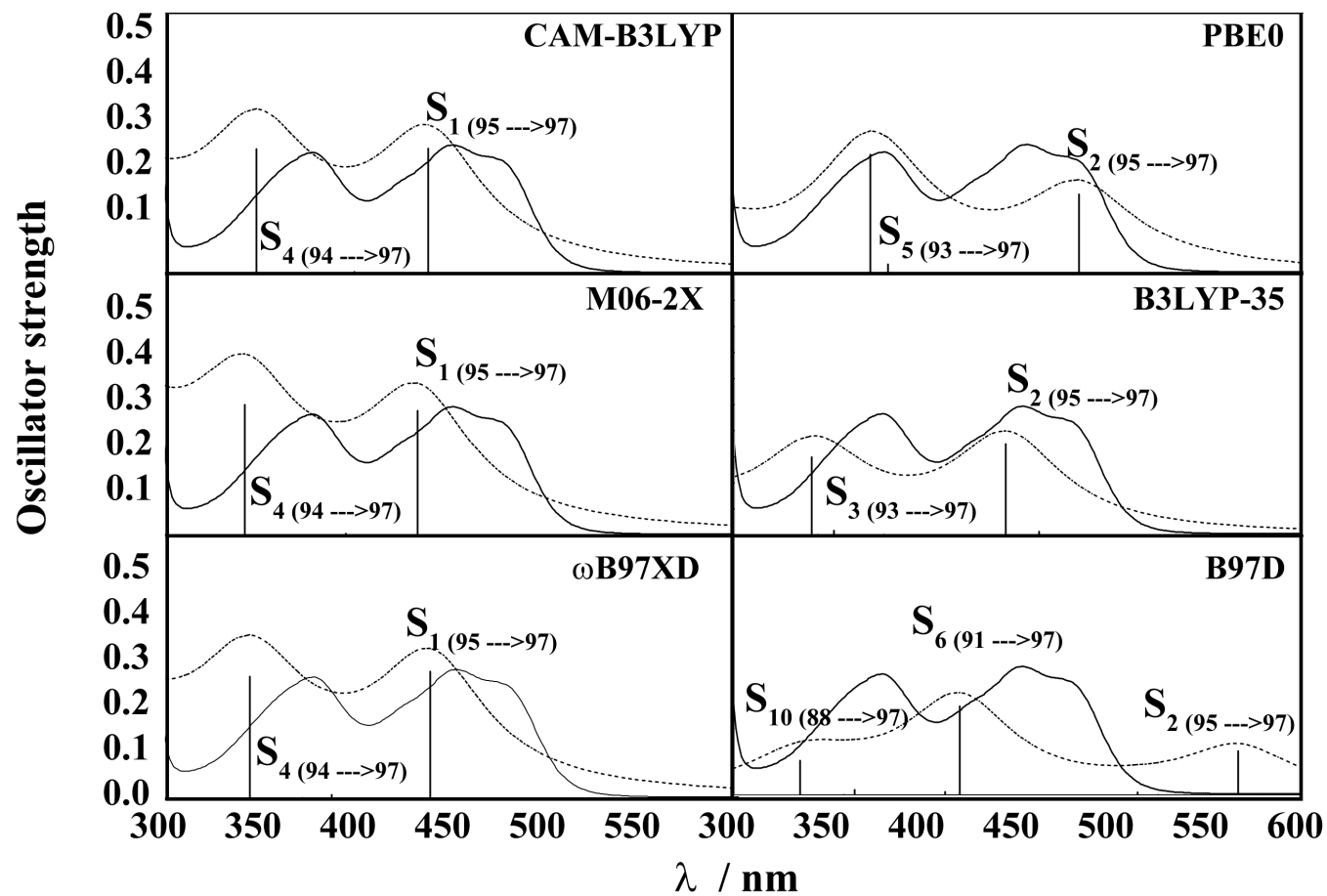


**Figure 7.4** Comparison of the experimental and calculated spectra of the TDDFT/TZVP of the X-ray configuration using water solvation model. The experimental spectra are shown as continuous line and the calculated spectra are shown as dashed line.

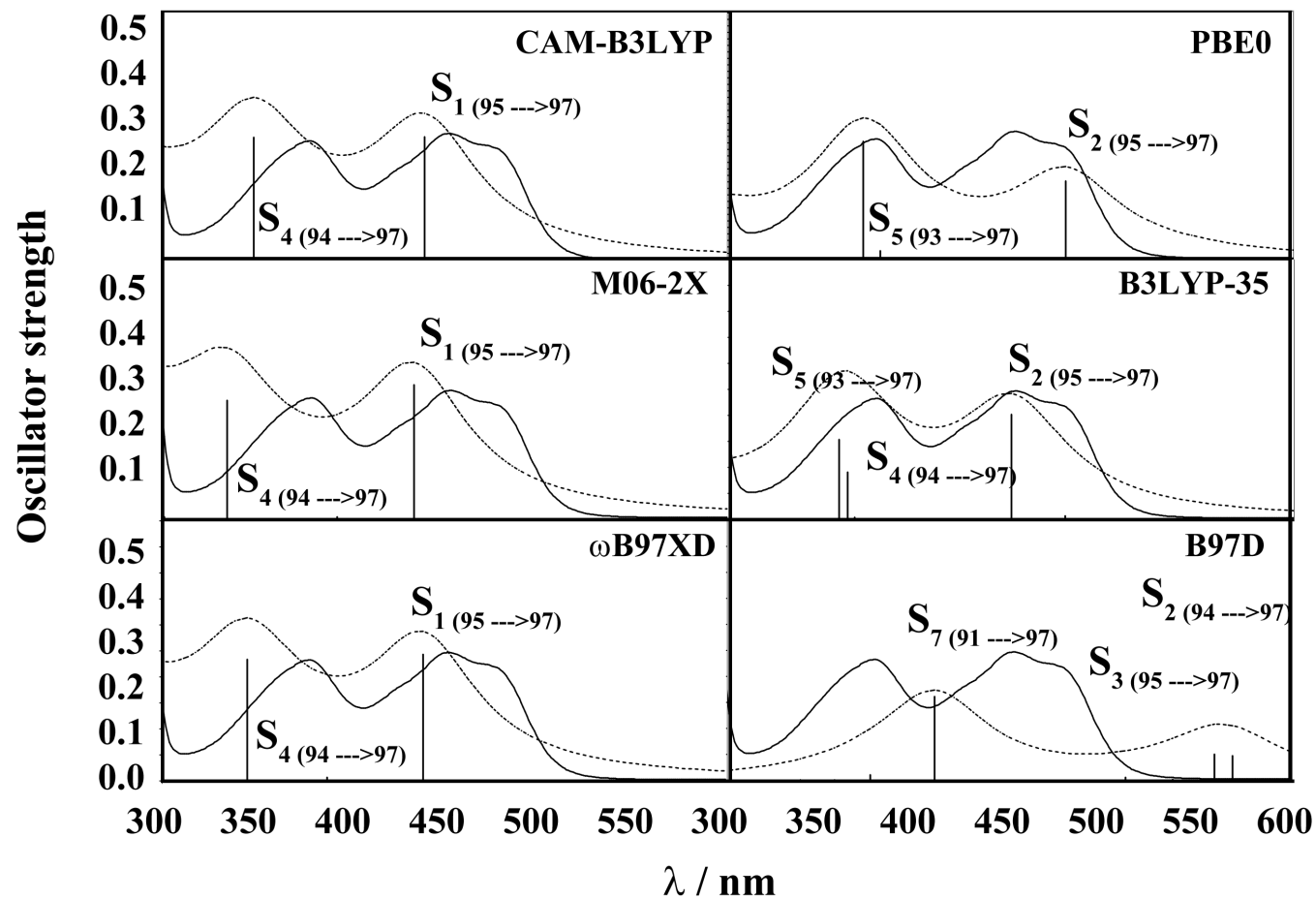


**Figure 7.5** Comparison of the experimental and calculated spectra of the TDDFT/TZVP of the X-ray configuration using dielectric constant equal 4. The experimental spectra are shown as continuous line and the calculated spectra are shown as dashed line.



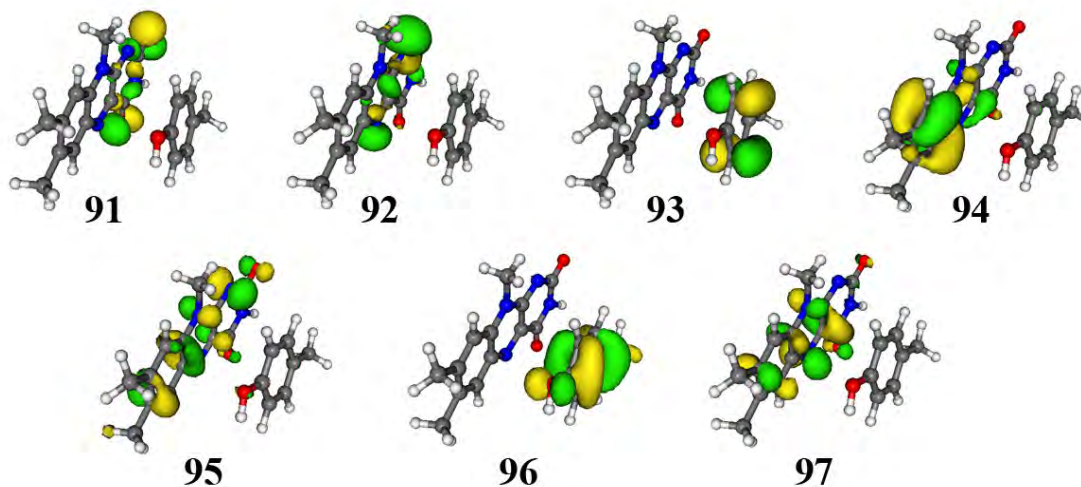


**Figure 7.6** Frontier molecular orbital of TD-CAM-B3LYP level of theory.

#### 7.4.2 RASSCF and MS-RASPT2 calculation

The RASSCF calculation is the multi-state calculations which have been successfully proved for evaluation of the electronic excited state of multi- $\pi$  electron systems. The RASSCF wave functions are obtained by using the state-average (SA) calculations over ten singlet electronic states with equal weight. The dynamic correlation was included in the MS-RASPT2 calculation. The RAS State Interaction method was employed in MS-RASPT2/RASSCF, for allowing the interacting between each electronic state. The calculations were done in gas phase environment due to the high computational cost for calculating PCM solvation model with multiconfigurational methods. Our strategy is to use this approach in order to verify the CT excited state in *H. pylori* FD upon light excitation by focusing extensively on the first two singlet excited state ( $S_1$  and  $S_2$ ). The MS-RASPT2/RASSCF can provide the vertical excitation energies, oscillator strength and the wave function of the CT transition as also collected in Table 7.1. The corresponding orbital numbering is depicted in Figure 7.2. Regarding to the TDDFT results as mentioned above, the time-dependent calculations with B3LYP-35, B97D and PBE0 show that the  $S_1$  can be assigned into dark CT character (mainly described by the transition between HOMO(96) to LUMO(97)), while the  $S_2$  show

LE phenomena (mainly described by the transition between HOMO-1(95) to LUMO(97)). On the other hand, using CAM-B3LYP,  $\omega$ B97XD and M06-2X functional we found that the  $S_1$  can be assigned to the LE state and the  $S_2$  shows the dark CT characteristic between HOMO and LUMO.

The MSRASPT2/RASSCF (26,2,2;11,4,8) calculations predict the excitation energies of  $S_0 \rightarrow S_1$  of 3.07 eV, and for  $S_0 \rightarrow S_2$  of 4.41, with the oscillator strength of 0.49 and 0.61, respectively. These values are seemed to be overestimated might be due to the gas phase environment. The SCF wave function of  $S_1$  show the LE character with the transition from HOMO(96) to LUMO(97) with 62% predominant, while the  $S_2$  is more pronounced to be the CT character from HOMO-1(95) to LUMO(97) with 70% predominant.

## 7.5 CONCLUSION

The absorption spectrum of FD from *H. pylori* has been investigated by performing the TDDFT and MS-RASPT2/RASSCF approaches using (26,2,2;11,4,8) level. The hybrid exact exchange and long-rang corrected functionals as B3LYP-35, PBE0, B97D, CAM-B3LYP, M06-2X and  $\omega$ B97XD have been employed in these calculations. The effect of solvation has been assigned by IEFPCM water solvation model. Furthermore, in order to mimic the protein environment the dielectric equal four has been assign in all TDDFT calculation. We found that the six TDDFT functionals as mentioned above provided the absorption results which can be categorized into two groups. First, it is comprised of B3LYP-35, PBE0 and B97D, while the second group is comprised of CAM-B3LYP, M06-2X and  $\omega$ B97XD. For the first group, the  $S_1$  state is assigned to be the dark CT state between Tyr and Iso subunit (HOMO(96) to LUMO(97)), whereas the  $S_2$  state is assigned to be the LE state of the conjugated  $\pi$  system within Iso subunit. The second group shows the proper absorption spectra. These functionals yielded the  $S_1$  state is pronounced to be the LE of Iso, while the  $S_2$  state is pronounced to be the CT state. These disagreements can be associated with the amount of exact exchange of TDDFT functionals. It seems that the increased amount of exact exchange (TD-M06-2X with amount of 54%) provided the more reasonable electronic CT as reflected by fitting

profile of spectrum. Moreover, the long-range correction functionals as TD-CAM-B3LYP and TD- $\omega$ B97XD also provided a good fitting profile. This might be due to the characteristic of the studied model in which the van der Waal interaction plays an important role for the stacking conformation. The difference of these TDDFT results has been further clearly investigated by using MS-RASPT2/RASSCF methodology. The MS-RASPT2/RASSCF (26,2,2;11,4,8) results show that the  $S_1$  state has the LE characteristic transition and the  $S_2$  excited state shows CT state phenomena. This clear observation coincides with the CAM-B3LYP and  $\omega$ B97XD and M06-2X. These results suggest the good performance to describe the CT excited state by the long-range corrected TD functionals. Comparison between the water solvation and mimicked protein with the dielectric equal four implied that the CT state are more affected and stabilized due to polar media. Even if the TDDFT and MS-RASPT2/RASSCF calculation clearly show the CT mechanism of FD from *H. pylori*, through the absorption spectra, the additional investigations on the related FDs are necessary to study in order to not only understanding their photophysics but also the improvement of calculations.

## CHAPTER VIII

### CONCLUSIONS

#### 8.1 CONCLUSIONS

In summary, we applied several computational chemistry techniques to investigate the dynamic and thermodynamic properties and the ET mechanism of two strains of flavodoxin. We choose FD-*Dv*MF as the first model due to the several information are available, except for the protein structures. Therefore, homology modeling method has been employed to predict the protein structures of WT and mutated variant FD-*Dv*MF (W59F, Y97F and W59F-Y97F). We successfully build protein structures up and subsequently applied the MD simulation technique to simulate those proteins in an explicit solvation model. In contrast to the FD-HP, its 3D protein structure is available. It is subjected with the similar MD simulation protocol to explore its dynamic and thermodynamic properties related to the FMN binding.

The molecular interactions of FMN with the protein parts in the four FD-*Dv*MF variants were studied by means of MM-PBSA. The order of the magnitude of the binding free energy and DC free energy per residue were Y97F > WT > W59F > DM. The 10-loop region in all FD-*Dv*MF variants shows the highest stabilization energy upon the FMN binding. This can be ascribed due to the H-bond formation between the phosphate oxygen atoms and the amino acid residues in the 10-loop region. The similar pattern of DC free energy is observed in FD-HP. The classification of such DC free energy into the contribution of van der Waals ( $E_{vdW} + G_{nonpol}$ ) and electrostatic ( $E_{ele} + G_{pol}$ ) energy shows that Asn-14, Thr-54 and Tyr-92 are dominantly influencing via van der Waals interactions. In addition to the binding mechanism of FMN molecule, the side-chain conformational analysis between holo-FD-HP and apo-FD-HP revealed that Asn14, Ala55, Gln61, Tyr-92, Thr-95 are influenced upon the cofactor association, described by the large deviation of side-chain dihedral angle.

To understand the photoinduced electron transfer mechanism of those FDs, we studied by combining the protein coordinates obtained from the previous MD simulations with the ET theory in

order to analyze their fluorescence decays. Firstly, the FD-*Dv*MFs variants were simultaneously analyzed. The obtained physical quantities are:  $\nu_0^q$  which related to the electronic interaction energy between the donor and the acceptor, the values of  $\nu_0^{Trp}$  and  $\nu_0^{Tyr}$  were 3090 and 2460 ps<sup>-1</sup>, respectively. The value of  $R_0^{Trp}$  was 0.772 nm which is considerably longer than  $R_0^{Tyr}$  of 0.676 nm. Considering the ET rate we surprisingly found that the distance between Tyr97 and Iso in W59F was shortest but the ET rate is not the fastest. As opposed to Trp59 in Y97F which show the ET fastest despite that it shows the longer in Rc. A similar result was also found in the WT FD-*Dv*MF, and these results suggest that the donor-acceptor distance and  $\nu_0^q$  are not always critically important to the ET rate in the proteins.

Secondly, The ET mechanism of WT FD-HP was analyzed. We found that the ultrafast fluorescence dynamics is ascribed to very fast ET from Tyr92 to Iso\* with the average of 22.5 ps<sup>-1</sup>. Comparison the ET rate in FD-HP and FD-*Dv*MF showing that the ET rate from Tyr92 to Iso\* was much faster than Tyr97 in WT FD-*Dv*MF (0.001 ps<sup>-1</sup>) and faster than Tyr97 in W59F (5.0 ps<sup>-1</sup>). The dependence of the logarithmic ET rate on the total free energy gap displayed the parabolic behavior as in FD-*Dv*MF. The parabolic behavior of the logarithmic ET rates is mainly ascribed to the net *ES* energy. This suggests that the net *ES* energy is a key factor for the ET rate.

In addition to understand the CT mechanism, the UV-visible spectra of FD-HP has been simulated by using the TDDFT and the wave function based approach as RASSCF/MS-RASPT2 with (26,2,2;11,4,8) level of theory. The high accuracy method as RASSCF/MS-RASPT2 revealed that the  $S_1$  state is pronounced to the LE transition and the  $S_2$  excites state shows CT state characteristic. This result is in accordance with those obtained from TDDFTs as; TD-M06-2X, TD-CAM-B3LYP, and TD- $\omega$ B97XD. These results suggesting that the increasing of amount of exact exchange and the long-range correction functional could provide the more reasonable electronic CT state which the ET donor and acceptor having the stacking conformation to each other.

## 8.2 RESEARCH LIMITATIONS

In this research there are some limitations due to the lack of experimental structure as the X-ray crystal structure of FD-*Dv*MF is not available. The starting structure of FD-*Dv*MF of both WT and mutated variants (W59F, Y97F, and double mutation) have to be built up based on the homology modeling technique.

## 8.3 SUGGESTION AND FUTURE WORK

FDs are the effective model to study the photochemistry, including the important interaction and amino acids involving for the FMN binding. The results of this dissertation could provide the ET mechanism of ET between aromatic amino acids to excited flavin. Moreover, the interactions involved for the flavin binding and their dynamic behavior at the atomistic level are provided. However, there are some questions need to be clearly answered leading to the future works as;

8.3.1 Recently, the computing facility is faster. Therefore, the high accuracy method such as QM/MM MD should be carried out. This method can be applied not only to study the important interaction for FMN binding but also the time-dependent CT between aromatic amino acid and Iso\*.

8.3.2 The folding-unfolding simulation should be studied to clearly explain the binding mechanism of FMN cofactor and the dynamic of amino acid during the binding.

8.3.3 The ability of our developed method should be applied by studying the photoexcitable system, for instant the dye-sensitized solar cell (DSSC) and related artificial photosynthetic system.

## SUPPLEMENTAL INFORMATION

## CHAPTER II

**Homology Modeling and Molecular Dynamics Simulations of Wild Type and  
Mutated Flavodoxins from *Desulfovibrio vulgaris* (Miyazaki F):  
Insight into FMN-Apoprotein Interactions**

---

This article has been published in Journal: Molecular Simulation. Page 1164-1178.

Volume: 37. Issue 14, Year: 2011.

---

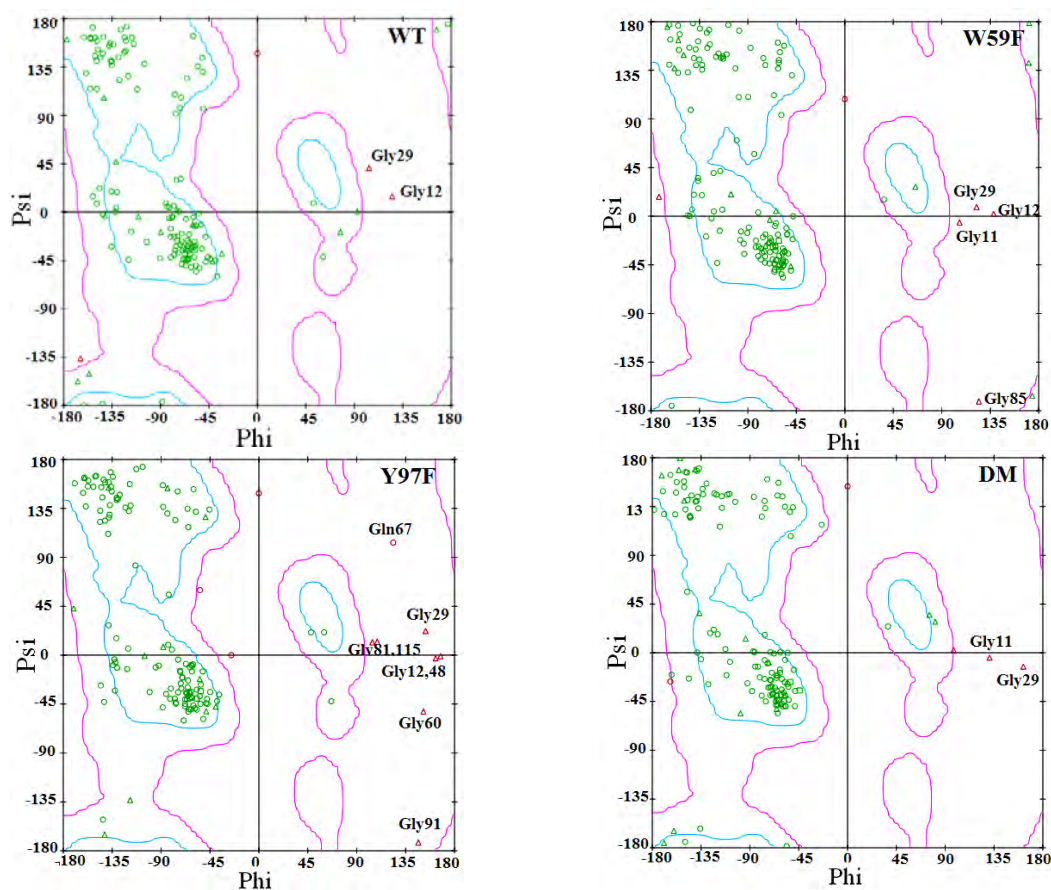


**Figure S2.1** Ramachandran plots of the four FD-DvMF variants (DM = W59F-Y97F).

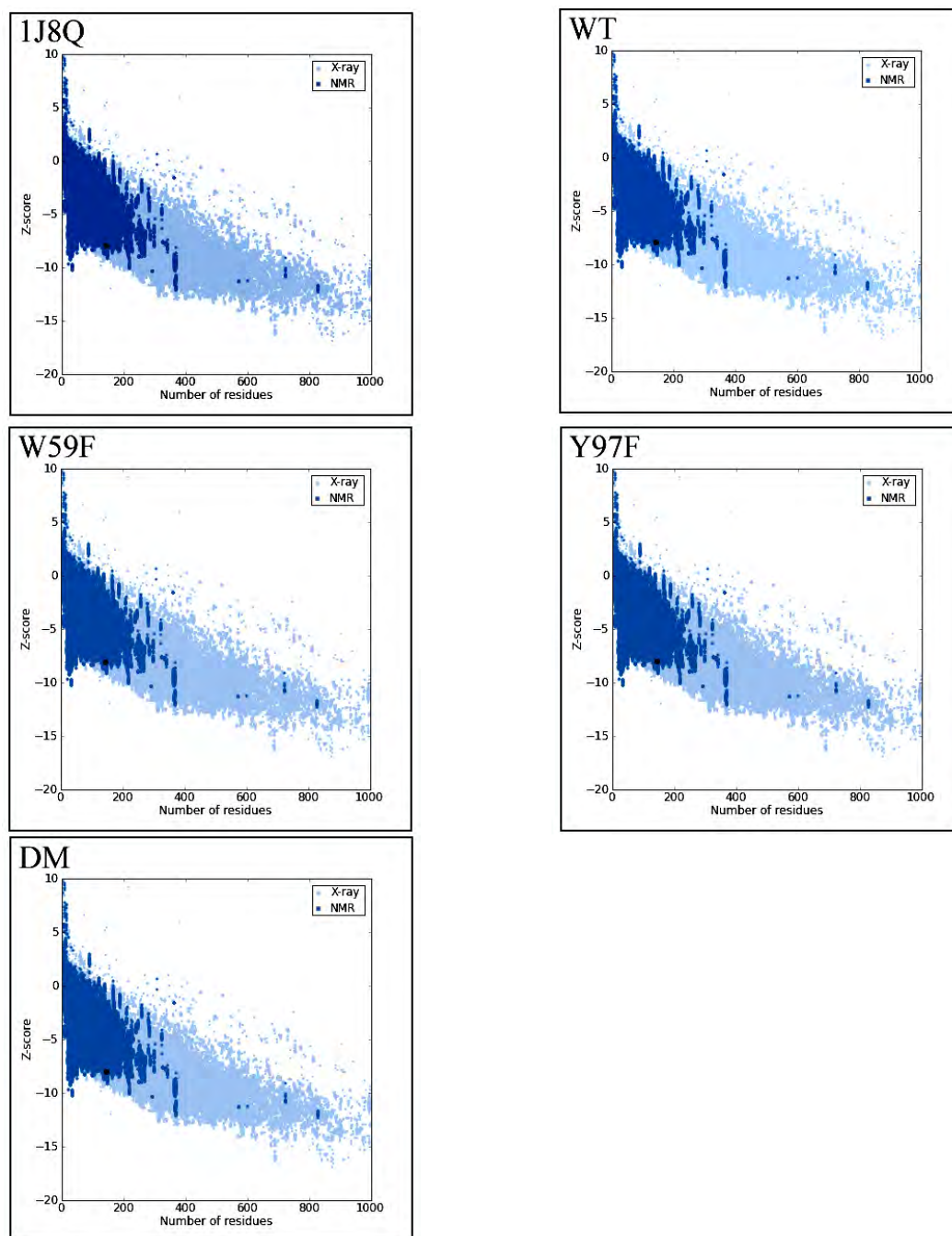


**Figure S2.2** ProSA-web Z-scores of the template (1J8Q) and four FD-DvMF variants.

The Z-scores were evaluated by X-ray crystallography (light blue) and NMR spectroscopy with respect to their length. The Z-score of each system was presented in black dot.



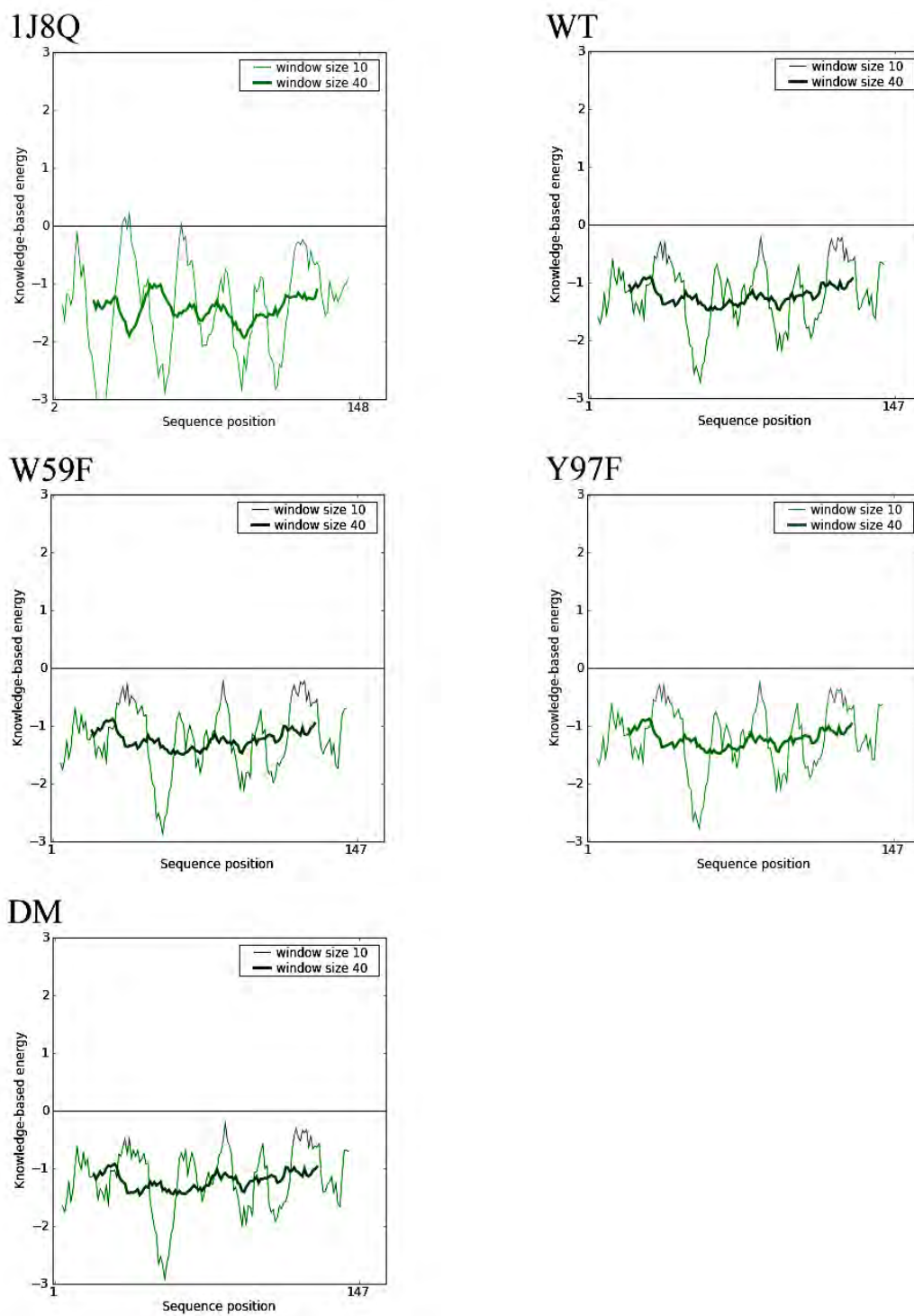


**Figure S2.3** ProSA-web energy profiles of the template and four predicted FD-DvMF variants.

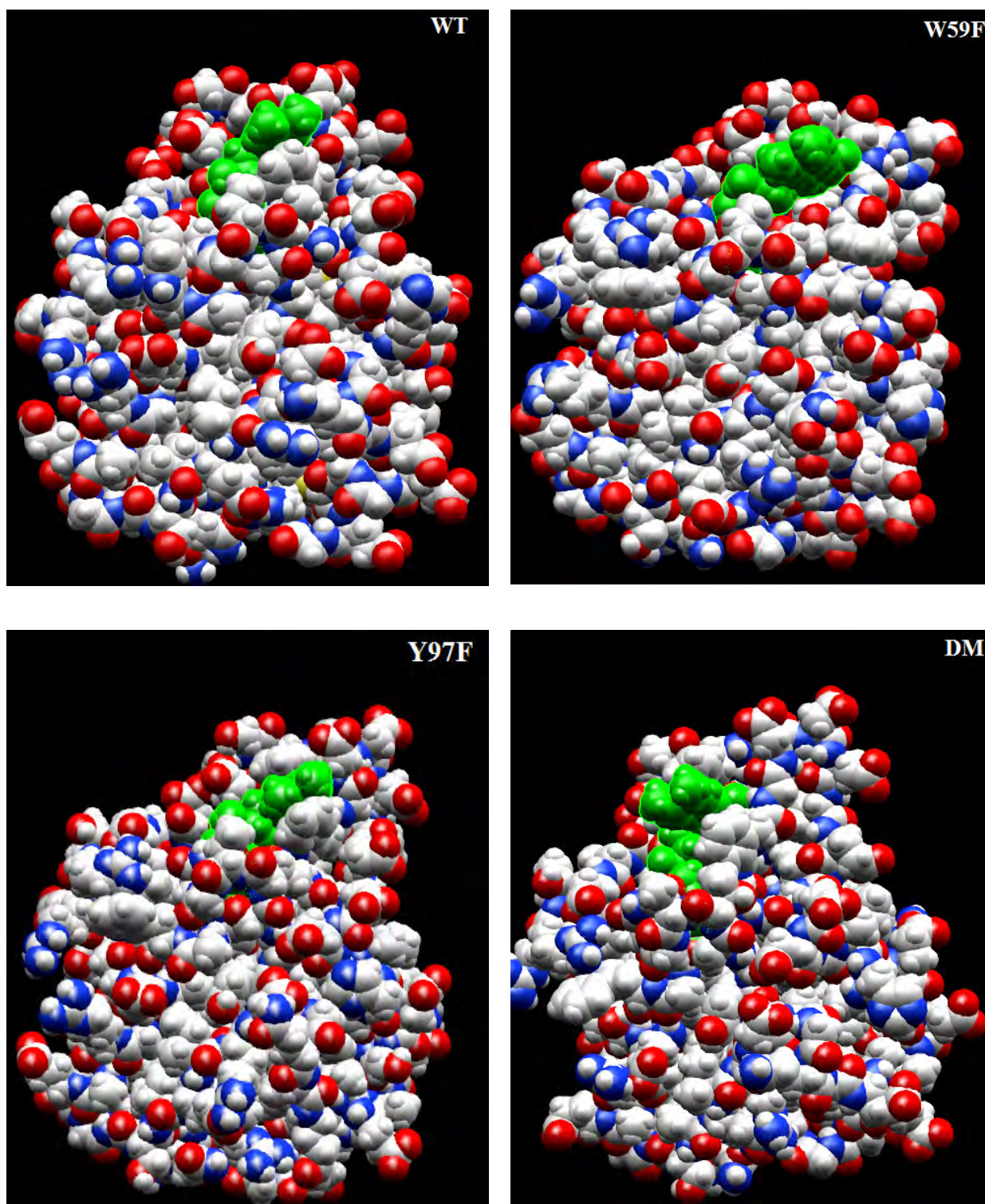


**Figure S2.4** Exposure of FMN into water layer expressed with space-filling model of the four FD-DvMF variants. The FMN is illustrated in green.

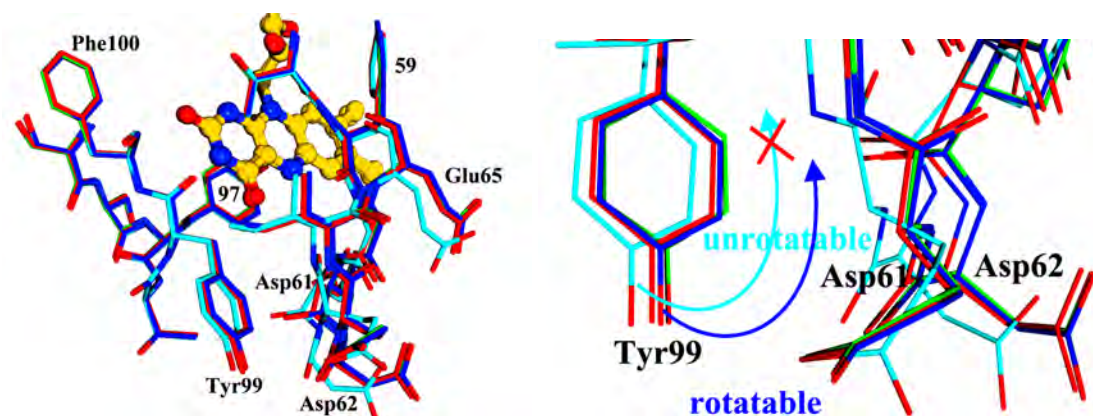


**Figure S2.5** The schematic representation of the structural conformations after minimization. The amino acids at the binding site were superimposed (left) and closed view at the Tyr99 (right). (WT is indicated in green, W59F in red, Y97F in deep blue and DM in light blue)

**Table S2.1** Comparison of the sequence identity and similarity, the amino acid residues at position 59 and 97 and the structural resolution among the four crystal structures of FD from *Desulfovibrio vulgaris*.

<b>PDB code</b>	<b>Strain / Type</b>	<b>Identity (%)</b>	<b>Similarity (%)</b>	<b>Residues at 59 / 97</b>	<b>Resolution (Å)</b>
1F4P	FD- <i>DvH</i> / Y98W	66	77	Trp / Trp	1.30
<b>1J8Q</b>	<b>FD-<i>DvH</i> / S35C</b>	<b>66</b>	<b>76</b>	<b>Trp / Tyr</b>	<b>1.35</b>
1FX1	FD- <i>DvH</i> / wild type	66	75	Trp / Tyr	2.00
1BU5	FD- <i>DvH</i> / wild type	66	76	Trp / Tyr	2.00

**SUPPLEMENTAL INFORMATION**

**CHAPTER III**

**Analysis of Photoinduced Electron Transfer in Flavodoxin**

**This article has been published in Journal: Journal of Photochemistry Photobiology A: Chemistry. Page 333-340. Volume: 217, Issue 2-3, Year: 2011**

**Comparison of the methods for numerical calculation of fluorescence decay between our method and one by Henry and Hochstrasser**

Expression for a calculated fluorescence dynamics by MD was first given by Henry and Hochstrasser [34] as Eq. (A1) (HH method).

$$F_{calc}(t) = \left\langle \exp\left\{-\int_{t'}^{t'+t} [k_0 + k_{ET}(\tau)] d\tau\right\} \right\rangle_{AV} \quad (A1)$$

$k_0$  is deactivation rate without ET, and  $k_{ET}(\tau)$  ET rate given by Eq. (A1) in Supplemental Material A. Here we assume that  $k_0$  is much less than  $k_{ET}(\tau)$ , and so negligible compared to ET rate.  $\langle \dots \rangle_{AV}$  denotes an averaging procedure with respect to  $t'$ . Lower and upper limit of the integration in the original equation given by Henry and Hochstrasser,[34] are 0 and  $t$ , but these should be  $t'$  and  $t' + t$  as in Eq. (A1).

$$F_{calc}(t) = \left\langle \exp\left\{-\Delta t \sum_{i=0}^n k_{ET}(j+i)\right\} \right\rangle_{AV} \quad (A2)$$

Figure A1 illustrates the method of numerical calculation for  $F_{calc}(t)$ . In Eq. (A2)

$\int_{t'}^{t'+t} k_{ET}(\tau) d\tau$  was approximated by a summation,  $\Delta t \sum_{i=0}^n k_{ET}(j+i)$ . More accurately, the

integral may be numerically calculated by Simpson method. In Eq. (A2)  $\Delta t = t/m$  and

$k_{ET}(j+i)$  denotes ET rate at  $t = t_{j+i}$ . Numerically  $\langle \dots \rangle_{AV}$  is also calculated by a summation as follows:

$$F_{calc}(t) = \frac{1}{m-n} \sum_{j=0}^{m-n} \exp\left\{-\left(\frac{t}{m}\right) \sum_{i=0}^n k_{ET}(j+i)\right\} \quad (\text{A3})$$

$n$  is number of data points of fluorescence decay, which is assumed that  $m$  is much larger than  $n$ .

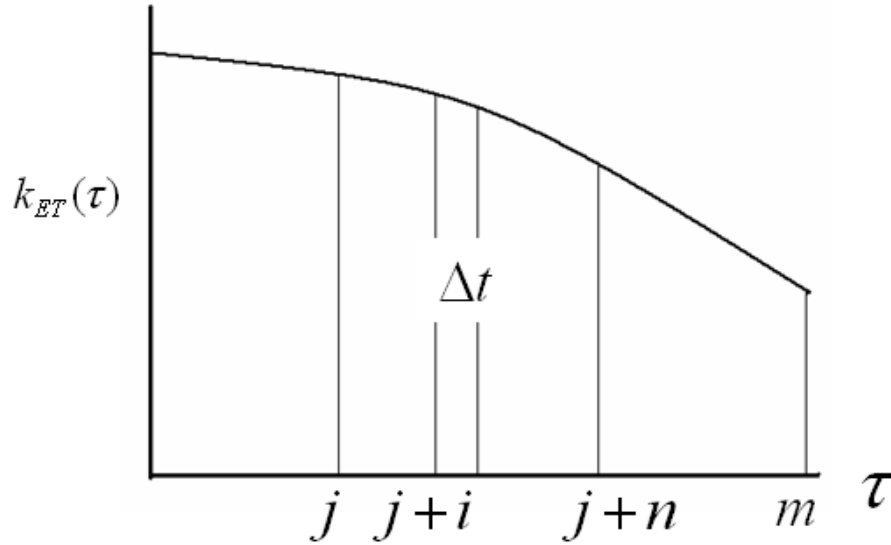


**Figure A1** Numerical calculation of fluorescence decay with  $k_{ET}(\tau)$ .

Time range of MD was divided into  $m$  intervals of  $\Delta t$ .  $\tau$  represents MD time. Fluorescence decay is to be calculated from  $t = t_j$  to  $t = t_{j+i}$ .  $\langle \dots \rangle_{AV}$  may be taken from  $t' = 0$  to  $t' = t_n$  ( $m=2n$ )

From Eq. (A3) we can see that  $k_{ET}(0)$  is used for the numerical calculation of fluorescence decay once,  $k_{ET}(1)$  twice,  $k_{ET}(2)$  three times, and  $k_{ET}(l)$  ( $l = i + j$ )  $l+1$  times, when  $l \leq n-1$ .  $k_{ET}(l)$  is used  $n+1$  times when  $n \leq l \leq m-n$ .  $k_{ET}(l)$  is used  $m-l+1$  times when  $l \geq m-n+1$ . This implies that  $k_{ET}(l)$  with  $n \leq l \leq m-n$  are most important upon the fluorescence decay, but  $k_{ET}(l)$  with  $l$  near 0 or  $m$  are not important. Namely, according to HH method, the values of  $k_{ET}(l)$  ( $0 \leq l \leq m$ ) are not equivalent for the calculation of fluorescence decay.

On the other hand our method is numerically calculated with Eq. (A4).

$$F_{calc}(t) = \frac{1}{m-n} \sum_{j=0}^{m-n} \exp\{-k_{ET}(j)t\} \quad (\text{A4})$$

$t$  extends from 0 to  $n\Delta t$ . In Eq (A4)  $k_{ET}(j)$  ( $j = 0$  to  $m$ ) is used only once. All values of  $k_{ET}(l)$  ( $n \leq l \leq m-n$ ) are used  $n+1$  times in the HH method, and 1 time in our method, so that after dividing  $F_{calc}(t)$  at every point of time by number of used frequency,  $F_{calc}(t)$  obtained by the both method should be same. Only the differences in  $F_{calc}(t)$  between the both method are time domain of MD average at  $l \leq n-1$  and at  $l \geq m-n+1$ . Accordingly, the both method should be equivalent, if  $m$  is much larger than  $n$ .

Calculation time of averaging procedure by HH method at each  $t$  may be

$$\begin{aligned} & 2\Delta t_c(1+2+3+\dots+n) + \Delta t_c(n+1)(m-2n+1) \\ & = \Delta t_c(n+1)(m-n+1) \end{aligned} ,$$

while the calculation time of our method is  $\Delta t_c m$  at each  $t$ .  $\Delta t_c$  denotes the calculation time of each step of the averaging procedure. Our method is much advantageous in the calculation time.

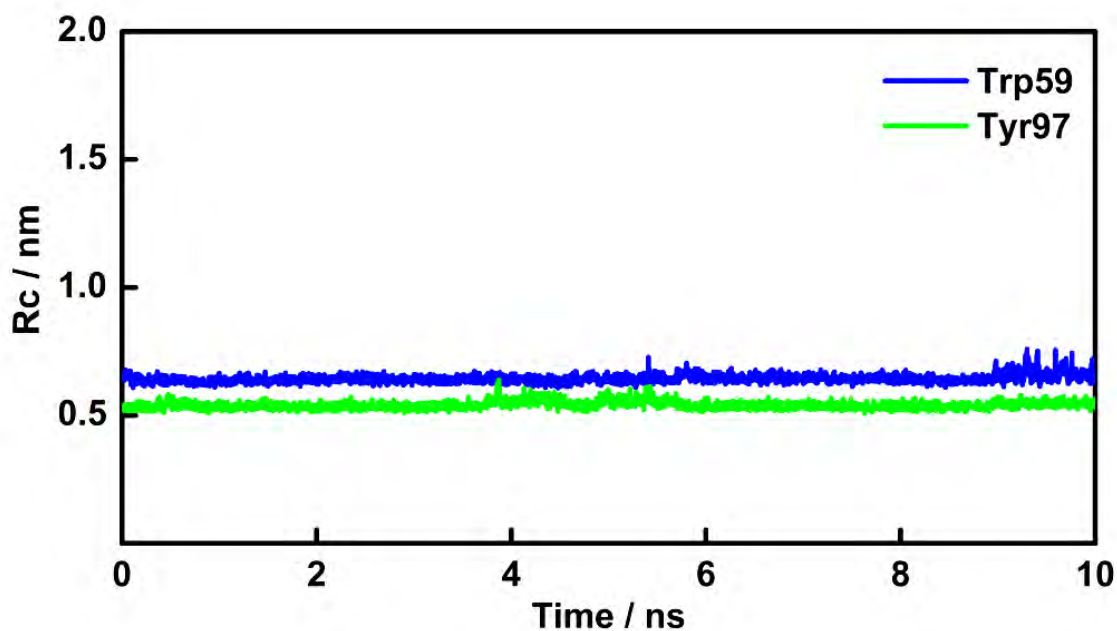


**Figure S3.1** Time-dependent changes in the Rc distance of Trp59 - Iso and Tyr97 - Iso, shown in blue and green, respectively.

## SUPPLEMENTAL INFORMATION

## CHAPTER IV

Photoinduced Electron Transfer in Wild Type and Mutated Flavodoxin from  
*Desulfovibrio vulgaris*, strain Miyazaki F.: Energy Gap Law

---

This article has been published in Journal: Journal of Photochemistry Photobiology A:

Chemistry. Page 32-41. Volume: 219, Issue 1, Year: 2011

---

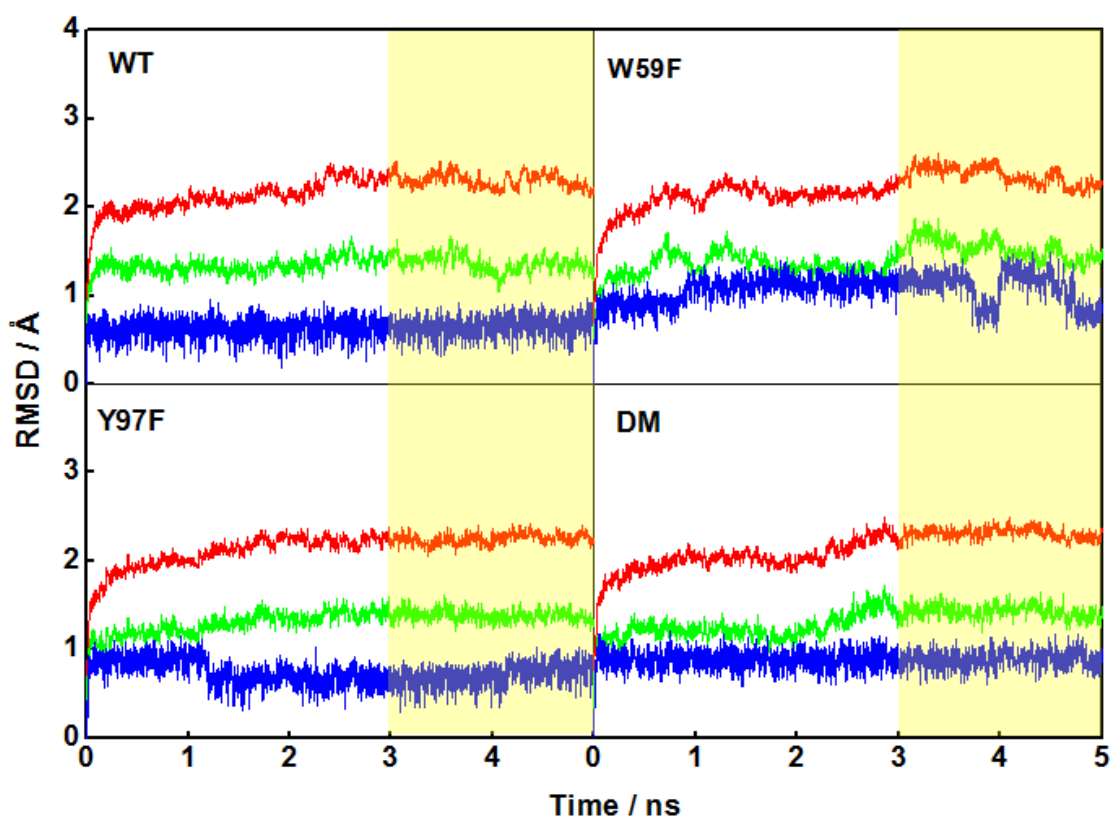


**Figure S4.1** Time-dependent changes in the RMSD of the four FD variants. Red lines indicated that for the entire protein, green lines the peptide backbone and blue lines the FMN molecule.

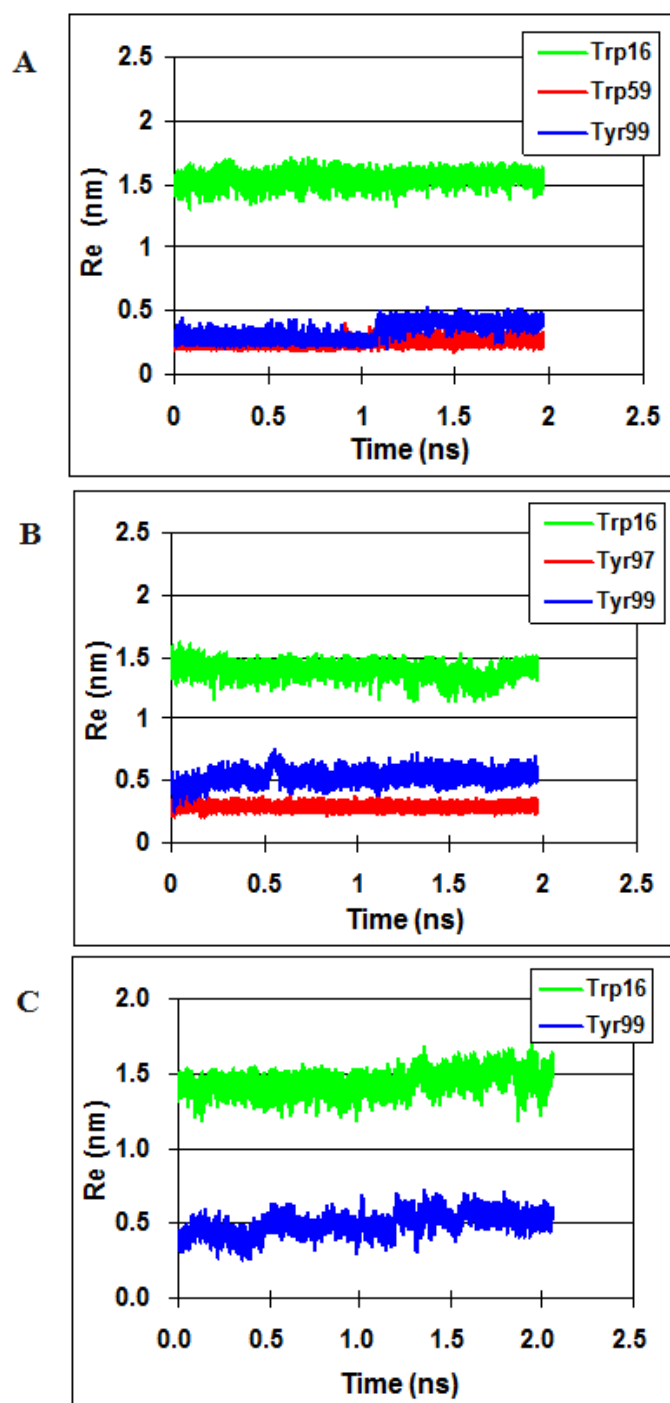


**Figure S4.2** Time-dependent changes in edge to edge distances between Iso and aromatic amino acids. A: Y97F, B: W59F and C: DM. Mean distances are listed in Table 4.1.



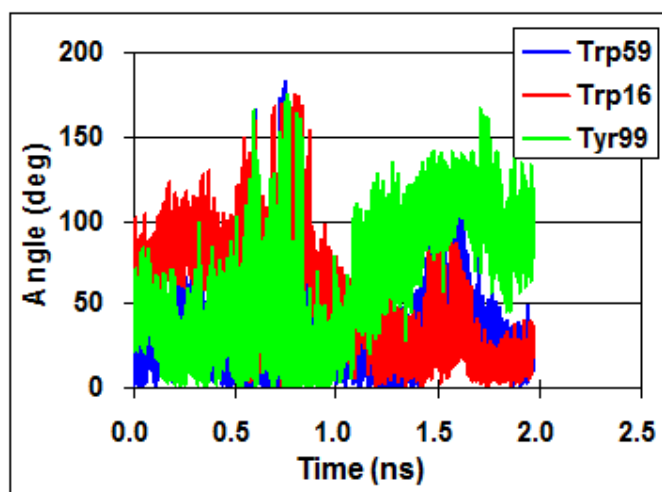


**Figure S4.3** Time-dependent change in the inter-planar angles between Iso and the aromatic amino acids in Y97F. The mean angles are listed in Table 4.1.

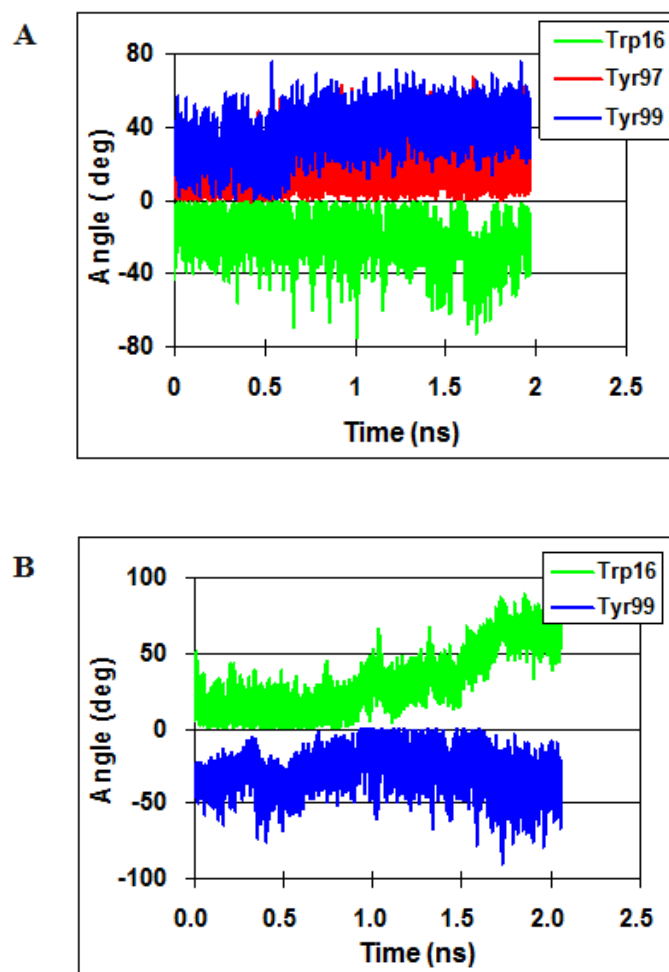


**Figure S4.4** Time-dependent changes in inter-planar angle between Iso and the aromatic amino acids in the W59F and DM FD variants. A: W59F and B: DM. The mean angles are listed in Table 4.1.

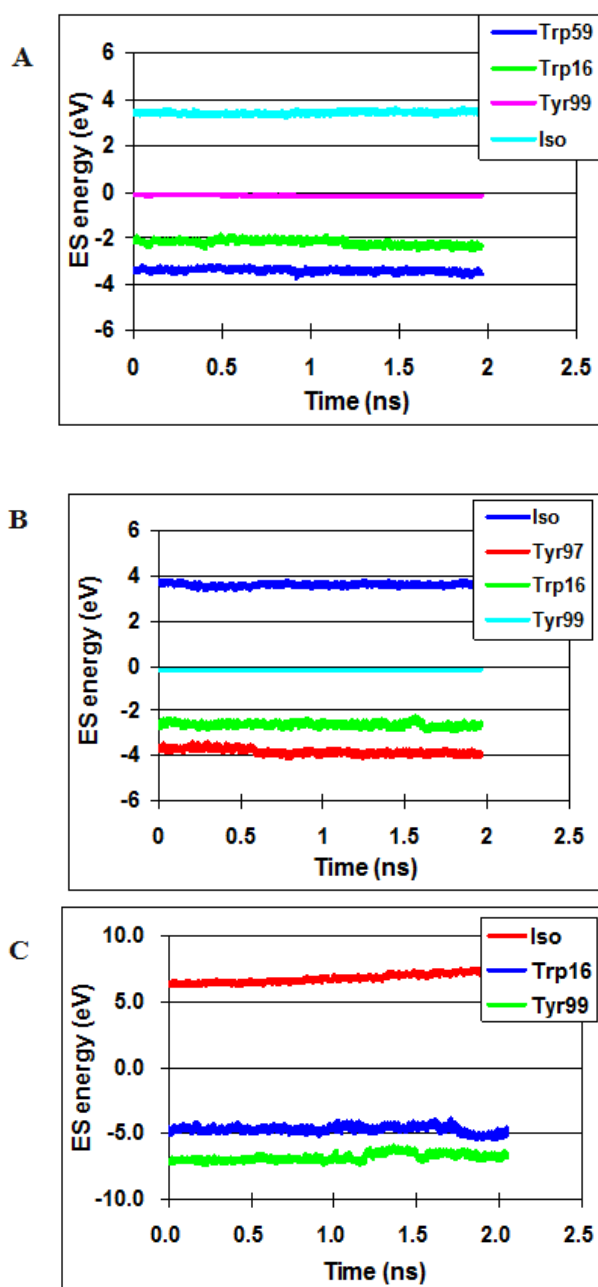


**Figure S4.5** *ES* energies in mutated FD systems.

A: Y97F, B: W59F, and C: DM. Iso represents *ES* energy between Iso anion and all other ionic amino acids including two phosphate anions. Trp59 and Trp16 indicate *ES* energy between Trp59 or Trp16 and all other ionic amino acids including two phosphate anions. Tyr97 and Tyr99 present *ES* energies between Tyr97 and Tyr99, respectively, and all other ionic amino acids including two phosphate anions. These *ES* energies were obtained by Eqs. (4-5), where the values of  $\epsilon_0$  were 4.78 in Y97F, 4.04 in W59F, and 2.28 in DM (see Table 4.2).

## SUPPLEMENTAL INFORMATION

## CHAPTER V

Conformational Flexibility and Thermodynamic properties of Holo and Apo  
*Helicobacter pylori* flavodoxin: Molecular Dynamic Simulation approaches

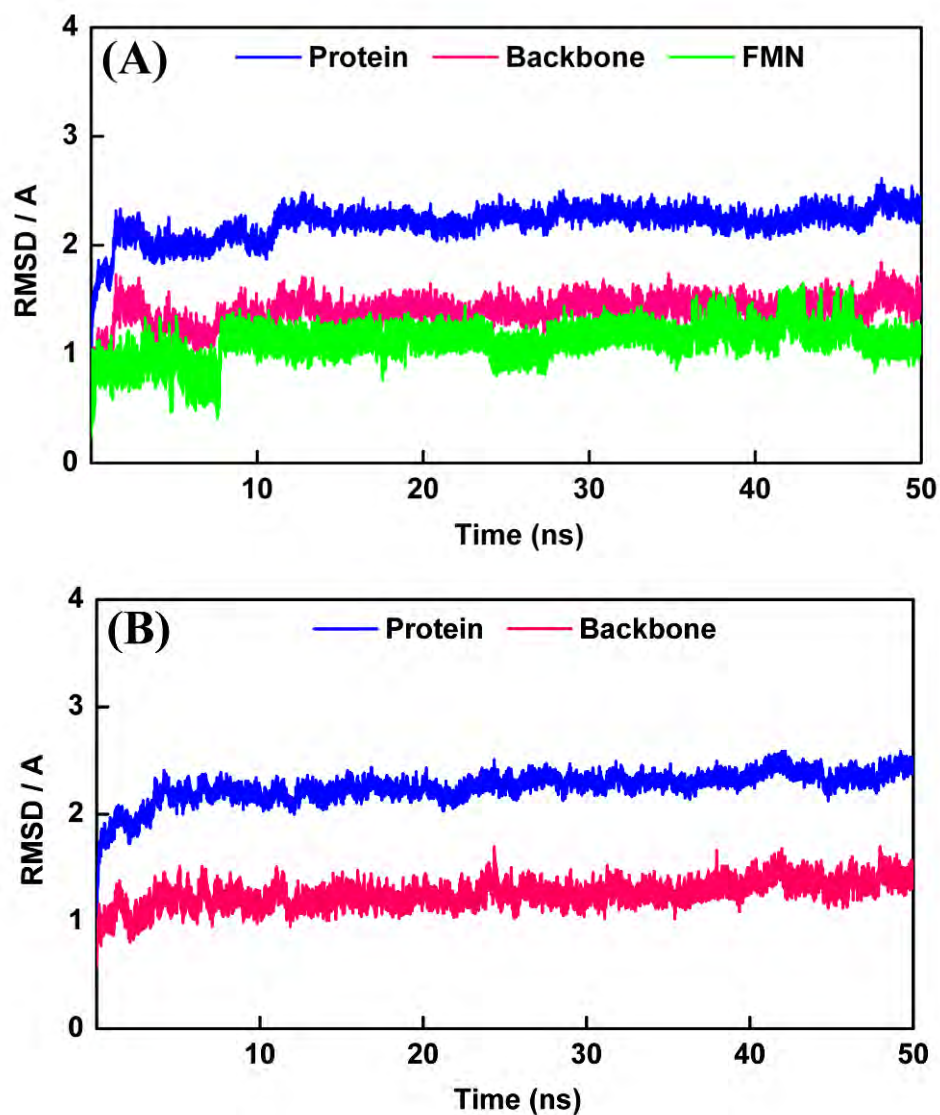


**Figure S5.1** Comparison the RMSD value between Holo-FD and Apo-FD.

Panel A shows Holo-FD, and panel B Apo-FD. The blue line indicates entries protein, the red line protein backbone and the green line FMN cofactor.

**Table S5.1** The dihedral angle parameter

Dihedral angle	$\chi_1$				$\chi_2$			
Thr-10	N	CA	CB	OG1	CA	CB	OG1	HG1
Ser-12	N	CA	CB	OG	CA	CB	OG	HG
Asn-14	N	CA	CB	CG	CA	CB	CG	ND2
Pro-53	N	CA	CB	CG	CA	CB	CG	OD1
Thr-54	N	CA	CB	OG1	CA	CB	OG1	HG1
Ala-55	H	N	CA	CB	N	CA	CB	HB1
Ala-57	H	N	CA	CB	N	CA	CB	HB1
Gly-58	H	N	CA	C	N	CA	C	O
Gln-61	N	CA	CB	CG	CA	CB	CG	OD1
Leu-86	N	CA	CB	CG	CA	CB	CG	CD1
Gly-87	H	N	CA	C	N	CA	C	O
Asp-88	N	CA	CB	CG	CA	CB	CG	OD1
Tyr-92	N	CA	CB	CG	CA	CB	CG	CD1
Thr-95	N	CA	CB	OG1	CA	CB	OG1	HG1
Phe-96	N	CA	CB	CG	CA	CB	CG	CD1
Ala-97	H	N	CA	CB	N	CA	CB	HB1
Glu-98	N	CA	CB	CG	CA	CB	CG	OD1

**Table S5.2** The mean RMSD of the Holo- and Apo-FDs<sup>a</sup>

Part	Holo	Apo
Entire protein	2.30	2.38
Backbone	1.46	1.38
Side-Chain	0.84	1.00
FMN	1.19	--

<sup>a</sup>The mean was taken over 30 ns of production time with 6 ps time intervals.

## SUPPLEMENTAL INFORMATION

## CHAPTER VI

**Mechanism of Photoinduced Electron Transfer from Tyrosine to the Excited  
Flavin in Flavodoxin from *Helicobacter pylori***

**Table 6.1S** Physical quantities related to ET in FD-*Dv*MF <sup>a)</sup>

Physical quantity	WT		Y97F		W59F	
	Trp59	Tyr97	Trp59	Tyr97	Trp59	Tyr97
$\ln k_{ET}^j$ <sup>b)</sup>	1.96	-6.68	1.14	1.60		
$\lambda_s^{qj}$ (eV)	1.53	1.54	1.20	1.47		
$ES_j$ <sup>d)</sup> (eV)	-0.0172	-0.0942	-0.219	-0.00159		
$-e^2 / \epsilon_0^q R_j$ <sup>e)</sup> (eV)	-0.384	-0.460	-0.652	-0.386		
$-\Delta G_T^{0j}$ (eV)	0.868	0.221	0.583	0.855		

<sup>a)</sup> Data are taken from Ref.[59].

## REFERENCES

- [1] Frago, S., Gomez-Moreno, C., and Medina, M. **Flavins and Flavoproteins 2008**. Prensas Universitarias de Zaragoza, 2008.
- [2] Sancho, J. Flavodoxins: sequence, folding, binding, function and beyond. **Cell. Mol. Life Sci.** 63 (2006): 855-864.
- [3] Yagi, T. Formate: Cytochrome Oxidoreductase of *Desulfovibrio vulgaris*. **J. Biochem. (Tokyo)** 66 (1969): 473-478.
- [4] Kitamura, M., Sagara, T., Taniguchi, M., Ashida, M., Ezoe, K., Kohno, K., Kojima, S., Ozawa, K., Akutsu, H., Kumagai, I., and Nakaya, T. Cloning and expression of the gene encoding flavodoxin from *Desulfovibrio vulgaris* (Miyazaki F). **J. Biochem.** 123 (1998): 891-898.
- [5] Okuno, T., Yamanaka, K., and Ogura, T. Flavodoxin, a new fluorescent substrate for monitoring proteolytic activity of FtsH lacking a robust unfolding activity. **J. Struct. Biol.** 156 (2006): 115-119.
- [6] Mataga, N., Chosrowjan, H., Taniguchi, S., Tanaka, F., Kido, N., and Kitamura, M. Femtosecond fluorescence dynamics of flavoproteins: Comparative studies on flavodoxin, its site-directed mutants, and riboflavin binding protein regarding ultrafast electron transfer in protein nanospaces. **J. Phys. Chem. B** 106 (2002): 8917-8920.
- [7] Lugsanangarm, K., Pianwanit, S., Kokpol, S., and Tanaka, F. Homology modelling and molecular dynamics simulations of wild type and mutated flavodoxins from *Desulfovibrio vulgaris* (Miyazaki F): insight into FMN–apoprotein interactions. **Mol. Simulat.** 37 (2011): 1164-1178.
- [8] Freigang, J., Diederichs, K., Schafer, K.P., Welte, W., and Paul, R. Crystal structure of oxidized flavodoxin, an essential protein in *Helicobacter pylori*. **Protein Sci.** 11 (2002): 253-261.
- [9] Bendall, D.S. **Protein Electron Transfer**. Oxford, UK: BIOS Scientific Publishers Ltd., 1996.
- [10] Anpo, M. and Matsuura, T. **Studies in Surface Science and Catalysis Vol.47**. Elsevier

- B.V., 1989.
- [11] Itamar, W. and Eugenie, K. **Bioelectronics**. Wiley-VCH, Weinheim, 2005.
- [12] Sattelle, B.M. and Sutcliffe, M.J. Calculating Chemically Accurate Redox Potentials for Engineered Flavoproteins from Classical Molecular Dynamics Free Energy Simulations†. **J. Phys. Chem. B** 112 (2008): 13053-13057.
- [13] Marcus, R.A. and Sutin, N. Electron transfers in chemistry and biology. **Biochim. Biophys. Acta**. 811 (1985): 265-322.
- [14] May, V. and Kuhn, O. **Charge and Energy Transfer Dynamics in Molecular Systems**. Weinheim: Wiley-VCH, Verlag GmbH Co., 2004.
- [15] Marcus, R.A. On the Theory of Oxidation-Reduction Reactions Involving Electron Transfer. I **J. Chem. Phys.** 24 (1956): 966-978.
- [16] Kakitani, T. and Mataga, N. New energy gap laws for the charge separation process in the fluorescence quenching reaction and the charge recombination process of ion pairs produced in polar solvents. **J. Phys. Chem.** 89 (1985): 8-10.
- [17] Nunthaboot, N., Pianwanit, S., Kokpol, S., and Tanaka, F. Simultaneous analyses of photoinduced electron transfer in the wild type and four single substitution isomers of the FMN binding protein from *Desulfovibrio vulgaris*, Miyazaki F. **Phys. Chem. Chem. Phys.** 13 (2011): 6085-6097.
- [18] Nunthaboot, N., Tanaka, F., Kokpol, S., Chosrowjan, H., Taniguchi, S., and Mataga, N. Simulation of ultrafast non-exponential fluorescence decay induced by electron transfer in FMN binding protein. **J. Photochem. Photobiol. A: Chem.** 201 (2009): 191-196.
- [19] Gray, H.B. and Winkler, J.R. Electron transfer in proteins. **Annu. Rev. Biochem.** 65 (1996): 537-561.
- [20] Cremades, N., Velazquez-Campoy, A.n., Martínez-Julvez, M., Neira, J.L., Pérez-Dorado, I., Hermoso, J., Jiménez, P., Lanás, A., Hoffman, P.S., and Sancho, J. Discovery of Specific Flavodoxin Inhibitors as Potential Therapeutic Agents against *Helicobacter pylori* Infection. **ACS Chem. Biol.** 4 (2009): 928-938.
- [21] Nelson, D.L. and Cox, M.M. **Lehninger Principles of Biochemistry**. 3 ed. New York: Worth Publisher, Inc., 2000.



- [22] Ludwig, M.L. and Luschinsky, C.L. **General properties of flavodoxins, in Chemistry and biochemistry of flavoenzymes (Müller, F., ed.)**.Vol.3. Boca Raton, Florida: CRC Press, 1992.
- [23] Mayhew, S.G. and Tollin, G. **General properties of flavodoxins, in Chemistry and biochemistry of flavoenzymes (Müller, F., ed.)**.Vol.3. Boca Raton, Florida, USA: CRC Press, 1992.
- [24] Crosson, S. and Moffat, K. Structure of a flavin-binding plant photoreceptor domain: insights into light-mediated signal transduction. **Proc. Natl. Acad. Sci. U.S.A.** 98 (2001): 2995-3000.
- [25] Zhong, D.P. and Zewail, A.H. Femtosecond dynamics of flavoproteins: Charge separation and recombination in riboflavine (vitamin B-2)-binding protein and in glucose oxidase enzyme. **Proc. Natl. Acad. Sci. U.S.A.** 98 (2001): 11867-11872.
- [26] van den Berg, P.A.W., Widengren, J., Hink, M.A., Rigler, R., and Visser, A.J.W.G. Fluorescence correlation spectroscopy of flavins and flavoenzymes: photochemical and photophysical aspects. **Spectrochim. Acta Part A.** 57 (2001): 2135-2144.
- [27] Pan, J., Byrdin, M., Aubert, C., Eker, A.P.M., Brettel, K., and Vos, M.H. Excited-state properties of flavin radicals in flavoproteins: Femtosecond spectroscopy of DNA photolyase, glucose oxidase, and flavodoxin. **J. Phys. Chem. B** 108 (2004): 10160-10167.
- [28] Karen, A., Sawada, M.T., Tanaka, F., and Mataga, N. Dynamics of excited flavoproteins-picosecond laser photolysis studies. **Photochem. Photobiol.** 45 (1987): 49-54.
- [29] Chosrowjan, H., Taniguchi, S., Mataga, N., Tanaka, F., Todoroki, D., and Kitamura, M. Comparison between ultrafast fluorescence dynamics of FMN binding protein from *Desulfovibrio vulgaris*, strain miyazaki, in solution vs crystal phases. **J. Phys. Chem. B** 111 (2007): 8695-8697.
- [30] Gauden, M., Yeremenko, S., Laan, W., van Stokkum, I.H.M., Ihalainen, J.A., van

- Grondelle, R., Hellingwerf, K.J., and Kennis, J.T.M. Photocycle of the flavin-binding photoreceptor AppA, a bacterial transcriptional antirepressor of photosynthesis genes. **Biochemistry** 44 (2005): 3653-3662.
- [31] Chosrowjan, H., Taniguchi, S., Mataga, N., Tanaka, F., Todoroki, D., and Kitamura, M. Ultrafast fluorescence dynamics of FMN-binding protein from *Desulfovibrio vulgaris* (Miyazaki F) and its site-directed mutated proteins. **Chem. Phys. Lett.** 462 (2008): 121-124.
- [32] Tanaka, F., Chosrowjan, H., Taniguchi, S., Mataga, N., Sato, K., Nishina, Y., and Shiga, K. Donor-acceptor distance-dependence of photoinduced electron-transfer rate in flavoproteins. **J. Phys. Chem. B** 111 (2007): 5694-5699.
- [33] Tanaka, F., Rujkorakarn, R., Chosrowjan, H., Taniguchi, S., and Mataga, N. Analyses of donor-acceptor distance-dependent rates of photo-induced electron transfer in flavoproteins with three kinds of electron transfer theories. **Chem. Phys.** 348 (2008): 237-241.
- [34] Henry, E.R. and Hochstrasser, R.M. Molecular dynamics simulations of fluorescence polarization of tryptophans in myoglobin. **Proc. Natl. Acad. Sci. U.S.A.** 84 (1987): 6142-6146.
- [35] Watenpaugh, K.D., Sieker, L.C., and Jensen, L.H. The binding of riboflavin-5'-phosphate in a flavoprotein: flavodoxin at 2.0-Angstrom resolution. **Proc. Natl. Acad. Sci. U.S.A.** 70 (1973): 3857-3860.
- [36] Drennan, C.L., Patridge, K.A., Weber, C.H., Metzger, A.L., Hoover, D.M., and Ludwig, M.L. Refined structures of oxidized flavodoxin from *Anacystis nidulans*. **J. Mol. Biol.** 294 (1999): 711-724.
- [37] Ludwig, M.L., Patridge, K.A., Metzger, A.L., Dixon, M.M., Eren, M., Feng, Y.C., and Swenson, R.P. Control of oxidation-reduction potentials in flavodoxin from *Clostridium beijerinckii*: The role of conformation changes. **Biochemistry** 36 (1997): 1259-1280.
- [38] Hoover, D.M. and Ludwig, M.L. A flavodoxin that is required for enzyme activation: The structure of oxidized flavodoxin from *Escherichia coli* at 1.8 angstrom resolution. **Protein Sci.** 6 (1997): 2525-2537.

- [39] Burkhart, B.M., Ramakrishnan, B., Yan, H., Reedstrom, R.J., Markley, J.L., Straus, N.A., and Sundaralingam, M. Structure of the Trigonal Form of Recombinant Oxidized Flavodoxin from *Anabaena*-7120 at 1.40 Angstrom Resolution. **Acta Crystallogr. D-Biol. Cryst.** 51 (1995): 318-330.
- [40] Fukuyama, K., Matsubara, H., and Rogers, L.J. Crystal structure of oxidized flavodoxin from a red alga *Chondrus crispus* refined at 1.8 Å resolution. Description of the flavin mononucleotide binding site. **J. Mol. Biol.** 225 (1992): 775-789.
- [41] Fukuyama, K., Wakabayashi, S., Matsubara, H., and Rogers, L.J. Tertiary structure of oxidized flavodoxin from an eukaryotic red alga *Chondrus crispus* at 2.35-Å resolution. Localization of charged residues and implication for interaction with electron transfer partners. **J. Biol. Chem.** 265 (1990): 15804-15812.
- [42] Mataga, N., Chosrowjan, H., Shibata, Y., Tanaka, F., Nishina, Y., and Shiga, K. Dynamics and mechanisms of ultrafast fluorescence quenching reactions of flavin chromophores in protein nanospace. **J. Phys. Chem. B** 104 (2000): 10667-10677.
- [43] Mataga, N., Chosrowjan, H., Shibata, Y., and Tanaka, F. Ultrafast fluorescence quenching dynamics of flavin chromophores in protein nanospace. **J. Phys. Chem. B** 102 (1998): 7081-7084.
- [44] Marti-Renom, M.A., Stuart, A.C., Fiser, A., Sanchez, R., Melo, F., and Sali, A. Comparative protein structure modeling of genes and genomes. **Annu. Rev. Biophys. Biomol. Struct.** 29 (2000): 291-325.
- [45] Havel, T.F. Predicting the Structure of the Flavodoxin from *Escherichia-Coli* by Homology Modeling, Distance Geometry and Molecular-Dynamics. **Mol. Simulat.** 10 (1993): 175-210.
- [46] Chen, H., Xu, H., Kweon, O., Chen, S., and Cerniglia, C.E. Functional role of Trp-105 of *Enterococcus faecalis* azoreductase (AzoA) as resolved by structural and mutational analysis. **Microbiology** 154 (2008): 2659-2667.
- [47] Zhou, H., Singh, N.J., and Kim, K.S. Homology modeling and molecular dynamics study of chorismate synthase from *Shigella flexneri*. **J. Mol. Graph. Model.** 25 (2006): 434-441.

- [48] Ji, H.F., Shen, L., Carey, J., Grandori, R., and Zhang, H.Y. Why WrbA is weaker than flavodoxin in binding FMN. A molecular modeling study. **J. Mol. Struct. (THEOCHEM)** 764 (2006): 155-160.
- [49] Castrignanò, T., De Meo, P.D.O., Cozzetto, D., Talamo, I.G., and Tramontano, A. The PMDB Protein Model Database. **Nucleic Acids Res.** 34 (2006): D306-D309.
- [50] Frisch, M.J., Trucks, G.W., Schlegel, H.B., Scuseria, G.E., Robb, M.A., Cheeseman, J.R., Montgomery, J.J.A., Vreven, T., Kudin, K.N., Burant, J.C., Millam, J.M., Iyengar, S.S., J., T., Barone, V., Mennucci, B., Cossi, M., Scalmani, G., Rega, N., Petersson, G.A., Nakatsuji, H., Hada, M., Ehara, M., Toyota, K., Fukuda, R., Hasegawa, J., Ishida, M., Nakajima, T., Honda, Y., Kitao, O., Nakai, H., Klene, M., Li, X., Knox, J.E., Hratchian, H.P., Cross, J.B., Adamo, C., Jaramillo, J., Gomperts, R., Stratmann, R.E., Yazyev, O., Austin, A.J., Cammi, R., Pomelli, C., Ochterski, J.W., Ayala, P.Y., Morokuma, K., Voth, G.A., Salvador, P., Dannenberg, J.J., Zakrzewski, V.G., Dapprich, S., Daniels, A.D., Strain, M.C., Farkas, O., Malick, D.K., Rabuck, A.D., Raghavachari, K., Foresman, J.B., Ortiz, J.B., Cui, Q., Baboul, A.G., Clifford, S., Cioslowski, J., Stefanov, B.B., Liu, G., Liashenko, A., Piskorz, P., Komaromi, I., Martin, R.L., Fox, D.J., Keith, T., Al-Laham, M.A., Peng, C.Y., Nanayakkara, A., Challacombe, M., Gill, P.M.W., Johnson, B., Chen, W., Wong, M.W., Gonzalez, C., and Pople, J.A., *Gaussian03*. 2003: Pittsburgh, PA.
- [51] Case, D.A., Darden, T.A., Cheatham, T.E., III, Simmerling, C.L., Wang, J., Duke, R.E., Luo, R., Crowley, M., Walker, R.C., Zhang, W., Merz, K.M., Wang, B., Hayik, S., Roitberg, A., Seabra, G., Kolossváry, I., Wong, K.F., Paesani, F., Vanicek, J., Wu, X., Brozell, S.R., Steinbrecher, T., Gohlke, H., Yang, L., Tan, C., Mongan, J., Hornak, V., Cui, G., Mathews, H.D., Seetin, M.G., Sagui, C., Babin, V., and Kollman, P.A., *AMBER10*. 2008, University of California: San Francisco.
- [52] Ryckaert, J.-P., Ciccotti, G., and Berendsen, H.J.C. Numerical integration of the cartesian equations of motion of a system with constraints: molecular dynamics of n-alkanes. **J. Comput. Phys.** 23 (1977): 327-341.
- [53] Kollman, P.A., Massova, I., Reyes, C., Kuhn, B., Huo, S., Chong, L., Lee, M., Lee, T.,

- Duan, Y., Wang, W., Donini, O., Cieplak, P., Srinivasan, J., Case, D.A., and Cheatham, T.E., 3rd. Calculating structures and free energies of complex molecules: combining molecular mechanics and continuum models. **Acc. Chem. Res.** 33 (2000): 889-897.
- [54] Kuhn, B. and Kollman, P.A. Binding of a diverse set of ligands to avidin and streptavidin: an accurate quantitative prediction of their relative affinities by a combination of molecular mechanics and continuum solvent models. **J. Med. Chem.** 43 (2000): 3786-3791.
- [55] Umamaheswari, A., Pradhan, D., and Hemanthkumar, M. Virtual screening for potential inhibitors of homology modeled *Leptospira interrogans* MurD ligase. **J. Chem. Biol.** 3 (2010): 175-187.
- [56] Azizian, H., Bahrami, H., Pasalar, P., and Amanlou, M. Molecular modeling of *Helicobacter pylori* arginase and the inhibitor coordination interactions. **J. Mol. Graph. Model.** 28 (2010): 626-635.
- [57] Luthy, R., Bowie, J.U., and Eisenberg, D. Assessment of protein models with three-dimensional profiles. **Nature** 356 (1992): 83-85.
- [58] Lugsanangarm, K., Pianwanit, S., Kokpol, S., Tanaka, F., Chosrowjan, H., Taniguchi, S., and Mataga, N. Analysis of photoinduced electron transfer in flavodoxin. **J. Photochem. Photobiol. A: Chem.** 217 (2011): 333-340.
- [59] Lugsanangarm, K., Pianwanit, S., Kokpol, S., Tanaka, F., Chosrowjan, H., Taniguchi, S., and Mataga, N. Photoinduced electron transfer in wild type and mutated flavodoxin from *Desulfovibrio vulgaris*, strain Miyazaki F.: Energy gap law. **J. Photochem. Photobiol. A: Chem.** 219 (2011): 32-41.
- [60] Dunning, T.H. A Road Map for the Calculation of Molecular Binding Energies. **J. Phys. Chem. A** 104 (2000): 9062-9080.
- [61] Decha, P., Rungrotmongkol, T., Intharathep, P., Malaisree, M., Aruksakunwong, O., Laohpongspaisan, C., Parasuk, V., Sompornpisut, P., Pianwanit, S., Kokpol, S., and Hannongbua, S. Source of high pathogenicity of an avian influenza virus H5N1: why H5 is better cleaved by furin. **Biophys. J.** 95 (2008): 128-134.
- [62] Rungrotmongkol, T., Nunthaboot, N., Malaisree, M., Kaiyawet, N., Yotmanee, P.,

- Meeprasert, A., and Hannongbua, S. Molecular insight into the specific binding of ADP-ribose to the nsP3 macro domains of chikungunya and venezuelan equine encephalitis viruses: Molecular dynamics simulations and free energy calculations. **J. Mol. Graph. Model.** 29 (2010): 347-353.
- [63] Lostao, A., El Harrous, M., Daoudi, F., Romero, A., Parody-Morreale, A., and Sancho, J. Dissecting the energetics of the apoflavodoxin-FMN complex. **J. Biol. Chem.** 275 (2000): 9518-9526.
- [64] Nunthaboot, N., Tanaka, F., Kokpol, S., Chosrowjan, H., Taniguchi, S., and Mataga, N. Simultaneous analysis of ultrafast fluorescence decays of FMN binding protein and its mutated proteins by molecular dynamic simulation and electron transfer theory. **J. Phys. Chem. B** 112 (2008): 13121-13127.
- [65] Nunthaboot, N., Tanaka, F., Kokpol, S., Chosrowjan, H., Taniguchi, S., and Mataga, N. Quantum mechanical study of photoinduced charge transfer in FMN binding protein. **J. Phys. Chem. B** 112 (2008): 15837-15843.
- [66] Nunthaboot, N., Tanaka, F., and Kokpol, S. Analysis of photoinduced electron transfer in AppA. **J. Photochem. Photobiol. A: Chem.** 207 (2009): 274-281.
- [67] Nunthaboot, N., Tanaka, F., and Kokpol, S. Simultaneous analysis of photoinduced electron transfer in wild type and mutated AppAs. **J. Photochem. Photobiol. A: Chem.** 209 (2010): 79-87.
- [68] Nishino, T.R., Miura, M., and Tanokura, K.F. **Flavins and Flavoproteins 2005**. Tokyo: Smallworld Publishing Co., 2005.
- [69] Masuda, S. and Bauer, C.E. AppA is a blue light photoreceptor that antirepresses photosynthesis gene expression in *Rhodobacter sphaeroides*. **Cell** 110 (2002): 613-623.
- [70] Gauden, M., Grinstead, J.S., Laan, W., van Stokkum, I.H.M., Avila-Perez, M., Toh, K.C., Boelens, R., Kaptein, R., van Grondelle, R., Hellingwerf, K.J., and Kennis, J.T.M. On the Role of Aromatic Side Chains in the Photoactivation of BLUF Domains†. **Biochemistry** 46 (2007): 7405-7415.
- [71] Kita, A., Okajima, K., Morimoto, Y., Ikeuchi, M., and Miki, K. Structure of a

- Cyanobacterial BLUF Protein, Tll0078, Containing a Novel FAD-binding Blue Light Sensor Domain. **J. Mol. Biol.** 349 (2005): 1-9.
- [72] Möglich, A., Yang, X., Ayers, R.A., and Moffat, K. Structure and Function of Plant Photoreceptors. **Annu. Rev. Plant. Biol.** 61 (2010): 21-47.
- [73] Marcus, R.A. Electrostatic Free Energy and Other Properties of States Having Nonequilibrium Polarization. I. **J. Chem. Phys.** 24 (1956): 979-989.
- [74] Moser, C.C., Keske, J.M., Warncke, K., Farid, R.S., and Dutton, P.L. Nature of biological electron transfer. **Nature** 355 (1992): 796-802.
- [75] Bixon, M. and Jortner, J. Non-Arrhenius temperature dependence of electron-transfer rates. **J. Phys. Chem.** 95 (1991): 1941-1944.
- [76] Mayhew, S.G., O'Connell, D.P., O'Farrell, P.A., Yalloway, G.N., and Geoghegan, S.M. Regulation of the redox potentials of flavodoxins: modification of the flavin binding site. **Biochem. Soc. Trans.** 24 (1996): 122-127.
- [77] Karen, A., Ikeda, N., Mataga, N., and Tanaka, F. Picosecond laser photolysis studies of fluorescence quenching mechanisms of flavin: a direct observation of indole-flavin singlet charge transfer state formation in solutions and flavoenzymes. **Photochem. Photobiol.** 37 (1983): 495-502.
- [78] Vorsa, V., Kono, T., Willey, K.F., and Winograd, N. Femtosecond Photoionization of Ion Beam Desorbed Aliphatic and Aromatic Amino Acids: Fragmentation via  $\alpha$ -Cleavage Reactions. **J. Phys. Chem. B** 103 (1999): 7889-7895.
- [79] Nunthaboot, N. and Tanaka, F. **Pure and Applied Chemistry International Conference 2009, Proceedings.** (2009): 495-498.
- [80] Chosrowjan, H., Taniguchi, S., Mataga, N., Nakanishi, T., Haruyama, Y., Sato, S., Kitamura, M., and Tanaka, F. Effects of the Disappearance of One Charge on Ultrafast Fluorescence Dynamics of the FMN Binding Protein. **J. Phys. Chem. B** 114 (2010): 6175-6182.
- [81] Kraft, B.J., Masuda, S., Kikuchi, J., Dragnea, V., Tollin, G., Zaleski, J.M., and Bauer, C.E. Spectroscopic and mutational analysis of the blue-light photoreceptor AppA: A novel photocycle involving flavin stacking with an aromatic amino acid. **Biochemistry** 42 (2003): 6726-6734.

- [82] Anderson, S., Dragnea, V., Masuda, S., Ybe, J., Moffat, K., and Bauer, C. Structure of a novel photoreceptor, the BLUF domain of AppA from *Rhodobacter sphaeroides*. **Biochemistry** 44 (2005): 7998-8005.
- [83] Masuda, S., Hasegawa, K., and Ono, T. Light-induced structural changes of apoprotein and chromophore in the sensor of blue light using FAD (BLUF) domain of AppA for a signaling state. **Biochemistry** 44 (2005): 1215-1224.
- [84] Laan, W., Gauden, M., Yeremenko, S., van Grondelle, R., Kennis, J.T.M., and Hellingwerf, K.J. On the mechanism of activation of the BLUF domain of AppA. **Biochemistry** 45 (2006): 51-60.
- [85] Gauden, M., van Stokkum, I.H.M., Key, J.M., Luhrs, D.C., Van Grondelle, R., Hegemann, P., and Kennis, J.T.M. Hydrogen-bond switching through a radical pair mechanism in a flavin-binding photoreceptor. **Proc. Natl. Acad. Sci. U.S.A.** 103 (2006): 10895-10900.
- [86] Jung, A., Reinstein, J., Domratcheva, T., Shoeman, R.L., and Schlichting, I. Crystal structures of the AppA BLUF domain photoreceptor provide insights into blue light-mediated signal transduction. **J. Mol. Biol.** 362 (2006): 717-732.
- [87] Toh, K.C., van Stokkum, I.H.M., Hendriks, J., Alexandre, M.T.A., Arents, J.C., Perez, M.A., van Grondelle, R., Hellingwerf, K.J., and Kennis, J.T.M. On the signaling mechanism and the absence of photoreversibility in the AppA BLUF domain. **Biophysical J.** 95 (2008): 312-321.
- [88] Domratcheva, T., Grigorenko, B.L., Schlichting, I., and Nemukhin, A.V. Molecular models predict light-induced glutamine tautomerization in BLUF photoreceptors. **Biophysical J.** 94 (2008): 3872-3879.
- [89] Yuan, H., Anderson, S., Masuda, S., Dragnea, V., Moffat, K., and Bauer, C. Crystal structures of the *Synechocystis* photoreceptor Slr1694 reveal distinct structural states related to signaling. **Biochemistry** 45 (2006): 12687-12694.
- [90] Takahashi, R., Okajima, K., Suzuki, H., Nakamura, H., Ikeuchi, M., and Noguchi, T. FTIR study on the hydrogen bond structure of a key tyrosine residue in the flavin-binding blue light sensor TePixD from *Thermosynechococcus elongatus*. **Biochemistry** 46 (2007): 6459-6467.



- [91] Bonetti, C., Mathes, T., van Stokkum, I.H.M., Mullen, K.M., Groot, M.L., van Grondelle, R., Hegemann, P., and Kennis, J.T.M. Hydrogen Bond Switching among Flavin and Amino Acid Side Chains in the BLUF Photoreceptor Observed by Ultrafast Infrared Spectroscopy. **Biophysical J.** 95 (2008): 4790-4802.
- [92] Wu, Q., Ko, W.H., and Gardner, K.H. Structural requirements for key residues and auxiliary portions of a BLUF domain. **Biochemistry** 47 (2008): 10271-10280.
- [93] Nagai, H., Fukushima, Y., Okajima, K., Ikeuchi, M., and Mino, H. Formation of Interacting Spins on Flavosemiquinone and Tyrosine Radical in Photoreaction of a Blue Light Sensor BLUF Protein TePixD $\dagger$ . **Biochemistry** 47 (2008): 12574-12582.
- [94] Fukushima, Y., Murai, Y., Okajima, K., Ikeuchi, M., and Itoh, S. Photoreactions of Tyr8- and Gln50-Mutated BLUF Domains of the PixD Protein of *Thermosynechococcus elongatus* BP-1: Photoconversion at Low Temperature without Tyr8 $\dagger$ . **Biochemistry** 47 (2007): 660-669.
- [95] Sadeghian, K., Bocola, M., and Schutz, M. A QM/MM study on the fast photocycle of blue light using flavin photoreceptors in their light-adapted/active form. **Phys. Chem. Chem. Phys.** 12 (2010): 8840-8846.
- [96] Unno, M., Kikuchi, S., and Masuda, S. Structural Refinement of a Key Tryptophan Residue in the BLUF Photoreceptor AppA by Ultraviolet Resonance Raman Spectroscopy. **Biophysical J.** 98 (2010): 1949-1956.
- [97] Dragnea, V., Arunkumar, A.I., Yuan, H., Giedroc, D.P., and Bauer, C.E. Spectroscopic Studies of the AppA BLUF Domain from *Rhodobacter sphaeroides*: Addressing Movement of Tryptophan 104 in the Signaling State. **Biochemistry** 48 (2009): 9969-9979.
- [98] Stelling, A.L., Ronayne, K.L., Nappa, J., Tonge, P.J., and Meech, S.R. Ultrafast Structural Dynamics in BLUF Domains: Transient Infrared Spectroscopy of AppA and Its Mutants. **J. Am. Chem. Soc.** 129 (2007): 15556-15564.
- [99] Brettel, K. and Byrdin, M. Reaction mechanisms of DNA photolyase. **Curr. Op. Struct. Biol.** 20 (2010): 693-701.

- [100] Kao, Y.-T., Tan, C., Song, S.-H., Öztürk, N., Li, J., Wang, L., Sancar, A., and Zhong, D. Ultrafast Dynamics and Anionic Active States of the Flavin Cofactor in Cryptochrome and Photolyase. **J. Am. Chem. Soc.** 130 (2008): 7695-7701.
- [101] Brazard, J., Usman, A., Lacombat, F., Ley, C., Martin, M.M., Plaza, P., Mony, L., Heijde, M., Zabulon, G.r., and Bowler, C. Spectro-Temporal Characterization of the Photoactivation Mechanism of Two New Oxidized Cryptochrome/Photolyase Photoreceptors. **J. Am. Chem. Soc.** 132 (2010): 4935-4945.
- [102] Tanaka, F. and Mataga, N. Ultrafast photophysics of flavins and flavoproteins. **Trends Chem. Phys.** 11 (2004): 59-74.
- [103] Bixon, M. and Jortner, J. Charge Separation and Recombination in Isolated Supermolecules. **J. Phys. Chem.** 97 (1993): 13061-13066.
- [104] Bixon, M., Jortner, J., Cortes, J., Heitele, H., and Michelbeyerle, M.E. Energy-Gap Law for Nonradiative and Radiative Charge-Transfer in Isolated and in Solvated Supermolecules. **J. Phys. Chem.** 98 (1994): 7289-7299.
- [105] Kakitani, T., Yoshimori, A., and Mataga, N. Effects of the donor-acceptor distance distribution on the energy gap laws of charge separation and charge recombination reactions in polar solutions. **J. Phys. Chem.** 96 (1992): 5385-5392.
- [106] Kakitani, T., Matsuda, N., Yoshimori, A., and Mataga, N. Present and Future Perspectives of Theoretical Aspects of Photoinduced Charge Separation and Charge Recombination Reactions in Solution. **Prog. React. Kinet.** 20 (1995): 347-381.
- [107] Yoshimori, A. and Kakitani, T. Energy Gap Dependence of the Solvent Dynamics Effect on Electron Transfer Rates in Non-Linear Response Systems. **J. Phys. Soc. Japan** 61 (1992): 2577-2592.
- [108] Jortner, J. and Bixon, M. Electron-Transfer and Intramolecular Radiationless Transitions. **J. Photochem. Photobiol. A: Chem.** 82 (1994): 5-10.
- [109] Burshtein, A.I. and Krissinel, E. Free Energy Gap Law under Diffusion Control. **J. Phys. Chem.** 100 (1996): 3005-3015.

- [110] Tachiya, M. and Seki, K. Energy gap law of electron transfer in nonpolar solvents. **J. Phys. Chem. A** 111 (2007): 9553-9559.
- [111] Mataga, N., Taniguchi, S., Chosrowjan, H., Osuka, A., and Kurotobi, K. Observations of the whole bell-shaped energy gap law in the intra-molecular charge separation (CS) from S-2 state of directly linked Zn-porphyrin-imide dyads: Examinations of wider range of energy gap ( $-\Delta G(\text{cs})$ ) for the CS rates in normal regions. **Chem. Phys. Lett.** 403 (2005): 163-168.
- [112] Iwaki, M., Kumazaki, S., Yoshihara, K., Erabi, T., and Itoh, S.  $\Delta G(0)$  dependence of the electron transfer rate in the photosynthetic reaction center of plant photosystem I: Natural optimization of reaction between chlorophyll a ( $A(0)$ ) and quinone. **J. Phys. Chem.** 100 (1996): 10802-10809.
- [113] Turro, C., Zaleski, J.M., Karabatsos, Y.M., and Nocera, D.G. Bimolecular electron transfer in the marcus inverted region. **J. Am. Chem. Soc.** 118 (1996): 6060-6067.
- [114] Parsonnet, J. The incidence of *Helicobacter pylori* infection. **Aliment. Pharmacol. Ther.** 9 (1995): 45-51.
- [115] Blaser, M.J. Hypotheses on the pathogenesis and natural history of *Helicobacter pylori*-induced inflammation. **Gastroenterol** 102 (1992): 720-727.
- [116] Lacy, B.E. and Rosemore, J. *Helicobacter pylori*: Ulcers and More: The Beginning of an Era. **J. Nutrition** 131 (2001): 2789S-2793S.
- [117] Parsonnet, J., Friedman, G.D., Vandersteen, D.P., Chang, Y., Vogelman, J.H., Orentreich, N., and Sibley, R.K. *Helicobacter pylori* infection and the risk of gastric carcinoma. **N. Engl. J. Med.** 325 (1991): 1127-1131.
- [118] Wotherspoon, A.C., Doglioni, C., Diss, T.C., Pan, L., Moschini, A., de Boni, M., and Isaacson, P.G. Regression of primary low-grade B-cell gastric lymphoma of mucosa-associated lymphoid tissue type after eradication of *Helicobacter pylori*. **Lancet.** 342 (1993): 575-577.
- [119] Hughes, N.J., Clayton, C.L., Chalk, P.A., and Kelly, D.J. *Helicobacter pylori* porCDAB

- and oorDABC genes encode distinct pyruvate:flavodoxin and 2-oxoglutarate: Acceptor oxidoreductases which mediate electron transport to NADP. **J. Bacteriol.** 180 (1998): 1119-1128.
- [120] D. Apiyo and P. Wittung-Stafshede. Presence of the cofactor speeds up folding of *Desulfovibrio desulfuricans* flavodoxin. **Protein Sci.** 11 (2002): 1129-1135.
- [121] Muralidhara, B.K. and Wittung-Stafshede, P. FMN binding and unfolding of *Desulfovibrio desulfuricans* flavodoxin: “hidden” intermediates at low denaturant concentrations. **Biochim. Biophys. Acta Protein Proteomics** 1747 (2005): 239-250.
- [122] Cremades, N., Bueno, M., Neira, J.L., Velázquez-Campoy, A.n., and Sancho, J. Conformational Stability of *Helicobacter pylori* Flavodoxin: fit to function at pH 5. **J. Biol. Chem.** 283 (2008): 2883-2895.
- [123] Martínez-Júlvez, M., Cremades, N., Bueno, M., Pérez-Dorado, I., Maya, C., Cuesta-López, S., Prada, D., Faló, F., Hermoso, J.A., and Sancho, J. Common conformational changes in flavodoxins induced by FMN and anion binding: The structure of *Helicobacter pylori* apoflavodoxin. **Protein Struct. Funct. Genet.** 69 (2007): 581-594.
- [124] Cremades, N., Velázquez-Campoy, A., Freire, E., and Sancho, J. The Flavodoxin from *Helicobacter pylori*: Structural Determinants of Thermostability and FMN Cofactor Binding†. **Biochemistry** 47 (2007): 627-639.
- [125] Ayuso-Tejedor, S., Abián, O., Velázquez-Campoy, A., and Sancho, J. Mechanism of FMN Binding to the Apoflavodoxin from *Helicobacter pylori*. **Biochemistry** 50 (2011): 8703-8711.
- [126] Lostao, A., Daoudi, F., Irún, M.P., Ramón, Á., Fernández-Cabrera, C., Romero, A., and Sancho, J. How FMN binds to Anabaena apoflavodoxin: A hydrophobic encounter at an open binding site. **J. Biol. Chem.** 278 (2003): 24053-24061.
- [127] S.G. Mayhew and Ludwig, M.L., *Flavodoxins and electron transferring flavoproteins.* 1975, Academic Press, New York.
- [128] Darrin, M.Y., Tom, A.D., and Pedersen, L.G. The effect of long-range electrostatic

- interactions in simulations of macromolecular crystals: A comparison of the Ewald and truncated list methods **J. Chem. Phys.** 99 (1993): 8345-8348.
- [129] Trylska, J., Grochowski, P., and McCammon, J.A. The role of hydrogen bonding in the enzymatic reaction catalyzed by HIV-1 protease. **Protein Science** 13 (2004): 513-528.
- [130] Copeland, R.A. Conformational adaptation in drug-target interactions and residence time. **Future Med. Chem.** 12 (2011): 1491-1501.
- [131] Genzor, C.G., Perales-Alcon, A., Sancho, J., and Romero, A. Closure of a tyrosine/tryptophan aromatic gate leads to a compact fold in apo flavodoxin. **Nat. Struct. Mol. Biol.** 3 (1996): 329-332.
- [132] Murray, T.A., Foster, M.P., and Swenson, R.P. Mechanism of Flavin Mononucleotide Cofactor Binding to the *Desulfovibrio vulgaris* Flavodoxin. 2. Evidence for Cooperative Conformational Changes Involving Tryptophan 60 in the Interaction between the Phosphate- and Ring-Binding Subsites. **Biochemistry** 42 (2003): 2317-2327.
- [133] Warshel, A., Chu, Z.T., and Parson, W.W. Dispersed polaron simulations of electron transfer in photosynthetic reaction centers. **Science** 246 (1989): 112-116.
- [134] Warshel, A. and Parson, W.W. Computer simulations of electron-transfer reactions in solution and in photosynthetic reaction centers. **Annu. Rev. Phys. Chem.** 42 (1991): 279-309.
- [135] Beratan, D., Betts, J., and Onuchic, J. Protein electron transfer rates set by the bridging secondary and tertiary structure. **Science** 252 (1991): 1285-1288.
- [136] Warshel, A. and Parson, W.W. Dynamics of biochemical and biophysical reactions: Insight from computer simulations. **Q. Rev. Biophys.** 34 (2001): 563-679.
- [137] Shibata, Y., Murai, Y., Satoh, Y., Fukushima, Y., Okajima, K., Ikeuchi, M., and Itoh, S. Acceleration of Electron-Transfer-Induced Fluorescence Quenching upon Conversion to the Signaling State in the Blue-Light Receptor, TePixD, from *Thermosynechococcus elongatus*. **J. Phys. Chem. B** 113 (2009): 8192-8198.
- [138] Weber, G. Fluorescence of riboflavin and flavin-adenine dinucleotide. **Biochem. J.** 47 (1950): 114-121.

- [139] McCormick, D.B. Interactions of flavins with amino acid residues: assessments from spectral and photochemical studies. **Photochem. Photobiol.** 26 (1977): 169-182.
- [140] van der Berg, P.A. and Visser, A.J.W.G. **New Trends in Fluorescence Spectroscopy. Applications to Chemical and Life Sciences.** First ed. Springer Series on Fluorescence, ed. Valeur, B. and Brochon, J.C. Berlin: Springer, 2001.
- [141] van den Berg, P.A.W., van Hoek, A., Walentas, C.D., Perham, R.N., and Visser, A.J.W.G. Flavin Fluorescence Dynamics and Photoinduced Electron Transfer in *Escherichia coli* Glutathione Reductase. **Biophys. J.** 74 (1998): 2046-2058.
- [142] Taniguchi, S., Chosrowjan, H., Tanaka, F., Nakanishi, T., Sato, S., Haruyama, Y., and Kitamura, M. A Key Factor for Ultrafast Rates of Photoinduced Electron Transfer among Five Flavin Mononucleotide Binding Proteins: Effect of Negative, Positive, and Neutral Charges at Residue 13 on the Rate. **Bull. Chem. Soc. Jpn** 86 (2013): 339–350.
- [143] Nueangaudom, A., Lugsanangarm, K., Pianwanit, S., Kokpol, S., Nunthaboot, N., and Tanaka, F. Structural basis for the temperature-induced transition of d-amino acid oxidase from pig kidney revealed by molecular dynamic simulation and photo-induced electron transfer. **Phys. Chem. Chem. Phys.** 14 (2012): 2567-2578.
- [144] Nueangaudom, A., Lugsanangarm, K., Pianwanit, S., Kokpol, S., Nunthaboot, N., and Tanaka, F. The mechanism of photoinduced electron transfer in the d-amino acid oxidase–benzoate complex from pig kidney: Electron transfer in the inverted region. **J. Photochem. Photobiol. A: Chem.** 250 (2012): 6-17.
- [145] Nunthaboot, N., Kido, N., Tanaka, F., Lugsanangarm, K., Nueangaudom, A., Pianwanit, S., and Kokpol, S. Relationship between rate of photoinduced electron transfer and hydrogen bonding chain of tyrosine-glutamine-flavin in flavin photoreceptors: Global analyses among four TePixDs and three AppAs. **J. Photochem. Photobiol. A: Chem.** 252 (2013): 14-24.
- [146] Kitamura, M., Kojima, S., Ogasawara, K., Nakaya, T., Sagara, T., Niki, K., Miura, K.,

- Akutsu, H., and Kumagai, I. Novel FMN-binding protein from *Desulfovibrio vulgaris* (Miyazaki F). Cloning and expression of its gene in *Escherichia coli*. **J. Biol. Chem.** 269 (1994): 5566-5573.
- [147] Nomura, A., Stemmermann, G.N., Chyou, P.-H., Kato, I., Perez-Perez, G.I., and Blaser, M.J. *Helicobacter pylori* Infection and Gastric Carcinoma among Japanese Americans in Hawaii. **N. Engl. J. Med.** 325 (1991): 1132-1136.
- [148] Yoshimori, A., Kakitani, T., Enomoto, Y., and Mataga, N. Shapes of the electron-transfer rate vs energy gap relations in polar solutions. **J. Phys. Chem.** 93 (1989): 8316-8323.
- [149] Matsuda, N., Kakitani, T., Denda, T., and Mataga, N. Examination of the viability of the Collins-Kimball model and numerical calculation of the time-dependent energy gap law of photoinduced charge separation in polar solution. **Chem. Phys.** 190 (1995): 83-95.
- [150] Mataga, N., Chosrowjan, H., and Taniguchi, S. Ultrafast charge transfer in excited electronic states and investigations into fundamental problems of exciplex chemistry: Our early studies and recent developments. **J. Photochem. Photobiol. C Photochem. Rev.** 6 (2005): 37-79.
- [151] Nunthaboot, N., Lugsanangarm, K., Pianwanit, S., Kokpol, S., Tanaka, F., Taniguchi, S., Chosrowjan, H., Nakanishi, T., Kitamura, M., and Submitted.
- [152] Lange, A.W., Rohrdanz, M.A., and Herbert, J.M. Charge-Transfer Excited States in a  $\pi$ -Stacked Adenine Dimer, As Predicted Using Long-Range-Corrected Time-Dependent Density Functional Theory. **J. Phys. Chem. B** 112 (2008): 6304-6308.
- [153] Lange, A.W. and Herbert, J.M. Both Intra- and Interstrand Charge-Transfer Excited States in Aqueous B-DNA Are Present at Energies Comparable To, or Just Above, the  $1\pi\pi^*$  Excitonic Bright States. **J. Am. Chem. Soc.** 131 (2009): 3913-3922.
- [154] Rohrdanz, M.A., Martins, K.M., and Herbert, J.M. A long-range-corrected density

- functional that performs well for both ground-state properties and time-dependent density functional theory excitation energies, including charge-transfer excited states. **J. Chem. Phys.** 130 (2009): 054112-054118.
- [155] Santoro, F., Barone, V., Lami, A., and Improta, R. The excited electronic states of adenine-guanine stacked dimers in aqueous solution: a PCM/TD-DFT study. **Phys. Chem. Chem. Phys.** 12 (2010): 4934-4948.
- [156] Improta, R. The excited states of  $\pi$ -stacked 9-methyladenine oligomers: a TD-DFT study in aqueous solution. **Phys. Chem. Chem. Phys.** 10 (2008): 2656-2664.
- [157] Chapman, S.K., Perham, R.N., and N.S., S. **Flavins and Flavoproteins**. Berlin: Rudolf Weber Agency for Scientific Publications, 2002.
- [158] Cremades, N., Bueno, M., Toja, M., and Sancho, J. Towards a new therapeutic target: *Helicobacter pylori* flavodoxin. **Biophys. Chem.** 115 (2005): 267-276.
- [159] Escudero, D. and González, L. RASPT2/RASSCF vs Range-Separated/Hybrid DFT Methods: Assessing the Excited States of a Ru(II)bipyridyl Complex. **J. Chem. Theor. Comput.** 8 (2011): 203-213.
- [160] Kupfer, S., Guthmuller, J., and González, L. An Assessment of RASSCF and TDDFT Energies and Gradients on an Organic Donor-Acceptor Dye Assisted by Resonance Raman Spectroscopy. **J. Chem. Theor. Comput.** (2012):
- [161] Runge, E. and Gross, E.K.U. Density-Functional Theory for Time-Dependent Systems. **Phys. Rev. Lett.** 52 (1984): 997-1000.
- [162] Furche, F. and Ahlrichs, R. Adiabatic time-dependent density functional methods for excited state properties. **J. Chem. Phys.** 117 (2002): 7433.
- [163] Scalmani, G., Frisch, M.J., Mennucci, B., Tomasi, J., Cammi, R., and Barone, V. Geometries and properties of excited states in the gas phase and in solution: Theory and application of a time-dependent density functional theory polarizable continuum model. **J. Chem. Phys.** 124 (2006): 094107-094115.
- [164] Tomasi, J., Mennucci, B., and Cammi, R. Quantum Mechanical Continuum Solvation Models. **Chem. Rev.** 105 (2005): 2999-3094.
- [165] Matute, R.A., Contreras, R., and González, L. Time-Dependent DFT on Phytochrome



- Chromophores: A Way to the Right Conformer. **J. Phys. Chem. Lett.** 1 (2012): 796-801.
- [166] M. J. Frisch, G.W.T., H. B. Schlegel, G. E. Scuseria, M. A. Robb, J. R. Cheeseman, G. Scalmani, V. Barone, B. Mennucci, G. A. Petersson, H. Nakatsuji, M. Caricato, X. Li, H. P. Hratchian, A. F. Izmaylov, J. Bloino, G. Zheng, J. L. Sonnenberg, M. Hada, M. Ehara, K. Toyota, R. Fukuda, J. Hasegawa, M. Ishida, T. Nakajima, Y. Honda, O. Kitao, H. Nakai, T. Vreven, J. A. Montgomery, Jr., J. E. Peralta, F. Ogliaro, M. Bearpark, J. J. Heyd, E. Brothers, K. N. Kudin, V. N. Staroverov, R. Kobayashi, J. Normand, K. Raghavachari, A. Rendell, J. C. Burant, S. S. Iyengar, J. Tomasi, M. Cossi, N. Rega, J. M. Millam, M. Klene, J. E. Knox, J. B. Cross, V. Bakken, C. Adamo, J. Jaramillo, R. Gomperts, R. E. Stratmann, O. Yazyev, A. J. Austin, R. Cammi, C. Pomelli, J. W. Ochterski, R. L. Martin, K. Morokuma, V. G. Zakrzewski, G. A. Voth, P. Salvador, J. J. Dannenberg, S. Dapprich, A. D. Daniels, Ö. Farkas, J. B. Foresman, J. V. Ortiz, J. Cioslowski, and D. J. Fox, Gaussian 09, R.A., Editor. 2009, Gaussian, Inc.: Wallingford CT.
- [167] Sauri, V., Serrano-Andres, L., Shahi, A.R.M., Gagliardi, L., Vancoillie, S., and Pierloot, K. Multiconfigurational Second-Order Perturbation Theory Restricted Active Space (RASPT2) Method for Electronic Excited States: A Benchmark Study. **J. Chem. Theor. Comput.** 7 (2010): 153-168.
- [168] Aquilante, F., De Vico, L., Ferré, N., Ghigo, G., Malmqvist, P.-å., Neogrády, P., Pedersen, T.B., Pitoňák, M., Reiher, M., Roos, B.O., Serrano-Andrés, L., Urban, M., Veryazov, V., and Lindh, R. MOLCAS 7: The Next Generation. **J. Comput. Chem.** 31 (2010): 224-247.
- [169] Veryazov, V., Widmark, P.-O., Serrano-Andrés, L., Lindh, R., and Roos, B.O. 2MOLCAS as a development platform for quantum chemistry software. **Int. J. Quant. Chem.** 100 (2004): 626-635.
- [170] Karlstrom, G., Lindh, R., Malmqvist, P.-Å.k., Roos, B.r.O., Ryde, U., Veryazov, V.,

Widmark, P.-O., Cossi, M., Schimmelpfennig, B., Neogrady, P., and Seijo, L.  
MOLCAS: a program package for computational chemistry. **Comput. Mater.  
Sci.** 28 (2003): 222-239.

## APPENDIX

### SCHOLARSHIP AND AWARDS

#### **2008 - 2012 (Ph.D. scholarship):**

The Royal Golden Jubilee Ph.D. Scholarship, by Chulalongkorn University and Thailand  
Research Fund

#### **2004 - 2008 (B.Sc. scholarship):**

The Science Achievement Scholarship of Thailand (SAST) by Commission on Higher Education,  
Thailand

#### **2012 (April) – 2012 (September):**

Training experience on the excited state calculation for electron transfer reaction, University of  
Vienna, Austria

#### **2010 (October) - 2011 (March):**

JASSO-JENESYS Program implemented by JSPS, Institute for Molecular Science, Japan

#### **2009 (December):**

Sokendai Asian Winter School 2009, organized by Institute for Molecular Science, Japan

### PUBLICATION IN THIS DESSERTATION

- 1. K. Lugsanangarm**, S. Pianwanit, S. Kokpol, F. Tanaka, H. Chosrowjan, S. Taniguchi, and N. Mataga, *Analysis of Photoinduced Electron Transfer in Flavodoxin* J. Photochem. Photobiol. A: Chem. 217 (2011), page 333-340.
- 2. K. Lugsanangarm**, S. Pianwanit, S. Kokpol, F. Tanaka, H. Chosrowjan, S. Taniguchi, and N. Mataga, *Photoinduced Electron Transfer in Wild Type and Mutated Flavodoxin from *Desulfovibrio vulgaris*, strain Miyazaki F., Energy Gap Law* J. Photochem. Photobiol. A: Chem. 219 (2011), page 32-41.

3. **K. Lugsanangarm**, S. Pianwanit, F. Tanaka, and S. Kokpol, *Homology Modeling and Molecular Dynamics Simulation of Wild Type and Mutated Flavodoxins from Desulfovibrio vulgaris (Miyazaki F.): Insight into FMN-Apoprotein Interaction*. Mol. Simulat. 37 (2011), page 1164-1178.

## I. CONFERENCES (POSTER PRESENTATION)

1. **K. Lugsanangarm**, S. Pianwanit, F. Tanaka, and S. Kokpol, *Theoretical Investigation on the Interaction between Flavin Mononucleotide and Flavodoxin for both Wild type and its Mutants by means of Molecular Dynamic Simulation*, The 35<sup>th</sup> Congress on Science and Technology of Thailand, Chonburi, Thailand, October 15 – 17, 2009.
2. **K. Lugsanangarm**, S. Pianwanit, F. Tanaka, and S. Kokpol, *Analysis on Ultrafast Fluorescence Dynamic and Electron Transfer of Flavodoxin from Desulfovibrio vulgaris (Miyazaki F)*, Sokendai Asian Winter School, IMS, Okazaki, Japan, December 1 - 4, 2009
3. **K. Lugsanangarm**, S. Pianwanit, F. Tanaka, and S. Kokpol, *Homology Modeling and Molecular Dynamics Simulation of Flavodoxin and Its Mutants: Insight into FMN-Apo Protein Interaction*, The 4<sup>th</sup> Asian Pacific Conference of Theoretical & Computational Chemistry, Port Dickson, Malaysia, December 21 – 23, 2009
4. **K. Lugsanangarm**, S. Pianwanit, F. Tanaka, S. Kokpol and S. Saito, *Theoretical prediction of the crucial interaction for inhibiting H. pylori flavodoxin: Molecular docking and MD simulations*, The Winter School of Sokendai/Asian CORE Program, Okazaki, Japan, February 19 - 22, 2011.
5. **K. Lugsanangarm**, S. Pianwanit, S. Kokpol and F. Tanaka, *Molecular Dynamic Simulation and Quantum Chemical Calculations for Analysis of Photoinduced Electron Transfer in Flavodoxin*, 14<sup>th</sup> Asian Chemical Congress (14ACC), Bangkok, Thailand, September 5 – 8, 2011.
6. **K. Lugsanangarm**, A. Nueangaudom, S. Pianwanit, S. Kokpol and F. Tanaka, *Molecular Orbital Study of the Effect of Dielectric constant on the Charge Transfer*

*Interaction in Flavodoxin*, Pure and Applied Chemistry International Conference (PACCON2012), Chiang Mai, Thailand, January 11-13, 2012.

7. **K. Lugsanangarm**, S. Pianwanit, S. Kokpol, F. Tanaka, N. Nunthaboot, H. Chosrowjan, S. Taniguchi, T. Nakanishi, K. Ogino, M. Kitamura, N. Kido, *Theoretical Analyses of Photoinduced Electron Transfer Mechanism of Flavodoxin From Helicobacter pylori and Desulfovibrio vulgaris (Miyazaki F)*, International Meeting on Atomic and Molecular Physics and Chemistry (IMAMPC2012), Pisa, Italy, September 12 – 14, 2012
8. **K. Lugsanangarm**, S. Pianwanit, S. Kokpol and F. Tanaka, *Theoretical Comparative Study of Intermolecular Electron Transfer in Flavodoxin from Helicobacter pylori and Desulfovibrio vulgaris, Miyazaki F*. 9th Thai Summer School of Computational Chemistry (9th TS2C2), Phattalung, Thailand, October 22 - 25, 2012

## **II. CONFERENCES (ORAL PRESENTATION)**

1. **Theoretical prediction of the crucial interaction for inhibiting *H. pylori* flavodoxin: Molecular docking and MD simulations**, The Winter School of Sokendai/Asian CORE Program, Okazaki, Japan, February 19 - 22, 2011
2. **Analysis of Photoinduced Electron Transfer Mechanism in Flavodoxin from *Helicobacter pylori***, The Science Forum 2013, Bangkok, Thailand, March 14 – 15, 2013
3. **Theoretical Analysis of Photoinduced Electron Transfer in Wild Type and Mutated Flavodoxin**, RGJ-Ph.D. Congress XIV, Chonburi, Thailand, April 5 – 7, 2013

## **III. RESEARCH VISITING**

1. October, 2009 – February, 2010  
Department of Theoretical and Computational Molecular Science, Institute for Molecular Science, with Prof. Shinji Saito
2. April, 2011 – September, 2011  
Institute for Theoretical Chemistry, University of Vienna, with Prof. Karl Peter Wolschann and Prof. Leticia González

## **BIOGRAPHY**

### **PERSONAL DATA**

**Name**            **Kiattisak Lugsanangarm**  
**Nationality**    **Thai**  
**Date of Birth**   **August 31, 1985**  
**E-mail**         **kiattisak.l@hotmail.com**

### **EDUCATION**

**2004 – 2008**    **B.Sc. in Chemistry (2<sup>nd</sup> honor)**  
**Department of Chemistry, Faculty of Science, UbonRatchathani University,**  
**UbonRatchathani, Thailand**

**2008 – 2011**    **Ph.D. in Physical Chemistry**  
**Department of Chemistry, Faculty of Science, Chulalongkorn University,**  
**Bangkok, Thailand**